SANDIA REPORT
SAND2006-2518
Unlimited Release
Printed April 2006

Closed Brayton Cycle Power Conversion Systems for Nuclear Reactors: Modeling, Operations, and Validation

Steven A. Wright, Ronald J. Lipinski, Milton E. Vernon, Travis Sanchez

Prepared by
Sandia National Laboratories
Albuquerque, New Mexico 87185 and Livermore, California 94550

Sandia is a multiprogram laboratory operated by Sandia Corporation,
a Lockheed Martin Company, for the United States Department of Energy's
National Nuclear Security Administration under Contract DE-AC04-94AL85000.

Issued by Sandia National Laboratories, operated for the United States Department of Energy by Sandia Corporation.

Available to DOE and DOE contractors from
U.S. Department of Energy
Office of Scientific and Technical Information
P.O. Box 62
Oak Ridge, TN 37831

Telephone: (865) 576-8401
Facsimile: (865) 576-5728
E-Mail: reports@adonis.osti.gov
Online ordering: http://www.osti.gov/bridge

Available to the public from
U.S. Department of Commerce
National Technical Information Service
5285 Port Royal Rd.
Springfield, VA 22161

Telephone: (800) 553-6847
Facsimile: (703) 605-6900
E-Mail: orders@ntis.fedworld.gov
Online order: http://www.ntis.gov/help/ordermethods.asp?loc=7-4-0#online

Table of Contents

Table of Contents 3
.List of Figures 5
List of Figures 6
List of Tables 15
Acknowledgements 18
Acknowledgements 18
Abstract 19
1 Introduction and Executive Summary 20
1.1 Dynamic Model Introduction 21
1.2 Sandia-Brayton Test-Loop 25
1.3 Model Comparison with Measured Data (Validation) 28
2 Integrated Dynamic Systems Models 31
2.1 History of Reactors and Closed Brayton Cycles 32
2.2 Recuperated Closed Brayton Cycle Introduction 35
2.2.1 Closed Brayton Cycle Control Issues 37
2.2.2 Thermodynamic Cycle Analysis of Closed Brayton Cycles 38
2.2.3 Scoping Calculations and Some Results 42
2.2.3.1 Chapman Enskog Theory for Properties of Mixed Gases 46
2.2.3.2 Gas Material Properties for Ideal and Monatomic Gases 46
2.2.3.3 Chapman Equation for C_p, k, and Viscosity for Gases 47
2.2.3.4 Mixture Rules for the He/Xe gas mixture 48
2.2.4 Trade Studies and Sizing Estimates 53
2.3 Characteristic Flow Curves for Radial Turbine and Compressors 55
2.3.1 Capstone C-30 Compressor and Turbine 55
2.3.2 Characteristic Flow Curves 58
2.3.2.1 C-30 Compressor Flow Map 60
2.3.2.2 C-30 Turbine Flow Map 64
2.3.3 132 kWe CBC Turbo-Compressor Description 67
2.3.3.1 NGST/CNREC 132 kWe Compressor Flow Map and Multivariate Polynomial Fit 68
2.3.3.2 NGST/CNREC 132 kWe Turbine Flow Map and Multivariate Polynomial Fit 71
2.3.4 Turbo-Compressor Working Line 73
2.4 Lumped Parameter Steady State Gas Cooled Reactor Model 76
2.4.1 Reactor Steady State Model 77
2.4.2 Recuperator Steady State Model 78
2.4.3 Turbo-Alternator-Compressor Steady State Model 79
2.4.4 Space Radiator Steady State Model 80
2.4.5 Gas Inventory Steady State Model 81
2.4.6 Steady State Equation Summary and Results for a Reactor Driven Brayton Cycle Power Conversion System 82
2.4.6.1 Steady State Operating Map at Constant Fuel Temperature 83
2.4.6.2 State Point Temperatures at Constant Shaft Speed 86
2.4.6.3 Stability Analysis 88

2.4.6.4 Control Issues and Discussion 91
2.5 Lumped Parameter Dynamic Model 91
2.5.1 Dynamic Lumped Parameter Reactor Model 91
2.5.2 Recuperator and Radiator Lumped Parameter Model 94
2.5.3 Radiator Lumped Parameter Model 94
2.5.4 Turbine, Alternator, and Compressor Lumped Parameter Model 95
2.6 Reactor Power and Control Simulator (RPCSIM) Dynamic Model 96
2.6.1 Other Dynamic Models for SP100 and TOPAZ 97
2.6.2 RPCSIM Simulink Dynamic Model Introduction 97
2.6.2.1 Simulink Development Environment 98
2.6.3 Dynamic Model Description and Assumptions for a Liquid Metal Cooled Reactor and a Gas Cooled Reactor 98
2.6.4 Gas Cooled Reactor Description and CBC Overview 102
2.6.4.1 Nuclear Reactor Core and Reflectors Description 106
2.6.4.2 Reactor Simulink Module 109
2.6.4.2.1 Point Kinetics Reactor Model 110
2.6.4.2.2 Feedback Mechanisms and Models 111
2.6.4.2.3 RPCSIM Gas Cooled Reactor Simulink Module 113
2.6.4.3 Turbine-Alternator-Compressor (TAC) Simulink Model 115
2.6.4.4 Heat Exchanger and Recuperator Simulink Module 117
2.6.4.5 Radiator Simulink Module 118
2.6.4.6 Gas Coolant Mass Constraint 121
2.6.4.7 Feedback Control Loops 123
2.6.4.7.1 Reactor Controller 124
2.6.4.7.2 PMAD or Turbo-Alternator-Compressor Controller 124
2.6.5 Simulink System Model and Equations 124
2.6.5.1 Simulink Fluid Thermal Hydraulics Models 125
2.7 Startup Transients for Reactor Driven Brayton Cycles 129
2.7.1 GCR Startup Transient with One Feedback Term 130
2.7.2 GCR Startup Transient with Three Feedback Terms 138
2.7.2.1 GCR Startup Transient with 3 Feedback Terms and Flow Starting well after Reactor Startup (Tinit + 300 K) 138
2.7.2.2 GCR Startup Transient with 3 Feedback Terms but with Flow Startup at 10 K above the Initial Temperature 142
2.7.2.3 GCR Startup Transient with Flow Startup Prior to Reactor Startup: Reactor has 3 Feedback Terms 143
2.7.2.4 Summary of the Three Startup Scenarios 147
2.7.3 Dynamic Stability 147
2.7.4 Consequences of Various Perturbations 152
2.7.4.1 What happens if the system pressure is increased? 153
2.7.4.2 What happens if the flow in the gas chiller is increased? 153
2.7.4.3 How long can the system run if the reactor power is turned off? 153
2.7.5 Liquid Metal Reactor Startup Transients 153
3 Sandia Brayton Test Loop Description 160
3.1 Closed Brayton Cycle Test-Loop Description 161
3.2 Capstone Turbo-Alternator-Compressor Modifications 165

3.3 Gas Heater Description 173
3.3.1 Electrical Power Description 180
3.4 Gas Cooler Description 182
3.5 Ducting and Instrumentation Description 187
3.5.1 Pressure Safety Overview 191
3.5.1.1 Pressure Ratings of Vessels and Components 192
3.5.1.2 Ducts and Vessels 192
3.6 CBC RT Controller Operation Summary 196
3.7 Alternative Working Fluid Gases and Electrical Breakdown in the Gas Cooling the Generator 202
3.7.1 Sandia Brayton Loop Paschen Effect Conditions 208
4 Operational Results, Validation, and Comparison of the Dynamic Model with the SBL-30 Operation 210
4.1 Brief Summary of Measurements from Three Transient Tests using the Sandia Brayton Loop 211
4.1.1 Introduction and Summary of Test TT4 211
4.1.2 Introduction and Summary of Test TT5 215
4.1.3 Introduction and Summary of Test TT6 217
4.2 Energy Balance 218
4.3 Comparison of Measured and Predicted Characteristic Flow Curves for the C30 Turbo-Compressor Set 221
4.4 Operations and Test Results of the Sandia Brayton Loop Tests TT5 and TT6223
4.4.1 Power Generated Versus Shaft Speed: Operational Curve 224
4.4.1.1 Test TT5 (880-K Turbine Inlet Temperature) 224
4.4.1.1.1 Impact of Power versus RPM “Operation Curve” 230
4.4.1.2 750-K Turbine Inlet Temperature measured Test TT6 232
4.4.1.3 700-K Turbine Inlet Temperature Measured in TT6 234
4.4.1.4 650-K Turbine Inlet Temperature Measured in TT6 236
4.4.1.5 600-K Turbine Inlet Temperature Measured in TT6 238
4.4.2 Power vs. Speed Summary of Measured Operations Curves for the Sandia Brayton Loop 240
4.5 Reactor Shutdown Simulations 241
4.5.1 Decay Heat Removal Issue Description 242
4.5.2 Sandia Brayton Loop Decay Heat Removal Test (TT5) 243
4.6 Dynamic Model Predictions of TT5 245
5 Summary and Conclusions 253

.

List of Figures

Figure 1-1: Simulink block diagram of the dynamic model for a gas cooled reactor coupled to a closed Brayton cycle. 23
Figure 1-2: Startup transient (ANS-3FB-300) for a 313 pin 100 kWe gas cooled space reactor with 3 feed-back coefficients coupled to a closed Brayton cycle. Coolant flow starts once the reactor average fuel temperature exceeds the initial temperature by 300 K. Pwr-Rx is the power in the reactor, Pwr Therm is the thermal power removed by the gas coolant from the reactor. Pwr-Rad-Therm is the power removed from the coolant by the space thermal radiator. Pwr-Rad-Space is the thermal power radiated to space, and Pwr Load-tot is the total load on the turbo-compressor shaft caused by the alternator and parasitic resistor. 24
Figure 1-3: Reactivity and flow rate input values for the gas cooled reactor startup transient ANS-3FB-300, where the HeXe gas flow starts when the fuel temperature exceeds the initial temperature by 300 K. The input values for reactivity and shaft rpm are coordinated to first bring the system to a low power level (4000-7000 s), followed by a ramp to full power (9000 – 14000 s). RhoDol-In is the reactivity in units of dollars inserted into the reactor by the control rods. RhoDol-Tot is the total reactivity (in dollars) which includes both the inserted reactivity and feedback effects. 25
Figure 1-4: Photo of the Sandia Brayton Loop (SBL-30) installed at Sandia. 26
Figure 1-5: Measured results of the Sandia Brayton Loop (SBL-30). The measured gas temperatures are shown on the left scale while the reactor power and shaft speed are shown on the right scale. The temperature nominclature starts at T100 (the turbine inlet), T200 is the turbine outlet and so on around the gas loop. T700 and 701 are water intlet and out let temperatures. The input power is in percent of full power (which is 62 kW) and the electrical power generated is in Watts/100. 28
Figure 1-6: Measured data for an early transient measurement to test the automatic control loop (May 13, 2005). 29
Figure 1-7: Screen shot of the dynamic model temperature predictions for the same measured transient shown in Figure 1-6 given input power, rpm, and water cooling temperatures. Gold is compressor inlet temperature (CIT), magenta is compressor outlet temperature, cyan is heater inlet temperature (HIT), red is turbine inlet temperature (TIT), green is turbine outlet temperature (TOT), and blue is gas chiller inlet temperature (GCIT). 30
Figure 2-1: Schematic of the ML-1 reactor showing the reactor on the right and the heat exchangers and turbo-machinery on the left. 33
Figure 2-2: One of 37 fuel elements that used UO2-BeO fuel clad with Hastelloy X in a water moderated gas cooled reactor. 34
Figure 2-3: Gas coolant temperature ant pressure state-points in the ML-1 reactor. 35
Figure 2-4: Schematic diagram of nuclear gas cooled reactor coupled to a simple recuperated Closed Brayton Cycle (CBC). 36
Figure 2-5: Temperature entropy diagram for a single staged helium Brayton cycle. 41
Figure 2-6: CBC cycle efficiency for HeXe (63 a/o He) as a function of pressure ratio and for two selected recuperator effectiveness values of 0.8 and .9. 44
Figure 2-7: CBC reactor inlet temperature as a function of compression ratio and recuperator effectiveness. 45
Figure 2-8: Mixed gas thermal conductivity and viscosity versus temperature or as a function of helium mole fraction. 51
Figure 2-9: Heat capacity as a function of Helium mole fraction. 52

Figure 2-10: Comparison of measured and predicted thermal conductivity for a He/Xe gas mixture containing 75 mole % He. 52
Figure 2-11: Comparison of calculated and measured viscosity for He/Xe gas mixture with 75 mole% He. 53
Figure 2-12. Reactor module mass vs. number of fuel pins. 54
Figure 2-13 Capstone C-30 compressor and turbine wheels include the gas thrust and journal bearings. The compressor is on the left side and is relatively cool, (green colors) and the turbine is on the right (red colors for the housing and bearings. (courtesy of NASA). 56
Figure 2-14: Face or front views of the Capstone C-30 compressor (left) and turbine. Note that the compress wheels blades are back swept while the turbine inlet blades are not. Also note that the turbine base is scalloped, this is likely done to help accommodate the gas flow from the inlet nozzle and presumably to help balance the thrust loads. 57
Figure 2-15: Compressor wheel and exit diffuser (left) and turbine inlet nozzle (right). 57
Figure 2-16 Characteristic curves for the Capstone C-30 compressor. The lower left figure shows the pressure ratio as a function of mass flow rate for constant rpm. The shaft rpm is shown parametrically. The lower right curve shows the temperature ratio, and the upper curve shows the isentropic efficiency. 60
Figure 2-17: Three dimensional plot of the C-30 compressor pressure ratio versus dimensionless flow and shaft speed. 63
Figure 2-18: C-30 Turbine flow map for pressure ratio as a function of dimensionless flow. In this curve the extrapolation to a pressure ratio of 1.0 at zero flow is shown. 65
Figure 2-19: C-30 turbine temperature ratio characteristic flow curve plotting the temperature ratio as a function of dimensionless flow for various rpm values. 65
Figure 2-20: 3-D plot of the Capstone C-30 turbine dimensionless flow map. 66
Figure 2-21: Power and efficiency for a 132 kWe gas cooled space reactor concept shown as a function of mass corrected mass flow rate for various shaft speed. The design shaft speed was 59,850 rpm. 69
Figure 2-22: Compressor temperature ratio (top) and pressure ratio for a 132 kWe gas cooled space reactor shown as a function of mass flow rate for various shaft speeds. Design shaft speed is 59,850 rpm. 70
Figure 2-23: Turbine temperature ratio (top) and pressure ratio for a 132 kWe gas cooled space reactor shown as a function of mass flow rate for various shaft speeds. Design shaft speed is 59,850 rpm. 72
Figure 2-24: Steady state working line (dotted red line) for the 132 kWe NGST/CNREC CBC system with a 400 K, 2.0 MPa compressor inlet pressure and a 1200 K turbine inlet temperature. The working curve is determined by the intersection of the turbine and compressor pressure ratio curves for the same rpm values. This intersection point guarantees that the mass flow, rpm, and pressure ratio through the turbine and compressor all equal each other. 74
Figure 2-25: Map of the 132 kWe NGST/CNREC turbo-compressor working line. 75
Figure 2-26: Transient behavior for shaft speed and flow accelerations (increases in power) and for deceleration (decreases in power). 75
Figure 2-27: Schematic diagram of nuclear gas cooled reactor coupled to a simple recuperated Closed Brayton Cycle (CBC). 77
Figure 2-28: Alternator or TAC shaft load plotted as a function of shaft speed for various fixed turbine inlet temperatures. 85

Figure 2-29: Reactor power shown as a function of shaft speed for various reactor average fuel temperatures. 86
Figure 2-30: Coolant temperatures at the stations around the Rx-CBC loop. 87
Figure 2-31: Average fuel temperature, reactor inlet and reactor outlet temperature at fixed speeds. 87
Figure 2-32: Reactor power level at several fixed shaft speeds shown as a function of TAC power or alternator power. 88
Figure 2-33: Excess power to spin the TAC shaft as a function of shaft rpm at various, but fixed, average fuel temperatures and for a fixed alternator load of 140 kW. When the excess shaft power is positive the shaft speed is increasing. When it is negative the shaft is slowing, and when the excess shaft power is zero, then steady state conditions are achieved. 89
Figure 2-34: Excess power to spin the TAC shaft as a function of shaft rpm at various, but fixed, alternator power levels and for a constant fuel temperature of 1150 K. When the excess shaft power is positive the shaft speed is increasing. When it is negative the shaft is slowing, and when the excess shaft power is zero, then steady state conditions are achieved. 90
Figure 2-35: Simulink™ schematic of a liquid metal cooled reactor (LMR). 99
Figure 2-36: Simulink™ schematic of a gas cooled reactor (GCR). 101
Figure 2-37: Conceptual layout for a direct gas cooled reactor coupled to two Brayton systems. Only one CBC loop is modeled in the present version of RPCSIM. 103
Figure 2-38: Approximate state points for the Closed Brayton Cycle System. 105
Figure 2-39: Nominal direct drive Gas-Cooled Reactor (GCR) ~400 kW_t showing the reactor, shield, inlet and outlet ducts, bypass flow, and radial reflectors (gray). 106
Figure 2-40: Close-up of Flow Through inlet nozzle, bypass, lower plenum, fuel pin flow annulus, and exit plenum and exit duct. 107
Figure 2-41: Axial flow paths in bypass flow channel and fuel channel with temperature distributions calculated in fuel, prism/block, and pressure vessel 110
Figure 2-42: Feedback Depends on Temperature of Fuel, Prism and Pressure Vessel (& Mounting Methods) 112
Figure 2-43: Simulink block diagram of GCR model. 114
Figure 2-44: Simulink feedback model. 114
Figure 2-45: Simulink compressor model. 116
Figure 2-46: Simulink turbine model. 117
Figure 2-47: Simulink recuperator module for RPCSIM. The model uses has a low pressure leg and a high pressure leg. Each leg uses a gas calculator and a heat transport calculator to determine the pressure drop through the system and the gas and structural temperatures in the recuperator. The model assumes a counter flow recuperator, and the above programming reverses the direction of the node numbers to simulate the counter flow characteristics of the recuperator. 119
Figure 2-48: Simulink Model for a NaK cooled space radiator. An additional submodule (cyan) is added to the standard heat transport module to account for radiation losses to space. 120
Figure 2-49: GCR Inventory Constraint to determine po5 123
Figure 2-50: RPCSIM thermal hydraulic models for coolant pressure drop (momentum) and heat transport (energy). The gas calculator determines the outlet pressure given the inlet flow rate, temperature and pressure and given the coolant hydraulic flow parameters such as hydraulic diameter, flow area, and flow length as well as the coolant material properties.

Likewise the gas outlet temperature and the time rate of change of the structural temperatures are determined by the heat transport module (heat exchanger). Again material properties and design geometries are required. 126
Figure 2-51: Input values for transient Tinit+300,1FB. The plot shows the inserted reactivity (Rho-Dol-In), the TAC shaft speed (Normalized Shaft Speed), the mass flow rate (Mass Flow Rate) and the total reactivity which is the sum of the inserted and feedback terms (Rho-Dol-Tot). The reactivity is given in dollars. 131
Figure 2-52: Reactor and CBC power levels for transient Tinit+300,1FB. The plot shows the fission power or reactor power, the thermal power transferred to the gas coolant, the power transferred from the coolant to the radiator structure (Pwr-Rad-Therm), the power radiated to space (Pwr-Rad-Space) and the alternator load or electrical power (Pwr-Load-tot). 132
Figure 2-53: Pressure values for transient Tinit+300,1FB. The plot shows the pressure at each station around the loop, but as can be seen the pressures really show the time dependent values of the low pressure leg and the high pressure leg. Pressure drop effects are observable, but they are small. 133
Figure 2-54: Station temperatures for transient Tinit+300,1FB. This plot shows the temperatures for the reactor outlet or turbine inlet (RxOT=TIT), the turbine outlet (TOT), the reactor inlet (RxIT), the radiator inlet (Rad IT), the compressor outlet (COT), and the compressor inlet (CIT). 135
Figure 2-55: Alternator power for transient Tinit+300;1FB. The time scale and power levels show the power required to motor the alternator. Self sustaining operations occur at 2850 seconds. 136
Figure 2-56: Reactor and CBC power levels for transient Tinit+300,3FB. The plot shows the fission power or reactor power (Pwr Rx), the thermal power transferred to the gas coolant (Pwr Therm), the power transferred from the coolant to the radiator structure (Pwr-Rad-Therm), the power radiated to space (Pwr-Rad-Space) and the alternator load or electrical power (Pwr-Load-tot). 139
Figure 2-57: Input values for transient Tinit+300,3FB. The plot shows the inserted reactivity (Rho-Dol-In), the TAC shaft speed (Normalized Shaft Speed), the mass flow rate (Mass Flow Rate) and the total reactivity which is the sum of the inserted and feedback terms (Rho-Dol-Tot). The reactivity is given in dollars. 140
Figure 2-58: Pressure values for transient Tinit+300,3FB. The plot shows the pressure at each station around the loop, but as can be seen the pressures really show the time dependent values of the low pressure leg and the high pressure leg. Pressure drop effects are observable, but they are small. 141
Figure 2-59: Station temperatures for transient Tinit+300,3FB. This plot shows the temperatures for the reactor outlet or turbine inlet (RxOT=TIT), the turbine outlet (TOT), the reactor inlet (RxIT), the radiator inlet (Rad IT), the compressor outlet (COT), and the compressor inlet (CIT). 141
Figure 2-60: Reactor and CBC power levels for transient Tinit+10,3FB. The plot shows the fission power or reactor power (Pwr Rx), the thermal power transferred to the gas coolant (Pwr Therm), the power transferred from the coolant to the radiator structure (Pwr-Rad-Therm), the power radiated to space (Pwr-Rad-Space) and the alternator load or electrical power (Pwr-Load-tot). The power pulse at A is caused by the latent heat effect, at B by the startup of coolant flow, and at C by the reactivity ramp. 142

Figure 2-61: Station temperatures for transient Tinit+10,3FB, This plot shows the temperatures for the reactor outlet or turbine inlet (RxOT=TIT), the turbine outlet (TOT), the reactor inlet (RxIT), the radiator inlet (Rad IT), the compressor outlet (COT), and the compressor inlet (CIT). All conditions are the same as in Figure 2-59 but the flow starts sooner, at the initial temperature + 10K. 143
Figure 2-62: Reactor and CBC power levels for transient Time500,3FB. The plot shows the fission power or reactor power (Pwr Rx), the thermal power transferred to the gas coolant (Pwr Therm), the power transferred from the coolant to the radiator structure (Pwr-Rad-Therm), the power radiated to space (Pwr-Rad-Space) and the alternator load or electrical power (Pwr-Load-tot). In this transient the CBC flow starts after reactor heating. 144
Figure 2-63: Input values for transient Time500,3FB. The plot shows the inserted reactivity (Rho-Dol-In), the TAC shaft speed (Normalized Shaft Speed), the mass flow rate (Mass Flow Rate) and the total reactivity which is the sum of the inserted and feedback terms (Rho-Dol-Tot). The reactivity is given in dollars. Note that the rpm and flow start at 500 seconds..... 145
Figure 2-64: Station temperatures for transient Time500,3FB, This plot shows the temperatures for the reactor outlet or turbine inlet (RxOT=TIT), the turbine outlet (TOT), the reactor inlet (RxIT), the radiator inlet (Rad IT), the compressor outlet (COT), and the compressor inlet (CIT). All conditions are the same as in Figure 2-59 but the flow starts at 500 seconds which is prior to reactor heating. 146
Figure 2-65: GCR startup transient Time500,3FB, showing alternator power as a function of time. This transient starts the CBC flow prior to reactor heat up and thus the motoring power (negative alternator powers) of almost 5 kW must be supplied for over 10 minutes before self-sustaining operations are observed. 146
Figure 2-66: RPM-Controller Simulink sub-module within Module PMAD1 (see Figure 2-36) . The RPM controller uses a proportional-integral feedback loop to dynamical keep the true shaft speed very close to the user defined reference shaft speed. 148
Figure 2-67: RPCSIM predicted steady state alternator power level shown as a function of shaft speed for two values of inserted reactivity ($1.65 and $1.12). Note that there are two shaft speeds that give the same alternator power level. 149
Figure 2-68: Steady state alternator and reactor power levels as a function of shaft speed.... 149
Figure 2-69: Plot of reactor power and alternator power to demonstrate that the lower shaft speed solution is dynamically unstable. At 11,000 seconds the RPM-Controller was turned off, which caused the shaft speed and reactor power level to increase. At 13,000 seconds the alternator load was decreaseed which caused an increase in reactor power and shaft speed... 150
Figure 2-70: Input values for reactivity, shaft speed, and mass flow rate for the dynamic stability demonstration transient. At 11,000 seconds the RPM-Controller is turned off, and the jump in rpm from 1000 rev/s to 1280 rev/s illustrates that the reactor CBC system goes through a transient to reach the dynamically stable point at 1280 rev/s. At 13,000 seconds the load is further decreased which causes an increase in shaft speed and flow rate, which in turn results in a reactor power level increase even though the load decreased. 151
Figure 2-71: Gas station temperature for the dynamic stability demonstration transient. Note that turbine inlet temperature(Tgas04) remains constant for the dynamically stable operating points, but the radiator temperature increases (Tgas06 and Tgas01 are the radiator inlet and outlet temperatures respectively) meaning that the thermodynamic cycle efficiency has decreased. 152

Figure 2-72: Startup transient showing reactor, radiator, and electrical power including the response to a turbine-coast-down transient. 157
Figure 2-73: Inserted and total reactivity for the startup and turbine-coast-down transient. .. 158
Figure 2-74: Shaft speed (rev per second) , lithium and HeXe flow rate (gm/s) for the LMR startup and turbine coast-down. 158
Figure 2-75: Temperatures of the LMR reactor inlet, outlet, fuel, and average lithium coolant temperature for the startup and turbine coast-down. 159
Figure 3-1: Block Diagram of the Closed-Brayton Cycle Test Loop. Cooler Exhaust Connects to the Inlet. 163
Figure 3-2: Measured (dark blue) and predicted (magenta squares) net electrical power as a function of shaft speed (rpm) at 1144 K. The measurements were made using the open cycle gas turbine operating conditions. The 1000K model predictions are colored red (Net electrical power) and cyan (total thermal power). 164
Figure 3-3: Predicted closed Brayton test loop power levels as a function of shaft speed for various turbine inlet temperatures. At 1100 F turbine inlet temperature the expected net power produced is about 7 kWe at 90,000 rpm. 165
Figure 3-4: Schematic of the unmodified C-30 with arrows illustrating the gas flow path and proposed housing modifications. 166
Figure 3-5: “Hot End” of the Capstone C-30 micro-turbine showing the turbine wheel, the combustor annulus, and the gas injector passages. 167
Figure 3-6: Photo of the 14 turbine exit blades, the turbine inlet annulus, and the high pressure recuperator exit. An annular shaped “combustor can” is slipped into the turbine inlet annulus to direct the gas exiting the recuperator through the injector ports to the heater. 167
Figure 3-7: “Hot” end of the connection flow paths between the injector ports and the heat inlet duct manifold for the C-30 Capstone Micro-Turbine assembly. 168
Figure 3-8: Capstone C-30 turbo-alternator-compressor cutaway with high-pressure zone highlighted. 168
Figure 3-9: Six tubes penetrating through the turbine exit dome, through the combustor dome shaped annulus (middle “dome”), and through the turbine inlet dome (smaller bottom dome shaped annulus) 169
Figure 3-10: Capstone C-30 turbo-alternator-compressor engineering drawing cutaway showing the gas flow path. Orange lines show the flow path through the compressor and recuperator, red lines show the flow path through the turbine and recuperator. 169
Figure 3-11: "Cold End" of the Capstone C-30 micro-turbine illustrating the spiral recuperator, the alternator, and the inlet cooling passages along the alternator. 170
Figure 3-12: Assembly drawing of the Sandia closed-Brayton-cycle test-Loop (SBL-30). ... 171
Figure 3-13: . Fully modified and assembled Capstone C-30 closed-Brayton loop as assembled at the manufactures (Barber-Nichols Inc.) is illustrated. The gas chiller is in the fore ground and the heater is on the left side of the image. 171
Figure 3-14: Sandia Brayton Loop as installed at Sandia. The loop is un-insulated in this figure. The heater is on the left, the gas chiller on the right, and the TAC in the middle. 172
Figure 3-15 Overview of the Sandia Brayton loop as viewed from the compressor inlet. 173
Figure 3-16: Fully installed and insulated Sandia Brayton Loop. 173
Figure 3-17: Watlow 80 kW Brayton loop gas heater and controller. 174

Figure 3-18: "U" shaped heater elements used in the Watlow heater. The photo shows the heater elements, the grid spacer wires, the baffle, and the gas exit thermocouple (vertical rod). 174
Figure 3-19 Watlow 80 kW gas heater element design drawings and specifications. 179
Figure 3-20: Electrical connection and cooling water supply for the SBL-30 as located in building 6585 room 2504. All power is supplied by the 480 3phase 100 amp service from the wall. The cooling water is provided by the building facilities manager. 181
Figure 3-21: Electrical Power circuit for the heater provided by Watlow. 182
Figure 3-22: Image of the Basco/Whitlock shell and tube gas chiller. Inlet water flows from the upper right side of the image to the lower left, while gas flows in the opposite direction. 184
Figure 3-23: View of the Basco/Whitlock shell and tube heat exchanger gas inlet flange, showing the stainless steel tubes. 184
Figure 3-24 Gas cooler specifications (1). 185
Figure 3-25 Gas cooler design specifications. 186
Figure 3-26: Top view schematic of Sandia Brayton Loop and location of major temperature and pressure sensors, and the controllers. 187
Figure 3-27: Turbine inlet temperature and pressure sensors and their feed through ports. Note that these instruments measure the gas temperature and pressure in one of the six heater exit tubes. 189
Figure 3-28 Compressor inlet temperature and pressure feed through port and sensors. 189
Figure 3-29: Schematic of the gas loop and water loop for the Sandia Brayton Loop. Various pressure safety devices and components are listed here. 195
Figure 3-30: This tab shows the main control screen. The top half shows a schematic of the loop with temperature, pressures, flow rates, alternator power, and shaft speed (rpm) displayed. The bottom have shows various control commands that the user can issue. 199
Figure 3-31: Charts tab, shows predefined plots of the gas temperature (top view), while the bottom view shows pressure, rpm and power. 200
Figure 3-32: Auxiliary charts can display any of the channels available to the system. Here the top chart shows the heater power and turbine exit pressure. The bottom chart shows the turbine inlet temperature. 201
Figure 3-33: This display show the "Channels Tab. It lists all of the data channels being recorded in real time. 202
Figure 3-34: Paschen curves for various gases at 20 ^{o}C (from Blair). 203
Figure 3-35. Paschen curves for various mixtures of He and Xe. 204
Figure 3-36. Paschen curves for different electrode materials. 204
Figure 3-37: Paschen model and data for various materials. 206
Figure 3-38: Modified Paschen model and data for various materials. 207
Figure 3-39: Modified Paschen model and data for HeXe mixtures. 208
Figure 3-40: Modified Paschen model coefficients vs. helium fraction for HeXe. 208
Figure 3-41: Alternator exposed electrical connections. The closest approach of two phase to phase wires is 1.6 cm. 209
Figure 4-1: Sandia Brayton Loop Transient Test 4 (TT4-050812) performance with no insulation and with the electrical power limited to 50% of full power or about 31 kW of heater power. 212
Figure 4-2: Summary data and plot of measured data from Transient Test 5, TT5-050913. This test was fully insulated and aimed at determining the energy balance at 100% power (62.3

kW), measuring the alternator power as a function of speed for fixed turbine inlet temperatures and in measuring decay heat removal capabilities after the heater power was turned off. 215
Figure 4-3: Summary data and plot of measured data from Transient Test 6, TT6-051017. This test was fully insulated and used the heater feedback controller to provide a user specified turbine inlet temperature. The test was used to determine curves for the power produced by the alternator as a function of rpm for various turbine inlet temperatures (TIT). The mass flow rate has units of gm/s. 217
Figure 4-4: Temperature of ducting and flanges for test TT5. The purple curve shows the heater exit flange temperature, and note that at 6800 seconds the flange temperature is not at steady state, though the other duct temperatures are. 220
Figure 4-5: Capstone operating curve based on the NASA off design performance curve mean line flow analysis models for the C30 turbine and compressor. The compressor inlet temperature is 300 K and the turbine inlet temperature is 1150 K. 222
Figure 4-6: Comparison of the measure operating curve (pressure ratio versus flow measured from test TT4) for the Capstone C30 turbine and compressor versus predicted curves (solid lines) based on the mean line flow analysis off-design performance models for a 285 K compressor inlet temperature and a 700 K turbine inlet temperature. The measured data (blue triangles) was corresponds to a shaft speed of 40, 46, 57, and 62 krpm. 223
Figure 4-7: Gas temperatures for SBL-30 run TT5-09-13-05 with TIT held at 880 K. 225
Figure 4-8: TT5 Turbine inlet temperature detail including shaft speed. 225
Figure 4-9: TT5Gas temperature details including shaft speed. 225
Figure 4-10: Measured Duct and flange temperatures for SBL-30 run TT5 with TIT held at 880 K. 226
Figure 4-11: Measured duct temperature details and shaft speed for test TT5. 226
Figure 4-12: Gas pressures for SBL-30 run TT5 with TIT held at 880 K. 227
Figure 4-13: Coolant water conditions for SBL-30 run with TIT held at 880 K. 228
Figure 4-14: Measured temperatures compared with model predictions for test TT5. The solid lines are measured data and the dotted lines are RPCSIM predictions. 229
Figure 4-15: Measured pressures compared with model predictions for test TT5. The solid lines are measured data and the dotted lines are RPCSIM predictions. 229
Figure 4-16: Measured power compared with model predictions for TT5. The solid lines are measured data and the dotted lines are RPCSIM predictions. 230
Figure 4-17: Heating power and alternator power vs. speed for TIT = 880 K. 232
Figure 4-18: TT6 measured data to determine alternator power for a fixed turbine inlet temperature of 750K at various shaft speeds. 233
Figure 4-19: TT6 measured pressure data for the 750 K alternator power versus shaft rpm data. 233
Figure 4-20: Extracted 750 K data of alternator power versus shaft speed for TT6. 234
Figure 4-21: Summary thermal data segment of TT6 to measure alternator power versus shaft speed at 700 K. 235
Figure 4-22: Pressure data for the TT6 segment kept at 700 K. 235
Figure 4-23: Extracted 700 K data of alternator power versus shaft speed for TT6. 236
Figure 4-24: Summary thermal data segment of TT6 to measure alternator power versus shaft speed at 650 K. 237
Figure 4-25: Pressure data for the TT6 segment kept at 650 K. 237
Figure 4-26: Extracted 650 K data of alternator power versus shaft speed for TT6. 238

Figure 4-27: Summary thermal data segment of TT6 to measure alternator power versus shaft speed at 600 K. 239
Figure 4-28: Pressure data for the TT6 segment kept at 600 K. 239
Figure 4-29: Extracted 600 K data of alternator power versus shaft speed for TT6. 240
Figure 4-30: Summary data of all power versus speed measurements made in tests TT5 and TT6. 241
Figure 4-31: Decay power levels after shutdown. 242
Figure 4-32: Predicted power produced by SBL-30 vs. turbine inlet temperature. 243
Figure 4-33: Gas temperatures for SBL-30 run with TIT held at 880 K. 244
Figure 4-34: RPCSIM block diagram of the Sandia Brayton Loop. 245
Figure 4-35: RPCSIM model power balance curves for TT5, given the input electrical power for the heater E-Htr-pwr and shaft speed. The Pwr-th curve shows the power transferred to the coolant. GCX-Power shows the wasted heat power rejected in the gas cooler heat exchanger and Alt-e-Pwr shows the power produced in the alternator. 247
Figure 4-36: RPCSIM input shaft speed (rpm) and predicted gas flow rate for TT5. 249
Figure 4-37: RPCSIM predicted gas temperatures for TT5 using measured input for the electrical heater power and the shaft speed. 250
Figure 4-38: RPCSIM calculated gas pressures at each station around the loop for test TT5 given the input power and rpm. The curves show the high and low pressure legs, and the small deviations due to frictional pressure drop simulated by the model. 251
Figure 4-39: Predicted compressor and turbine pressure ratio for test TT5. 251

List of Tables

Table 2-1: Operating parameters for the ML-1 US Army mobile reactor and turbo-generator. 34
Table 2-2: Station locations for temperature and pressure at various locations around the loop. The abbreviations such as CIT and TIT refer to the compressor and turbine inlet temperatures. 36
Table 2-3: Ideal gas properties for helium and xenon and their mixture at 63.5 a% helium. ... 47
Table 2-4: Density, speed of sound, and heat capacity equations for ideal gases with the heat capacity of He/Xe at 63.5 a% listed. 47
Table 2-5: Estimate of Capstone C-30 Compressor Dimensions 58
Table 2-6: Estimate of Capstone C-30 Turbine Dimensions 58
Table 2-7: Capstone C-30 Compressor flow map using the multivariate polynomial fit for the pressure ratio and temperature ratio. 64
Table 2-8: Capstone C-30 turbine flow map using multivariate polynomial fits for the pressure ratio and temperature ratio as a function of dimensionless flow and speed. 67
Table 2-9: Estimate of NGST/CNREC 132 kWe compressor dimensions. 68
Table 2-10: Estimate of NGST/CNREC 132 kWe Turbine Dimensions 68
Table 2-11: NGST/CNREC 132 kWe Compressor flow map using the multivariate polynomial fit for the pressure ratio and temperature ratio. 71
Table 2-12: NGST/CNREC 132 kWe turbine flow map using the multivariate polynomial fit for the pressure ratio and temperature ratio 73
Table 2-13: Lumped parameter steady state reactor and heat transfer equations 78
Table 2-14: Steady state counter flow recuperator model with recuperator effectiveness set to 0.95. 79
Table 2-15: Turbo-alternator-compressor steady state model, based on the 132 kWe NGST/CNREC turbo-compressor set. 80
Table 2-16: Space radiator steady state model. 81
Table 2-17: Gas inventory steady state model. 82
Table 2-18: Complete set of steady state equations for a reactor coupled to a closed Brayton cycle 84
Table 2-19: Dynamic Lumped parameter reactor point kinetics model 92
Table 2-20: Lumped parameter heat transport model for the reactor 93
Table 2-21: Lumped parameter coefficients for a 313 pin ~ 400 kWth Gas Cooled Reactor ... 93
Table 2-22: Recuperator Lumped parameter model. 94
Table 2-23: Lumped parameter dynamic model of space based radiator 95
Table 2-24: Lumped parameter equations for the Turbo-Alternator-Compressor (TAC) 96
Table 2-25: Design Dimensions of GCR Fuel Pin 108
Table 2-26: Major dimensions and components of the GCR. 109
Table 2-27: Estimates of feedback coefficients for the GCR/ 112
Table 2-28: Estimates of feedback coefficients for an LMR/ 113
Table 2-29: Summary of feedback model used for the Simulink GCR. 113
Table 2-30: Recuperator design dimensions and other properties 118
Table 2-31: Radiator design dimensions and other properties 121
Table 2-32: Table of GCR ducting component volume, length, diameter or and mass. In some cases the reactor, recuperator or radiator or gas chiller heat exchanger data must be used. 122

Table 2-33: Simulink gas calculator and equations used within the module. The gas calculator internal model calculates the gas density, the gas velocity, the Reynolds number, the friction factor, the heat transfer coefficient, and the node-to-node pressure drop. Green ovals represent input values to the module and red ovals represent the outputs. 127
Table 2-34: Simulink sub-module and equation set for the heat transport calculator. 129
Table 3-1: Measured operating conditions of the open cycle C-30 gas-micro-turbine (Column 2) and expected operating conditions of the CBC test loop (columns 3 & 4) at 1000 K and 1144 K with a compressor inlet pressure of .0825 MPa. 164
The Brayton loop gas heater was designed to add about 80 kW of thermal power to the gas which would heat the flowing nitrogen or air to about 1000 K for a flow rate of about 0.25 kg/s. The heater and controller were designed and fabricated by Watlow Inc., Wright City, Mo. A photo of the heater and controller is shown in Figure 3-17 and in many of the other photos already shown. In general the heater consists of a horizontal 12" diameter schedule 300 304 stainless steel vessel through which 54 "U" shaped heater elements are placed. The heater elements are 0.430" inches in diameter and have a leg length of 71" (see Figure 3-18). The gas flows in an "L" shaped fashion through the heater, but 7 baffles force the gas flow into a serpentine path the crosses the heater elements. The inlet flow is downward, and the exit flow is horizontal. The heater element power density is about 5 Watt/in^2 and requires a supply voltage of 480 V 3 phase. The heaters are wired into two banks of three phase resistance bridges with each leg of the resistance bridge having a resistance that varies from 10.55 – 12.22 ohms. The vessel is designed to ASME specifications and it was designed for a fill gas pressure of up to 42 psia at a vessel temperature of 1425 K. The vessel was hydrostatically pressure tested to 474 pisg. Detailed engineering design specifications for the vessel and for the heater elements are listed in Table 3-3 and Table 3-4. The design drawings for these two components are provided in Table 3-2 and in Figure 3-19. 173
Table 3-3: Watlow 80 kW gas heater vessel product specifications. 175
Table 3-4: Watlow gas heat product specifications for the immersion heaters and their material specifications. 176
Table 3-5: Fluid hydraulic and heat transfer properties used in the RPCSIM for the Sandia Brayton Loop SBL-30. 177
Table 3-6 Watlow gas heater vessel design drawings and specifications. 177
Table 3-7: Maximum and Typical Power Draws/ Supply form Capstone Power Management Circuitry 180
Table 3-8: Basco/Whitlock gas chiller hydraulic and heat transfer properties used in the RPCSIM model for the Sandia Brayton Loop 183
Table 3-9: Description of instrumentation, feedthroughs, and connectors at each station identified in Figure 3-26. 188
Table 3-10 Volumes on the components in the gas loop. 190
Table 3-11 Total volume gas loop. 191
Table 3-12: Duct and component volumes, mass, length, and hydraulic diameter. 191
Table 3-13: SBL-30 components, material, dimensions, and calculated UTS pressure. 193
Table 3-14: SBL-30 components, material, dimensions, and calculated yield pressure. 193
Table 3-15: Summary of low pressure leg and high pressure leg limiting MAWP at various operating conditions. 194
Table 3-16: Empirically determined constants for the modified Paschen model. 206
Table 3-17: Modified Paschen model constants for HeXe mixtures using F=0.75 207

Table 4-1: List of recorded data channels, providing the channel number, name, display name and a brief description of each recorded channel. 214
Table 4-2: Table of measured gas and water temperatures used to determine the mass balance. The power levels report the power in kW based on the corrected gas flow rate..... 218
Table 4-3: Average nitrogen heat capacity used for the heater and the gas chiller..... 218

Acknowledgements

The authors wish to thank the Management of Sandia National Laboratories and the Lab Directed Research and Development Program for funding and supporting this project. The authors especially want to thank Ken Nichols and Robert Fuller at Barber Nichols Inc. for the design and manufacture of the Brayton loop, and for the rapid correction of initial hardware problems, for working closely with the authors to keep the development costs on schedule and on budget, and for developing and delivering a working set of hardware, electronics, and instrumentation that is fun to operate. Thanks also goes to Keith Barrett at Prime Core Corporation for the development of the control and data analysis software, which is a pleasure to use.

The authors also wish to thank the numerous student interns who helped assemble the hardware, arranged for the delivery of the hardware, and assured that the system dimensions and design would fit in the laboratory and in the elevator leading to the laboratory. These students include Jennifer Jablonski, Travis Sanchez, Sherry Stout, Alex Padilla, Matt Humberstone, and Andrew March. Finally we wish to thank Sandia Facilities, John Scott and other staff members for accommodating our needs and working with us to install the water cooling, insulation, and additional electrical power in a timely and cost affordable manner.

Abstract

This report describes the results of a Sandia National Laboratories internally funded research program to study the coupling of nuclear reactors to gas dynamic Brayton power conversion systems. The research focused on developing integrated dynamic system models, fabricating a 10-30 kWe closed loop Brayton cycle, and validating these models by operating the Brayton test-loop.

The work tasks were performed in three major areas. First, the system equations and dynamic models for reactors and Closed Brayton Cycle (CBC) systems were developed and implemented in SIMULINK™. Within this effort, both steady state and dynamic system models for all the components (turbines, compressors, reactors, ducting, alternators, heat exchangers, and space based radiators) were developed and assembled into complete systems for gas cooled reactors, liquid metal reactors, and electrically heated simulators. Various control modules that use proportional-integral-differential (PID) feedback loops for the reactor and the power-conversion shaft speed were also developed and implemented. The simulation code is called RPCSIM (Reactor Power and Control Simulator).

In the second task an open cycle commercially available Capstone C30 micro-turbine power generator was modified to provide a small inexpensive closed Brayton cycle test loop called the Sandia Brayton test-Loop (SBL-30). The Capstone gas-turbine unit housing was modified to permit the attachment of an electrical heater and a water cooled chiller to form a closed loop. The Capstone turbine, compressor, and alternator were used without modification. The Capstone system's nominal operating point is 1150 K turbine inlet temperature at 96,000 rpm. The annular recuperator and portions of the Capstone control system (inverter) and starter system also were reused. The rotational speed of the turbo-machinery is controlled by adjusting the alternator load by using the electrical grid as the load bank. The SBL-30 test loop was operated at the manufacturers site (Barber-Nichols Inc.) and installed and operated at Sandia. A sufficiently detailed description of the loop is provided in this report along with the design characteristics of the turbo-alternator-compressor set to allow other researchers to compare their results with those measured in the Sandia test-loop.

The third task consisted of a validation effort. In this task the test loop was operated and compared with the modeled results to develop a more complete understanding of this electrically heated closed power generation system and to validate the model. The measured and predicted system temperatures and pressures are in good agreement, indicating that the model is a reasonable representation of the test loop. Typical deviations between the model and the hardware results are less than 10%. Additional tests were performed to assess the capability of the Brayton engine to continue to remove decay heat after the reactor/heater is shutdown, to develop safe and effective control strategies, and to access the effectiveness of gas inventory control as an alternative means to provide load following. In one test the heater power was turned off to simulate a rapid reactor shutdown, and the turbomachinery was driven solely by the sensible heat stored in the heater for over 71 minutes without external power input. This is an important safety feature for CBC systems as it means that the closed Brayton loop will keep cooling the reactor without the need for auxiliary power (other than that needed to circulate the waste heat rejection coolant) provided the heat sink is available.

1 Introduction and Executive Summary

Small innovative nuclear power systems are receiving increasing attention as the enabling technology for new and challenging Department of Energy (DOE), National Aeronautics and Space Administrations (NASA), Department of Defense (DoD), commercial space and terrestrial applications. One of the more important research areas required to enable these missions is the development of more efficient electrical power conversion systems that result in lower weight and more cost effective systems. Directly coupling high-temperature gas turbine cycles to gas cooled nuclear reactors has the potential to yield cycle efficiency up to 35% for space applications and up to 50% for terrestrial applications. Such significant efficiency improvements would enable next generation power systems such as Next Generation High Temperature Gas Reactors (HTGR), or nuclear electric propulsion and power for NASA or commercial space systems, or for specialized advanced DoD missions.

This report describes the results of a Sandia National Laboratories internally funded research program to study the coupling of nuclear reactors to gas dynamic Brayton power conversion systems. The title of this Laboratory Directed Research and Development effort (LDRD) is "Advanced High Efficiency Direct Cycle Gas Power Conversion Systems for Small Special Purpose Nuclear Power Reactors". The research focused on developing integrated dynamic system models, fabricating a 10-30 kWe closed loop Brayton cycle, and validating these models by operating the Brayton test-loop. Operation of the test-loop and developing the system models has allowed Sandia to validate a set of tools and models that can be used to determine how nuclear reactors operate with gas turbine power conversion systems. These tools are proving useful for evaluating control strategies, and for modeling even larger reactor systems, such as High Temperature Gas reactors and other Next Generation Systems.

The work tasks were performed in three major areas. First, the system equations and dynamic models for reactors and closed Brayton cycle systems were developed and published in several reports (Wright 2003a, 2003b, 2003c). Within this effort, both steady state and dynamic system models for all the components (turbines, compressors, reactors, ducting, alternators, heat exchangers, and space based radiators) were developed and assembled into complete systems for Gas Cooled Reactors, Liquid Metal Reactors, and electrically heated simulators. This report provides a complete description of these equations, models and results.

In the second task an open cycle commercially available Capstone C30 micro-turbine power generator (Capstone, 2005) was modified to provide a small inexpensive closed Brayton cycle test-loop. The test-loop was operated at the manufacturer's site, Barber-Nichols Inc. (Barber-Nichols, 2005) and installed and operated at Sandia during the summer of 2005. A sufficiently detailed description of the Sandia Brayton test-Loop (SBL-30) is provided in this report along with the design characteristics of the turbo-alternator-compressor set to allow other researchers to compare their results with those measured in the Sandia test-loop.

The third task consisted of a validation effort. In this task the test loop was operated and compared with the modeled results to develop a more complete understanding of this electrically heated closed power generation system. Tests are currently on going to assess the effect that gas conductivity, molecular weight, and gas pressure have on the test loop. Other tests are also being performed to assess the capability of the Brayton engine to continue to remove decay heat after the reactor/heater is shutdown, to develop safe and effective control strategies, and to asses the effectiveness of gas inventory control to provide load following.

Brief descriptions of the dynamic model, the Sandia Brayton Loop-hardware and operational results, along with early comparisons of the measurements with the model are provided in this introduction and executive summary.

1.1 Dynamic Model Introduction

The dynamic modeling effort has been very useful in supporting this LDRD effort and in supporting related development of space nuclear power systems (Wright, et al, 2005) because there is very little experience in coupling nuclear reactors to closed Brayton cycle gas power conversion systems. A number of gas-cooled reactors have been coupled to coolant circulators, but only the ML-1 reactor (Brunhouse and Titus, 1961) has been coupled directly to a closed-loop Brayton-cycle. The use of gas circulators (or pumps) versus turbo-machinery induced coolant flow is an important distinction, because the systems that used circulators/pumps have independent electrical motors that force the coolant through the reactor. Therefore, with circulators, the reactor operator has direct control of coolant flow through the reactor. In contrast, the balance of power/torque in the turbo-alternator-compressor machinery provides the shaft power to force the coolant through the reactor. For a reactor that is cooled by a Brayton cycle, the electrical load and the operating state (temperature, pressure, revolutions per minute/rpm) of the turbo-alternator machinery and gas loop directly affect the flow through the reactor; and therefore, it also affects the reactor power level as well. The dynamic system model was developed because of this intimate coupling between reactor power and flow created by the balance of power within the turbo-alternator-compressor within the CBC system. This work provides a basis for multiple future SNL programs in the ongoing DOE, NASA, commercial, and defense applications.

The dynamic reactor and CBC system model uses a lumped capacitance model for the system components. The major assumption used by the model is that the flow rate is constant around the loop and that the pressure drop in a component is determined by the quasi-steady state frictional drag or form drag through all non-rotating components. The flow is always assumed to be incompressible (except in the turbine and compressors), but density changes caused by changes in temperature are accounted for, as are pressure drops due to frictional drag and due to form losses. The dynamic model was developed and implemented in SIMULINK™ (Simulink, 2005). SIMULINK™ is a development environment packaged with MatLab™ (MatLab, 2005) that allows for the creation of dynamic state flow models. Simulation modules for liquid metal, gas cooled reactors, and electrically heated systems were developed, as have modules for components such as, ducting, heat exchangers, turbines, compressors, permanent magnet alternators, load resistors, and gas bearings. Various control modules that use proportional-integral-differential (PID) feedback loops for the reactor and the power-conversion shaft speed have also been developed and implemented.

The modules are compiled into libraries and can be easily connected in different ways to explore the operational space of a number of potential reactor, power-conversion system configurations, and control approaches. The modularity and variability of these SIMULINK™ models provides a way to simulate a variety of complete power generation systems. Current efforts are focused on improving the fidelity of the existing SIMULINK™ modules, extending them to include full scale High Temperature Gas Cooled Reactors, small isotopic heaters, heat pipes, Stirling gas dynamic engines, and on developing state flow logic to provide intelligent

autonomy and control. The simulation code is called RPCSIM (Reactor Power and Control Simulator).

The Closed Brayton Cycle (CBC) model equations were described in the proceedings of the "*1st International Energy Conversion Engineering Conference"* (Wright, 2003). A more detailed version of these equations was implemented in Simulink (Wright, 2005). This model requires the knowledge of the characteristic flow curves for the turbine and compressor. The required curves consist of the pressure ratio and temperature ratio versus dimensionless (or corrected) flow rate through both the turbine and the compressor (including the inlet and outlet diffusers). Estimates of these curves were obtained by using mean line flow analysis curves/maps obtained from the NASA off normal design codes (Wasserbauer 1975, and Galvas 1973) and by selecting appropriate properties for the wheel diameter, blade angles and other design properties.

The other CBC components (recuperator, ducting, heater, and chiller) were modeled by using simple multi-nodal models to estimate the pressure drop, flow rate, Reynolds number, friction factor, heat transfer coefficient, and heat transfer to solid structures within ducts, heat exchangers and radiators. If a reactor is involved, then the standard six group point kinetics equations are used to model the reactor (Keepin, 1965 and Hetrick, 1971). A block diagram description of this model is shown in Figure 1-1 which is arranged in blocks that represent the reactor, ducting, the turbine and compressor, the alternator, pumps and heat exchangers. The system model illustrated in Figure 1-1 is for a space reactor thus one of the heat exchangers (Radiator1) is a waste heat rejection system that uses thermal radition to radiate the waste heat to space. These models are described in more detail in subsequent sections.

A separate model also exists for the Sandia Brayton Loop. This model looks very much like the model shown in Figure 1-1 except that the reactor is replaced with an electrical heater. Both the dynamic model for the electrically heated CBC test loop and the reactor heated loops use a feedback control loop to control the shaft speed. This control loop uses a parasitic load resistor (or coupling of power to the electrical grid) to adjust the total torque or load on the shaft to control the shaft speed. A feedback loop forces the load to follow a reference shaft speed that is provided via input. The electrical heater or reactor uses a multi-node model to calculate the fuel pin or heater element temperature, the gas temperature and the heater wall temperature along the length of the heater (any number of nodes can be used, though typically we use 10-30). Thermal capacitance, heat transfer areas, flow areas, and hydraulic diameters, and mass are required for each component. The system runs quickly and depending on the number of nodes used and the detail of the input reference rpm levels can easily simulate a 14,000 second startup transient in only 30-300 seconds of computer time.

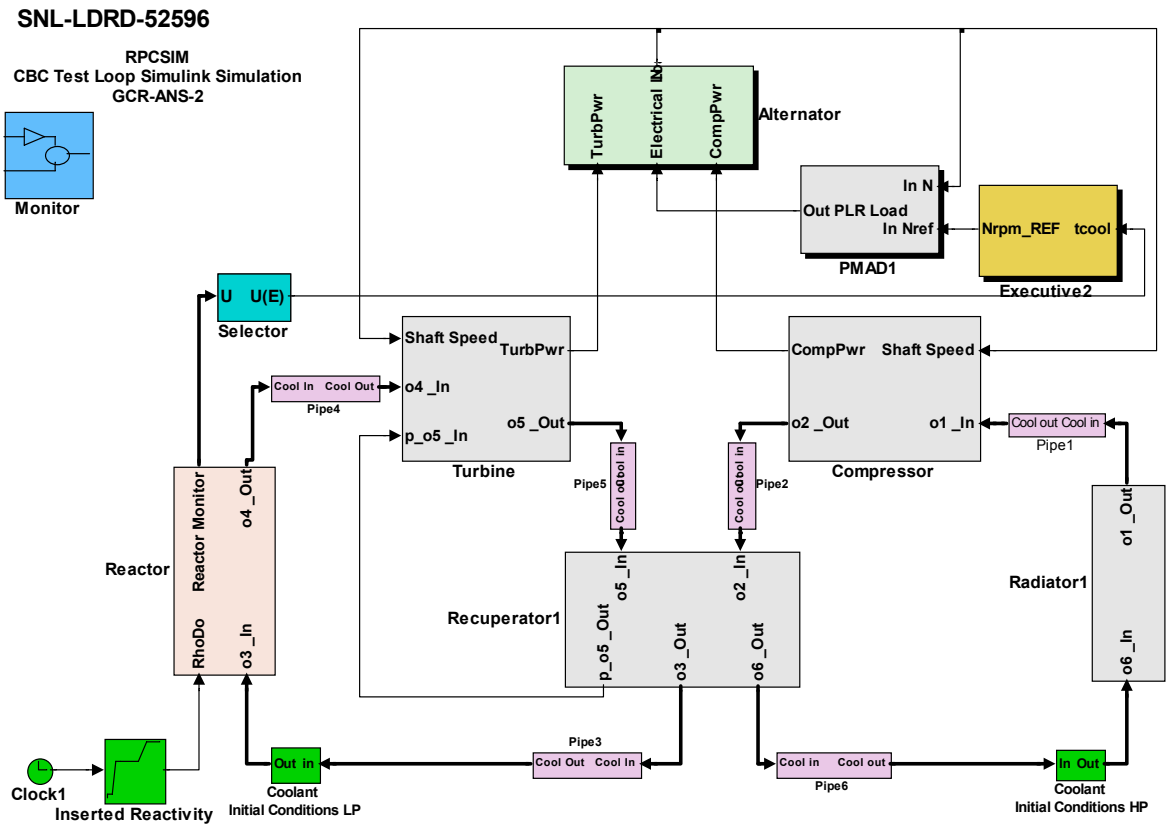

Figure 1-1: Simulink block diagram of the dynamic model for a gas cooled reactor coupled to a closed Brayton cycle.

A number of startup transients have been run with RPCSIM. Figure 1-2 and Figure **1-3** show the results of a startup transient for a 313 pin gas cooled reactor that is coupled to a 100 kWe Brayton engine. The reactor has 3 negative feedback coefficient terms that account for axial fuel expansion, core lattice expansion, and radial expansion of the BeO radial reflectors. The transient is designated (ANS-3FB300): details of this model and other information are provided in the main body of this report. The transient shown in Figure 1-2 and Figure **1-3** was designed to test the model and to take the Space Reactor Power system through a complete startup in which the reactor is heated prior to starting coolant flow. The transient that was modeled is simply one of many and represents only one approach to startup and may not represent the startup sequence that may actually be used for a space reactor.

The startup transient performs a variety of activities; it increases reactor temperature, ramps the Turbo-Alternator-Compressor shaft speed to a desired set point, and increases reactor temperature in coordination with the increase flow or turbo-alternator-compressor (TAC) shaft speed. The transient has two steady-state regions or phases (4000-7000 s and 9000–14000 s) where the closed loop hardware and structure are allowed to approach equilibrium. The startup transient begins by increasing the reactor power via adding reactivity and then starting up the CBC system. The reactivity is inserted as a step insertion of 12 cents which causes the reactor power to increase from mWatts to kW in a period of about 80 seconds. Next the reactivity is increased in a ramp from 12 cents to about 80 cents. During this reactivity ramp the average fuel temperature increases. When the fuel temperature exceeds the initial temperature by 300

K the TAC shaft speed is increased rapidly to 40% of full speed (60,000 rpm is full speed). Between 4000 s and 7000 s the system is allowed to reach equilibrium. The model indicates that the fuel temperature reaches about 700 K during this time period. Between 7000 s and 9000 s both the reactivity and rpm are ramped to their full values ($1.45 and 60,000 rpm). After 9000 s the system is again allowed to achieve equilibrium. Figure 1-2 shows the predicted reactor fission power, the thermal power transferred to the HeXe coolant, the thermal power transferred from the coolant to the radiator structure, and the power radiated to space. The electrical power generated is also shown. Figure 1-3 shows the reactor input values which consist of inserted reactivity and the TAC shaft rpm.

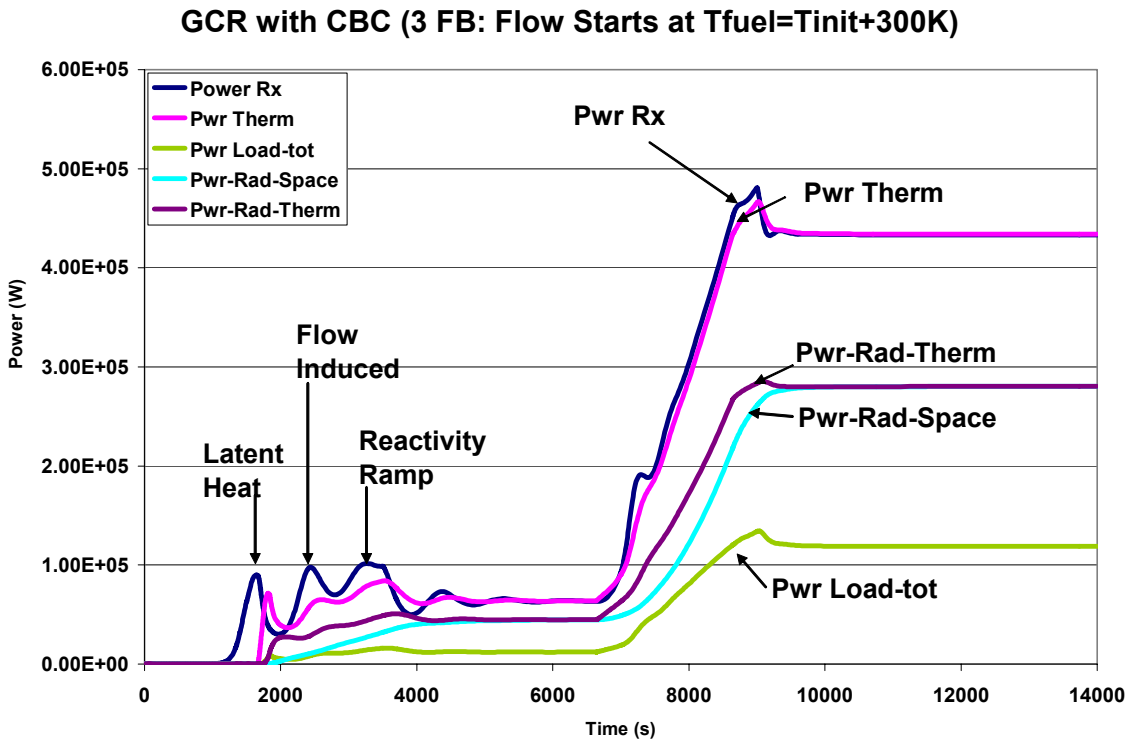

Figure 1-2: Startup transient (ANS-3FB-300) for a 313 pin 100 kWe gas cooled space reactor with 3 feed-back coefficients coupled to a closed Brayton cycle. Coolant flow starts once the reactor average fuel temperature exceeds the initial temperature by 300 K. Pwr-Rx is the power in the reactor, Pwr Therm is the thermal power removed by the gas coolant from the reactor. Pwr-Rad-Therm is the power removed from the coolant by the space thermal radiator. Pwr-Rad-Space is the thermal power radiated to space, and Pwr Load-tot is the total load on the turbo-compressor shaft caused by the alternator and parasitic resistor.

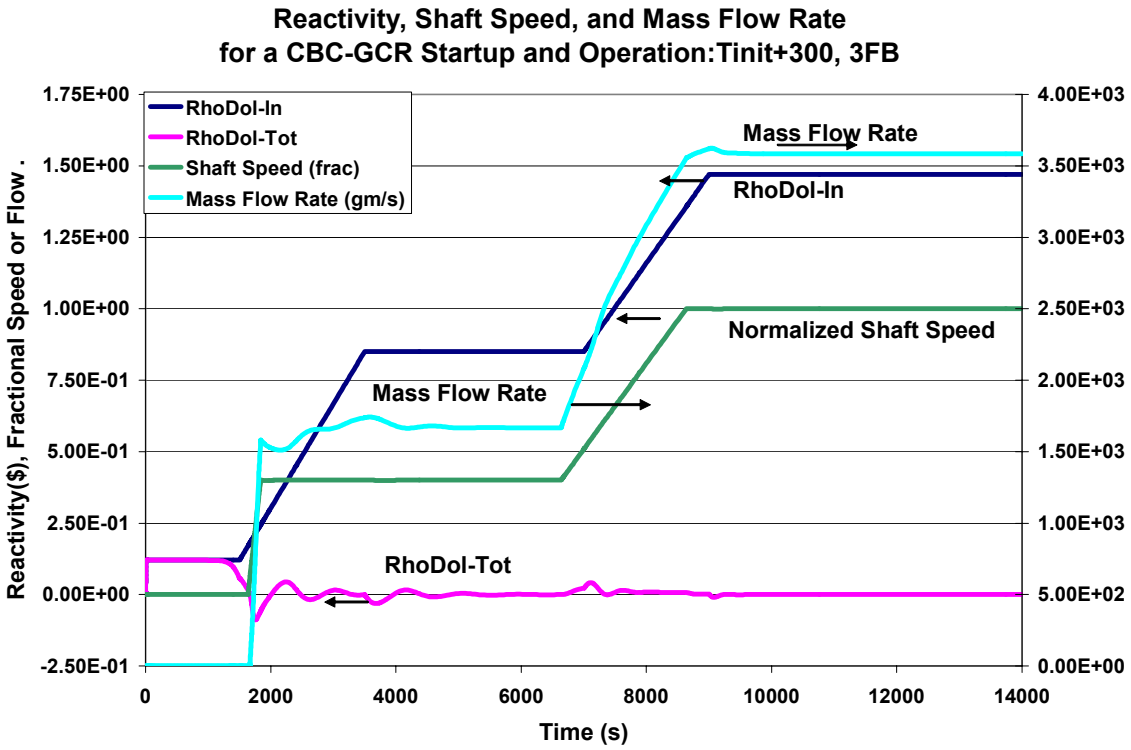

Figure 1-3: Reactivity and flow rate input values for the gas cooled reactor startup transient ANS-3FB-300, where the HeXe gas flow starts when the fuel temperature exceeds the initial temperature by 300 K. The input values for reactivity and shaft rpm are coordinated to first bring the system to a low power level (4000-7000 s), followed by a ramp to full power (9000 – 14000 s). RhoDol-In is the reactivity in units of dollars inserted into the reactor by the control rods. RhoDol-Tot is the total reactivity (in dollars) which includes both the inserted reactivity and feedback effects.

1.2 Sandia-Brayton Test-Loop

Because very little experience exists regarding the operational behavior of these systems, Sandia has developed a closed-loop test bed that can be used to determine the operational behavior of these systems and to validate models for these systems. Sandia contracted Barber-Nichols Inc. to design, fabricate, and assemble a Closed-loop Brayton Cycle (CBC) system (contract number 178743). This system was developed by modifying commercially available hardware. It uses a 30 kWe Capstone C-30 gas-turbine unit www.capstoneturbine.com) with a modified housing that permits the attachment of an electrical heater and a water cooled chiller that are connected to the turbo-machinery in a closed loop. The test-loop uses the Capstone turbine, compressor, and alternator without modification. The Capstone system's nominal operating point is 1150 K turbine inlet temperature at 96,000 rpm. The annular recuperator and portions of the Capstone control system (inverter) and starter system are also reused. The rotational speed of the turbo-machinery is controlled by adjusting the alternator load by using the electrical grid as the load bank. The Sandia Brayton Loop SBL-30 hardware is shown in Figure 1-4. The number 30 is used because the system is based on the Capstone C-30 gas turbine power unit. It is currently configured with a Watlow™ (Watlow 2005) heater that is

limited to 62 kW_t. The expected maximum turbine inlet temperature is 900-1000 K at 90,000 rpm. Electrical power levels exceeding 10 kW_e have been produced at rotating speeds of 90,000 rpm. Future upgrades to the heater could increase the electrical heater power to 100 kW_t, 1150 K turbine inlet temperature, and produce up to 30 kW_e.

The test-loop is controlled by National Instruments Field Point Real Time computer (RT) controller and Field Point modules (FP). The RT computer communicates with the Watlow™ heater controller through a 4-20 mA loop, and it also communicates with the Capstone C-30 controller via an RS-232 link to select the shaft speed (and therefore the electrical load) and to read a variety of currents, voltages, and power levels used within the Capstone inverter hardware. The RT computer is programmed in a LabView™ Virtual Interface (VI) to provide for configuration setup, data acquisition and storage of the temperature, pressure and flow sensors, to control the electrical heater, and to communicate with the Capstone controller. A separate Lab View Virtual Interface (CBC_Control_Panel) communicates with the RT VI controller via an Ethernet connection and is the user's primary interface to the RT controller. In the CBC_Control_Panel the user provides information for the setup and calibration of all the channels, and displays a number of screens that allow the user to control the test-loop or to display all the data.

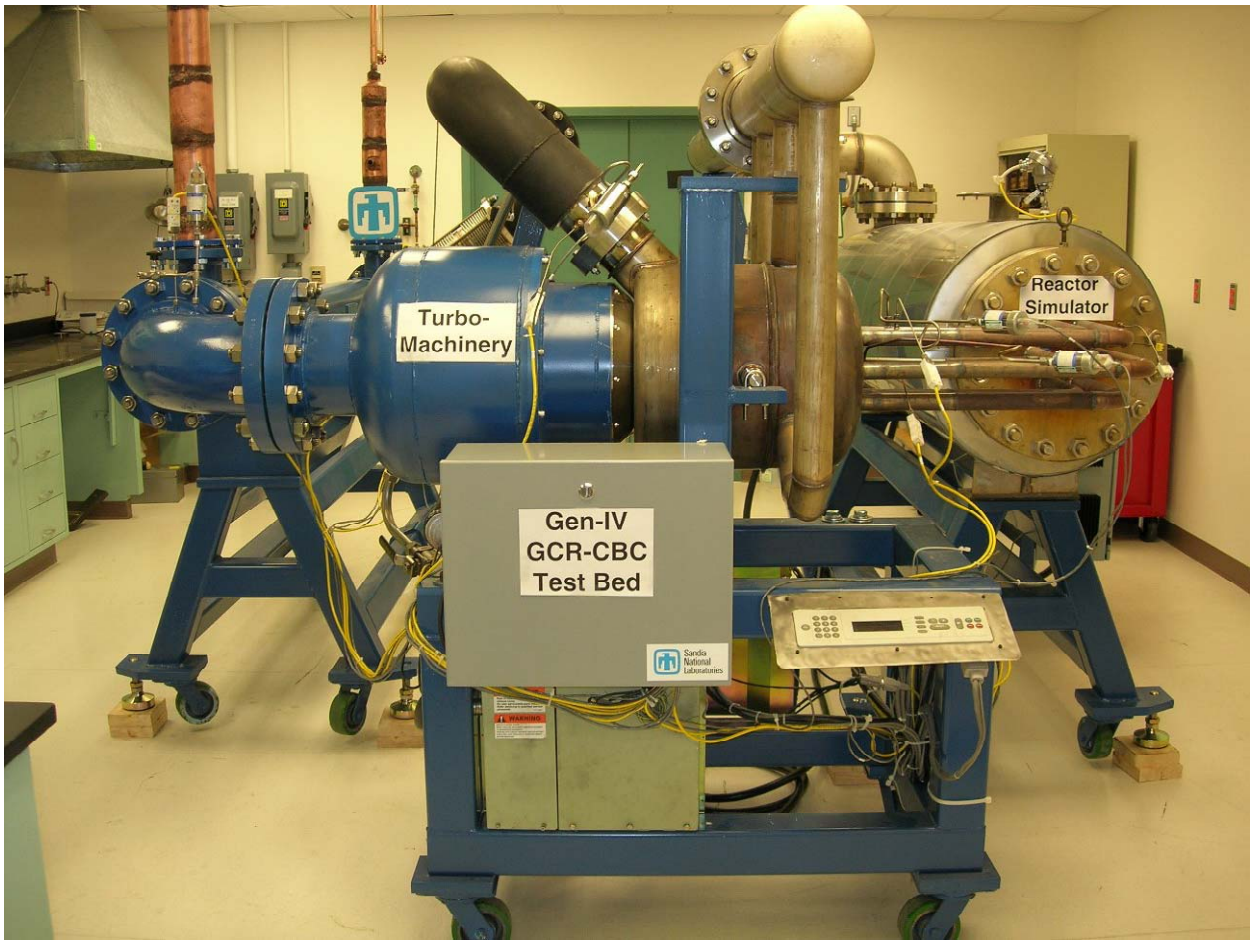

Figure 1-4: Photo of the Sandia Brayton Loop (SBL-30) installed at Sandia.

The test loop is instrumented with temperature and pressure sensors located at the inlet or outlet of all components, on the water chiller, and on some of the hotter structural components. In addition an orifice was installed to measure the flow rate through the loop using an ASME procedure.

The system operator controls the loop by controlling the power sent to the electrical heater and the turbo-compressor shaft speed. The heater power can be manually varied from zero to 100% of full power (~62.5 kW_{th}), or controlled by a PID feedback loop that automatically adjusts the heater power to force the turbine inlet temperature to move to the user specified set point. The turbo-compressor shaft speed is controlled by the Capstone Controller and the 480 V three-phase inverter circuitry. At low turbine inlet temperatures the alternator is motored to achieve the user specified shaft speed. In general the shaft speed controller causes the voltage and phase angle from the DC-AC invertor to lead or lag the grid voltage by the proper amount to achieve the user specified shaft speed. When the inverter lags the grid voltage the alternator is being motored; when it leads the grid voltage then the power produced by the altenator is put on the grid. In this manner the power produced by the alternator can be smoothly controlled from negative levels of -3kW (motoring) up to 30 kWe of power production. When the operator requests a shaft speed, the Capstone control automatically adjusts the inverter phase angle via a feedback loop (which is equivalent to changing the electrical load) to balance the net power from the turbo-compressor shaft.

Figure 1-5 shows some of the measured data for obtained by operating the heater at 50% of full power from 2500-4000 s and 60% of full power until 17000 s (full power is 62.35 kW). The measured gas temperatures are shown on the left scale, while the electrical heater power, power produced by the alternator and the shaft rpm are shown on the right. In this test, near steady state conditions were achieved at approximately 12,000 s. This was then followed by transient step shaft speed that resulted in increases and decreases in electrical power produced by the alternator (12000-15000 s). (*Note, the shaft speed is changed by temporarily unbalancing the torques or powers generated in the turbine, compressor, and alternator. Postive excess torque/power will increase the shaft speed while negative excess torque/power will slow down the shaft speed. This is automatically performed by a feedback loop within the Capstone controller.)* Between 16,000 s and 17000 s a new steady state level was achieved. Between about 17000 s and 17600 s reactor shutdown was simulated by turning off the electrical heater at 17000 seconds. Since a reactor continues to generate decay power after shutdown, it is important to show that some flow through the core can be maintained after shutdown. The shutdown portion of the test showed that flow could be maintained, and furthermore that some positive power could be generated by the alternator, for over 18 minutes before motoring was required. This is an important safety feature for these systems as it means that the closed Brayton loop will keep circulating and remove reactor decay power without the need for auxiliary power (provided there is a path for waste heat rejection).

The nomenclature used in the plots, and descriptions of instrumentation and other measured data are described in sections 3.5 and 4.1 of this report.

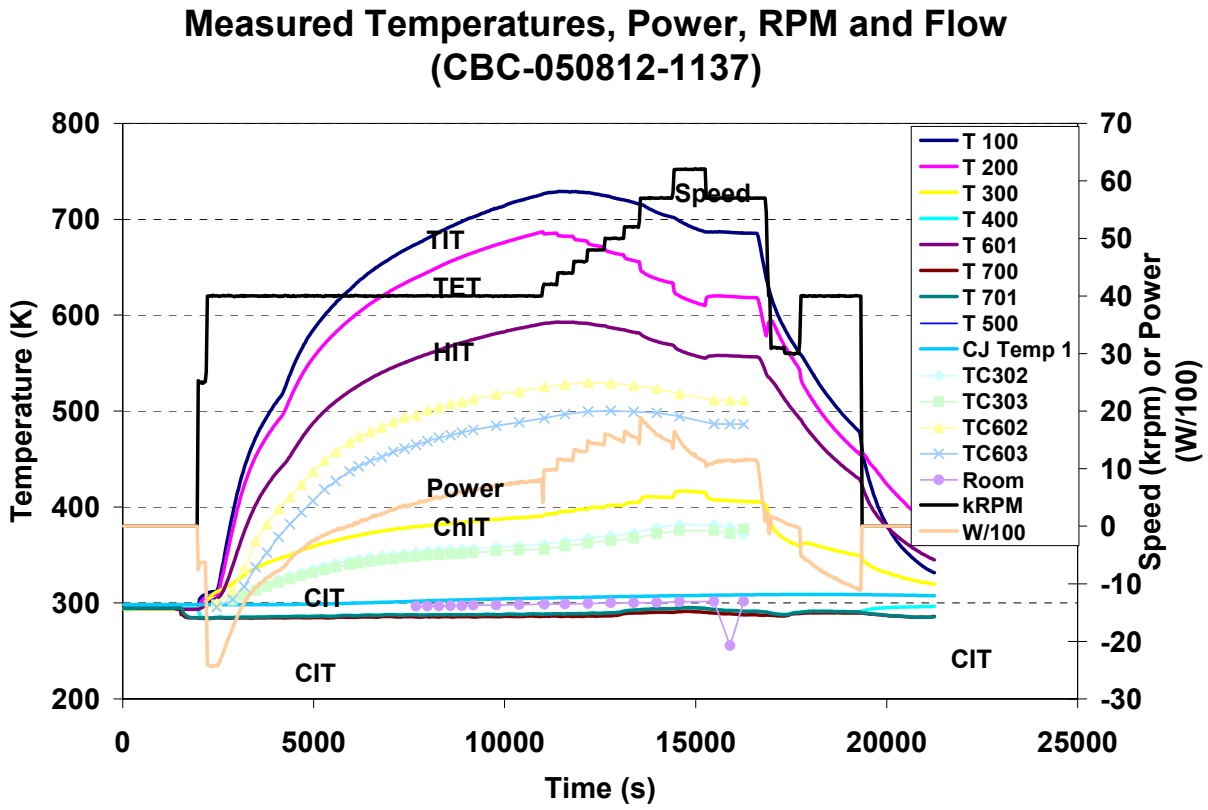

Figure 1-5: Measured results of the Sandia Brayton Loop (SBL-30). The measured gas temperatures are shown on the left scale while the reactor power and shaft speed are shown on the right scale. The temperature nominclature starts at T100 (the turbine inlet), T200 is the turbine outlet and so on around the gas loop. T700 and 701 are water intlet and out let temperatures. The input power is in percent of full power (which is 62 kW) and the electrical power generated is in Watts/100.

1.3 Model Comparison with Measured Data (Validation)

Some early comparisons of the measured data with the dynamic model predictions modeled data are provided in Figure 1-6 and Figure 1-7. The transient shown in Figure 1-6 was made May 13, 2005 at Barber-Nichols Inc. prior to shipping the hardware to Sandia. This test data was designed to test the CBC_RT controller and display panel. It also was designed to test the automatic control loop that adjusts the electrical heater power to provide a desired turbine inlet temperature. Figure 1-6 shows the measured gas temperatures at various locations around the test-loop for the input heater power and shaft rpm (not shown). Figure 1-7 shows the dynamic model predictions for the same temperature locations. This comparison was made by using the measured input heater power, shaft speed, and cooling water temperature. Note that the heater power was adjusted to account for heat losses in the system due to limited amounts of insulation on the hardware ducting.

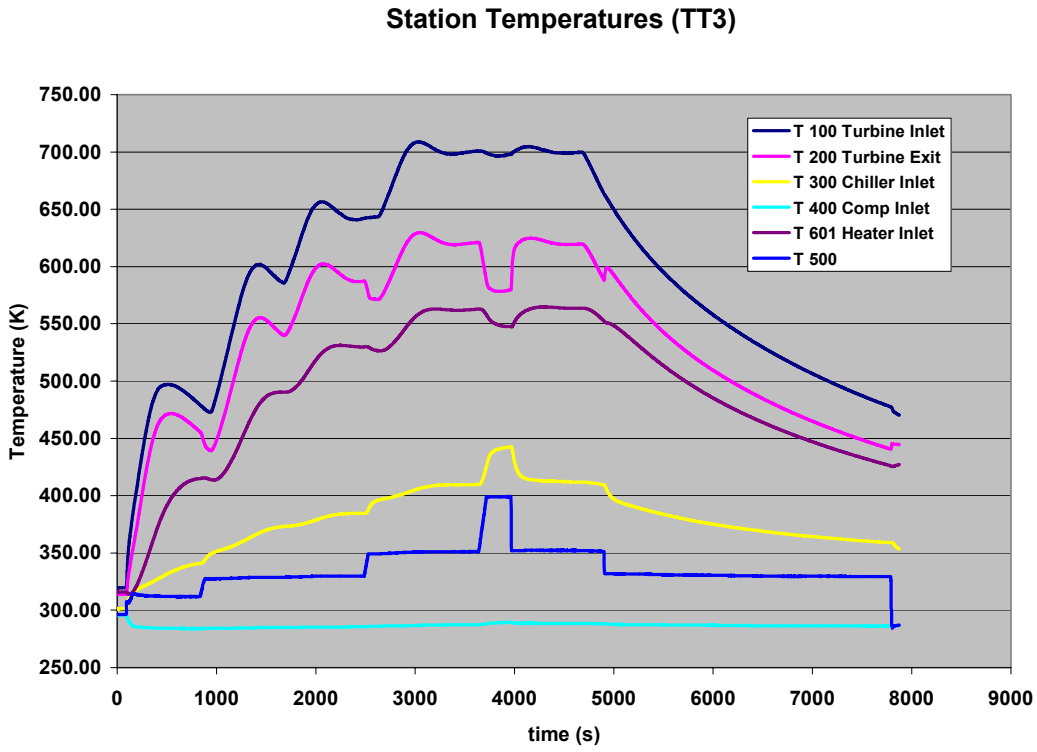

Figure 1-6: Measured data for an early transient measurement to test the automatic control loop (May 13, 2005).

Note that the measured and predicted temperatures are very similar, indicating that the model is a reasonable representation of the test loop. Comparisons of other information such as pressure and power are also similar, but do reveal some areas where the model needs additional work. This data and other more recent data taken at Sandia are presented in more detail within the body of this report.

The validation effort is continuing. Additional data are being recorded and the test loop hardware is being further instrumented, insulation is being added, heat balances are being performed, and additional power is being added to the facility so that higher temperatures and power levels can be achieved. The modeling efforts are also continuing and additional models to better represent heat loses, pressure drops, and the alternator circuitry are being improved.

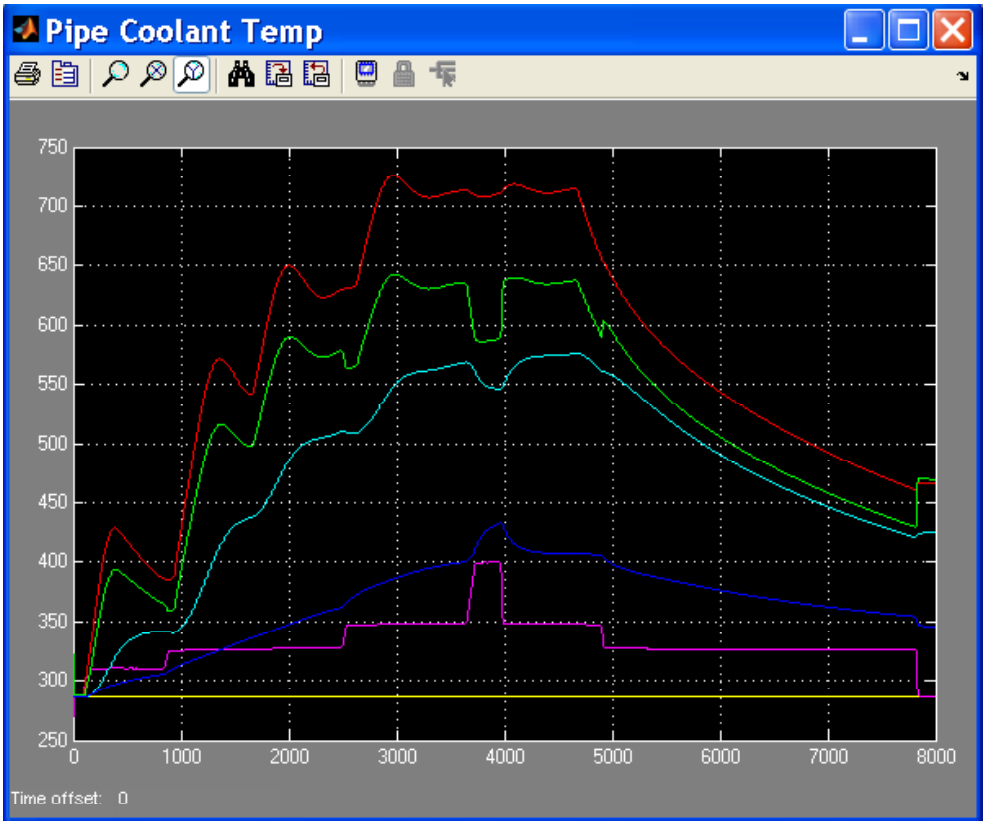

Figure 1-7: Screen shot of the dynamic model temperature predictions for the same measured transient shown in Figure 1-6 given input power, rpm, and water cooling temperatures. Gold is compressor inlet temperature (CIT), magenta is compressor outlet temperature, cyan is heater inlet temperature (HIT), red is turbine inlet temperature (TIT), green is turbine outlet temperature (TOT), and blue is gas chiller inlet temperature (GCIT).

Overall, this program has contributed greatly to the understanding of reactors and turbomachinery, it has developed and operated a closed Brayton test loop at reasonable costs and in a timely manner. In addition the early model comparisons indicate that the model accurately predicts all the major phenomena observed in the tests performed to date. Differences between the model and the measurements do exist and we expect to improve our models over time.

2 Integrated Dynamic Systems Models

Few reactors have ever been coupled to closed Brayton-cycle systems. As a consequence of this lack of experience, the system behavior under dynamically varying loads, during startup and shut down conditions, and the requirements for safe and autonomous operation are largely unknown or unfamiliar to the nuclear community of scientists and engineers. The dynamic system model was developed because of this lack of experience, and because of the intimate coupling between the reactor power and the flow within the CBC system. This section of the report describes steady-state and dynamic models for closed-loop turbo-compressor systems (for space power systems, for terrestrial power plants, and for electrically heated test-loops). These models and their predictions are beginning to provide a basic understanding of the dynamic behavior and stability of the coupled reactor and power generation system. The model described in this report is a lumped capacitance model of the reactor, turbine, compressor, recuperator, radiator/waste-heat-rejection system and generator.

The intimate coupling between closed Brayton cycle power conversion systems and reactors is often not immediately obvious because most gas cooled reactors use coolant circulators or pumps to directly cool the reactor. Only the ML-1 reactor has been coupled directly to a closed-loop Brayton-cycle system. The use of circulators (or pumps) versus closed-loop Brayton cycle circulation is important, because the systems that use circulators/pumps have independent electrical motors that force the coolant through the reactor. For these circulator /pumped reactor systems, the reactor operator has direct control of coolant flow through the reactor by simply adjusting the power to the compressor or circulator. In contrast, for a reactor coupled directly (or even indirectly through a heat exchanger) to a closed-Brayton system loop, the balance of power/torque in the turbo-alternator-compressor machinery provides the shaft power to force the coolant through the reactor. In this way the electrical load and the operating state (temperature, pressure, revolutions per minute/rpm) of the turbo-alternator machinery and gas loop directly affect the flow through the reactor. Because the turbo-machinery state-points determine the flow through the reactor, it also affects the reactor power level.

The Closed-Brayton-Cycle (CBC) model equations that are described in this report were first briefly described in the proceedings of the "*1st International Energy Conversion Engineering Conference"* (Wright, 2003). A more detailed version of these equations was implemented in Simulink™ and reported in the proceedings *of Space Technology and Applications International Forum*: STAIF-2005, (Wright, 2005). The majority of the results presented in this report are based on the equations and solution methods described in the STAIF-2005 report. Both steady-state and dynamic models were developed.

The key to solving the set of system equations is in understanding and having accurate knowledge of the characteristic flow curves for the turbine and compressor. These curves consist of the pressure ratio and temperature ratio versus dimensionless (or corrected) flow rate through both the turbine and the compressor (including the inlet and outlet diffusers). Estimates of these curves were obtained by using mean line flow analysis curves/maps. Simple versions of the flow maps are described in numerous turbo-machinery text books and were developed by the authors. However more reliable results were obtained by using characteristic flow maps purchased from turbo-machinery vendors or obtained from the NASA off normal design codes (Wasserbauer 1975, and Galvas 1973). These codes require the user to select appropriate properties for the working fluid, wheel diameter, blade angles, blade height,

backsweep and other design properties. Models for the other CBC components (recuperator, ducting, heater, and chiller) consist of simple multi-nodal models to estimate the pressure drop, flow rate, Reynolds number, friction factor, heat transfer coefficient, and heat transfer to solid structures within ducts, heat exchangers and radiators.

These integrated system models versions are providing crucial information in developing procedures for safe start up, shut down, safe-standby, stability modeling, and other autonomous operating modes. The dynamic modeling effort has been very useful in supporting this LDRD effort and in supporting related development of space nuclear power systems (ref to NGST, NRPCT and DOE).

In the following sections of this report we begin by describing the only reactor that has been coupled to a closed Brayton loop, the ML-1 reactor. This reactor was a US Army mobile reactor that used a turbo-generator-compressor set to produce up to 300 kWe. This is then followed by a brief, but typical description of a thermal dynamic model of a closed Brayton cycle. These models illustrate the standard approach that one uses to predict the steady-state temperatures, pressures, and flow in a CBC system. However, the limitations of this simiple thermodynamic cycle analysis model are that the model incorporates no knowledge of the rotating machinery size, rotational speed, or other parameters. This section nevertheless introduces the CBC system and identifies the nomenclature used in this report. The third subsection introduces the characteristic curves for a turbo-compressor set and discusses "matching" and the "nominal" steady-state operating curves that are based on the characteristic flow curves of the turbine and compressor. The details of how one generates these curves are not provided, but references to numerous turbo machinery text books are provided that do illustrate how this is done. In addition references to the publicly available NASA off design performance tools for radial compressors and turbines are provided. The NASA off design performance codes are described and the results of these codes are used to develop the characteristic flow curves for the Sandia Brayton test-Loop.

Once the off design performance flow curves are available we then develop and provide the lumped parameter steady-state performance model for a reactor coupled to a closed Brayton cycle. The results of this model are used to generate a set of "standard" operating curves during steady state conditions. These steady state operating curves can then be compared with the simple thermodynamic or cycle analysis models at the desired operating point. In this report, the steady-state curves are then generalized and stability criteria are examined. The complete set of lumped parameter dynamic equations are then introduced. This section is then followed by a summary of the Simulink™ version of the dynamic model, which extends the simple lumped parameter model to include multimodal components for subsystems including the reactor, recuperator, ducting, and heat exchangers. The Simulink™ model is called RPCSIM for Reactor Power and Control Simulator. The RPCSIM Gas Cooled Reactor (GCR) model is described including illustrations of the results of the GCR simulation for a 130 kWe class space reactor. Comparisons with the steady-state lumped parameter model are provided as are comparisons with the typical thermodynamic model.

2.1 History of Reactors and Closed Brayton Cycles

The ML-1 reactor was part of the US Army's Nuclear Power Program (Brunhouse, 1961, and Suid 1990). The reactor, shown in Figure 2-1, first generated electricity on September 21, 1962. At that time, it was the smallest reactor power plant to produce electricity, had the

highest reactor coolant exit temperature of a reactor to produce electricity, and was the first plant in which the reactor was coupled directly to a closed-cycle, gas-driven turbo-machine.

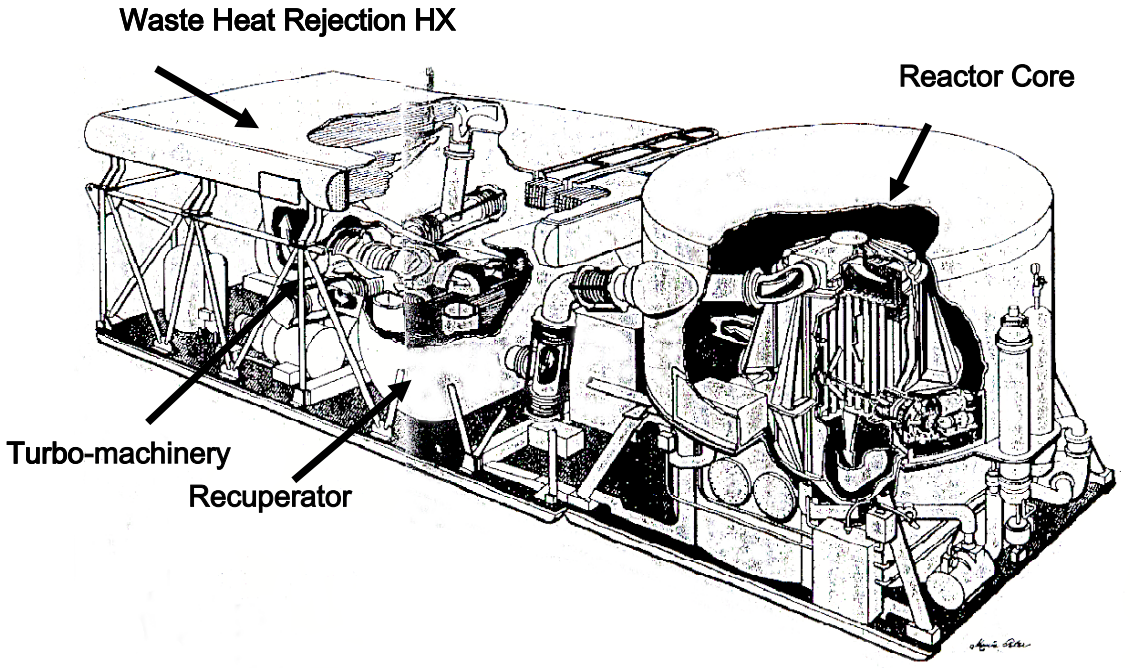

Figure 2-1: Schematic of the ML-1 reactor showing the reactor on the right and the heat exchangers and turbo-machinery on the left.

The ML-1 reactor used UO_2BeO fuel that was clad with Hastelloy X in 19 pin bundles (see Figure 2-2). Thirty-seven of the bundles were located in a water-moderated array. The pin bundles were cooled with Nitrogen or air. The reactor coolant inlet temperature was 677 K, the turbine inlet temperature (reactor exit temperature) was 936K, and the compressor inlet temperature was 311 K. Other state points are shown in Figure 2-3. This reactor operated at power levels up to 3.3 MW_t and the net electrical power produced was 330 kW_e. Aerojet-General Corporation fabricated the reactor and power plant, and it was tested at the National Reactor Testing Station (now INEEL).

The startup sequence consisted of first motoring the turbine-alternator-compressor and then increasing the reactor power (and subsequently the turbine inlet temperature) until self-running conditions were achieved with no load (Atomic Energy Commission Report, no date). After a system check, the system was brought to full power with no load (presumably full flow and full rpm) followed by transitioning to on-line operations. No further startup or operational details have been discovered by the authors within the scope of our research effort.

The ML-1 reactor operated for almost three years. In spite of the successes and many firsts for this reactor and power plant, the plant suffered from regular mechanical breakdowns, emitted more radiation than expected, and was too costly to justify its continued development.

Table 2-1: Operating parameters for the ML-1 US Army mobile reactor and turbo-generator.

ML-1 Reactor (US Army, Mobile Reactor and Turbo-Generator)	
Reactor Fission Power	3.3 MWt
Electrical Power	~300 kWe
Moderator	Water and BeO
Fuel	UO2 BeO
Cladding	Hastelloy X
Turbo-Compressor Working Fluid	Air/Nitrogen
Turbine Inlet Temperature	1200 F 650 C
Date of first Operation	9/21/1962
Manufacturer	Aerojet Corporation

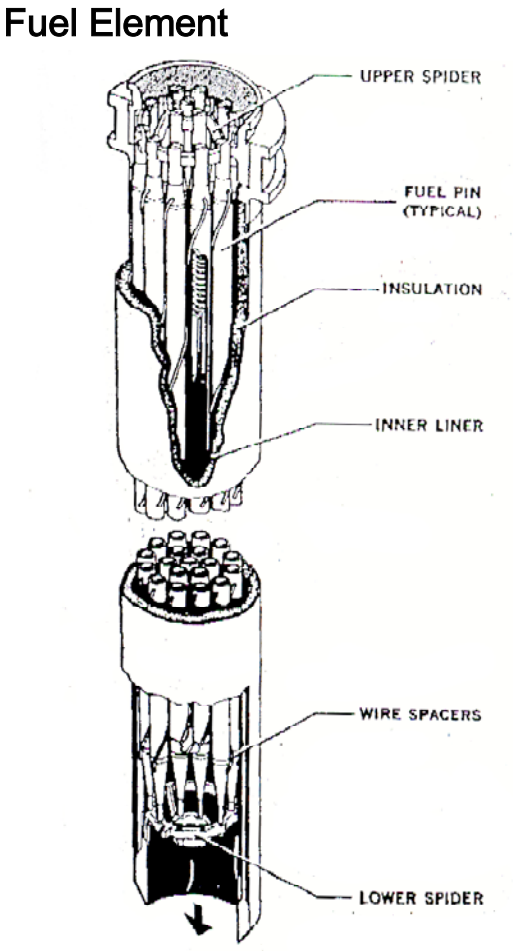

Figure 2-2: One of 37 fuel elements that used UO2-BeO fuel clad with Hastelloy X in a water moderated gas cooled reactor.

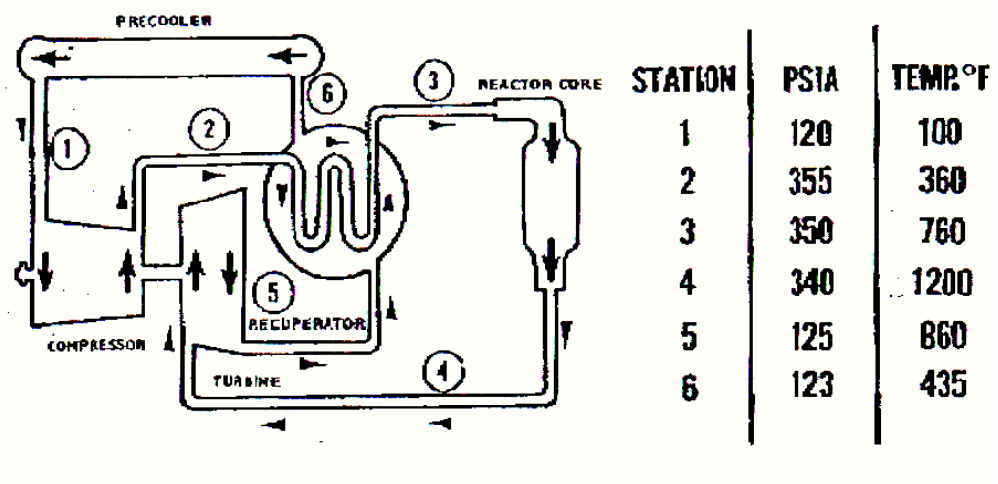

STATION	PSIA	TEMP.°F
1	120	100
2	355	360
3	350	760
4	340	1200
5	125	860
6	123	435

Figure 2-3: Gas coolant temperature ant pressure state-points in the ML-1 reactor.

2.2 Recuperated Closed Brayton Cycle Introduction

Most gas turbine power generation systems are open cycles and use air as the working fluid. In open cycle systems the compressor inlet pressure is essentially one atmosphere or less if it is operated at altitude. For small auxiliary power systems or micro-turbine systems, the turbine inlet temperature is typically limited to about1150 K because of material property limitations, but also for economic reasons. Most of the smaller systems (less than 500 kWe) use radial compressors and turbines rather than axial machines. For space reactor systems or advance terrestrial systems the designer has flexibility in the choice of working fluids and the system pressure. The fact that the pressure can be increased well above atmospheric levels is one of the great advantages of closed Brayton cycles. For space applications a gas mixture of helium-xenon is normally proposed for use with the helium mole fraction varying from 60-90%. For large terrestrial applications the working fluid is normally pure helium at elevated pressures.

The schematic diagram for a recuperated closed Brayton cycle system is shown in Figure 2-4. The cycle is completely closed and gas flows through the compressor, recuperator, into the reactor, then into the turbine, then back into the recuperator and finally into waste heat rejection system (the space radiator, or gas cooler). The reactor is shown on the left side of figure and the waste heat rejection system (space radiator) is shown on the right. The red numbers identify the station locations with 1 corresponding to the compressor inlet, 2 corresponds to the low temperature (high pressure) leg of the recuperator, and so on around the loop. Table 2-2 lists all the station locations and the common abbreviations used for these locations.

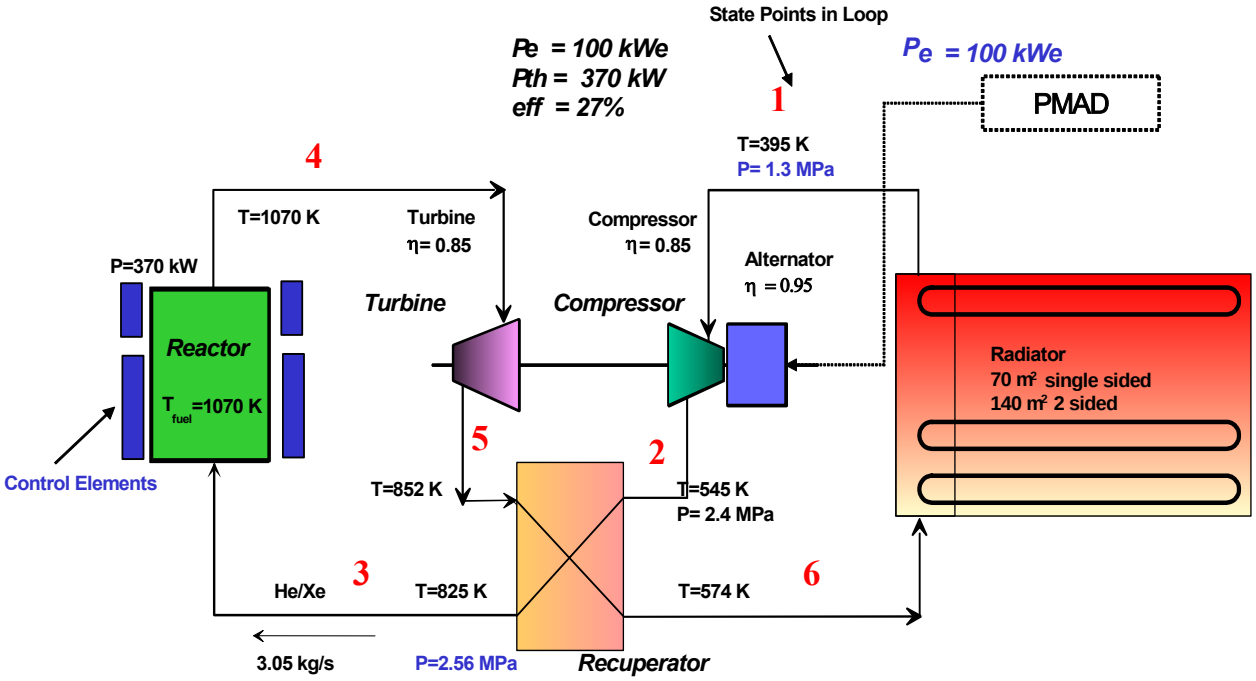

Figure 2-4: Schematic diagram of nuclear gas cooled reactor coupled to a simple recuperated Closed Brayton Cycle (CBC).

Table 2-2: Station locations for temperature and pressure at various locations around the loop. The abbreviations such as CIT and TIT refer to the compressor and turbine inlet temperatures.

Station Number	Inlet Component	Outlet Component
1	Compressor Inlet (CIT)	Gas Chiller Outlet
2	Recuperator Inlet Low Temp Leg	Compressor Outlet (COT)
3	Reactor Inlet (RIT, HIT)	Recuperator Outlet LT Leg
4	Turbine Inlet (TIT)	Reactor Outlet (ROT, HOT)
5	Recuperator Inlet High Temp Leg	Turbine Outlet (TOT)
6	Waste Heat Rejection, Radiator Inlet, Gas Chiller/Cooler	Recuperator Outlet HT Leg

An important point to note about the CBC schematic is that the turbine, compressor, and alternator are all mounted on the same shaft, therefore they rotate at the same speed. (This is not always a requirement, because some systems can use two shafts. The first shaft may have a turbine and compressor and is used solely for pumping the working fluid around the loop. The second shaft has only a turbine and alternator. It spins at a different speed than the high temperature pumping shaft and is used for producing electrical power.) For the simple recuperated CBC systems shaft speeds generally proposed for space systems generally vary between 40,000-100,000 revolutions per minute (rpm) depending on the gas molecular weight, gas pressure, and wheel size for the turbine and compressor. For space power systems a permanent magnet alternator is used with a stator coil that is wired to produce 3 phase power at the frequency of revolution of the shaft (Mason, 1997). An additional component for space

power systems is the Power Management And Distribution subsystem (PMAD). The PMAD is responsible for rectifying and regulating the 3 phase voltage and current and distributing power to the load and bus. It also has another extremely important function because it is also used to regulate the total electrical load and thereby the frequency rotational speed of the turbo-alternator-compressor (TAC) (Mason, 1997). The design variations of the PMAD system are extremely important as they are highly coupled to the operation of the reactor, but the design of PMAD systems is not the focus of this report.

For terrestrial applications there is a strong desire to have the alternator/generator rotate at 3600 rpm regardless of the load. This enables the power plant to produce 60 Hz power directly. In this instance bypass flow paths are used to control shaft speed for short term (seconds) load following capability, and fill gas inventory is used for long term (hours) load following (ref, GA paper). Alternatively, it may be advantageous to use a multi-shaft system that has a separate pumping/circulating shaft and a separate power takeoff shaft.

2.2.1 Closed Brayton Cycle Control Issues

The above discussion introduces some issues associated with the controllability of reactors and CBC systems. Because of the limited experience of coupling reactors and CBC systems, the accurate modeling of these systems is extremely important. The CBC schematic in Figure 2-4 is useful because it can be used to illustrate the various types of control methods that can be employed. The following list briefly describes some of the main control approaches, and some of the advantages or disadvantages are discussed.

1. The PMAD system can be used to increase or decrease the total electrical load by use of a parasitic load resistor that is wired in parallel with the normal system load. This is normally done by using a feedback circuit that adjusts the total load (as seen by the alternator) to force the TAC shaft rpm to follow a reference or requested speed. This is normally the type of control that is proposed for space power applications. For small terrestrial systems, instead of using a parasitic load, the electrical power grid can be used as the load (Capstone, 2005). These types of control (parasitic load resistor or grid loading) are very fast. If the parasitic load is used it keeps the thermal efficiency very high, but strongly affects the electrical efficiency. If the grid is used as the load then both electrical and thermal efficiencies can be kept very high, but it assumes that the grid is infinite and is always available.
2. Another method of control is to increase or decrease the average fuel temperature of the reactor by moving the reactor control rods/elements. This has the effect of continually changing the reactor temperature which may lead to reactor fuel reliability issues due to thermal cycling. It also requires frequent and continuous motion of the control elements and thereby introduces more lifetime/reliability concerns. This type of control is slow and will be dominated by the thermal inertia of the reactor and other hardware components. Control initiated by changing the reactor temperature is normally considered for startup, shutdown, for long term power level changes, for accident and off-normal response, or for compensation caused by fuel burnup.
3. Bypass valves may be used for control because they can rapidly shunt gas from a high pressure leg to a low pressure leg. For example a bypass valve could be used to shunt some of the gas flow from leg 2 to leg 6 or leg 3 to leg 5 (see Figure 2-4). This approach prevents over-speeding of the TAC shaft by shunting some of the gas around

the reactor and turbine. In this way the power produced by the turbine is reduced which in turn reduces the shaft speed. This type of control is rapid (within seconds), but severely affects overall thermal and electrical power generation efficiency.

4. A throttle valve, placed at a low temperature location within the loop, can be used for control because it can be used to restrict gas flow through the loop. It restricts the working fluid flow rate by increasing the loop pressure drop. This type of control is rapid, but severely affects overall thermal and electrical efficiency.
5. Inventory control can also be used. This type of control uses machinery to increase or decrease the absolute pressure of the loop. Generally, increases in pressure will increase the power generated for the same reactor temperature. This is generally a slow process (minutes to hours), but can be used to keep both thermal and electrical efficiency very high.
6. Another control approach is to adjust the compressor inlet temperature by increasing or decreasing the heat removal capability of the gas cooler. For space reactors this could be accomplished by increasing or decreasing the space radiator coolant flow or by shutting off portions of the space radiator.

2.2.2 Thermodynamic Cycle Analysis of Closed Brayton Cycles

The thermodynamic cycle for closed Brayton cycles is conveniently illustrated in a temperature entropy diagram. This is shown in Figure 2-5. The drawing was developed for a terrestrial system that used pure helium as the working fluid, and the peak coolant exit temperature was set at 1000 K while the compressor inlet temperature was set at 300 K. The corresponding temperatures other state point variables for a space reactor (1070 K and 395 K) are shown in Figure 2-4. The T-s diagram lists the same state points, 1 through 6, that were identified in the CBC schematic of Figure 2-4. The following discussion of the T-s diagram will use the values for the terrestrial reactor.

The cycle starts at station 1 with the inlet working fluid temperature set at 300 K and the pressure at 5 MPa. The compressor (with inlet state 1 and outlet state 2) has a compression ratio of about 2:1 and therefore increases the pressure by this ratio. As the gas is compressed, it heats, resulting in increased temperature of the gas at station 2 according to

$$\frac{T_{o2}}{T_{o1}} = 1 + \frac{\left(p_{o2}/p_{o1}\right)^{\frac{\gamma-1}{\gamma}} - 1}{\eta_{sC}} = \left(\frac{p_{o2}}{p_{o1}}\right)^{\frac{\gamma-1}{\gamma}/\eta_{pC}} \qquad 2\text{-}1$$

where T_{o1}, T_{o2}, P_{o1}, and P_{o2} are the total temperature and pressure of the gas at the inlet and exit of the compressor and associated diffusers, γ is the ratio of heat capacities at constant pressure and volume, $\gamma = C_p/C_v$ for an ideal gas, η_{sC} is the isentropic efficiency of compression and η_{pC} is the polytropic efficiency of compression. (See Japikse 1997, Balje 1981, and Wilson 1988 to determine how to convert isentropic efficiency to polytropic efficiency.) The total temperature and pressure are defined as

$$T_o = 1 + \frac{v^2}{2\,C_p T_s} \qquad 2\text{-}2$$

$$p_o = p_s \left(\frac{T_o}{T_s} \right)^{\frac{\gamma - 1}{\gamma}} \qquad 2\text{-}3$$

The subscript o refers to total temperature or pressure, and the subscript s refers to the static values for temperature and pressure. The work performed by the compression process is simply W_{comp} = mdot ·Cp·(T_{o2} - T_{o1}), where mdot is the mass flow rate, and Cp is the coolant heat capacity at constant pressure.. In the example, the inlet gas is compressed from 5 MPa to 10 MPa, and the gas heats from 300 K to 411 K. For this example η_{sC} =0.85 and γ = 1.66 for pure helium.

The recuperator (process 2-3) is a heat exchanger that transfers residual heat from the exhaust of the turbine to preheat the compressor exit gas before entering the reactor. In the recuperator the gas is heated to temperature T_{o3} by the hot gas that comes from the turbine exhaust. Within each of the recuperator flow passages (low and high temperature legs) heat transfer is occurring at approximately constant pressure, though small pressure drops do occur because of frictional drag within the components. The heat transferred in the recuperation process Q_{23} = mdot ·Cp·(T_{o3} - T_{o2}). Naturally, during steady state conditions, the heat gained in the low temperature leg must equal the heat lost in the high temperature leg. Thus, $Q_{23} = Q_{56}$ which is equivalent to T_{o3} - T_{o2}= T_{o5} - T_{o6}. The temperature increase is defined by the effectiveness of the recuperator. For a counter flow heat exchanger with the same gas in each leg, and for the same mass flow rate the effectiveness is defined as (Holman, 2001)

$$\varepsilon_x = \frac{T_{o3} - T_{o2}}{T_{o3} - T_{o2}} = \frac{T_{o5} - T_{o6}}{T_{o3} - T_{o2}} \qquad 2\text{-}4$$

In the example, the recuperator heats the gas to T_{o3} = 750 K.

Once the gas exits the recuperator, the gas is heated in a near constant pressure process (see Figure 2-5) by the reactor to its maximum temperature T_{o4}, which in the example is set to about 1000 K. Again this heating process (3-4) is assumed to occur at constant pressure.

Expansion in the turbine is process 4-5, and it results in a pressure drop that is nearly equal to the pressure rise in the compressor. The gas expansion in the turbine produces power or work. The amount of work produced is W_{45} = mdot ·Cp·(T_{o4} - T_{o5}) In the example, the expansion process (4-5) lowers the gas pressure from approximately 10 MPa to 5 MPa with a corresponding decrease in gas temperature. The turbine exit temperature is related to the inlet temperature and pressure by

$$\frac{T_{o5}}{T_{o4}} = 1 - \eta_{sT}\left(1 - \left(p_{o5}/p_{o4}\right)^{\frac{\gamma-1}{\gamma}}\right) = \left(\frac{p_{o5}}{p_{o4}}\right)^{\frac{\gamma-1}{\gamma}*\eta_{pT}} \quad \text{2-5}$$

where T_{o4}, T_{o5}, P_{o4}, and P_{o5} are the total temperature and pressure of the gas at the inlet and exit of the turbine associated diffusers, η_{sT} is the isentropic efficiency of expansion in the turbine and η_{pT} is the polytropic efficiency of expansion in the turbine.

Next the expanded turbine gas enters the high temperature leg of the recuperator which transfers some of its heat to the low temperature gas in leg (2-3). The exit temperature T_{o6} is determined by the right hand side of equation (4) as described earlier.

The last portion of the cycle is completed by the gas that flows through the waste heat rejection system or gas cooler. This is process (6-1) and results in heat flowing out of the cycle to the environment as required by the second law of thermodynamics. The heat rejection temperature in the early stages of design is set as a goal. For example in Figure 2-5 the compressor inlet temperature (CIT) is set to $T_{o1} = 300$ K. Similarly, the exit temperature from the reactor is normally set as a goal. In the example $T_{o4} = 1000$ K.

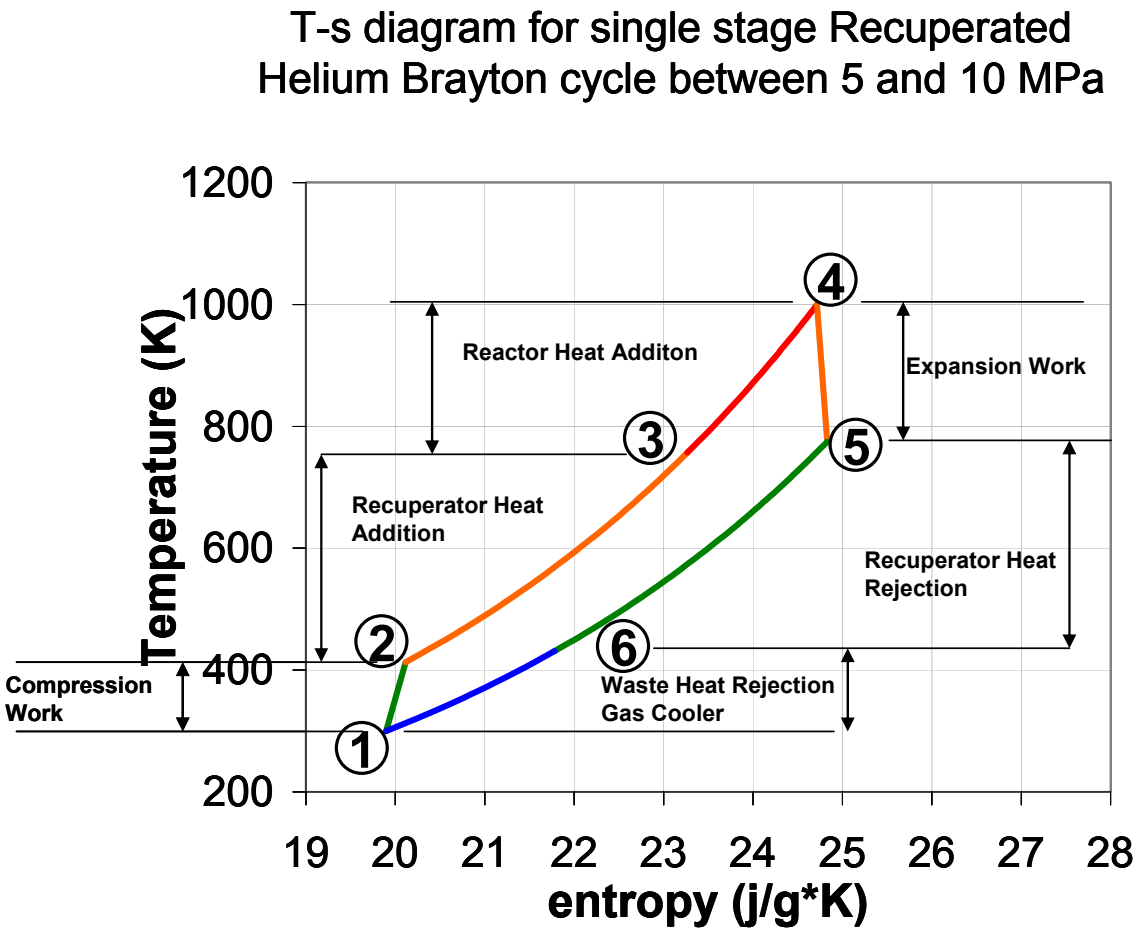

Figure 2-5: Temperature entropy diagram for a single staged helium Brayton cycle.

These equations have been conveniently collected together by (Wilson 1988) into a system of equations that use the above thermodynamic cycle equations to determine the mass flow rate, state-point temperatures and pressures, electrical efficiency, the electrical power generated given the thermal power, recuperator effectiveness, maximum temperature ratio T_{o4}/T_{o1}, pressure ratio $r = p_{o2}/p_{o1}$, and the fractional pressure drop through the cycle. These equations follow.

$$E = \frac{T_{o4} - T_{o5}}{T_{o4}} = 1 - \left(\left(1 - f_{dp} \left(p_{o2} / p_{o1} \right) \right)^{R/Cp \cdot \eta_{pT}} \right) \qquad 2\text{-}6$$

Where E is the coefficient of expansion term,

$$f_{dp} = \sum_{components} dp_o / p_o \qquad 2\text{-}7$$

f_{dp} is the fractional pressure drop within all components

$$r = p_{o2} / p_{o1} \quad 2\text{-}8$$

r is the compressor pressure ratio,

$$R = R_{ugc} / MW \quad 2\text{-}9$$

R is the gas constant, MW is the molecular weight of the working fluid, and R_{ugs} is the universal gas constant.

$$C = \frac{T_{o2} - T_{o1}}{T_{o1}} = \left(r^{R/Cp \cdot \eta_{pC}} - 1 \right) \quad 2\text{-}10$$

C is the coefficient of compression term

$$\eta_{th} = \frac{T_{o4} - T_{o5}}{T_{o4}} = \frac{E \cdot \left(T_{o4} / T_{o1} \right) - C}{\left(T_{o4} / T_{o1} \right)\left(1 - \varepsilon_x (1 - E_1)\right) - (1 + C)\,(1 - \varepsilon_x)} \quad 2\text{-}11$$

η_{th} is the thermal efficiency,

$$W = \dot{m} \cdot C_p \left(T_{o4} - T_{o5} \right) - \dot{m} \cdot C_p \left(T_{o2} - T_{o1} \right) \quad 2\text{-}12$$

W is the total shaft work produced by the turbo-compressor,

$$W_{rx} = \dot{m} \cdot C_p \left(T_{o4} - T_{o3} \right) \quad 2\text{-}13$$

and W_{rx} is the total thermal power produced in the reactor or heater.

These equations assume that the mass flow rate through the turbine and compressor are the same. In real systems some gas flow may be bypassed to cool machinery or even for control purposes. In addition, for non-ideal gases (such as air), the heat capacity is different in the turbine than in the compressor because the heat capacity, Cp is a function of temperature. Corrections to account for these effects are easily incorporated into the above set of equations and they are described in (Wilson, 1984).

These equations are very useful for performing a variety of scoping calculations and to estimate the size, mass, operating temperature and pressure, of all components. They are also useful for making a variety of trade studies to determine the pressure and molecular weight of the gas can be used in the Brayton cycle. A few conclusions from these scoping calculations are presented below.

2.2.3 Scoping Calculations and Some Results

Two design goals of most space reactors or other small reactors are to reduce the system mass and to maximize the amount of power produced by the system. The mass of the reactor and the power conversion system is in part controlled by critical mass limits of the reactor, but also by

the pressure, thermal conductivity, and mass flow rate of gas working fluid. The selection of the gas conductivity, gas pressure, and system cycle efficiency (maximum and minimum cycle temperatures) have the greatest impact on the system specific mass (kg/kWe) because these variables, to a large degree, control the heat removal capability, and thus the size of the reactor.

To achieve high thermal cycle efficiencies an even more important goal is to select a design that can achieve high gas exit temperatures but still keep the temperatures and stresses of the pressure boundaries within the limits of available materials. For a gas cooled reactor this can be achieved by selecting the reactor inlet temperature to be sufficiently low such that the inlet gas can be used to cool the pressure vessel and all other components. Where high temperatures are required, such as in the reactor exit duct, it is important to balance the pressures across the high temperature materials so that the stress levels are minimized (Wright and Lipinski, 2003). These design principles allows the designer to used non-refractory metals for the pressure vessel wall and ducting materials while still allowing the gas exit temperature to be heated to as high as 1150 K or even higher. These design principles and engineering features can be used to greatly lower programmatic risk because they lower both the cost and shorten the schedule, by allowing the use of widely available well characterized materials while avoiding the development of refractory metal components and eliminating the need to use liquid metal coolants (Na or lithium) that must operate at temperatures well above the Liquid Metal Fast Breeder Reactor (LMFBR) operational and design experience.

Examination of the simple set of equations described above indicate that the cycle efficiency (ratio of power produced to thermal power input) is determined largely by the compression ratio (r), and the peak to minimum temperature ratio (T_{o4}/T_{o1}). The reactor inlet temperature is also mostly affected by the pressure ratio, but also by the effectiveness of the recuperator.

Some of the design issues for a Gas Cooled reactor are illustrated here by applying the above set of equations to determine the optimum pressure ratio and to show how the pressure ratio and recuperated effectiveness can be selected to permit the use of superalloys for the reactor pressure vessel when cooled by the reactor inlet gas. For the purposes of illustration, the authors assume that the superalloys can operated at temperatures less than 900 K (generally limited by thermal creep). Furthermore the results shown here use a helium-xenon gas mixture that is 63.5 a% helium. The molecular weight for a gas mixture is just the mole fraction average of the individual molecular weights. However, other properties such as gas conductivity, viscosity, and Prandtl number do not scale this way (see section 2.2.3.3). For a gas mixture of 63.5% He and 36.5 % (percent by mole fraction) the heat capacity is Cp = 414.37 J/kg-K. Other values used in this section are 0.84/0.861 and 0.88/0.863 for the isentropic/polytropic efficiency of the compressor and turbine.

Figure 2-6 shows the CBC cycle efficiency as a function of pressure ratio. Note that it has a maximum value of for a compression ratio of about 1.7-1.8, assuming a total fractional pressure drop (dp) through the loop of 5%. This figure also shows that the higher effectiveness recuperator significantly improves the total cycle efficiency and reduces the required pressure ratio. If no recuperator were used, then for the same temperatures T_{o4} and T_{o1} the peak efficiency occurs at a pressure ratio of about 3.5, but the efficiency is still less than that of the recuperated system.

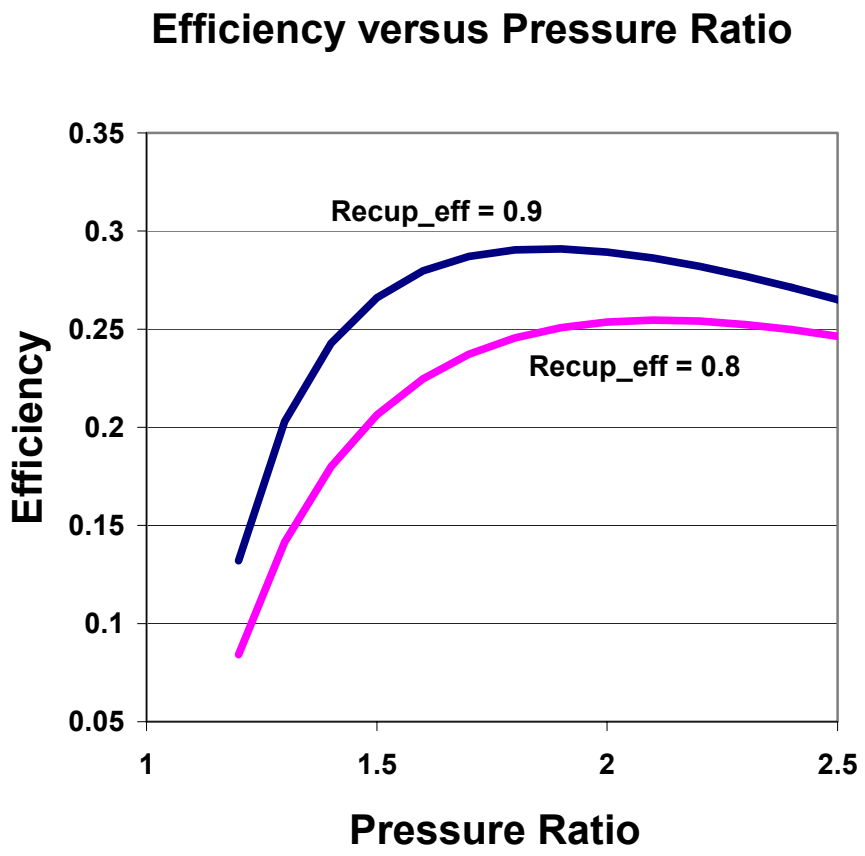

Figure 2-6: CBC cycle efficiency for HeXe (63 a/o He) as a function of pressure ratio and for two selected recuperator effectiveness values of 0.8 and .9.

Figure 2-7 shows the reactor inlet temperature for the same range of pressure ratios and recuperator effectiveness. Because material compatibility properties limit the superalloy temperature to less than 900 K, the pressure ratio should be > 1.9 to keep reactor inlet temperature less than 900 K (for a recuperator effectiveness of 0.9). But because the efficiency of the system is decreasing above 1.7-1.8 (see Figure 2-6), the design is restricting both the compression ratio and the recuperator effectiveness. Compression ratios near 1.8-1.9 and recuperator effectiveness near 0.9 seem to be near the ideal values. Of course more detailed analysis may shift these numbers somewhat, but they appear to be good starting points for design purposes.

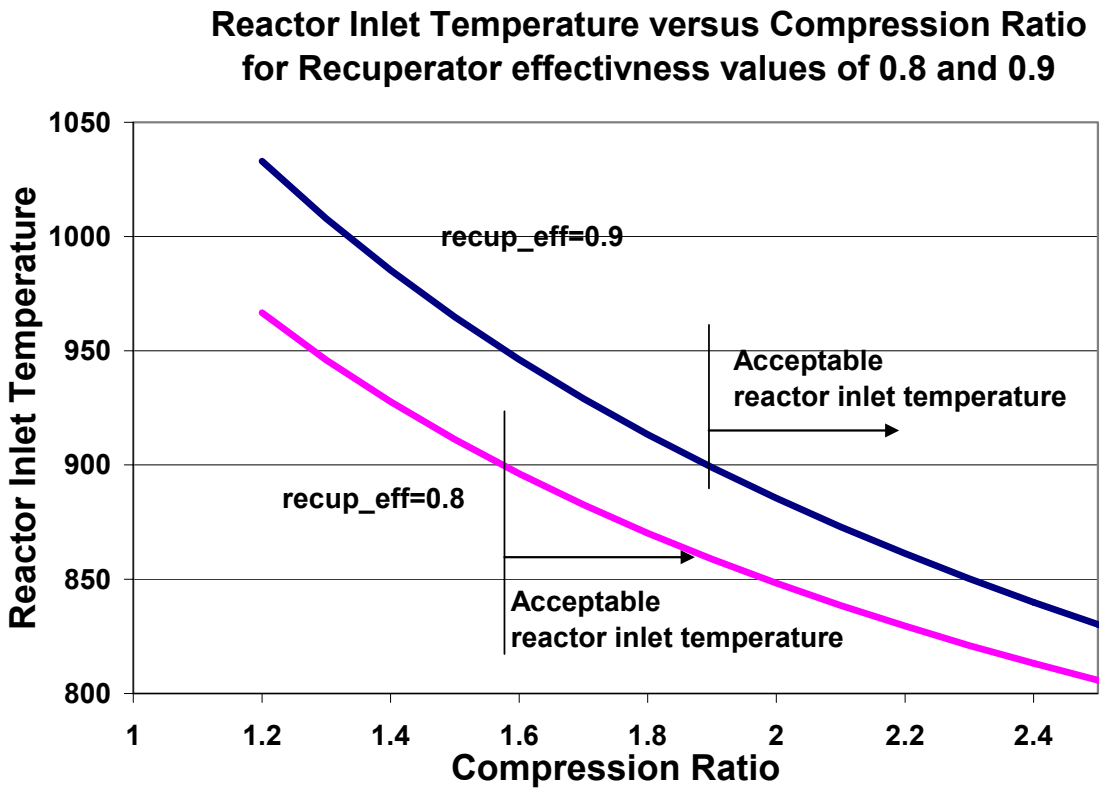

Figure 2-7: CBC reactor inlet temperature as a function of compression ratio and recuperator effectiveness.

2.2.3.1 Chapman Enskog Theory for Properties of Mixed Gases

It is relatively easy to expand the thermodynamic cycle analysis described above to perform additional scoping calculations that can be used to estimate the size of the reactor and its associated components, and some results of these trade studies are described in section 2.2.4. This requires knowledge of the fundamental hydrodynamic properties of the mixed (or pure) gas such as gas heat capacity, gas thermal conductivity, viscosity, and Prandtl number. These properties are required to estimate the heat transfer coefficient, mean flow velocities and pressure drops, Reynolds and Nusselt numbers.

Mixed gases are often considered for use in space and other special purpose applications because, for the same molecular weight, a mixed gas has a higher thermal conductivity than the pure gas. If pure helium at high pressures were used in a small power conversion system the turbo-machinery design would be very small and operate at extremely high shaft rotation speeds (> 100,000 rpm). The small size and high speed introduces loss and tolerance issues and it also complicates the design and operational limits of the alternator. Furthermore there is a specific speed (a dimensionless value) that must be met and a dimensionless diameter constraint as well. The specific speed is related to the rotational speed, the volumetric flow rate, and adiabatic temperature rise. The specific diameter constraint is related to the actual diameter, the volumetric flow rate and the adiabatic temperature rise. These values set constraints on the design and introduces tradeoffs that limit the pressure and molecular weight of the gas mixture.

We use the Chapman-Enskog theory to determine the transport properties for the low density monatomic gases helium and xenon. These properties are mixed according to a method by Mason and Saxena (1957) that is an approximation to a more accurate method developed by Hirschfelder (1954). These transport properties are described in Bird-Stewart-&-Lightfoot (Bird 1960).

Given the molecular weight of the ideal gases, the mole fraction of the gas mixture, the universal gas constant, and the ratio of the specific heats (constant pressure to constant volume) γ, one can then determine the specific heat, molecular weight, speed-of-sound, density, and specific heat ratio for the gas mixture. These equations for a 90% helium fraction are described below.

2.2.3.2 Gas Material Properties for Ideal and Monatomic Gases

The gas properties for the molecular weight (MW), and specific heat ratio (γ) of pure helium and xenon as well as their mixed values are listed below.

Table 2-3: Ideal gas properties for helium and xenon and their mixture at 63.5 a% helium.

Xenon Molecular Weight MW_{Xe}	MW_{Xe} = 131.3 gm/mole	**2-14a**
Helium Molecular Weight MW_{He}	MW_{He} = 4 gm/mole	**b**
Ratio of C_p/ C_v for He	γ_{Xe} = 1.66	**c**
Ratio of C_p/C_v for Xe	γ_{Xe} = 1.66	**d**
Xenon Mole Fraction	f_{Xe} = 0.365, 36.5 a%	**e**
Helium Mole Fraction	f_{He} = 1- f_{Xe} = 0.635 , 63.5 a%	**f**
Average γ = Cp/Cv ratio	$\gamma = f_{Xe}\gamma_{Xe} + (1- f_{Xe})\gamma_{Xe}$	**g**
Average Molecular Weight	MW_o = 50.465 gm/le	**h**
Gas Constant for mixed gas property	$R_o = R_{ugc} / MW_o$ = 164.749 J/kg-K	**i**

With these properties for the He and Xe mixture properties the equations for the density, the speed-of-sound, and the specific heat are:

Table 2-4: Density, speed of sound, and heat capacity equations for ideal gases with the heat capacity of He/Xe at 63.5 a% listed.

Density equation for an Ideal Gas	$\rho(T,P) := \frac{P}{R_o \cdot T}$	**2-15a**
Speed of sound equation for a gas mixture at temperature T	$c(T) := \sqrt{\gamma \cdot R_o \cdot T}$	**b**
Heat capacity equation for an ideal gas	$C_{fp}(\gamma, MW) := \frac{R_{ugc}}{MW \cdot \left(1 - \frac{1}{\gamma}\right)}$	**c**
Heat capacity for 63.5 a% He mixture	Cp = 414.37 J/kg-K	**d**

2.2.3.3 Chapman Equation for C_p, k, and Viscosity for Gases

The Lennard-Jones potentials along with the molecular theory of gases and liquids can be used to predict the viscosity and the conductivity of gases at low densities. The Lennard-Jones potential values used are from Hirschfelder (1954). A simple and concise summary of this

theory is in Bird (1960, pp 744-746). The Lennard-Jones potentials for He and Xe are given below.

Lennard-Jones Parameters for He $\varepsilon_{He} = 10.2$ K $\sigma_{He} = 2.576$ 2-16

Lennard-Jones Parameters for Xe $\varepsilon_{Xe} = 229$ K $\sigma_{Xe} = 4.055$ 2-17

This data is used with a transport theory prediction curve $\Omega(T)$ to obtain the viscosity and conductivity at low densities for monatomic gases as a function of temperature and gas mixture. (Hirschfelder, 1954).

$$\Omega(t) := 0.92495 + 2.073681\,10^{-3}\cdot t + \left[.719288(t)^{(-1.151049)} - 5.464521\,10^{-2}\cdot\sqrt{t}\right] \quad \textbf{2-18}$$

Given this equation, the viscosity for a low density monatomic gas (Bird, Stewart, and Lightfoot, 1969) is defined by

$$\mu(MW,\varepsilon,\sigma,T) := \frac{\sqrt{\frac{MW}{\left(\frac{gm}{mole}\right)}\cdot\frac{T}{K}}}{\sigma^2\cdot\Omega\left(\frac{T}{\varepsilon}\right)}\cdot 2.669\,10^{-6}\cdot\frac{kg}{m\cdot s} \quad \textbf{2-19}$$

For example, the viscosity for helium at 300 K and 1000 K is 1.979 x 10^{-5} Pa-s and 4.306 x 10^{-5} Pa-s respectively. Similarly, the conductivity for a low density monatomic gas, with $\gamma >$ 1.63, is defined by (ibid, pg 255):

$$k1(MW,\varepsilon,\sigma,T) := 8.322\,10^{-2}\cdot\frac{W}{m\cdot K}\cdot\frac{\sqrt{\frac{\frac{T}{K}}{\left[\frac{MW}{\left(\frac{gm}{mole}\right)}\right]}}}{\sigma^2\cdot\Omega\left(\frac{T}{\varepsilon}\right)} \quad \textbf{2-20}$$

At 300 K and 1000 K the gas conductivity for helium is 0.154 and 0.336 W/m-K.

2.2.3.4 Mixture Rules for the He/Xe gas mixture

The semi-empirical formula from Wilke (1950) is used to determine the mixed gas properties for thermal conductivity and for viscosity. (See also Bird, 1960, pp 24 and 258.) These rules are listed below.

$$\phi_{HX\_mix}(T) := \frac{1}{\sqrt{8}}\cdot\left(1+\frac{MW_{He}}{MW_{Xe}}\right)^{-.5}\cdot\left[1+\left(\frac{\mu_{He\_o}(T)}{\mu_{Xe\_o}(T)}\right)^{.5}\cdot\left(\frac{MW_{Xe}}{MW_{He}}\right)^{.25}\right]^2 \quad \textbf{2-21}$$

$$\phi_{XH\_mix}(T) := \frac{1}{\sqrt{8}} \cdot \left(1 + \frac{MW_{Xe}}{MW_{He}}\right)^{-.5} \cdot \left[1 + \left(\frac{\mu_{Xe\_o}(T)}{\mu_{He\_o}(T)}\right)^{.5} \cdot \left(\frac{MW_{He}}{MW_{Xe}}\right)^{.25}\right]^2 \quad \textbf{2-22}$$

$$k_{mix}(T) := \frac{f_{He} \cdot k_{He}(T)}{f_{He} \cdot 1 + f_{Xe} \cdot \phi_{HX\_mix}(T)} + \frac{f_{Xe} \cdot k_{Xe}(T)}{f_{He} \cdot \phi_{XH\_mix}(T) + f_{Xe} \cdot 1} \quad \textbf{2-23}$$

$$\mu_{mix}(T) := \frac{f_{He} \cdot \mu_{He\_o}(T)}{f_{He} \cdot 1 + f_{Xe} \cdot \phi_{HX\_mix}(T)} + \frac{f_{Xe} \cdot \mu_{Xe\_o}(T)}{f_{He} \cdot \phi_{XH\_mix}(T) + f_{Xe} \cdot 1} \quad \textbf{2-24}$$

The Prandtl number for the He/Xe gas mixture is now defined as

$$\Pr = Cp\frac{\mu}{k} \quad \textbf{2-25}$$

where the mixed properties for Cp, viscosity and conductivity are used.

These equations were programmed in the programming environments Mathcad™, Excel™, MatLab™, and Simulink™ to specify the state properties of the closed Brayton cycle system described in the previous section. In addition the complete theory (Hirschfield, 1954) was programmed into Mathcad and compared with the simple theory described here (Wilke 1950). An internal SNL memo is available on the complete theory. The more complete theory was developed because the Prandtl numbers for the individual gases are very similar, but the Prandtl number for the mixture is much lower than the individual values. Because the Prandtl number plays an important role in the heat transfer coefficient from the fuel pin to the gas coolant, we felt that it was important to verify this behavior especially for gas mixtures with very different molecular weights. We observed very little difference between the more complete theory and the condensed semi-empirical theory.

Figure 2-8shows the results of the Chapman-Enskog theory predictions for the thermal conductivity, viscosity and Prandtl number for various Helium Xenon gas mixtures. The results provide some insight to the design of reactors and small gas-dynamic power conversions systems. First, both the conductivity and viscosity show the standard square-root of temperature dependence that is expected. For increasing helium content the gas conductivity increases monotonically, however, for the viscosity the values remains relatively constant or increase slightly, but then the viscosity drops dramatically at high helium fractions (> 80 a%). Because leak rates will be greater for helium than for xenon, there will be a tendency for the mole fraction of helium to decrease over the life of the system. Depending on the leak rates, this could result in increased viscosity and lower conductivities. Such changes are not likely to seriously affect the design, but they do introduce expected deviations that will have to be accommodated by providing adequate design margin.

As mention earlier the Prandtl number shows unexpected behavior with respect to changes in helium fraction. Both helium and xenon have Prandtl numbers near 0.7, however the mixture shows a very reduced value (Pr = 0.2) at mixtures containing about 60 a% helium.

Figure 2-9 shows the constant pressure heat capacity (Cp) as a function of Helium mole fraction. Note that because the model assumes that the gas mixture is an ideal gas, that there is no temperature dependence for the heat capacity.

The data was also compared with measurements. In general the comparison between measured data and predicted data are good. However, the conductivities appear higher than the measured values (by about 6-10%), while the viscosities are virtually identical. Figure 2-10 and Figure 2-11 show the comparison between the theory and measurements for thermal conductivity and viscosity (Hirschfelder, 1954). This experimental and predicted behavior are for a gas mixture with 75% mole fraction of Helium, and as mentioned above the agreement is better for the viscosity than for the thermal conductivity. The theory and equations can be used for other binary gas mixtures simply by changing the molecular weight, the specific-heat ratio, and the Lennard-Jones potentials.

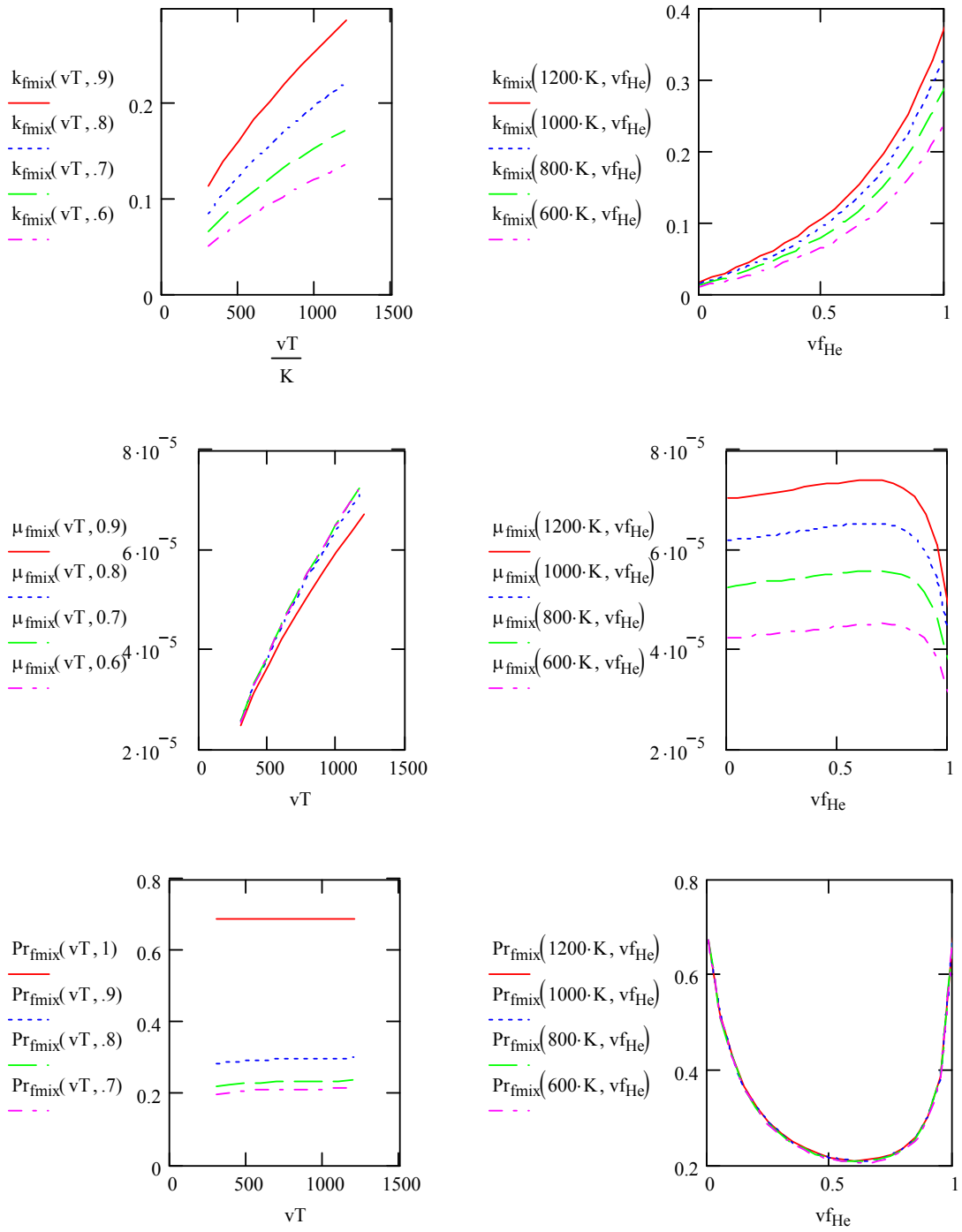

Figure 2-8: Mixed gas thermal conductivity and viscosity versus temperature or as a function of helium mole fraction.

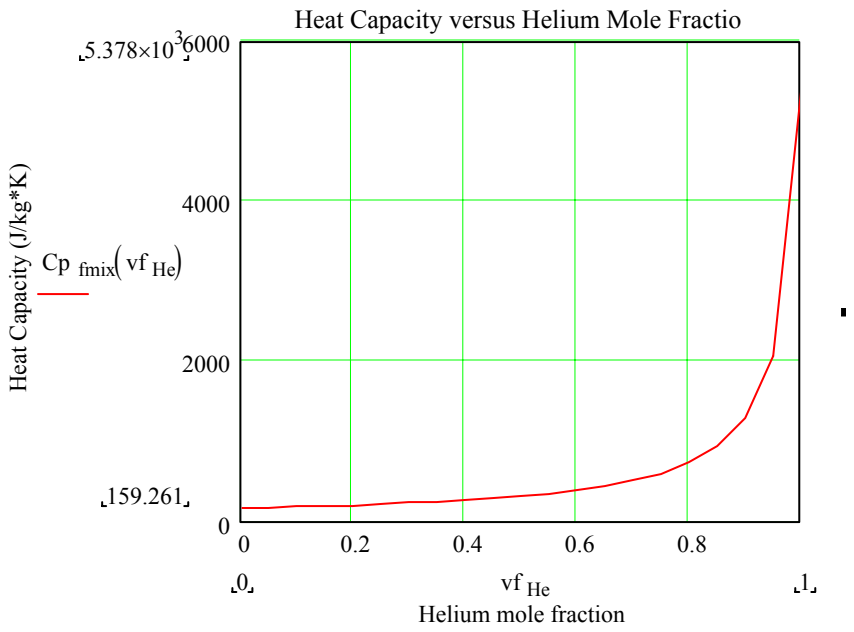

Figure 2-9: Heat capacity as a function of Helium mole fraction.

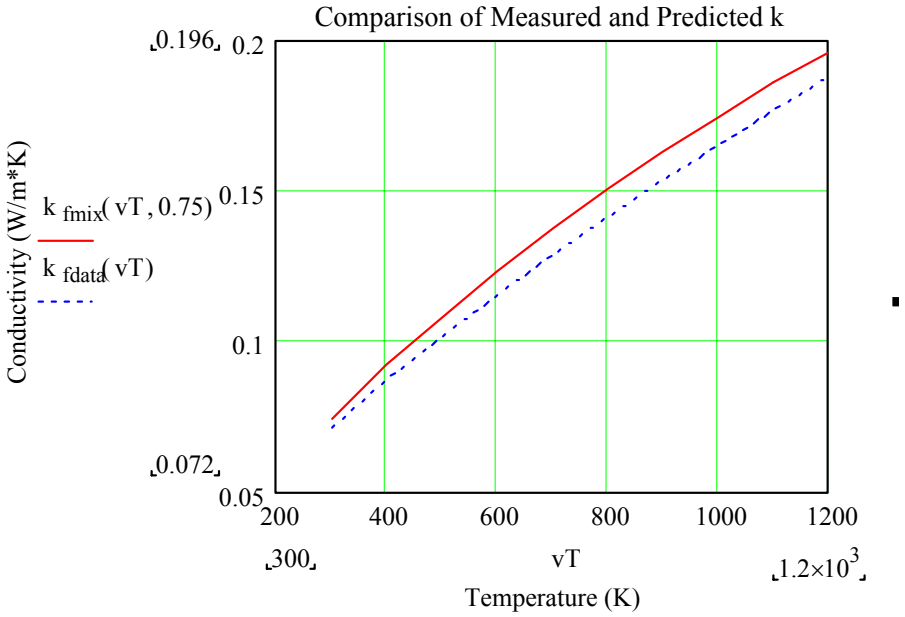

Figure 2-10: Comparison of measured and predicted thermal conductivity for a He/Xe gas mixture containing 75 mole % He.

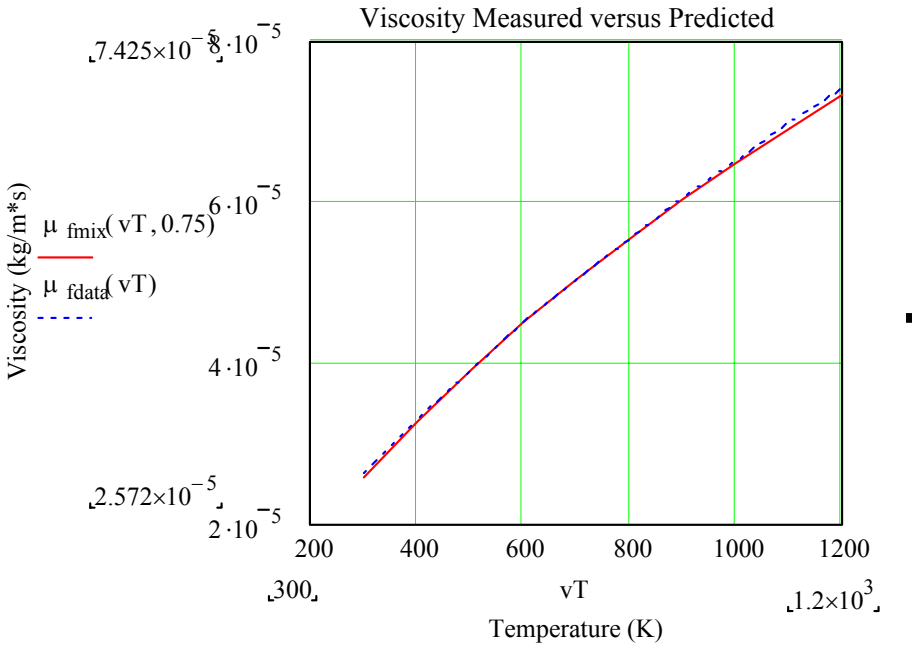

Figure 2-11: Comparison of calculated and measured viscosity for He/Xe gas mixture with 75 mole% He.

2.2.4 Trade Studies and Sizing Estimates

The thermodynamic cycle analysis equation sets (described above) were extend to include the thermal physical data such as conductivity, viscosity, and Prandtl number so that size and mass estimates could be made. In addition other limitations such as limiting the flow velocities to 10% of the sound speed, and selecting reasonable values for the efficiencies/effectiveness of turbines, compressors, alternators, recuperators, and electronics were assumed. When this is done, it is then possible to perform a variety of trade studies to determine the size and mass of various nuclear systems and how these change with different assumptions such as gas pressure, and gas molecular weight.

For space systems these trades must include the power to mass trade-offs of the system as well as the mission, as these values determine the lifetime of a mission. The results of this type of effect of gas molecular weight and pressure were evaluated in a series of trade studies.

A quick inspection of the equations listed above shows that the cycle thermal efficiency is primarily dependent on the heat capacity of the gas, efficiency of the turbine and compressor, cycle high and low temperatures, and loop pressure drop fraction. If the molecular weight of a noble gas mixture is changed (e.g. changing the helium fraction in a HeXe mixture), the ratio γ of the constant pressure to constant volume heat capacity of the mixture (γ) remains fixed at 1.66. At first blush this would imply that the cycle thermal efficiency would remain unchanged. However, in a system such a change would result in a number of other changes that would impact efficiency. For example, the turbine and compressor efficiencies would change, the thermal conductivity and recuperator effectiveness would change, and the loop pressure drop would change. All of these changes could be overcome by a redesign of the components, but that would result in a mass change. So it is important to clearly define what is held constant when one parameter is varied when performing trade studies.

For a space reactor, one of the most important parameters is system mass for a given electrical power. A trade study was performed under a NASA contract to determine how the reactor and radiation shield mass changed for a CBC system directly driven by a GCR. In this study, the reactor coolant passages were adjusted to keep the reactor pressure drop at 3% of the reactor gas pressure. In addition, the amount of spectral-shifting neutron absorbing material was adjusted so that for launch safety reasons the reactor would remain subcritical when submerged in water. Finally, enough fuel was included to allow operation at full power for 10 years. With these constraints, the mass of the reactor and radiation shield (plus 350 kg for structures and controls) was determined. The results are shown in Figure 2-12. The reactor thermal power was held at 400 kW. The number of fuel pins was varied (with a resulting change in pin diameter) as part of the parameter scan. The baseline gas composition was 10% helium (by mass) and 90% xenon. The various curves are for different gas pressures. There also is a curve for 99% helium (by mass) and a lower fractional pressure drop through the reactor. The red circles identify the minimum allowable number of pins if the clad must remain below 1250 K.

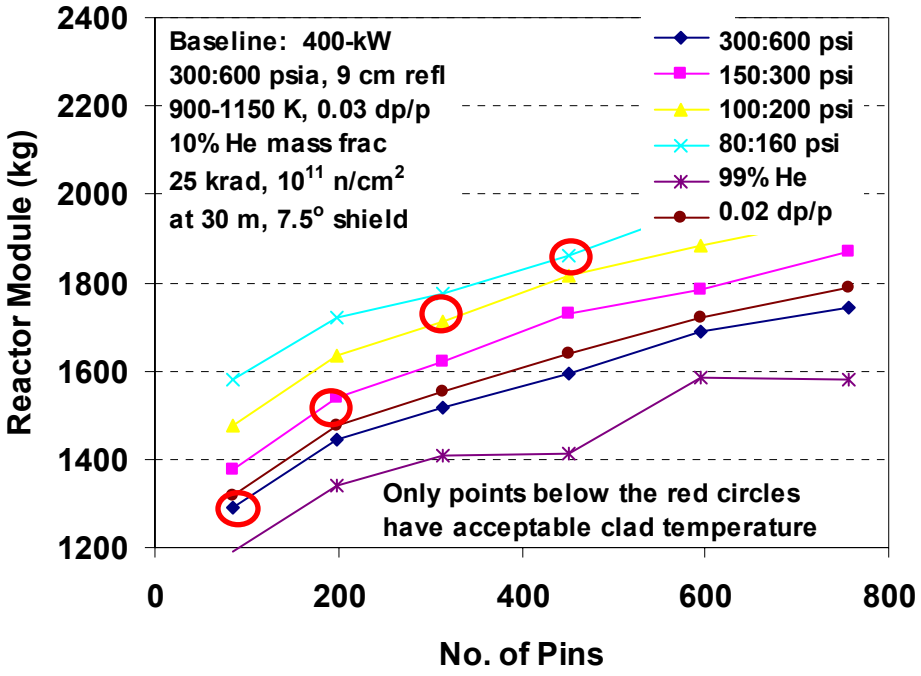

Figure 2-12. Reactor module mass vs. number of fuel pins.

The result of this study shows that the reactor mass is reduced if the pressure is increased. This is because the denser gas can transport the heat with smaller flow channels. One of the curves also shows that a higher helium fraction reduces the reactor mass. This is because the higher specific heat and lower viscosity allows smaller flow channels. Finally, the plot shows that requiring a lower pressure drop in the reactor does not cause a substantial mass increase.

These results are interesting, but they are incomplete without knowledge of how these changes affect the power conversion efficiency and system mass. For example, increasing the system pressure will change the efficiency for a given turbomachinery design. To reach a new

optimum configuration, the turbomachinery unit will probably be smaller (if the electrical power is held fixed). The smaller unit might be less efficient if it leaks more gas around the turbine and compressor blade ends. It also will spin faster, which might impact the generator mass.

As another example, increasing the helium fraction also will change the efficiency of a given design. Optimizing the design will probably result in a larger turbomachinery unit. This larger unit might have a smaller gas bypass fraction and thus be more efficient. This might offset the higher mass.

The bottom line is that an accurate model for system component design and cycle efficiency is needed and should be coupled with the parameter scan of reactor mass to find a system-wide minimum mass configuration.

2.3 Characteristic Flow Curves for Radial Turbine and Compressors

This section of the report develops the characteristic flow curves for radial turbines and compressors. Prior to developing these curves it is useful to present detailed descriptions and photos of the Capstone C-30 compressor and turbine. This description is useful because it illustrates why some of the assumptions were made for the dynamic model, and it illustrates some of the design trade-offs that must be made for the turbine and compressor such as thrust load balancing, temperatures of the gas bearings, and flow of gas within the bearings.

2.3.1 Capstone C-30 Compressor and Turbine

A photo of the complete compressor and turbine for the Capstone C-30 (30 kWe) wheel set, including gas bearings, is shown in Figure 2-13 (Photos courtesy of NASA Glenn Research Center). The entire wheel set for this 30 kWe system is less than 6 inches long and the wheel diameters are around 4 inches. The reader should note that the dimensions for a 132 kWe turbo-compressor set that is designed for He/Xe at 2 MPa are about the same. The small dimensions of the turbine and compressor and the high flow velocities through the turbine and compressor (about 70% the speed of sound) mean that the gas flow can achieve equilibrium conditions very rapidly (on the order of 0.3 – 0.4 ms). Thus pressure changes caused by speed changes or temperature or pressure changes will result in new equilibrium flow rates within about 1 ms or faster. A quasi-steady state approach to estimating the pressure changes and flow rates through the rotating machinery, such as used in the mean-line flow analysis methods is therefore justified. Because the flow and pressures reach their equilibrium flow conditions so rapidly (within the turbo-compressor wheel set), the time rate of change in flow through the system will be governed mainly by the rate of change of rpm which is in turn controlled by the moment of inertia of the shaft, wheels, and alternator as well as by the misbalance in the torque/power in the turbine, alternator, and compressor. The inertia due to the mass of gas with in the entire ducting network is currently ignored in the models. By way of comparison, we estimate the mass of the rotating turbomachinery components including alternator to be approximately 20-30 kg, while the mass of the coolant in the loop is only about 5 kg. Infact one way to account for the mass of the coolant is to add its inertia to the rotating components.

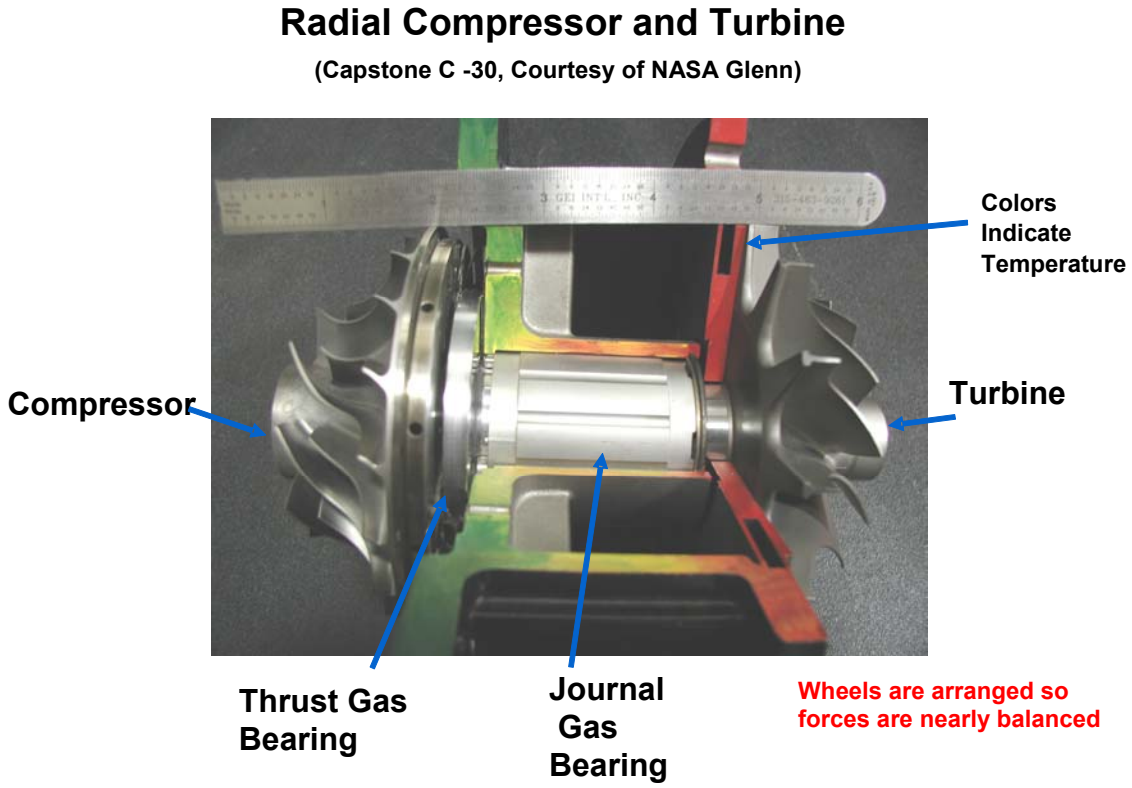

Figure 2-13 Capstone C-30 compressor and turbine wheels include the gas thrust and journal bearings. The compressor is on the left side and is relatively cool, (green colors) and the turbine is on the right (red colors for the housing and bearings. (courtesy of NASA).

Figure 2-13 also shows the gas journal bearing and the gas thrust bearing of the turbocompressor. The face side of the compressor and turbine are shown in Figure 2-14, and Figure 2-15 shows the compressor outlet diffuser and the turbine inlet nozzle. The bearings and turbo-compressor wheels are arranged so that the pressure difference across the face of the compressor wheel is balanced by the pressure difference across the turbine wheel. Also note that the bearings and shaft materials are cooler closer to the compressor than on the turbine side. Gas flow in the bearings is from the compressor side to the turbine side (from cold to hot) because the turbine inlet pressure is less than the compressor exit pressure.

The permanent magnet alternator shaft (not shown) is connected to the compressor and turbine shaft via a small rod or pencil-like shaft. The compressor inlet gas is the coldest gas in the entire CBC loop thus it is used to cool the alternator. The gas flows from the left side of Figure 2-13 into the compressor inlet and then is flung radially outward where it goes to the recuperator and then ultimately to the reactor. The hot gas from the reactor/heater enters in a narrow annulus in the right side of Figure 2-13, through the nozzle and then radially inward where it impacts and expands against the turbine blades and then flows axially out of the turbine face.

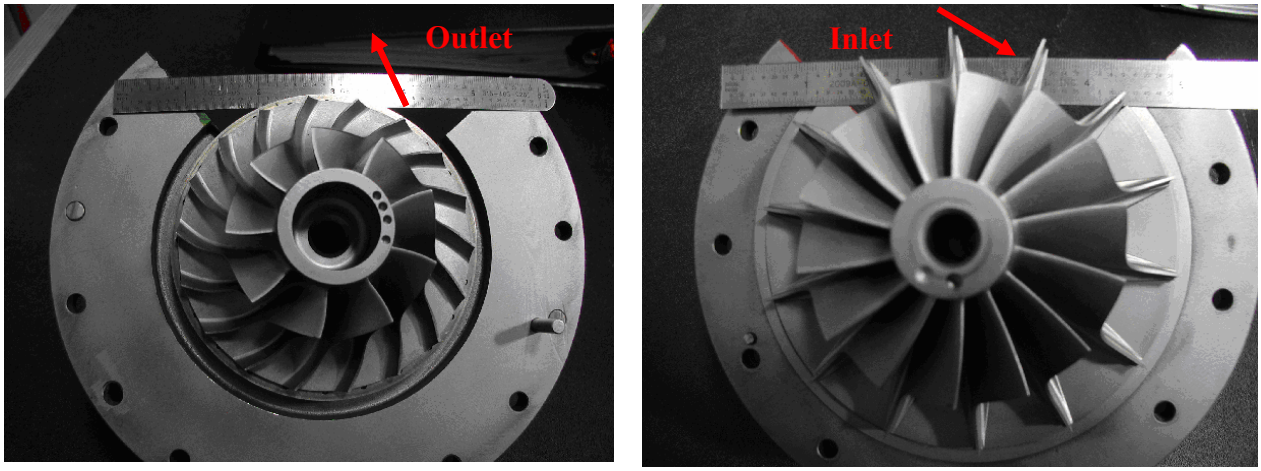

Figure 2-14: Face or front views of the Capstone C-30 compressor (left) and turbine. Note that the compress wheels blades are back swept while the turbine inlet blades are not. Also note that the turbine base is scalloped, this is likely done to help accommodate the gas flow from the inlet nozzle and presumably to help balance the thrust loads.

Based on these images and on others made during fabrication by Barber-Nichols Inc. (manufacturer of the Sandia Brayton Loop), we have been able to estimate most of the dimensions required to determine the characteristic flow curves. Table 2-5 and Table 2-6 summarize the approximate dimensions for the Capstone C-30 compressor and turbine.

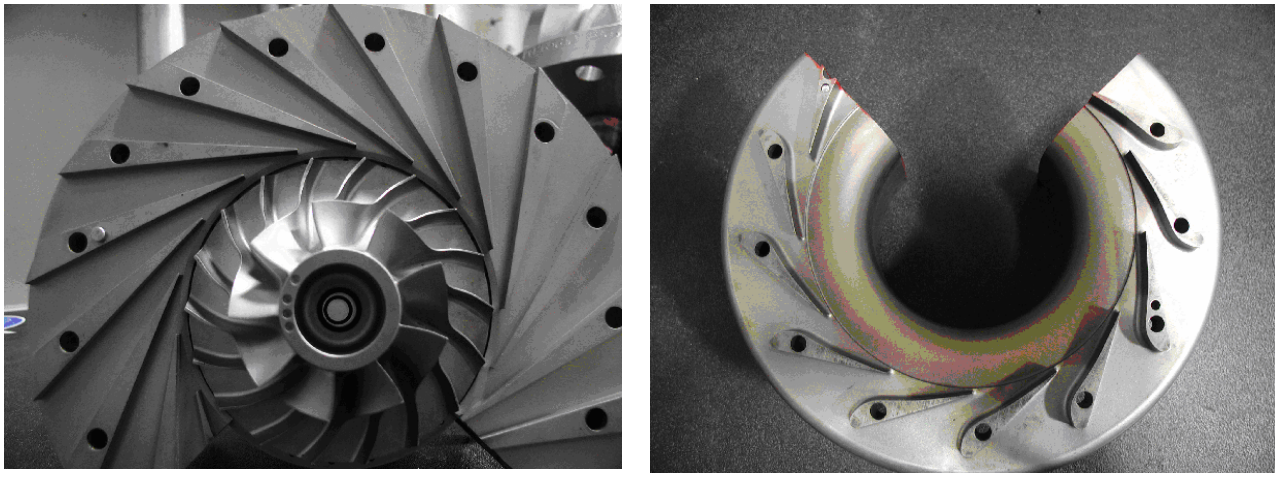

Figure 2-15: Compressor wheel and exit diffuser (left) and turbine inlet nozzle (right).

Table 2-5: Estimate of Capstone C-30 Compressor Dimensions

Capstone C-30 Compressor Dimensions (approximate)		
Description	**Variable Name**	**Value**
Tip Radius	r_{tip}	54.61 mm
Hub Radius	r_{h1}	11.73mm
Shroud Radius	r_{s1}	37.82 mm
Blade Height	b_2	7 mm
Blade Exit Angle	β_{2b}	-55 degrees
Blade Thickness	t_b	0.7 mm
Number of Blades	Z_r	18/9 (split + full / full)
Design rpm	N_{rpm}	96,000 rpm
Design Pressure Ratio p_{o2}/p_{o1}	r_c	3.7

Table 2-6: Estimate of Capstone C-30 Turbine Dimensions

Capstone C-30 Turbine Dimensions (approximate)		
Description	**Variable Name**	**Value**
Tip Radius	r_{tip}	50.81 mm
Hub Radius	r_{h1}	12.83 mm
Shroud Radius	r_{s1}	27.95 mm
Blade Height	b_2	3.6 mm
Blade Exit Angle	β_{2b}	-45 degrees
Blade Thickness	t_b	1.8 mm
Number of Blades	Z_r	18/9 (split + full / full)
Design rpm	N_{rpm}	96,300 rpm
Design Pressure Ratio p_{o2}/p_{o1}	r_c	3.7

2.3.2 Characteristic Flow Curves

As described in the introduction, the balance of power/torque in the turbo-alternator-compressor machinery provides the shaft power to force the coolant through the reactor. Therefore, the electrical load and the operating state (temperature, pressure, flow rate, revolutions per minute/rpm) of the turbo-alternator machinery and the state of the gas loop directly affect the flow through the reactor; and consequently affect the reactor power level as well.

The key to understanding and modeling this highly coupled process requires knowledge of the flow characteristics of the turbine and compressor and how the mass flow rate, and pressure drop in the turbine and pressure increase in the compressor are affected by the inlet temperature, pressure, and shaft speed.

It is not the intent of this report to describe how to design radial turbines or centrifugal compressors, or how to calculate the off-design flow performance curves for these devices. A number of excellent textbooks are available that describe how mean line flow analysis methods can be used to calculate the flow curves (Balje, Wilson, Walsh, Japikse). Also mean line flow

analysis tools and computer codes are available from NASA (NASA, 2005) that can be used to design and to determine off design performance for radial inflow turbines and centrifugal compressors (Wasserbauer, 1975) and (Galvas, 1983). Other codes are available for axial flow rotating machinery as well.

This report uses characteristic flow curves that were generated for two turbo-machinery sets. One is for the Sandia Brayton Loop that is based on the Capstone C-30 microturbine for which the compressor and turbine wheels have already been described. The other model is for a conceptual gas cooled space reactor concept that operates with a 132 kWe turbo-alternator-compressor set. Both systems use radial compressors and turbines, and as it turns out they are about the same size.

The characteristic flow curves for the C-30 turbine and compressor were generated from NASA off-design performance codes. For the 132 kWe Gas Cooled Reactor concept, we used flow curves that were generated by Concepts NREC under contract by Northrop Grumman Corporation. Concepts NREC has design and analysis software and classes that are available for purchase. These curves are used and presented with permission from Northrop Grumman Corporation. Characteristic mean line flow analysis curves for both TAC sets are presented.

The mean line flow curves were generated from the four NASA codes (rtd, rtod, ccd-quik, and ccodp, see NASA Software Index 2005). The code rtd is a radial turbine design code, rtod is a radial turbine off design performance code, ccd-quik is a centrifugal compressor design code and ccodp is a centrifugal compressor off design performance code. The codes, including source code, are freely available from NASA upon request. The input files were based on the dimensions shown in Table 2-5 and Table 2-6.

The fundamental assumption made by the dynamic model is that the flow is constant around the loop. With this assumption it is necessary to define the equations for each component that can give the outlet temperature and pressure given the inlet temperature, pressure, and flow rate. Therefore the characteristic flow curves must provide the exit temperature and pressure given the inlet conditions. The characteristic flow curves are defined as four functions:

$$\frac{p_{o2}}{p_{o1}} = f_{prC}(T_{o1}, p_{o1}, mdot, N_{rpm}), \quad 2\text{-}26$$

$$\frac{p_{o4}}{p_{o5}} = f_{prT}(T_{o4}, p_{o4}, mdot, N_{rpm}), \quad 2\text{-}27$$

$$\frac{T_{o2}}{T_{o1}} = f_{TrC}(T_{o1}, p_{o1}, mdot, N_{rpm}), \quad 2\text{-}28$$

$$\frac{T_{o4}}{T_{o5}} = f_{TrT}(T_{o4}, p_{o4}, mdot, N_{rpm}). \quad 2\text{-}29$$

These functions give the turbine and compressor temperature and pressure ratio as a function of inlet temperature and pressure and as a function of mass flow rate (mdot) and shaft speed (N_{rpm}). The shaft speed (N_{rpm}) is directly related to the mass flow rate through the turbine and compressor characteristic flow equations. Both the steady state and dynamic models use

multivariate polynomial fits to define these functions. Lookup tables can also be used, though we have not had much success with them.

2.3.2.1 C-30 Compressor Flow Map

The flow curves for the C-30 compressor are shown in Figure 2-16. These curves were generated by using the NASA code ccodp.exe and the input file is listed in Appendix A. The figure shows three plots, though only the pressure ratio and temperature ratio curve are needed. Each curve shows the efficiency, pressure ratio or temperature ratio as a function of corrected mass flow rate for various shaft speeds, the design shaft speed is 96,300 rpm.

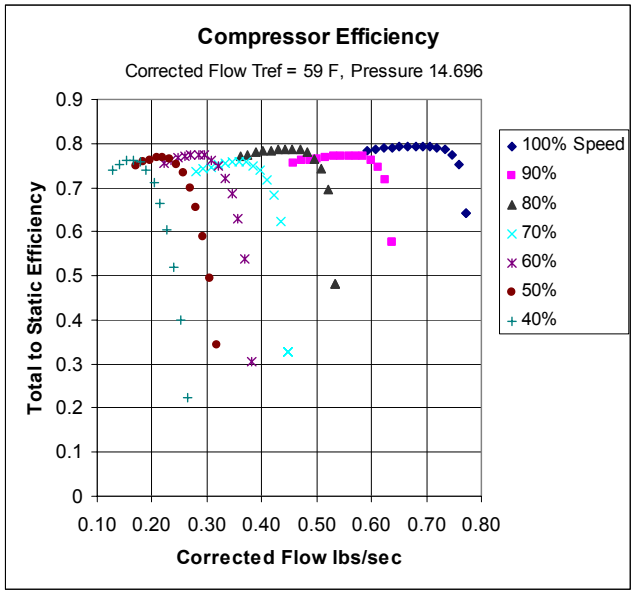

Figure

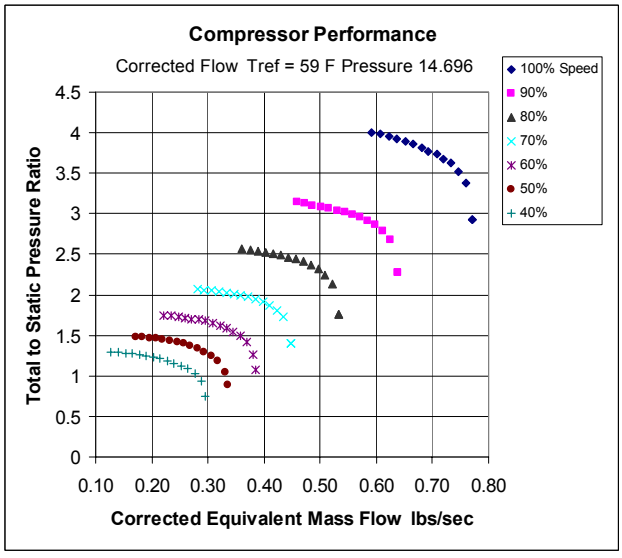

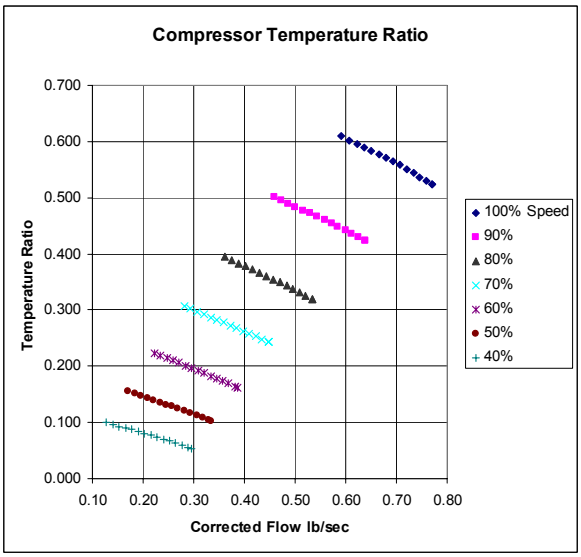

2-16

Figure 2-16 Characteristic curves for the Capstone C-30 compressor. The lower left figure shows the pressure ratio as a function of mass flow rate for constant rpm. The shaft rpm is shown parametrically. The lower right curve shows the temperature ratio,

and the upper curve shows the isentropic efficiency.

The corrected flow is defined as:

$$W_{eq} = \text{actual mass flow rate} * \sqrt{\left(\frac{T}{T_{std}} \Big/ \frac{P}{p_{std}} \right)} \qquad \textbf{2-30}$$

where T_{std} = 288.15 K and p_{std} = 101.3252 kPa. Note that for a fixed rpm the compressor pressure ratio decreases with increased flow rate, but at a certain flow rate the pressure ratio begins to decrease very rapidly, this represents the beginning of choked flow where the gas velocities are beginning to approach sonic speeds. At 96,300 rpm choked flow starts at a corrected flow rate of about 0.74 lb/s. Also note that as the rpm increases the pressure ratio increases even more (as illustrated by the increased spacing between the curves) which is evidence that the pressure ratio is roughly proportional to rpm^2.

The compressor efficiency curves show a few interesting trends. First for a given shaft speed, the efficiency has a maximum value, thus at flow rates above or below this optimum value the efficiency falls off dramatically. The width of the plateau around the maximum efficiency (versus flow) increases with increasing shaft speed. In addition the magnitude of the maximum efficiency also increases slightly with rpm. Overall though, it is seen that even at low shaft speeds (here at 40% of the design shaft speed) that good efficiencies can be achieved even at low speeds (close to 75% isentropic efficiency). At low speeds the efficiency appears to be about 5% less than at the design speed (at the ideal flow rate and design speed the maximum isentropic efficiency is 80%). It is possible to convert the efficiency and pressure ratio curves to the temperature ratio curves via equation 2-1 and the definition for polytropic efficiency.

An important limitation of these curves is that they are only valid over a range of shaft speeds and pressure ratios. During startup transients or other off-normal transients it will be important to assure that the system is operating within the range of validity. A related but different issue is that the dynamic and steady state models require some form of functional fit to these curves. We have found it necessary to extrapolate the data at low flows, at high flows and at low shaft speeds so that the functional fits provide physically meaningful results. Generally we use linear extrapolation rules, but at zero flow or zero rpm we assume that the pressure and temperature ratios extrapolate to 1.0.

The functional relationships for pressure ratio and temperature ratio can be greatly simplified if they are rewritten in terms of dimensionless flow and dimensionless speed. When this is done the equations for f_{PrC}, f_{PrT}, f_{TrC}, and f_{TrT} become functions of only the dimensionless flow and dimensionless speed. The dimensionless flow $\dot{m}'$ and N' are defined as

$$\dot{m}' = \frac{\dot{m} \cdot \sqrt{\frac{T_{in}\ R_o}{\gamma}}}{\left(2\ r_{tip}\right)^2\ P_{in}} \qquad \textbf{2-31}$$

$$N' = \frac{N \cdot 2\, r_{tip}}{\sqrt{\gamma\, R_o T_{in}}} \qquad \textbf{2-32}$$

Here N' has units of revolutions/sec. Thus the pressure and temperature ratio equations become

$$\frac{p_{o2}}{p_{o1}} = f_{prC}(T_{o1}, p_{o1}, mdot, N_{rpm}) = f_{prC}(m', N'), \qquad \textbf{2-33}$$

$$\frac{p_{o4}}{p_{o5}} = f_{prT}(T_{o4}, p_{o4}, mdot, N_{rpm}) == f_{prT}(m', N'), \qquad \textbf{2-34}$$

$$\frac{T_{o2}}{T_{o1}} = f_{TrC}(T_{o1}, p_{o1}, mdot, N_{rpm}) = f_{TrC}(m', N'), \qquad \textbf{2-35}$$

$$\frac{T_{o4}}{T_{o5}} = f_{TrT}(T_{o4}, p_{o4}, mdot, N_{rpm}) == f_{TrT}(m', N'). \qquad \textbf{2-36}$$

One of the benefits of using the non-dimensional form for the characteristic flow maps is that once they have been determined, they can be used for gases other than the one they were generated for. Likewise they can be used at other pressures, temperatures, and other sized wheels. This similarity concept is based on a dimensional analysis known as the Buckingham Pi Theory (Buckingham, 1914). The similarity concept is extremely useful because it means that turbo machines that are physically similar have similar velocity triangles, have similar ratios of gravitational to inertial forces, and when operating with fluids with the same thermodynamic quality will have equal fluid dynamic characteristics, and efficiencies.

A three dimensional plot of the dimensionless flow map for the C-30 compressor is shown in Figure 2-17. Note the grouping of points near the bend in the curve is where choked flow conditions are being approached. These data represent the original data as generated by the NASA ccodp.exe code and then converted to dimensionless form. The widely separated points to the left of this region are extrapolations, as is the single point at zero rpm and zero flow. The data in this curve was fit to a multivariate polynomial using the tools within Mathcad™. The multivariate polynomial equation is shown in

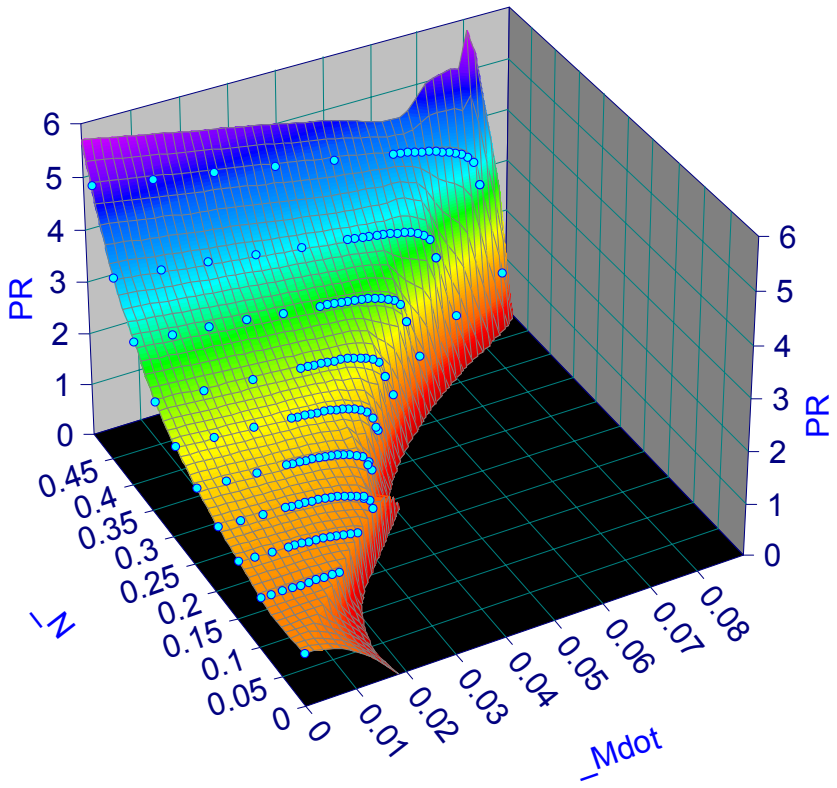

Figure 2-17: Three dimensional plot of the C-30 compressor pressure ratio versus dimensionless flow and shaft speed.

in equations 2-37 and 2-38. For the compressor the index i goes from 0…20, thus *i*max=20.

$$\Pr(x,y) = \sum_{i=0}^{i\max} Pcoeffs_i \cdot x^{II_{i,0}} \cdot y^{II_{i,1}} \qquad \textbf{2-37}$$

$$Tr(x,y) = \sum_{i=0}^{i\max} Tcoeffs_i \cdot x^{II_{i,0}} \cdot y^{II_{i,1}} \qquad \textbf{2-38}$$

The x variable represents the independent variable for dimensionless flow and the y variable represents the dimensionless speed. The exponential index numbers for x=flow and y=speed are listed in the II array that is listed in the first column of Table 2-7 , and the pressure coefficients are listed in the $Pcoeffs_i$ array, while the temperature coefficients are listed in the $Tcoeffs_i$. array. These arrays are provided below in Table 2-7. As a note, the same multivariate fitting process was also used for the turbine.

Table 2-7: Capstone C-30 Compressor flow map using the multivariate polynomial fit for the pressure ratio and temperature ratio.

C-30 Compressor Multivariate Polynomial Coefficients and Exponents

II =

	0	1
0	1	4
1	0	5
2	0	4
3	0	3
4	1	3
5	2	3
6	0	2
7	1	2
8	2	2
9	3	2
10	0	1
11	1	1
12	2	1
13	3	1
14	4	1
15	0	0
16	1	0
17	2	0
18	3	0
19	4	0
20	5	0

Pressure Coefficients

Pcoeffs =

	0
0	-917.428
1	349.506
2	-308.4632
3	128.3404
4	$-4.8109 \cdot 10^{3}$
5	$3.3625 \cdot 10^{5}$
6	-14.5707
7	$1.8121 \cdot 10^{3}$
8	$-1.334 \cdot 10^{4}$
9	$-7.0096 \cdot 10^{6}$
10	1.5794
11	202.9079
12	$-5.8758 \cdot 10^{4}$
13	$2.5136 \cdot 10^{6}$
14	$3.2199 \cdot 10^{7}$
15	0.9918
16	-63.2992
17	$6.8113 \cdot 10^{3}$
18	$-5.6204 \cdot 10^{4}$
19	$-8.6898 \cdot 10^{6}$
20	$-3.4187 \cdot 10^{7}$

Temperature Coefficients

Tcoeffs =

	0
0	-727.0394
1	83.7951
2	-95.0968
3	38.5725
4	647.6114
5	$9.3597 \cdot 10^{3}$
6	-2.776
7	-215.7061
8	$-1.909 \cdot 10^{3}$
9	$-1.4899 \cdot 10^{5}$
10	0.3769
11	28.1037
12	$-1.0167 \cdot 10^{3}$
13	$5.5081 \cdot 10^{4}$
14	$6.3814 \cdot 10^{5}$
15	0.9998
16	-2.4983
17	25.2698
18	$3.4158 \cdot 10^{3}$
19	$-2.4576 \cdot 10^{5}$
20	$-2.8537 \cdot 10^{5}$

2.3.2.2 C-30 Turbine Flow Map

The procedure for developing the flow map for the C-30 turbine was the same as for the compressor except that the NASA rtod.exe code was used were used to generate the flow data. This data was then non-dimensionalized and then fit using the multivariate process just described. The dimensionless flow maps are listed in Figure 2-18 and in Figure 2-19. These curves show both the temperature ratio (total-total) versus the dimensionless flow. Note that the curves show a different behavior than the compressor curves. For the turbine the pressure ratio increases with increasing flow, while it decreases for the compressor. Increased flow results in increasing pressure drop and is the same behavior that one would expect for a non-rotating component such as a duct or orifice. In the turbine the pressure ratio curves increase monotonically, in a manner that is roughly proportional to mass flow rate squared. Again higher rpm values produce higher pressure ratios, and at very high flow rates the curves begin to approach the choked flow region. The data in Figure 2-18 was extrapolated to 1.0 at zero

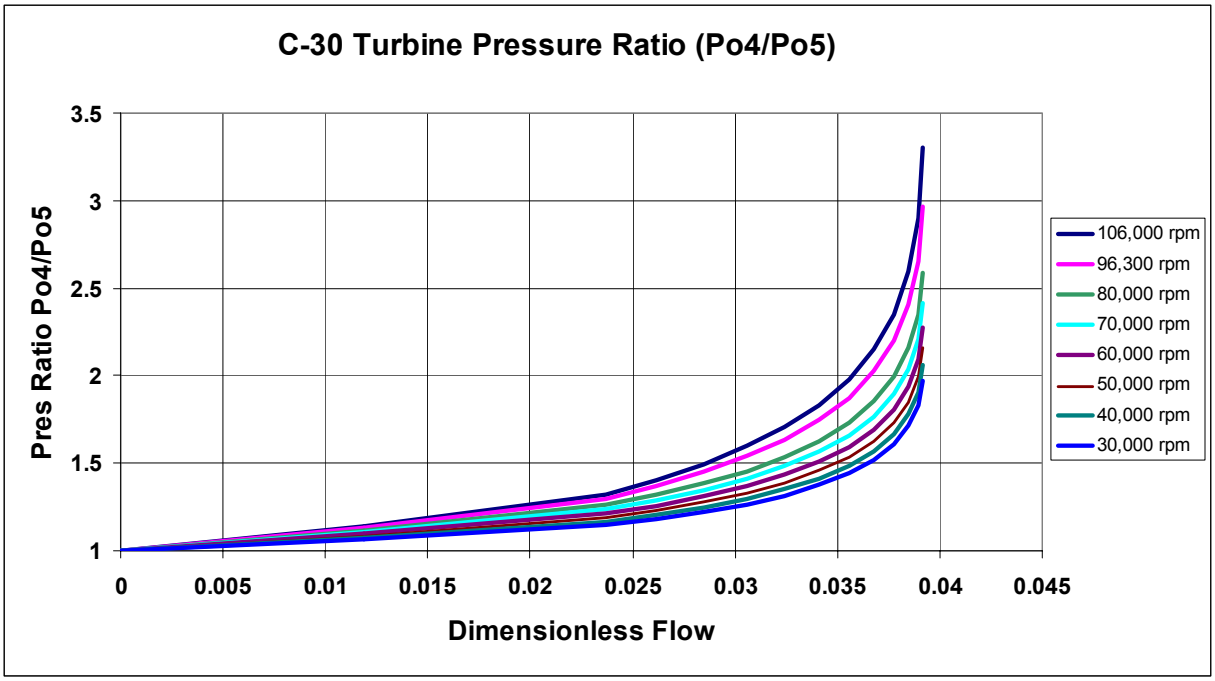

Figure 2-18: C-30 Turbine flow map for pressure ratio as a function of dimensionless flow. In this curve the extrapolation to a pressure ratio of 1.0 at zero flow is shown.

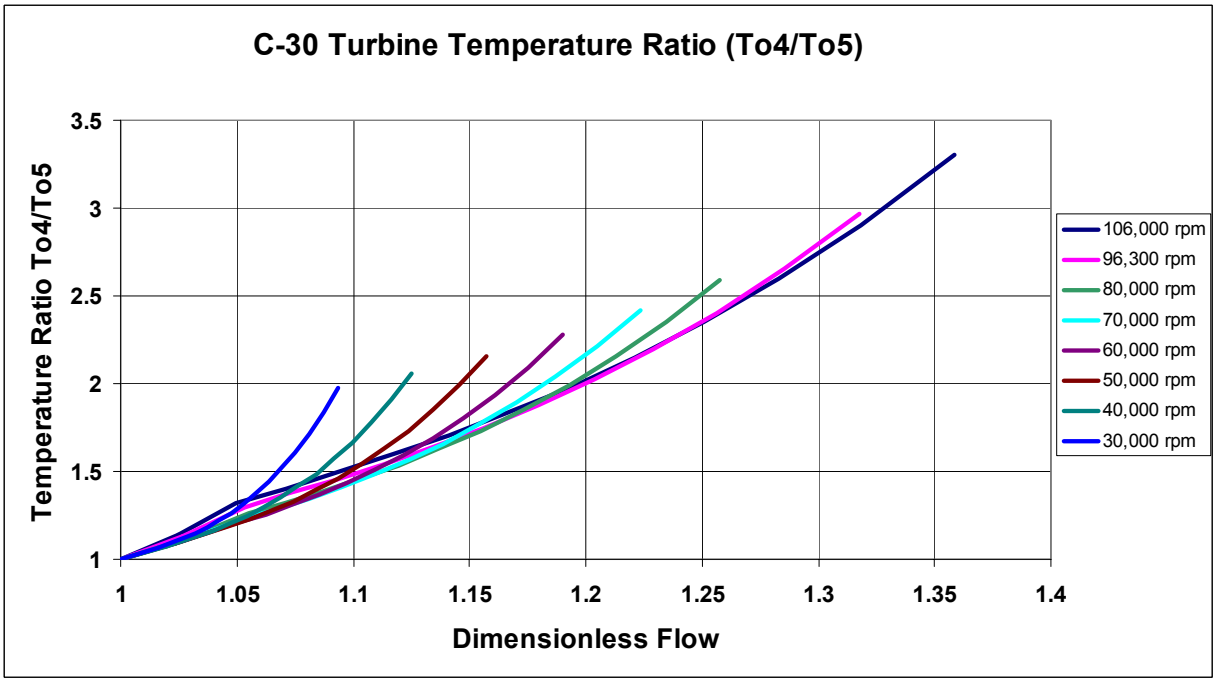

Figure 2-19: C-30 turbine temperature ratio characteristic flow curve plotting the temperature ratio as a function of dimensionless flow for various rpm values.

flow. The temperature ratio curves shown in Figure 2-19 were extrapolated to a temperature ratio of 1.0 at zero flow, but as seen in these curves an extrapolation to a value that is greater than 1.0 would appear to produce smoother characteristics. Figure 2-19 shows the same data

but plotted in a three dimensional map. Note that this form of display illustrates the need to extrapolate the data to zero rpm but for varying flow rates. At the time of writing of this report these extrapolations to zero rpm were not yet made.

As in the compressor the non-dimensional form of the flow curves for pressure and temperature ratio were fit to multivariate polynomials. The fits are identical to those described above however the index of iteration may vary. For the C-30 turbine the index i iterates from 0 to a max of 9. The same equations are used to determine the dimensionless flow and speed, but the dimensions for the turbine must be used for the tip radius. The parameters used in the multivariate fit for the turbine are shown in Table 2-8.

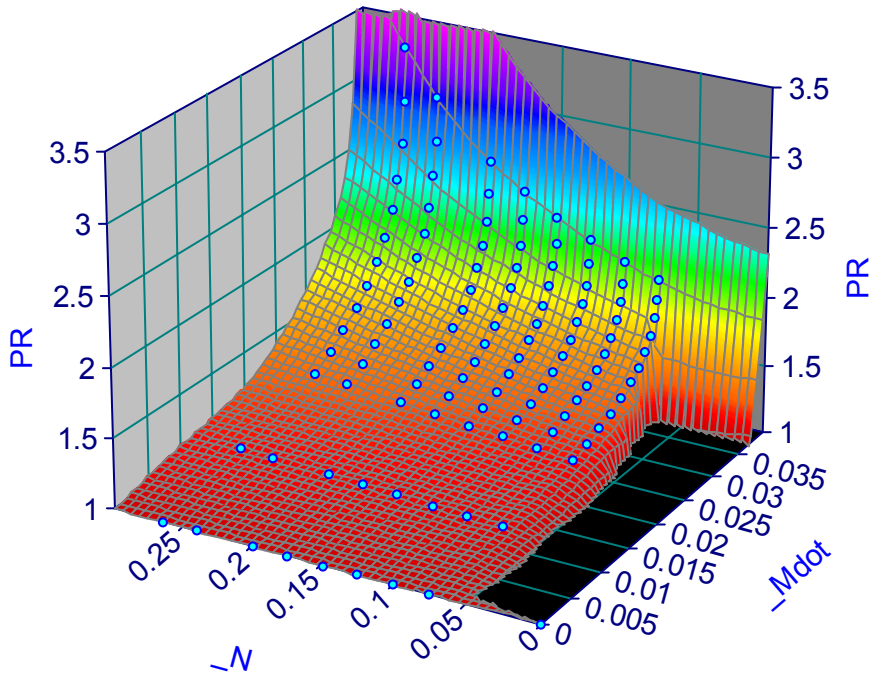

Figure 2-20: 3-D plot of the Capstone C-30 turbine dimensionless flow map.

Table 2-8: Capstone C-30 turbine flow map using multivariate polynomial fits for the pressure ratio and temperature ratio as a function of dimensionless flow and speed.

C-30 Turbine Multivariate Polynomial Coefficients and Exponents

II exponent for x = dimensionless flow and y = dimensionless speed

II =

	0	1
0	1	2
1	0	3
2	0	2
3	0	1
4	1	1
5	2	1
6	0	0
7	1	0
8	2	0
9	3	0

Pressure Coefficients

Pcoeffs =

	0
0	43.2342
1	-11.1408
2	-0.0125
3	1.5912
4	-116.9112
5	$1.4233 \cdot 10^3$
6	1
7	-19.583
8	$1.1588 \cdot 10^3$
9	$-2.2834 \cdot 10^4$

Temperature Coefficients

Tcoeffs =

	0
0	-14.2665
1	-4.4851
2	2.0369
3	1.624
4	-120.2468
5	$1.4829 \cdot 10^3$
6	1
7	-20.1697
8	$1.314 \cdot 10^3$
9	$-2.2362 \cdot 10^4$

2.3.3 132 kWe CBC Turbo-Compressor Description

A second set of turbo-compressor maps were developed to simulate the behavior of nuclear space reactors connected to closed Brayton cycle systems. These flow maps were developed by NGST (Northrop Grumman Space Technologies) as part of a trade study performed for the NASA Prometheus project (Wollman, 2005). The flow maps were generated for a helium-xenon gas mixture that assumed 5 weight percent He which is equivalent to 63.5 mole % He. The goal of this design was to select a system that had a relatively high reactor pressure (near 4 MPa) and turbine inlet temperature (1194 K). These values were selected in part to show that small radial turbines and compressors could be designed to operate with high efficiency (84.5 %, isentropic) at these relatively high pressures. As shown in the trade studies (2.2.4) the mass of the reactor and power conversion system can be reduced at high pressures. Other design conditions were that the compressor inlet temperature would be 400 K at 2.068 MPa, and the shaft rpm was selected to be 59,850 rpm. For these conditions compressor and turbine wheel design conditions (at least those values that were reported to Sandia by Concepts NREC) are listed in Table 2-9 and Table 2-10.

Table 2-9: Estimate of NGST/CNREC 132 kWe compressor dimensions.

Capstone C-30 Compressor Dimensions (approximate)		
Description	**Variable Name**	**Value**
Tip Radius	r_{tip}	50.81 mm
Hub Radius	r_{h1}	12.83 mm
Shroud Radius	r_{s1}	27.95 mm
Blade Height	b_2	3.6 mm
Blade Exit Angle	β_{2b}	-45 degrees
Blade Thickness	t_b	1.8 mm
Number of Blades	Z_r	18/9 (split + full / full)
Design rpm	N_{rpm}	96,300 rpm
Design Pressure Ratio p_{o2}/p_{o1}	r_c	3.7

Table 2-10: Estimate of NGST/CNREC 132 kWe Turbine Dimensions

Capstone C-30 Turbine Dimensions (approximate)		
Description	**Variable Name**	**Value**
Tip Radius	r_{tip}	54.61 mm
Hub Radius	r_{h1}	11.73mm
Shroud Radius	r_{s1}	37.82 mm
Blade Height	b_2	7 mm
Blade Exit Angle	β_{2b}	-55 degrees
Blade Thickness	t_b	0.7 mm
Number of Blades	Z_r	18/9 (split + full / full)
Design rpm	N_{rpm}	96,000 rpm
Design Pressure Ratio p_{o2}/p_{o1}	r_c	3.7

2.3.3.1 NGST/CNREC 132 kWe Compressor Flow Map and Multivariate Polynomial Fit

The flow maps or characteristic curves were generated by Concepts NREC corporation using their mean line flow analysis codes "COMPAL", and "RIT". Four curves for the compressor are presented here. Figure 2-21 shows the plots for the compressor power and the total-static isentropic efficiency for the compressor. Note that the efficiency curve shape is similar to the efficiency curve developed for the C-30 compressor using the NASA ccodp code, see Figure 2-16. The power plot is simply a reflection of mdot*Cp*dT. The temperature and pressure ratio characteristic curves are shown in Figure 2-22. The compressor curves are plotted as a function of corrected flow (as indicated in the flow title bar on the x-axis). Again it is seen that the shapes of these curves strongly resemble the shapes of the curves generated for the C-30 compressor, see Figure 2-16 .

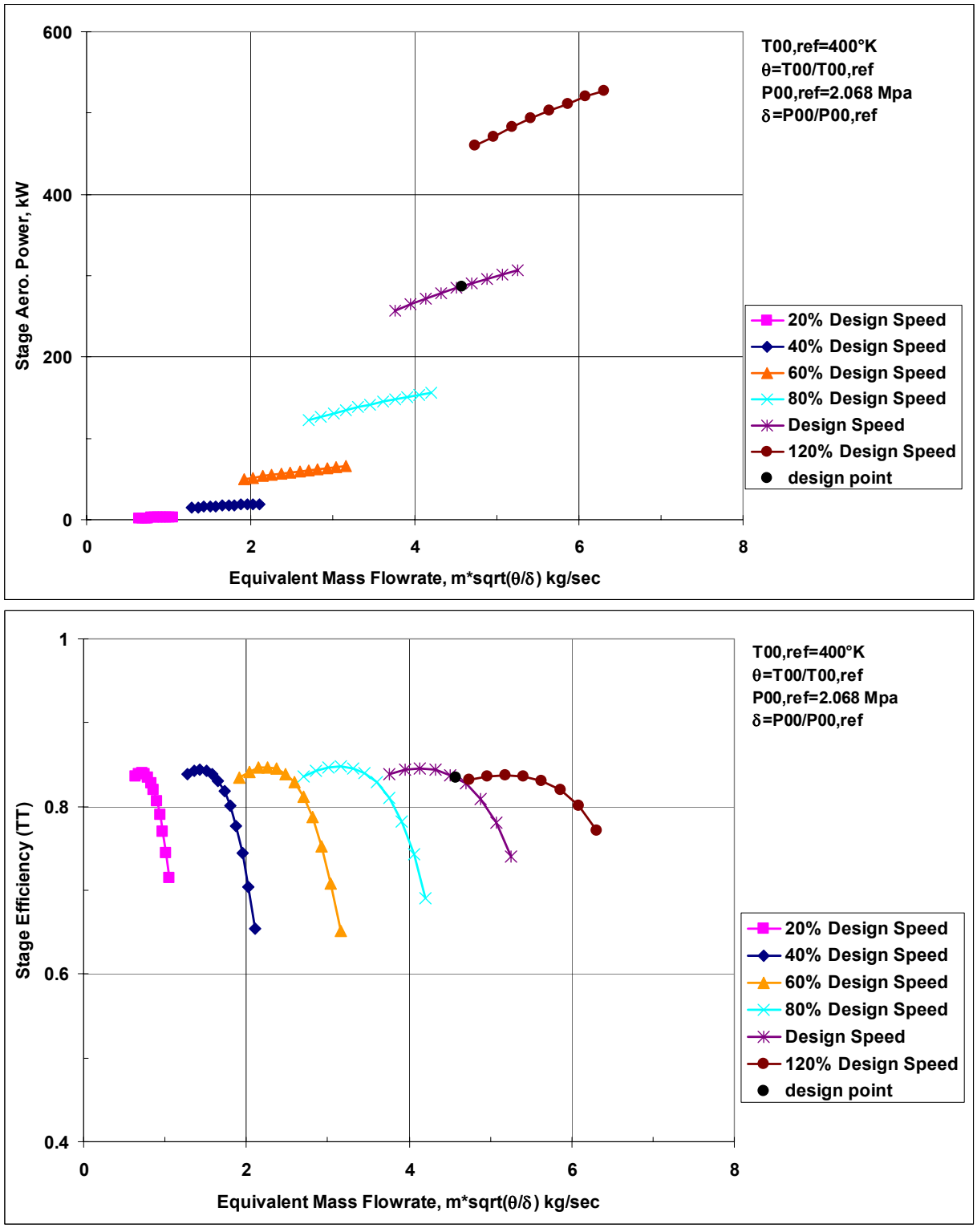

Figure 2-21: Power and efficiency for a 132 kWe gas cooled space reactor concept shown as a function of mass corrected mass flow rate for various shaft speed. The design shaft speed was 59,850 rpm.

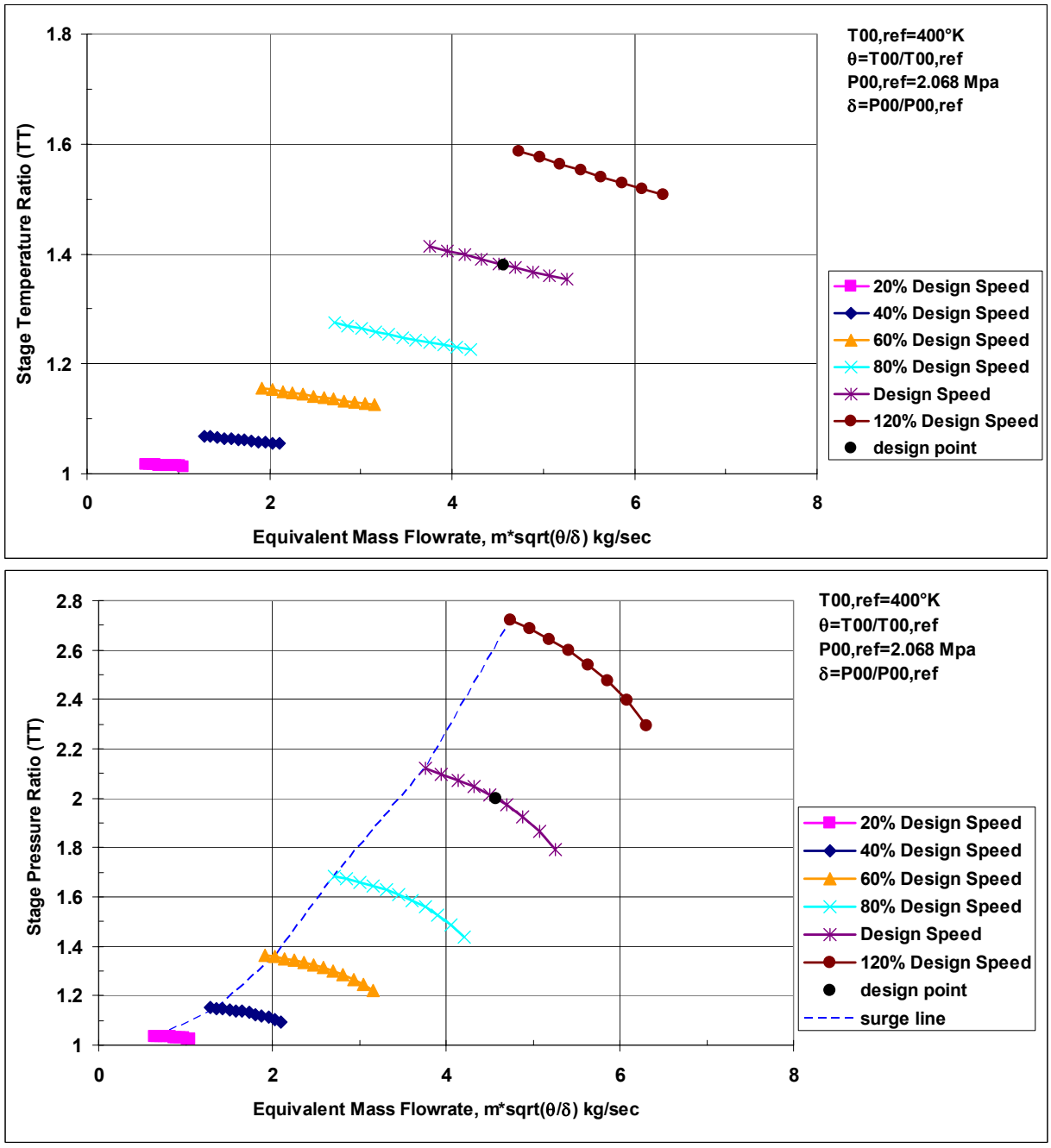

Figure 2-22: Compressor temperature ratio (top) and pressure ratio for a 132 kWe gas cooled space reactor shown as a function of mass flow rate for various shaft speeds. Design shaft speed is 59,850 rpm.

Table 2-11: NGST/CNREC 132 kWe Compressor flow map using the multivariate polynomial fit for the pressure ratio and temperature ratio.

NGST/CNREC 132 kWe Compressor Multivariate Polynomial Coefficients for Pressure Ratio and Temperature Ratio

II

II =

	0	1
0	1	3
1	0	4
2	0	3
3	0	2
4	1	2
5	2	2
6	0	1
7	1	1
8	2	1
9	3	1
10	0	0
11	1	0
12	2	0
13	3	0
14	4	0

Pressure Coefficients

cPcoeffs =

	0
0	$1.8031 \cdot 10^{4}$
1	-520.6477
2	34.5007
3	19.6882
4	$-1.8386 \cdot 10^{3}$
5	$-2.0698 \cdot 10^{5}$
6	-0.4882
7	-76.4001
8	$2.1884 \cdot 10^{4}$
9	$9.7017 \cdot 10^{5}$
10	0.9977
11	5.0964
12	-240.0294
13	$-6.794 \cdot 10^{4}$
14	$-1.588 \cdot 10^{6}$

Temperature Coefficients

Tcoeffs =

	0
0	-640.9217
1	26.1363
2	-5.9262
3	6.8463
4	130.3498
5	$5.7131 \cdot 10^{3}$
6	$-7.1431 \cdot 10^{-3}$
7	-27.0913
8	-855.8704
9	$-2.2354 \cdot 10^{4}$
10	0.9999
11	0.1408
12	34.8095
13	$2.2679 \cdot 10^{3}$
14	$2.7907 \cdot 10^{4}$

2.3.3.2 NGST/CNREC 132 kWe Turbine Flow Map and Multivariate Polynomial Fit

The flow maps or characteristic curves for the turbine were generated by Concepts NREC corporation using their mean line flow analysis code "RIT". The temperature and pressure ratio characteristic curves are shown inFigure 2-23. The turbine curves are plotted as a function of actual flow. Again it is seen that the shapes of these curves strongly resemble the shapes of the curves generated for the C-30 turbine, see Figure 2-18.

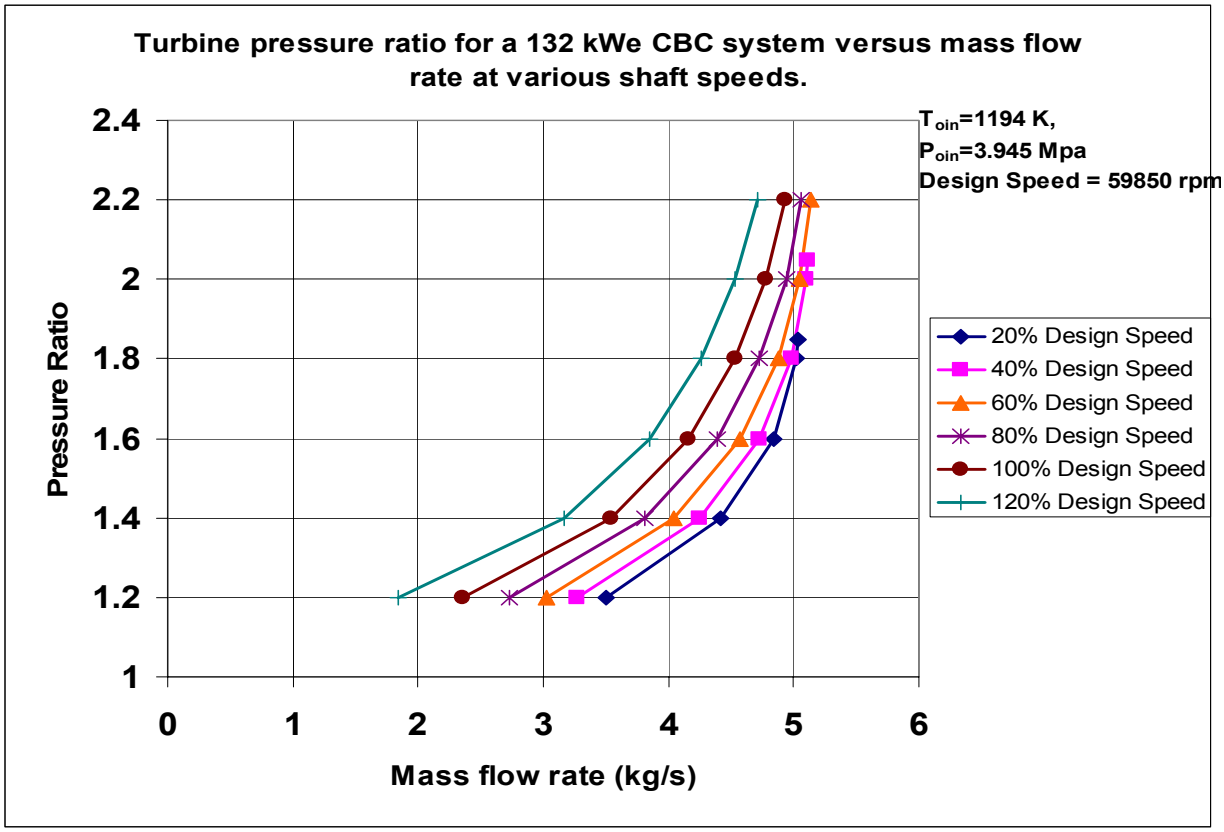

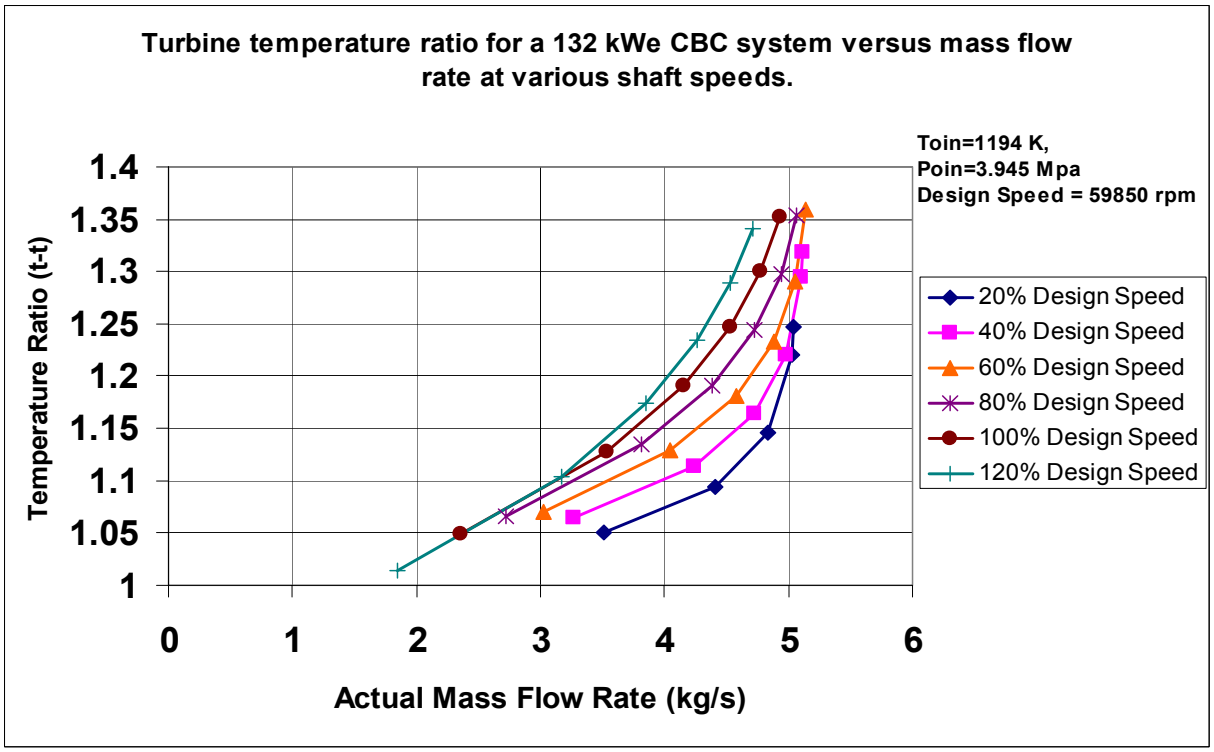

Figure 2-23: Turbine temperature ratio (top) and pressure ratio for a 132 kWe gas cooled space reactor shown as a function of mass flow rate for various shaft speeds. Design shaft speed is 59,850 rpm.

Table 2-12: NGST/CNREC 132 kWe turbine flow map using the multivariate polynomial fit for the pressure ratio and temperature ratio.

NGST/CNREC 132 kWe Turbine Multivariate Polynomial Coefficients for Pressure Ratio and Temperature Ratio

II

	0	1
0	1	2
1	0	3
2	0	2
3	0	1
4	1	1
5	2	1
6	0	0
7	1	0
8	2	0
9	3	0

Pressure Coefficients

	0
0	43.2342
1	-11.1408
2	-0.0125
3	1.5912
4	-116.9112
5	$1.4233 \cdot 10^3$
6	1
7	-19.583
8	$1.1588 \cdot 10^3$
9	$-2.2834 \cdot 10^4$

Temperature Coefficients

	0
0	-14.2665
1	-4.4851
2	2.0369
3	1.624
4	-120.2468
5	$1.4829 \cdot 10^3$
6	1
7	-20.1697
8	$1.314 \cdot 10^3$
9	$-2.2362 \cdot 10^4$

2.3.4 Turbo-Compressor Working Line

The tables Table 2-11 and Table 2-12 provide functional relationships that determine the temperature and pressure ratio as a function of inlet temperature, pressure, flow and shaft speed. For a CBC system with the turbine and compressor mounted to a single shaft, both the turbine and compressor are spinning at the same speed. Furthermore since the flow is in a closed loop the mass flow rate through the two devices is the same. Also to first order (neglecting pressure loss effects) the pressure rise in the compressor equals the pressure drop in the turbine (i.e., the turbine and compressor have the same pressure ratio). With these assumptions it is possible to plot the turbine and compressor pressure ratio curves onto a single plot to determine the steady-state operating line for a specified compressor inlet pressure (CIP) and temperature (CIT) and for a selected turbine inlet temperature (TIT).

Figure 2-24 shows this plot for the 132 kWe NGST/CNREC turbo-compressor set. This plot was made by plotting the compressor pressure ratio (black lines) for various rpm values but always assuming that the inlet temperature was 400 K, also the compressor inlet pressure was assumed to be 2.0 MPa. Likewise the turbine pressure ratio curves (blue lines) were made by assuming that the reactor provides a constant turbine inlet temperature (1200 K), but the turbine inlet pressure was determined by the compressor pressure ratio relationship. The intersection of the compressor and turbine pressure ratio curves, for the same rpm, also satisfy the constraint that the mass flow rate and pressure ratio are equal. The set of intersecting pressure ratio versus mass flow points defined by this intersection and at different rpm values define the operating line or steady-state working line (dotted red line) for the turbo-compressor.

As an example, for the specified TIT, CIT and CIP, the CBC loop can have a mass flow rate of 3kg/s only if the shaft speed is about 42,000 rpm and the pressure ratio is about 1.4. Of course this situation represents a lower power operation because we are not at the design point of 4.5 kg/s, 60,000 rpm and a pressure ratio of about 1.9.

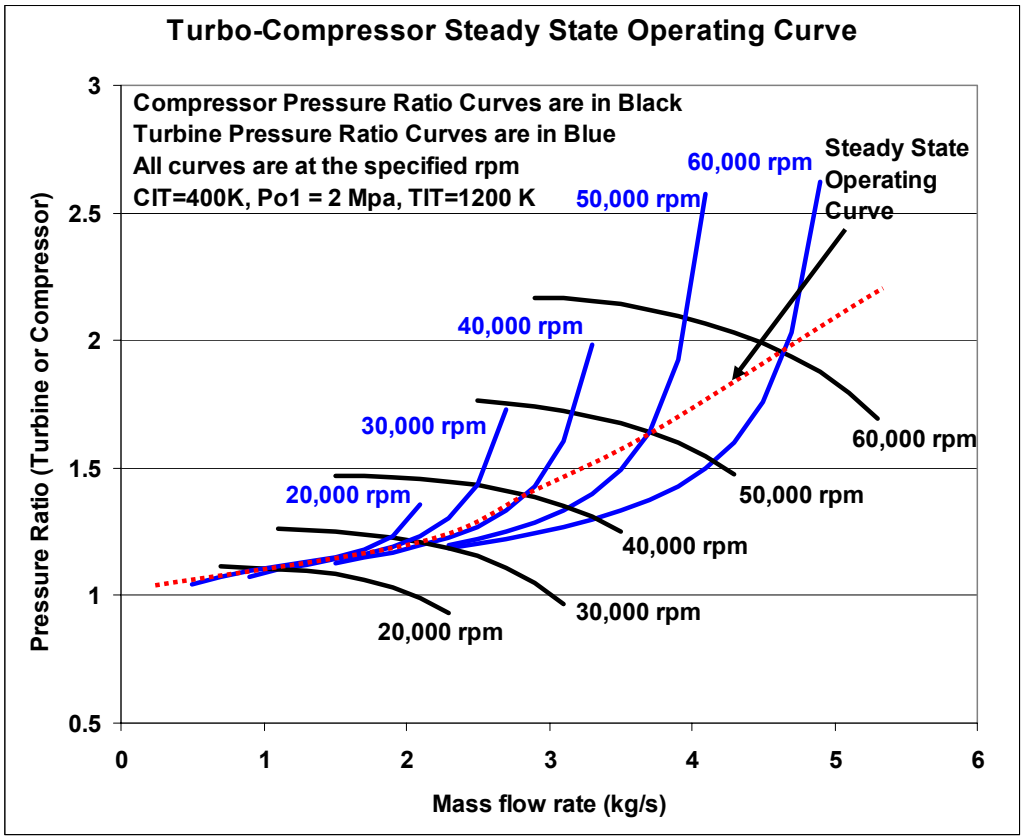

Figure 2-24: Steady state working line (dotted red line) for the 132 kWe NGST/CNREC CBC system with a 400 K, 2.0 MPa compressor inlet pressure and a 1200 K turbine inlet temperature. The working curve is determined by the intersection of the turbine and compressor pressure ratio curves for the same rpm values. This intersection point guarantees that the mass flow, rpm, and pressure ratio through the turbine and compressor all equal each other.

Similar steady state operating lines can be developed for other turbine inlet temperatures. For a lower TIT, the working-line would lie below the higher TIT working line. In this manner an entire operating map for the turbo compressor set can be filled out. A portion of this map is notionally illustrated in Figure 2-25. This figure has simplified the curve a bit by eliminating the turbine pressure ratio curves.

This type of plot is also useful for illustrating the dynamic behavior. Because the curve was generated for steady-state, accelerations or decelerations in rpm and flow will fall off the working-line. To accelerate the shaft speed requires additional pressures above what is needed for steady-state. Therefore accelerating transients will shift above the line (this is illustrated in Figure 2-25).

These working line curves and turbo-compressor operating maps are beginning to explain a number of features of the CBC system, but they are still incomplete, because they do not take into account the entire closed loop, or the reactor characteristics. These curves work very nicely for open gas turbine systems because the inlet pressure and temperature are indeed very nearly constant, and the turbine inlet temperature can be rapidly adjusted by scheduling fuel

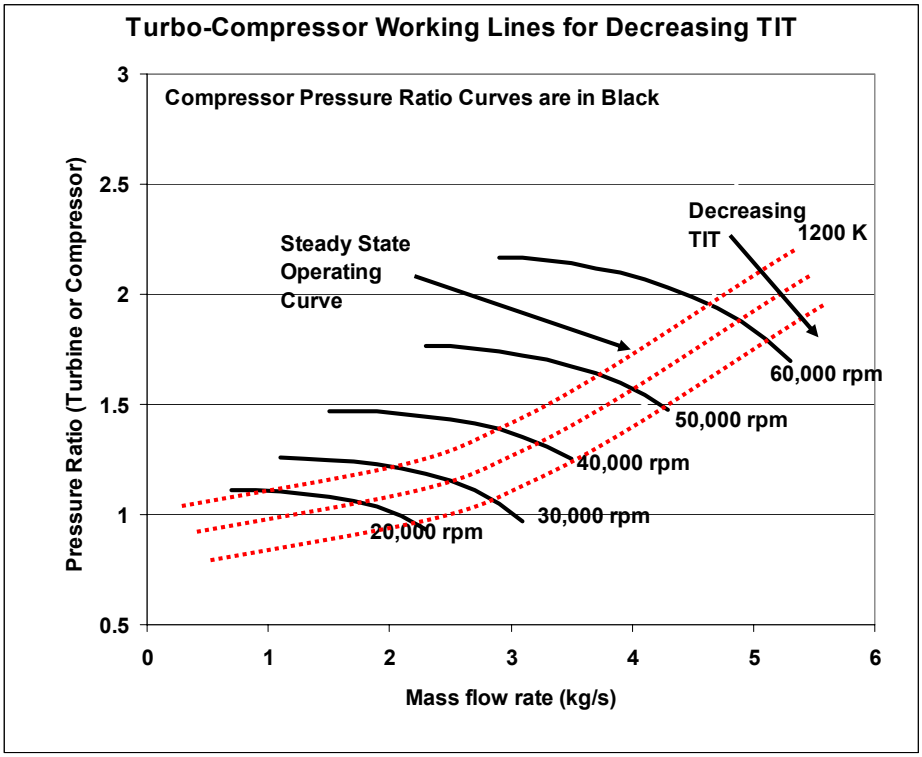

Figure 2-25: Map of the 132 kWe NGST/CNREC turbo-compressor working line.

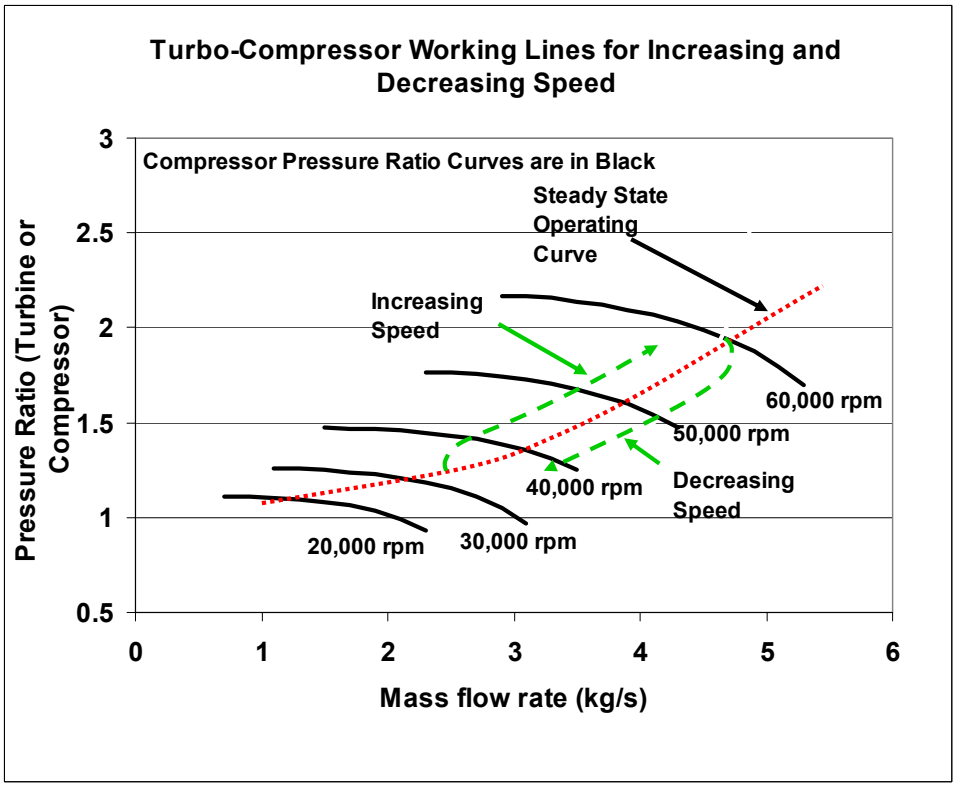

Figure 2-26: Transient behavior for shaft speed and flow accelerations (increases in power) and for deceleration (decreases in power).

to the combustor. Similar power or temperature control for a reactor driven CBC loop is not practical because it means rapidly cycling and changing the reactor fuel temperature. It can be done in principle, but it is relatively hard to do because the reactor mass is sufficiently large that the thermal capacitance will limit the rate at which temperature changes can occur. It would also reduce the lifetime of the materials due to the thermal cycling. The situation is even more complex, because the turbine and compressor are in a closed loop and have limited amounts of coolant volume. Thus accelerations in rpm will result in a larger pressure ratio, but they will also have a tendency to decrease the compressor inlet pressure, as the average pressure in the loop is staying constant. Therefore any model of the reactor driven CBC system must include these effects. These issues and many others are addressed in the next section where the steady state solution to a lumped parameter model of the reactor and CBC loop are modeled.

2.4 Lumped Parameter Steady State Gas Cooled Reactor Model

A simple lumped parameter steady state model for a reactor driven closed Brayton cycle is developed in this section. For convenience, the schematic diagram of a gas cooled reactor that is coupled to a CBC space reactor system is repeated in Figure 2-27. The temperature and pressures around the loop are indicated by subscripts beginning with o1 for the compressor inlet and o2 for the compressor outlet. The index increases in the direction of flow around the loop.

The model consists of a set of equations for each component, and one of the main goals in developing this model is to keep it as simple as possible. By keeping the model simple it is hoped that it will be easier to attribute reasons and simple explanations for some of the behavior observed in the CBC system. In addition, future work may attempt to provide limited forms of analytic solutions, thus simple models will be required. For the sake of simplicity, no pressure or temperature losses are assumed in the ducts, therefore T_{o3} which is the recuperator low temperature leg exit temperature is also the reactor inlet temperature. Likewise, T_{o4} is both the reactor outlet temperature and the turbine inlet temperature. In addition all temperatures and pressures are assumed to be the total temperature and the total pressure. The subscript o refers to the total temperature or pressure. The model also assumes that the coolant is a mixture of helium and xenon with 63.5 a% He.

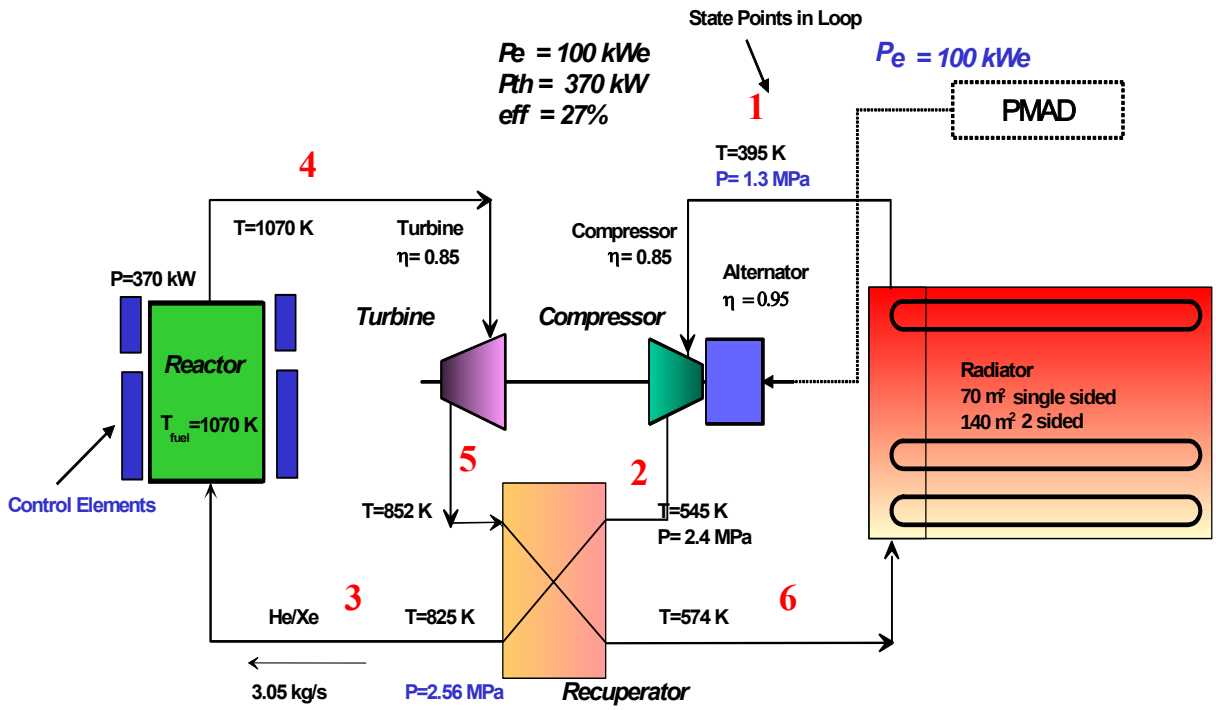

Figure 2-27: Schematic diagram of nuclear gas cooled reactor coupled to a simple recuperated Closed Brayton Cycle (CBC).

This section assembles the whole system of equations and presents some results. Once the steady state model is developed, it is relatively straight forward to generalize it so that the transient model can be solved.

2.4.1 Reactor Steady State Model

The equations for a simple steady state reactor are presented in Table 2-13 . In steady state the point kinetics model (Hetrick, 1971) solution is trivial for a reactor that has one negative feedback term that depends only on the average temperature of the fuel. In this case a steady state reactor behaves very much like a constant temperature machine and adjusts the reactor power level to keep the average fuel temperature constant with the fuel temperature being proportional to the amount of reactivity inserted.

Table 2-13: Lumped parameter steady state reactor and heat transfer equations.

Steady state equations for the reactor

$T_f = T_o + \rho_{insert} / \alpha_T$	Rx(1)	T_f	is the average fuel temperature
		T_o	is the initial fuel temperature (225 K)
$P_{th} = \dot{m} C_p \left(T_{o4} - T_{o3}\right)$	Rx(2)	α_T	is the negative fuel temperature feedback coefficient (cents/K) α_T = .02 cents/K
$P_{th} = h_A \cdot A_f \left(T_f - T_c\right)$	Rx(3)		cent = $\rho / (100\,\beta)$
		β	is the delayed neutron fraction = 0.0064
$T_c = (T_{o4} + T_{o3}) / 2$	Rx(4)	ρ_{insert}	is the inserted reactivity
		$h_A \cdot A_f$	is the effective heat transfer coefficient times the area from the fuel to the coolant A_f = 3.933 m^2, and h_A = *396.7* W/(m^2-K)
		C_p	is the heat capacity of the coolant C_p = 421.8 J/(kg-K)
		$\dot{m}$	is the mass flow rate through the CBC loop (kg/s)
		T_{o3}	is the reactor inlet temperature (K)
		T_{o4}	is the reactor outlet temperature (K)
		T_c	is the average coolant temperature

Table 2-13 lists the equations for the reactor, equations Rx(1) through Rx(4). As seen in this table the reactor is assumed to have one average fuel temperature, T_f. The average coolant temperature, T_c, is taken to be the average of the coolant inlet and outlet temperatures, and the steady state thermal power produced by the reactor is proportional to the temperature difference between the fuel and coolant, and the heat transferred to the coolant results in a net temperature increase of the fluid (To4 – To3).

The heat transfer coefficients and mass estimates were developed for a 313 pin reactor that uses UN fuel and was clad with Nb1Zr. The fuel diameter was 9 mm and the clad thickness was 0.5 mm. Each fuel pin was assumed to be 0.4 m long. These values were used to estimate the heat transfer coefficients and the thermal capacitance of the reactor. The mass of the pressure vessel and other structures were ignored in this form of the steady state model.

2.4.2 Recuperator Steady State Model

The recuperator model assumes a simple counter flow heat exchanger with the same fluid flowing through both legs of the heat exchanger. This type of model is fully described in Chapman, 1967 and Holman, 2001). The equations that were used are listed in Table 2-14 in

equations Rcp (1) through Rcp (2). The effectiveness was optimistically estimated to be 0.95. Given estimates of the materials and dimensions of the heat exchanger it is possible to determine the overall heat transfer coefficient of the heat exchanger and relate this via the NTU (Number of heat Transfer Units) to the effectiveness of the recuperator. The effectiveness is the ratio of the actual heat transferred to the maximum heat that could be transferred in an ideal heat exchanger (a counter flow heat exchanger of infinite area). It is in effect a measure of how closely the cooler temperature on the each side of the heat exchanger approaches the maximum temperature possible.

Table 2-14: Steady state counter flow recuperator model with recuperator effectiveness set to 0.95.

Recuperator steady state model

$T_{o3} = \varepsilon_x (T_{o5} - T_{o2}) + T_{o2}$	Rcp(1)	T_{o2}	is the compressor outlet temperature
		T_{o5}	is the turbine outlet temperature (K)
$T_{o6} = T_{o5} - \varepsilon_x (T_{o5} - T_{o2})$	Rcp(2)	T_{o6}	is the radiator/gas cooler inlet temperature (K)
		ε_x	is the effectiveness of the recuperator $\varepsilon_x = 0.95$

2.4.3 Turbo-Alternator-Compressor Steady State Model

Next the system of equations for the turbo-alternator-compressor (TAC) is described. For the turbine and compressor these equations are essentially the characteristic flow model described in the previous section of this report, however, we have made a few additional corrections to account for the pressure drop through the loop which is assumed to be 5% of the loop pressure.

Equations TAC(1) through TAC(4) are the characteristic flow equations through the compressor and turbine. TAC(1) defines the temperature ratio for the compressor, TAC(2) defines the temperature ratio for the turbine, TAC(3) defines the pressure ratio for the turbine, and TAC (4) defines the pressure ratio for the compressor. TAC(5) states that turbine inlet pressure p_{o4} is the compressor outlet pressure reduce by (5%) the fractional pressure drop in the loop. The fractional pressure drop is defined as the sum of all the fractional pressure drops for each component within the loop. We make the assumption that ε_{dp} = 5%. Equation TAC(6) is a new equation. It states that the power produced by the turbine less the power used by the compressor equals the power or load on the turbo-alternator-shaft. Effectively it is the alternator load. (Note that the electrical power produced by the alternator would be the load power times the efficiency of the alternator.) These three power terms must be in balance during steady state conditions, otherwise the TAC shaft speed would be increasing or decreasing.

Table 2-15: Turbo-alternator-compressor steady state model, based on the 132 kWe NGST/CNREC turbo-compressor set.

Turbo-Alternator Compressor Steady State Model

$$\frac{T_{o2}}{T_{o1}} = f_{TrC}(T_{o1}, p_{o1}, \dot{m}, N_{rpm}) \quad \text{TAC(1)}$$

$$\frac{T_{o4}}{T_{o5}} = f_{TrT}(T_{o4}, p_{o4}, \dot{m}, N_{rpm}) \quad \text{TAC(2)}$$

$$\frac{p_{o1}}{p_{o4}} \cdot = f_{prT}(T_{o4}, p_{o4}, \dot{m}, N_{rpm}) \quad \text{TAC(3)}$$

$$\frac{p_{o2}}{p_{o1}} = f_{prC}(T_{o1}, p_{o1}, \dot{m}, N_{rpm})(1-\varepsilon_{dp}) \quad \text{TAC(4)}$$

$$p_{o4} = p_{o2}(1-\varepsilon_{dp}) \quad \text{TAC(5)}$$

$$P_{load} = \dot{m} C_p (T_{o4} - T_{o5}) - \dot{m} C_p (T_{o2} - T_{o1}) \quad \text{TAC(6)}$$

$$\varepsilon_{dp} = \sum_{i=all\ components} \frac{dp_i}{p_o} \quad \text{TAC(7)}$$

T_{o2} is the compressor outlet temperature

T_{o5} is the turbine outlet temperature (K)

T_{o6} is the radiator/gas cooler inlet temperature (K)

ε_x is the effectiveness of the recuperator $\varepsilon_x = 0.95$

P_{load} is the power load on the TAC shaft

N_{rpm} is the shaft speed (revolutions/s or revolutions per minute)

ε_{dp} is the fractional pressure drop in the CBC loop, $\varepsilon_{dp} = 0.05$

2.4.4 Space Radiator Steady State Model

The space based radiator model is described in Table 2-16. Again a very simple model is used. In steady state it simply states that the heat or power lost by the coolant is radiated to space. The model assumes that there is a gas chiller or heat exchanger that transports the heat from the coolant to the radiator surface, with a constant temperature drop dT_{drop} of 50 K. In reality the temperature drop will depend on the power being radiated, but for this model a constant value is assumed. The thermal power total temperature difference between the radiator coolant inlet and outlet, $\dot{m}$ Cp (T_{o6} -T_{o1}) equals the power radiated to space as described in equation (RAD(1). The radiator is assumed to have a constant width and temperature for each radiating surface incremental area dA.

Table 2-16: Space radiator steady state model.

Turbo-Alternator Compressor Steady State Model

$$\frac{A_{rad}\,\sigma\,\varepsilon_{rad}}{\dot{m}\,C_p} = \int_{T_{o1}-dT_{drop}}^{T_{o6}-dT_{drop}} \frac{1}{T^4 - T_{space}^{\ 4}}\,dT \qquad \text{RAD(1)}$$

T_{o1} is the radiator coolant outlet temperature (K)

T_{o6} is the radiator coolant inlet temperature (K)

ε_{rad} is the emissivity the radiator $\varepsilon_{rad} = 0.9$

σ is the Stefan-Boltzmann Constant $\sigma = 5.67 \times 10^{-8}$ W/(m^2-K^4)

dT_{drop} is the temperature drop between the radiator coolant and the radiating surface per incremental area dA, $dT_{drop} = 50$ K

A_{rad} is the radiating area of the radiator (m^2), $A_{rad} = 300$ m^2

T_{space} is the effective temperature of space, in near earth orbit this value is taken to be $T_{space} = 225$ K

2.4.5 Gas Inventory Steady State Model

The last equations that are required to complete the set of equations is the gas inventory model. Even though the turbo-compressor model determines the pressure ratios and the mass flow rate, the absolute pressure is determined by the amount of coolant gas that is contained in the closed loop. For the sake of simplicity, the loop is assumed to have two effective coolant volumes, one for the low pressure leg of the loop and one for the high pressure leg of the loop. Each volume has a near constant pressure and an effective average temperature. The sum of the mass of coolant within each volume therefore equals the total mass in the loop which is kept constant.

Table 2-17: Gas inventory steady state model.

Turbo-Alternator Compressor Steady State Model

$$m_{fill} = \frac{P_{o1} \cdot V_{lp}}{R_o \cdot \overline{T}_{lp}} + \frac{P_{o2} \cdot V_{hp}}{R_o \cdot \overline{T}_{hp}} \qquad \text{INV(1)}$$

$$\overline{T}_{lp} = 0.2 \cdot T_{o1} + 0.8 \cdot T_{o6} \qquad \text{INV(2)}$$

$$\overline{T}_{hp} = \frac{T_{o3} + T_{o4}}{2} \qquad \text{INV(3)}$$

P_{o1} is the compressor inlet total pressure (Pa)

P_{o2} is the compressor outlet total pressure (Pa)

R_o is the gas constant $R_o = R/MW_{He/Xe}$ = 164.75 (J/kg-K)

T_{lp} is the effective average temperature of the low pressure leg

T_{hp} is the effective average temperature of the high pressure leg

V_{lp} is the low pressure leg volume, V_{lp} =0.1 m^3

V_{hp} is the high pressure leg volume, V_{hp} =0.15 m^3

m_{fill} is the CBC loop fill mass, m_{fill} =5.8735 kg

2.4.6 Steady State Equation Summary and Results for a Reactor Driven Brayton Cycle Power Conversion System

The complete set of equations is defined in Table 2-13 through Table 2-17. These tables correspond to the various CBC components including the reactor, the recuperator, the turbo-alternator-compressor (TAC), the space radiator, and they include the gas inventory constraint equation. With minor simplifications all of these equations have been collected into Table 2-18. Table 2-18 displays the equations in the form used for Mathcad™ Version 11.2a (Mathsoft, 2005) which was used to solve the equation set. One of the internal non-linear equation solvers (Levenberg-Marquardt) was used. The equation set lists the equations and variables introduced and counts or keeps track of them. The problem set consists of 14 equations with 16 unknowns. Because there are two more unknowns than equations, solutions can be only be obtained if two of the variables are treated as input parameters. The solution used here treats the reactor fuel temperature and the shaft rpm as the independent variables. Other pairs of independent variables have been used as well. For example, the same set of equations has also been solved using the TAC load and fuel temperature as the independent variables. Because the equations are non-linear, an iterative solution technique was used along with initial guesses for the solutions. Many of the initial guess values for the variables are listed on the right side of Table 2-18.

2.4.6.1 Steady State Operating Map at Constant Fuel Temperature

A very useful plot that illustrates many of the features of reactor driven closed Brayton cycle power conversion systems is illustrated in Figure 2-28 and in Figure 2-29. In Figure 2-28 the TAC shaft load (equivalent to the alternator electrical power produced divided by the turbo-alternator-compressor (TAC) shaft power is plotted as a function of shaft speed (rpm) for various average reactor fuel temperatures. The TAC power is equivalent to the alternator power divided by the total alternator efficiency that includes windage and electrical effects. We sometimes refer to this power as the alternator power. For completeness we also show the reactor power for the same conditions (see Figure 2-29). First let's examine the alternator power versus shaft rpm in Figure 2-28. The non-linear nature of the reactor driven Brayton cycle is illustrated in this plot. Note that for a given load (say 100 kW) at an average fuel temperature of 1100 K, that there are two shaft speeds that give steady state solutions. These are 47,000 rpm and 62,000 rpm. It is obvious that only one of these solutions will be the true value that the system will operate at because the shaft can only spin at one speed, but under what conditions? Before answering this question first observe in Figure 2-29 that the reactor power level at the lower rpm is about 280 kW_t while at 62,000 rpm the reactor power is about 400 kW_t. Obviously it would be highly desirable to operate at the lower shaft speed because much higher thermal dynamic cycle efficiencies could be achieved at the lower shaft speeds.

As will be shown later, for the set of equations listed in Table 2-18, the higher shaft speed is the only dynamically stable point. The lower rpm value is indeed a steady-state solution, but it is dynamically unstable without implementing some type of dynamic control system. Because the equations are steady state solutions, the dynamic effects are not captured in the solution.

In fact dynamic solutions of these equations show that for a fixed TAC load and for shaft speeds below the lower rpm steady-state point, the CBC loop will result in a system wide "stall"; that is, the shaft rpm will continue to decrease in speed until it stops. Similarly if the shaft speed is above the lower rpm "stall" value (again for fixed load), the shaft speed will increase and dynamically stabilize at the higher steady state rpm. These effects and more will be explained in more detail in subsequent sections of this report.

Other important data such as the "break-even" or "self-starting" conditions can also be obtained from the plot of TAC load (alternator power) versus shaft speed. The zero crossing locations indicate the "break-even" or self-starting / self-operating conditions for the reactor driven power conversion system. Thus at 25,000 rpm the average fuel temperature must be at least 500 K or greater for positive power to be produced, that is for the system to self start. At 40,000 rpm shaft speed the self-starting fuel temperature must be near 600 K and at 60,000 rpm the self-starting rpm is 800K. Some caution is advisable here, because the fits and extrapolations used to make the characteristic flow maps have inaccuracies at low shaft speeds and low flow rate. Nevertheless, we believe the trends and rough numbers as described here to be roughly correct. Future values may change as we improve our ability to model the flow curves near zero flow and zero rpm.

Table 2-18: Complete set of steady state equations for a reactor coupled to a closed Brayton cycle.

Given	Eqns	Variables	No of Variables	
$P_{th} = hAbar \cdot (T_f - T_{cbar})$	1	P.th T.f T.cbar	3	$P_{th} = 4.3548\times 10^{5}\,kg\,m^{2}\,s^{-3}$
$P_{th} = mdot \cdot Cp \cdot (T_{o4} - T_{o3})$	2	mdot T.o4 T.o3	4 5 6	
$T_{cbar} = \frac{T_{o4} + T_{o3}}{2}$	3			$T_{cbar} = 885.4227K$
$T_{o2} = rTrComp(T_{o1}, P_{o1}, Nrpm, mdot)$	4	T.o2 T.o1 P.o1 Nrpm	7 8 9 10	$T_{o2} = 521.3507K$
$T_{o5} = rTTurb(T_{o4}, P_{o4}, Nrpm, mdot)$	5	T.o5 P.o4	11 12	$T_{o5} = 783.3174K$
$T_{o3} = \varepsilon_x \cdot (T_{o5} - T_{o2}) + T_{o2}$	6			$T_{o3} = 770.2191K$
$T_{o6} = T_{o5} - \varepsilon_x \cdot (T_{o5} - T_{o2})$	7	T.o6	13	$T_{o6} = 534.4491K$
				$Nrpm = 1\times 10^{3}\,s^{-1}$
$p\_C = rprComp(T_{o1}, P_{o1}, Nrpm, mdot)$	8	p_C	14	p_C = 3.6171MPa
$p\_T = rprTurb(T_{o4}, P_{o4}, Nrpm, mdot)$	9	p_T	15	p_T = 1.8277MPa
$P_{o1} = p\_T \cdot (1)$	10			$P_{o1} = 1.782MPa$
$P_{o4} = p\_C \cdot (1 - \varepsilon_{dp})$	11			
$A_{rad} = \frac{mdot \cdot Cp}{\sigma \cdot \varepsilon_{rad}} \cdot \int_{T_{o1}-dT_{drop}}^{T_{o6}-dT_{drop}} \frac{1}{T^4 - T_{space}^4}\,dT$	12			$A_{rad} = 300m^{2}$
$P_{th} = P_{load} + [mdot \cdot Cp \cdot (T_{o6} - T_{o1})]$	13	P.load	16	
$mdot \cdot Cp \cdot (T_{o4} - T_{o5}) - mdot \cdot Cp \cdot (T_{o2} - T_{o1}) = P_{load}$				
$m_{fill} = \frac{P_{o1} \cdot V_{lp}}{R_o \cdot (.2T_{o1} + .8 \cdot T_{o6})} + \frac{p\_C \cdot V_{hp}}{R_o \cdot \frac{(T_{o3} + T_{o4})}{2}}$	14	Since this equation assumes no volume in the recuperator I should use the average temperature across the Rx and Radiator		

1 2 3 4 5 6 7 8 9 10 11 12 13 14

$cbcSys2(T_f, Nrpm) := Find(P_{th}, T_{cbar}, mdot, T_{o6}, T_{o5}, T_{o4}, T_{o3}, T_{o2}, T_{o1}, p\_C, p\_T, P_{load}, P_{o1}, P_{o4})$

Another important behavior illustrated in Figure 2-28 answers the question, what happens if I increase the flow rate by 10%. The answer is that it clearly depends on where you are on the curves shown in Figure 2-28. Because the equations are non-linear, the response to perturbations depends on the initial conditions. For example, if the initial operating point is on the positive slope of the curve, say at the red dot (P_{load_TAC}=100 kW, rpm =47,000, T_f=1100 K) then a small increase in shaft speed will result in an increase in the electrical load or TAC power level.

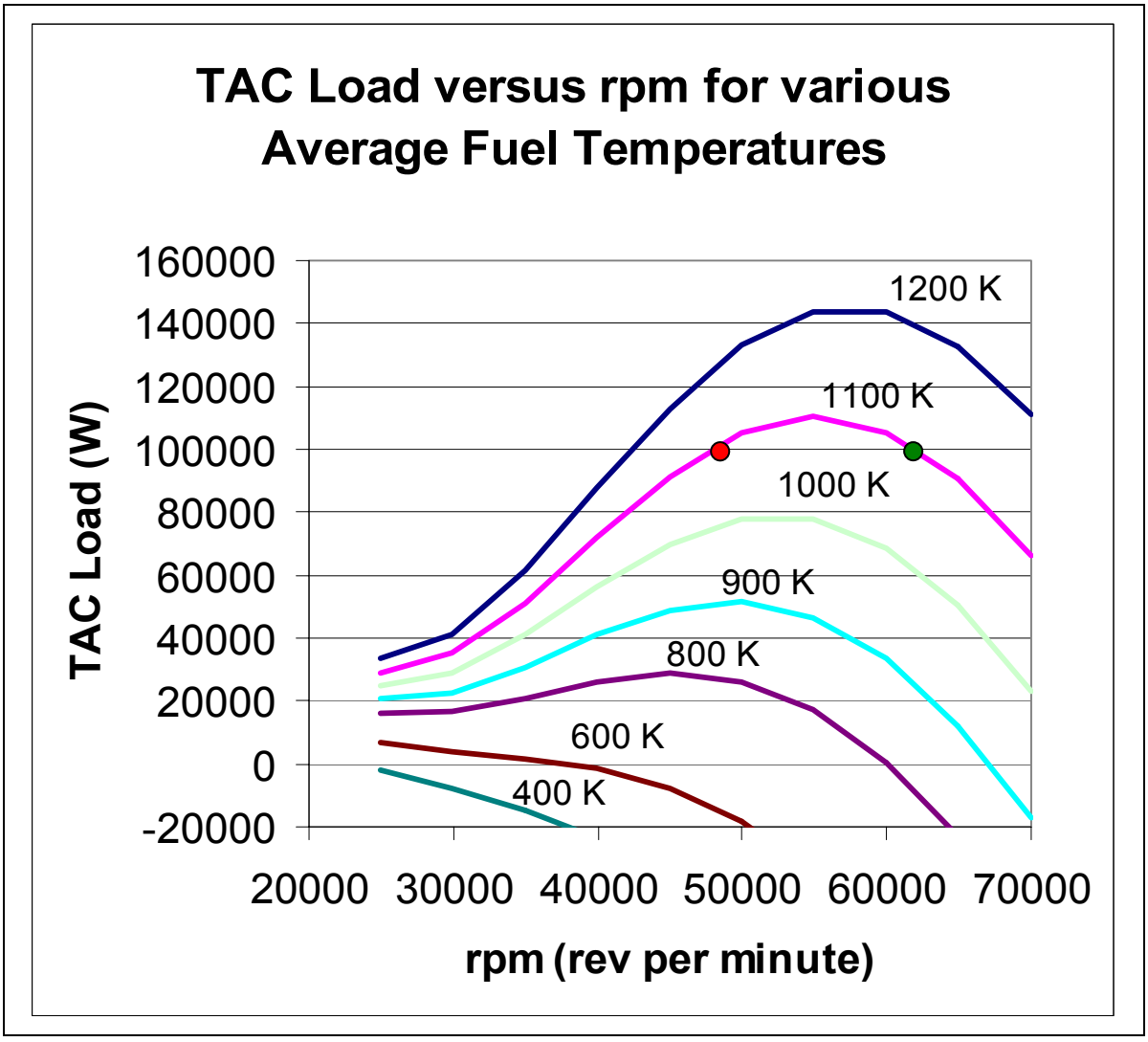

Figure 2-28: Alternator or TAC shaft load plotted as a function of shaft speed for various fixed turbine inlet temperatures.

Likewise if the initial operating point has a negative slope (for example at the green dot, P_{load_TAC}=100 kW, T_f=1100K, rpm=63,000) then a small increase in shaft speed will result in a decrease in TAC load or power generated. This behavior is real, and it has indeed been measured in the Sandia Brayton Loop (see Section 4.4).

The behavior of the reactor driven CBC system (on the negatively sloped portion of the plot) is counter intuitive as a decrease in load results in an increase in rpm but with a corresponding increase in reactor power. It is stable, and it will load follow, but it is probably not how one desires to operate the reactor and CBC machinery. Clearly operations on the left side or the positively sloped portion of the plot is more desirable as increases in rpm result in increased, power generation and increased reactor power level. As mentioned, this will require the use of an active feedback control system.

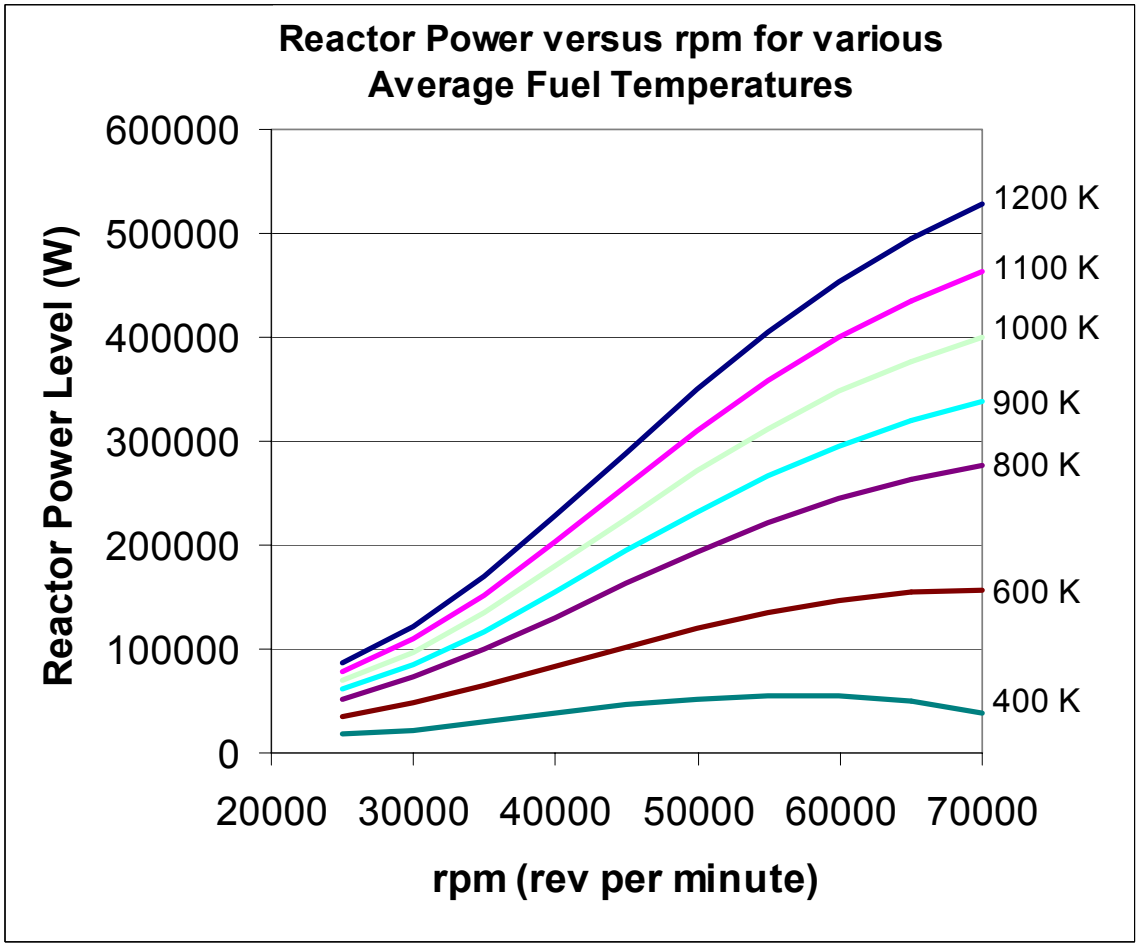

Figure 2-29: Reactor power shown as a function of shaft speed for various reactor average fuel temperatures.

2.4.6.2 State Point Temperatures at Constant Shaft Speed

Another interesting set of operating curves that can be determined from the steady state set of equations uses the TAC load, and the shaft speed as independent variables. When this is done we can solve the equations to determine the state point coolant temperatures, fuel temperature, and reactor power level that can be achieved a various fixed shaft speeds. Figure 2-32 shows how the gas temperatures vary for several values of fixed shaft speed. Note that fixed shaft speeds are equivalent to plotting the operating conditionsfor the Reactor CBC system based on a vertical line as shown in Figure 2-28. Note, that for the fixed speed cases, as one increases the electrical or alternator load, the turbine inlet temperature (and all other temperatures) also increases. The shapes of these curves, see Figure 2-30, are almost linear (straight lines) with respect to TAC power level. Also observe that the slope of the compressor inlet temperature is almost flat (due largely to the T^4 power removal capability of the radiator. This means that even for a space based system as the requested power levels go up the low temperature side of the radiator stays relatively constant. It also means that the reactor fuel temperature must increase if the power level increases (for fixed shaft speed). Because the average fuel temperature is related to the inserted reactivity, this means that for constant shaft speed

operations that reactivity will have to be inserted so that the required turbine inlet temperature can be maintained. The fuel temperature curves are is illustrated in

Figure 2-31.

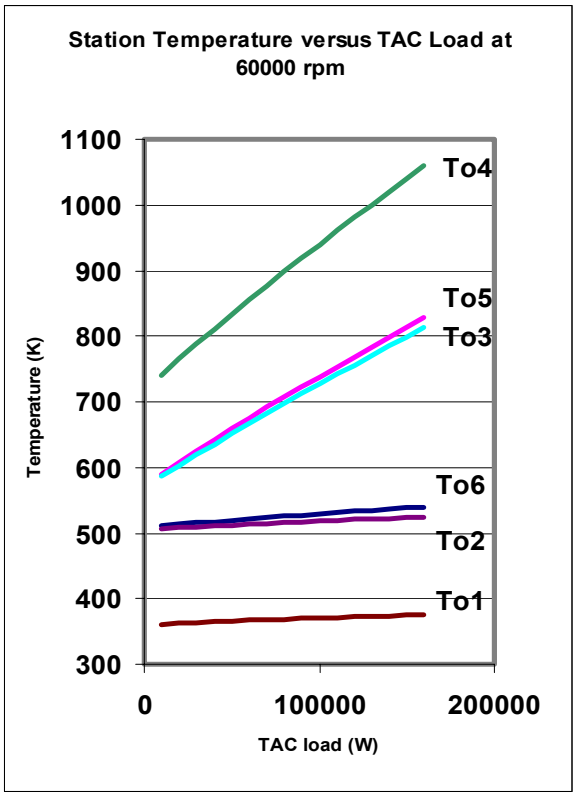

Figure 2-30: Coolant temperatures at the stations around the Rx-CBC loop.

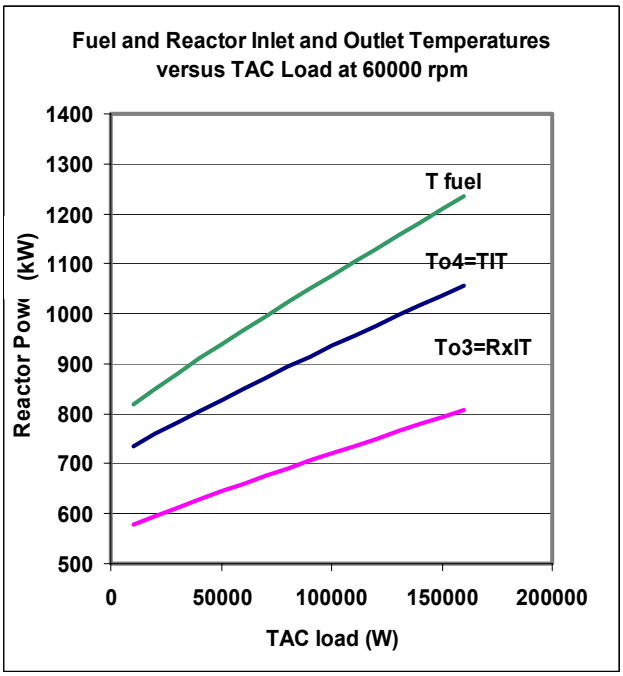

Figure 2-31: Average fuel temperature, reactor inlet and reactor outlet temperature at fixed speeds.

A related plot is shown in Figure 2-32. Here, for the same conditions as shown in Figure 2-30 the reactor power level is plotted as a function of requested TAC load or alternator power. Again a linear relationship is observed at various levels of shaft speed. At the lower shaft speeds the conditions required to extract large power levels require very high temperatures, so high that they will exceed the materials limits of the reactor and the turbomachinery.

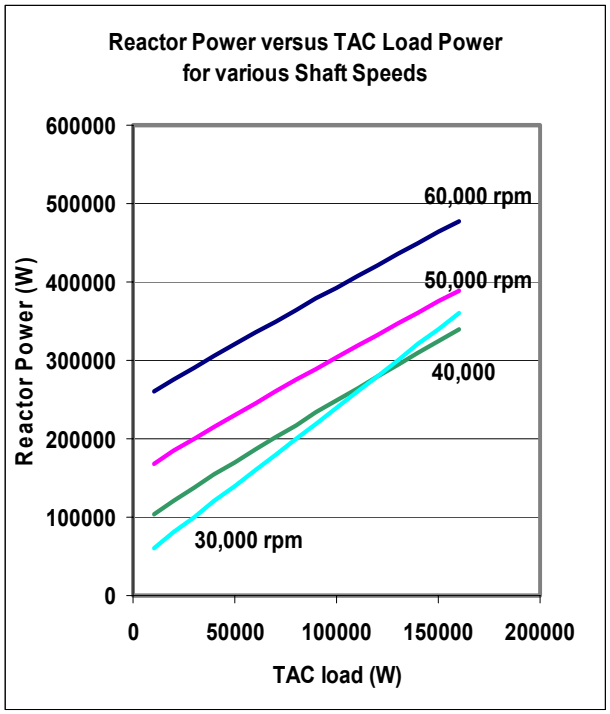

Figure 2-32: Reactor power level at several fixed shaft speeds shown as a function of TAC power or alternator power.

2.4.6.3 Stability Analysis

The analysis presented so far describes the steady state operating conditions, but it does not tell us much about the stability of the system nor how to control the system. One way that we have been able to understand the stability of the Rx-CBC system is to make a minor change to the steady-state equations so that it can be solved with an additional parameter that is sensitive to the dynamics of the system. During steady state the flow rate through the loop must be fixed, but during a transient the flow will likely be changing due to a misbalance of the torque or excess load/power on the TAC shaft. The shaft torque or excess power can be solved for if equation TAC(6) is modified so that the balance of the turbine power, compressor power and alternator power is determined, rather than being forced to be zero. With this change equation TAC(6) now becomes

$$P_x = P_{load} + \dot{m} C_p \left(T_{o4} - T_{o5}\right) - \dot{m} C_p \left(T_{o2} - T_{o1}\right) = P_{Load} + P_{turbine} - P_{comp} \qquad \textbf{2-39}$$

where P_x is the excess power to the shaft. Note that the torque is just power divided by angular frequency, thus $\tau_{TAC}=P_x / (2\pi N)$, where N is just the shaft rotational speed in revolutions per second. When the excess power to the TAC shaft is positive, the shaft speed will be increasing, likewise when the excess TAC shaft power is negative, it will be slowing down; and when it is zero the shaft speed will not be changing.

The equation set introduces a new independent variable P_x, into the solution. For the solution method we take the TAC load, the fuel temperature, and the shaft speed as the independent variables (P_{load}, T_f, and N_{rpm}) and now solve for P_x among other variables such as fuel temperature reactor power level, gas temperatures and gas pressures. A plot of P_x as a function

of rpm can now be made for various fuel temperatures. This plot is shown in Figure 2-33 for fixed fuel temperatures (1050 K, 1100 K, and 1150 K), and when the alternator load (P_{load}) is set to 100 kWe. The plot is repeated in Figure 2-34 for fixed power levels that are parametrically varied from 100 kWe to 130 kWe in increments of 10 kWe for a fixed fuel temperature of 1200 K.

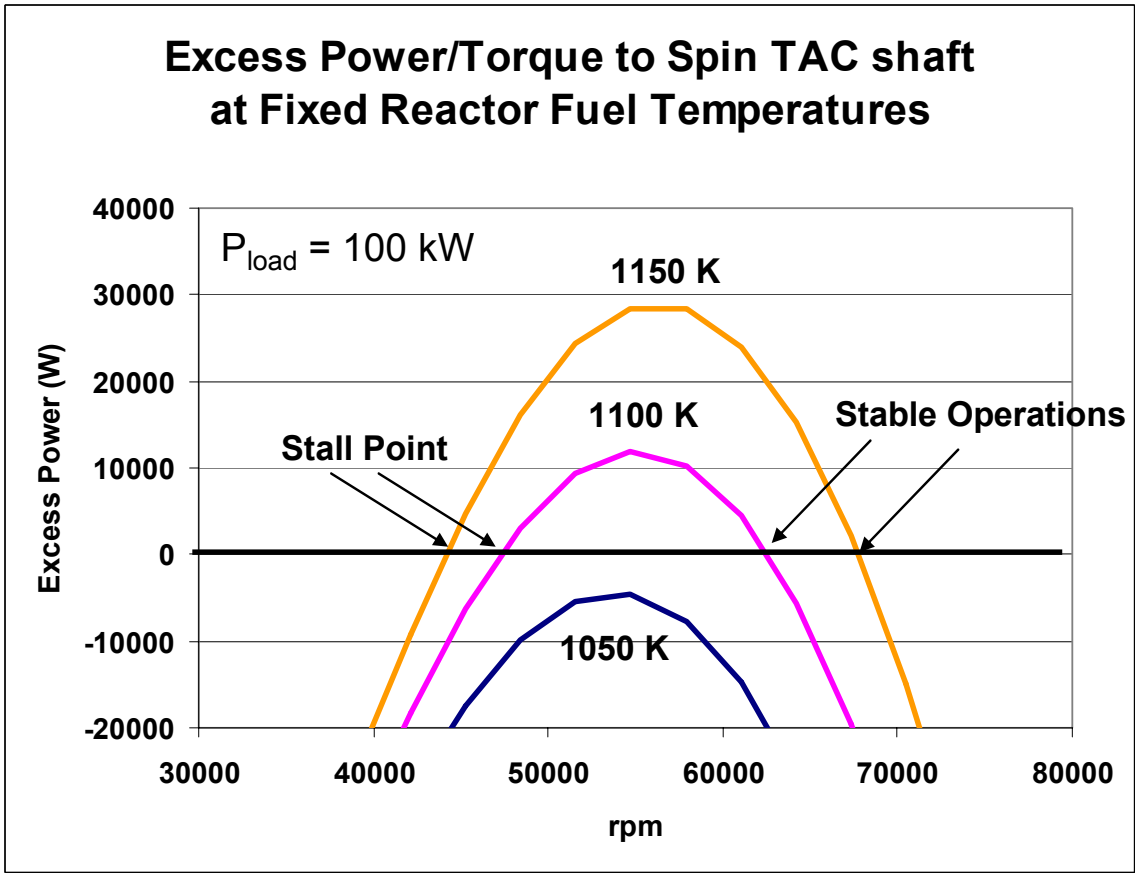

Figure 2-33: Excess power to spin the TAC shaft as a function of shaft rpm at various, but fixed, average fuel temperatures and for a fixed alternator load of 140 kW. When the excess shaft power is positive the shaft speed is increasing. When it is negative the shaft is slowing, and when the excess shaft power is zero, then steady state conditions are achieved.

First again note that for a fixed load that there are two steady state operating points as predicted earlier. For example a 100 kWe alternator load with an 1100 K average fuel temperature has two shaft speeds with $P_x = 0$, and these speeds are 47 ,000 rpm and 63,000 rpm. Note that these values are the same as those predicted in Figure 2-28, for the 1100 K average fuel temperature case with 100 kWe as the TAC load. Also observe that there are some conditions that have no steady state solution, such as the 1050 K fuel temperature line at 100 kWe. This is simply a reflection of the fact that the fuel temperature (or turbine inlet temperature) must be above some value (defined by the curves in Figure 2-28) in order to operate.

Now let's look more closely at these two steady state points. Let's assume that we are at steady state at 100 kWe, with $T_{fuel} = 1100$ K, and with a shaft speed of 67,000 rpm. If some perturbation caused the rpm level to increase a bit, the plot in Figure 2-33 shows that P_x

decreases and becomes negative. A negative excess power or torque will slow the shaft speed forcing the rpm to return to its original value. Likewise if the perturbation decreased the speed from 67,000 to a smaller value, then the excess torque or power becomes positive which will increase the shaft rpm and return it to the original value. Therefore, we see that the zero crossing points with negative slopes are stable operating locations. Indeed we have run dynamic models and found these points to be stable.

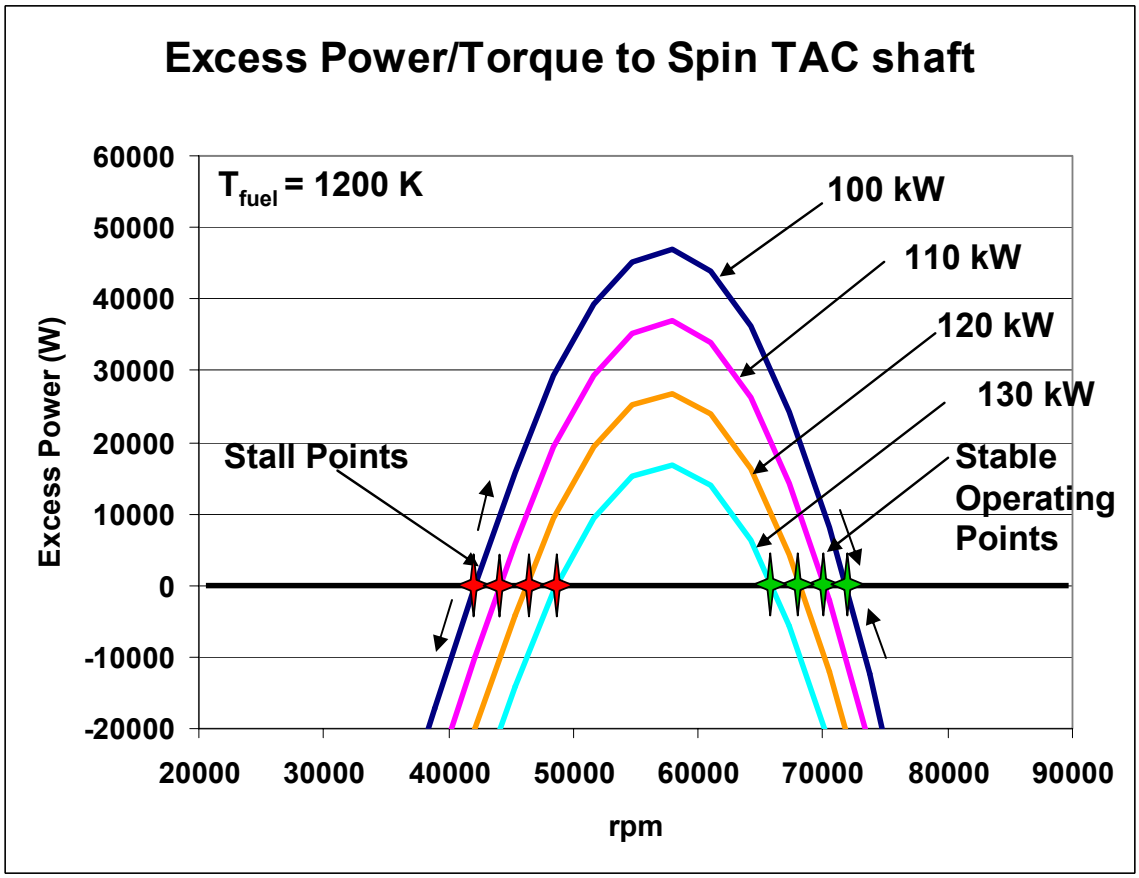

Figure 2-34: Excess power to spin the TAC shaft as a function of shaft rpm at various, but fixed, alternator power levels and for a constant fuel temperature of 1150 K. When the excess shaft power is positive the shaft speed is increasing. When it is negative the shaft is slowing, and when the excess shaft power is zero, then steady state conditions are achieved.

Now let's look at the steady state (zero crossing points) with positive slope, (i.e. the zero crossing locations at lower shaft speeds). Assume that the alternator power is 100 kWe, the rpm is 47,000, and the average fuel temperature is 1100 K. This corresponds to the zero crossing location for the purple curve in Figure 2-33. Now lets assume that a perturbation decreases the shaft speed. In this case the torque or excess alternator power becomes negative which further slows the shaft speed. This slowing will continue resulting in a system wide "stall". In contrast, if the perturbation increases the rpm, a positive excess torque on the shaft is created and this will increase the speed of the shaft even more, which results in even more positive torques that further increase the speed. The speeds and power levels will follow the

constant temperature curve around the hump in the curve until it reaches the stable point where it stabilizes.

Therefore we see that the steady state locations with negative slopes with respect to power or torque are stable at a system level and have a tendency to return to their equilibrium or steady state level. In contrast, the steady state points with positive slope with respect to power or torque are unstable. As mentioned earlier, the stable operating characteristics are a bit counter intuitive because decreases in load will result in increased shaft speeds and higher power levels. Even though this behavior is stable, and will load follow it is not how we wish to operate the power plant largely because it is not as efficient an operating point.

2.4.6.4 Control Issues and Discussion

The preceding analysis and discussion shows that an active control system will be needed to provide controlled perturbations that have the effect of operating at or near the positively sloped portion of the power rpm curves (lower rpm side of the curve).

The stability discussion above suggests that an active load control scheme will be capable of keeping the shaft rpm at the desired rate if a feedback loop is inserted into the control system that continually adjusts or dithers the TAC load to keep the shaft rpm at the requested set point. Furthermore, if the system wide state points are very close to the steady state solution then the amount or size of the perturbations/dithering required to keep the system at the requested rpm can be very small. This type of control system is used in the solar dynamic model that was tested at Glenn Research Center, NASA, (Mason, 1997), and it is also the type of system that is used in the Sandia Brayton Loop. Because the rotational inertia of the TAC shaft is so small only small levels or excess torque or power will be required to keep the shaft speed at the desired rpm.

2.5 Lumped Parameter Dynamic Model

For the sake of completeness the equations for the lumped parameter dynamic model are described here, this will be followed later by the more accurate and better behaved Simulink description of the dynamic equation set. Time dependent solutions to these equations are provide in reference (Wright, 2003); however, the solutions reported in this reference use a different set of flow characteristic curves and thus are not one-to replications of the examples illustrated in this report. Overall the solutions in the AIAA confirm the dynamic stability issues described in the preceding section here.

2.5.1 Dynamic Lumped Parameter Reactor Model

The point kinetics model was used to describe the reactor and the equations for it are shown in Table 2-19. The point kinetics model assumes that the shape of the reactor power distribution and neutron flux are maintained and are only proportional to power level. The model also includes a negative feedback term α to account for the reactivity changes due to fuel expansion or other effects. Other feedback terms such as those due to lattice expansion or changes in moderator temperature can be included in a similar fashion, however they have been omitted in here. Six delayed neutron groups are used.

The reactor power, temperature, and reactivity behave in the following manner. The power level increases for positive reactivity ρ, and it decreases for negative reactivity ρ. The reactor

is said to be critical and thus at steady state when $\rho = 0$. Therefore at steady state power levels, the inserted reactivity determines the fuel temperature by the relationship $\rho_{in} = \alpha * T_f$. Reactivity is often described in terms of percent dK/K or in dollars. A dollar of reactivity is just (dK/(K) / β), where K is the multiplication constant and is equivalent to the average number of neutrons generated in the next generation over the current generation.

During steady-state the reactor power is determined by the difference in the fuel temperature $T_{f.}$ and the average coolant temperature T_{34} (see Table 2-20). The inserted reactivity affects the power level only because it can change the average fuel temperature $T_{f,}$, but the power level is determined not so much by the fuel temperature but by the temperature difference between the fuel temperature and the coolant temperature. Clearly the coolant flow rate will also strongly affect the power level. The point kinetics model for a lumped parameter reactor with one average fuel temperature is described in Table 2-19.

Table 2-19: Dynamic Lumped parameter reactor point kinetics model

$\frac{dP_{rx}}{dt} = \frac{(\rho - \beta)}{\Lambda} \cdot P_{rx} + \sum_{i=1}^{6} (\lambda_i C_i)$ RPK-1	Where
$\frac{d}{dt} C_i = \frac{\beta_i}{\Lambda} \cdot P_{th} - \lambda_i \cdot C_i$ RPK-2	P_{rx} = Reactor or Fission Power
$\beta := \sum_{i=1}^{6} \beta_i$ RPK-3	P_{th} = Thermal Reactor Power (W) or heat transferred to coolant
$\rho := \rho_{in}(t) - \alpha \cdot T_f$ RPK-4	ρ = total reactivity (inserted + feedback)
$P_{th} = mdot \cdot Cp \cdot (T_{o4} - T_{o3})$ RPK-5	β = total delayed neutron fraction (0.0064)
	β_i = i th delayed neutron group fraction
	Λ = Prompt neutron generation time (1 x 10^{-5} s)
	λ_i = i th delayed neutron group decay constant (s^{-1})
	C_i = concentration of i th delayed neutron group (W)
	$\rho_{in}(t)$ = reactivity inserted by control rods
	α = Feedback Coefficient (-1.28 x 10^{-5} dk/k / K = -.02 cents/K)

The heat transfer reactor model and the coupling between the fission power and the reactor power is described in (equation RPK-5) and in

Table 2-20. These equations govern the transport of heat from the fuel to the coolant and also determine the reactor power level. In a transient the fission power (P_{rx}) may exceed the thermal power (P_{th}) that is being removed from the reactor. When this occurs, the temperature of the reactor will be increasing. Equation RPK-5 in Table 2-19 shows how the flow rate and heat transport to the coolant affect the coolant temperatures. This equation describes the

amount of thermal heat (P_{th}) being removed by the coolant, but note that it is dependent on the reactor inlet temperature which depends on the conditions of the turbomachinery and the effectiveness of the recuperator, thus the actual power level is intimately wrapped up with the condition of the CBC loop. Note that the thermal power (P_{th}) is not necessarily equal to the fission or reactor power (P_{rx}). The remaining reactor heat transport (RHT) equations and terms are defined in

Table 2-20. Here equation RHT2-1 relates the reactor fission power to the thermal capacitance of the fuel ($1/\kappa_f$) and the time constant of heat transfer from the fuel pin to the coolant ($1/\gamma_f$). Note that $\gamma_f / \kappa_f = h_{eff}*A$ where h_{eff} is the effective heat transfer coefficient from the fuel pin to the coolant and A is the heat transfer area. .

Table 2-20: Lumped parameter heat transport model for the reactor

$\frac{dT_f}{dt} = \kappa_f \cdot P_{rx} - \gamma_f \cdot (T_f - T_{34})$ RHT-1 $T_{34} := \frac{T_{o3} + T_{o4}}{2}$ RHT-2	where T_f = Fuel Temperature (K) κ_f = Inverse Thermal Capacitance of Fuel Pin (K/J) γ_f = Inverse time constant of heat transfer from fuel to coolant (1/s) T_{34} = Average of Rx inlet and outlet coolant Temperature (K) Cp = Heat Capacity of the He/Xe coolant (J/kg-K) T_{o3} = Reactor Inlet Temperature (K) T_{o4} = Reactor Outlet Temperature (K) mdot = Mass flow rate through the CBC loop (kg/s)

The lumped parameter coefficients for κ_f, $\gamma_{f.}$, and h_{eff} were estimated for a 313 pin gas cooled reactor. The fuel pins were assumed have a diameter of 9 mm, a length of 0.4 m, and a clad thickness of 0.5 mm. The cladding was Nb1Zr. Table 2-21 gives numeric values for these coefficients.

Table 2-21: Lumped parameter coefficients for a 313 pin ~ 400 kWth Gas Cooled Reactor

κ_f	=	3.425 E-5	(K / J)	κ_f	= Inverse Thermal Capacitance of Fuel
γ_f	=	0.0534	(1 / s)	γ_f	= Inverse time constant of heat transfer from fuel to coolant (1/s)
h_{eff} * A	=	1560	(W / K)	h_{eff} * A	= Heat transfer coefficient time area

2.5.2 Recuperator and Radiator Lumped Parameter Model

The equations for the recuperator model are described in Table 2-22. It essentially assumes that there is an average coolant temperature T_{23} (in the high-pressure leg) and an average temperature T_{56} (in the low-pressure leg) that controls the rate of energy flowing into or out of the recuperator structure. The balance of heat flowing into the recuperator structure determines the rate of change of the recuperator temperature T_{rcp}.

The recuperator model is not the simple effectiveness model that was used for the steady state solution. Instead it requires input parameters for the effective heat transfer coefficient times area of heat transfer hA_{rcp}, the heat capacitance of the recuperator structure Cp_{rcp}, and the mass of the recuperator structure M_{rcp}. These values were estimated for a recuperator that has a heat transfer area of 40 m^2, a mass of 140 kg, and a wall thickness of 0.4 mm and are provide in Table 2-22.

Table 2-22: Recuperator Lumped parameter model.

$$\frac{d}{dt}T_{rcp} := \frac{hA_{rcp}}{M_{rcp}\cdot Cp_{rcp}}\cdot\left(T_{56}-T_{rcp}\right)-\frac{hA_{rcp}}{M_{rcp}\cdot Cp_{rcp}}\cdot\left(T_{rcp}-T_{23}\right) \quad 3\text{-}1$$

$$T_{23} := \frac{T_{o2}+T_{o3}}{2} \quad 3\text{-}2$$

$$T_{56} := \frac{T_{o5}+T_{o6}}{2} \quad 3\text{-}3$$

where

T_{rcp} = recuperator structure temperature (K)

hA_{rcp} = heat transfer coefficient * area (W/K)

Cp_{rcp} = heat capacity of recuperator structure (J/kg-K)

T_{56} = Average gas temperature of low pressure leg of the recuperator (K)

T_{23} = average gas temperature of high pressure leg of the recuperator (K)

A_{rcp}	= 40 m^2	heat transfer area of recuperator
h_{eff_rcp}	= 743.7 W/ (m^2- K)	effective heat transfer coefficient
M_{rcp}	= 140 kg	Mass of recuperator
$Cp_{rcp} = Cp_{718}$	= 634 J/(kg- K)	Heat capacity of recuperator
t_{wall_rcp}	= 0.4 mm	Wall thickness of recuperator

2.5.3 Radiator Lumped Parameter Model

The radiator model is similar to the recuperator model. The equations for the radiator are defined in Table 2-23. These equations equate the time rate of change of the radiator structure temperature to the net thermal power transferred to the radiator structure minus the thermal power radiated to space. Again reasonable estimates are needed for the radiator heat transfer area, radiating area, emissivity, and heat transfer coefficients. Briefly summarized the radiator was assumed to have a 300 m^2 radiating area, with an emissivity of 0.9. The effective or average radiating temperature was selected to be ($0.8*T_{o6} + 0.2*T_{o1}$). These and other values are listed in the table.

Table 2-23: Lumped parameter dynamic model of space based radiator

$$\frac{dT_{rad}}{dt} = \frac{'\sigma \cdot 'A_{rad} \cdot \varepsilon_{rad}}{'M_{rad} \cdot 'Cp_{Al}} \cdot \left('T_{rad}^{4} - 'T_{space}^{4}\right) - \left[\frac{'\sigma \cdot 'A_{rad} \cdot \varepsilon_{rad}}{'M_{rad} \cdot 'Cp_{Al}} \cdot \left('T_{rad}^{4} - 'T_{space}^{4}\right)\right]$$ 4-1 $$T_{61} = .8 \cdot T_{o6} + .2 \cdot T_{o1}$$ 4-2	where T_{rad} = average radiator structure temperature (K) $hAbar_{gRad}$ = heat transfer coefficient * area (W/K) from coolant to radiator structure; 3.6 kW/K Cp_{rcp} = heat capacity of recuperator structure (J/kg-K) T_{61} = Average radiator gas temperature (K) T_{o6} = radiator gas inlet temperature (K) T_{o1} = radiator gas outlet temperature (K) M_{rad} = Radiator structure mass (kg); 855 kg A_{rad} = Radiator area (m^2) 300 m^2 σ = Stefan Boltzmann Constant ε_{Rad} = Emissivity of Radiator (0.9) Cp_{Al} = Heat Capacity of Radiator (Radiator material is aluminum) used T_{space} = Effective temperature of space (225 K in near earth orbit)

2.5.4 Turbine, Alternator, and Compressor Lumped Parameter Model

The last set of equations governs the behavior of the turbo-compressor, for a specified load. These equations are described in Table 2-24. Equation 5-1 describes the power balance on the TAC shaft. Essentially, the power that remains after that produced by the turbine less the power used by the compressor and less that produced by the generator equals the excess power to spin the shaft. Positive excess shaft power P_X will make the shaft spin faster, negative P_X will slow the shaft. The fourth equation 5-4 relates the angular acceleration to the excess power or torque. Also because the CBC loop is closed variations in compressor speed will continually change the pressure ratio in the loop based on the initial fill mass and other system parameters (temperature and volume). This relationship is given in equation 5-5. The final equations are the "characteristic curves" that determine the outlet temperature and pressure for the turbine and compressor (equations 5-6).

Table 2-24: Lumped parameter equations for the Turbo-Alternator-Compressor (TAC)

$P_X := P_{turb} - P_{comp} - P_{load}$ (5-1)	where
$P_{turb} := mdot \cdot Cp_{HeXe} \cdot (T_{o4} - T_{o5})$ (5-2)	P_X = Excess power to spin the TAC shaft (W)
$P_{comp} := modt \cdot Cp_{HeXe} \cdot (T_{o2} - T_{o1})$ (5-3)	P_{turb} = Power produced by the turbine (W)
$\frac{d}{dt} Nrpm := \frac{P_X}{I_{tac} \cdot Nrpm \cdot 4 \cdot \pi^2}$ (5-4)	P_{comp} = Power consumed by the compressor (W)
$m_{fill} := \frac{P_{o4} \cdot V_{hp}}{R_o \cdot T_{o3}} + \frac{P_{o1} \cdot V_{lp}}{R_o \cdot T_{o6}}$ (5-5)	Cp_{HeXe} = Heat Capacity of the HeXe coolant (J/kg*K); 421.8 J/(kg-K)
$fp_{turb}(....), fT_{turb}(.....), fp_{comp}(.....), fT_{comp}(.....)$ (5-6)	T_{o1} = Compressor Inlet Temperature (K)
	T_{o2} = Compressor Outlet Temperature (K)
	Nrpm = Rotational Speed of the TAC shaft (s^{-1})
	I_{tac} = Rotational moment of inertia for the TAC and shaft;(0.036 $kg.m^2$)
	m_{fill} = Total mass of He/Xe in system (kg); 5.87 kg
	V_{lp}, V_{hp} = Low and High Pressure Volumes V_{lp}= 100 liter; V_{hp}=150 liter
	P_{o4} = Inlet pressure to the Turbine (Pa)
	P_{o1} = Inlet pressure to the Compressor (Pa)
	R_o = Gas constant for the HeXe mixture (J/kg-K)
	T_{o6} = Radiator gas inlet Temperature (K)

2.6 Reactor Power and Control Simulator (RPCSIM) Dynamic Model

This section of the report describes an integrated dynamic system model called RPCSIM that is capable of dynamically simulating the behavior of a wide number of terrestrial and space reactors, power-conversion systems, and control methodologies. RPCSIM is a Reactor, Power, and Control Simulator (RPCSIM) that was programmed in SIMULINK™ (Simulink, 2005) which is specifically design to solve time dependent state flow systems. The basic equations for the reactor model and for the Closed-Brayton-Cycle (CBC) power-conversion system were described in the preceding sections of this report. These models were developed to understand the behavior of a Space Reactor coupled to a closed-Brayton-power conversion system under dynamically varying conditions such as startup, shut down, normal, and off normal operating conditions. By exercising the simulation tool RPCSIM, the control approaches, stability criterion, and the requirements for safe and autonomous operation are also being developed. System validation of RPCSIM is being performed using the closed-Brayton-cycle loop hardware, which is described in a subsequent section of this report.

2.6.1 Other Dynamic Models for SP100 and TOPAZ

Dynamic models for other space reactors such as TOPAZ and SP100 space reactor programs were developed and reported in Yahalom, 1994 and El-Genk, 1993, and Kwan, 1994. The SP100 program reports the results of a dynamic model that simulates the thaw process and the startup of the reactor and pumps for a liquid metal reactor coupled to a thermal electric power conversion system (Yahalom, 1994). In spite of the passive nature of the thermoelectric power conversion system, significant power transients were predicted when the liquid metal pumps start. In the TOPAZ dynamic model the reactor is strongly coupled to the behavior of the thermionic power conversion elements which are intimate components of the fuel elements (El-Genk, 1993) and (Kwan, 1994). The startup scenario reported for the TOPAZ reactor showed only mild transients, largely because the NaK coolant was always liquid (no thaw process was required) which permits near continuous coolant flow while the reactor is started. RPCSIM differs from these earlier dynamic models because it focuses primarily on the behavior of reactor systems that are coupled to gas-dynamic power conversion systems (e.g. closed-Brayton-cycle systems), rather than the more passive thermoelectric and thermionic power conversion systems.

2.6.2 RPCSIM Simulink Dynamic Model Introduction

RPCSIM implements the system equations in SIMULINK™ (Simulink, 2005). SIMULINK™ is a visual programming environment specifically designed to simulate dynamic state flow systems. The RPCSIM includes modules for gas and liquid metal cooled reactors, closed-Brayton-cycle power conversions systems, heat exchangers, ducting, radiators, alternators, power management devices, reactor controllers and other systems.

RPCSIM has extended the dynamic models to include control systems for the reactor and for the turbo-machinery shaft speed. The reactor control system regulates the reactor power and temperature by varying the inserted reactivity, while the Power Management and Distribution (PMAD) control system regulates the shaft-speed by varying the load on the alternator. RPCSIM currently uses proportional, integral, differential (PID) controllers to adjust the reactivity and parasitic load so that reference shaft speed and fuel temperature are sufficient to provide the requested electrical power to the space craft ion thrusters. Overall, the task of the reactor controller and the PMAD controller is to prevent over-speed of the TAC (turbo-alternator-compressor), to avoid over-temperatures within the reactor and other components, to motor the alternator for starting, to avoid turbo-machinery stall, and in general to respond to a large number of other control behavior situations. The job of the autonomous control system will be to recognize the various operational states of the system, and to select appropriate actions such as lowering the reactor temperature, increasing the shaft speed, starting and stopping pumps or other responses based on ground commands or based on the mission profile. It is clear that the two controllers for the reactor and turbomachinery require a great deal of coordination to recognize the actions that are desired and to implement controller responses that produce the correct action such as increasing power, lowering power, or performing some diagnostic behavior. These types of coordinated operations represent the autonomous control that will be required. We hope to extend the results of RPCSIM to the realm of autonomous reactor operations in the future.

2.6.2.1 Simulink Development Environment

SIMULINK™ is a development environment that is packaged with MatLab™ (MatLab, 2005), and it allows the creation of dynamic state flow models. Simulink provides a visual way to observe how the components of a model are linked together and how they impact each other. SIMULINK™ subsystems act like functions in a programming language, and can call programs written in other languages to increase speed. These simulations can run entirely in C or FORTRAN, or they can run using the visualization programming tools that are part of SIMULINK™. The C and FORTRAN code is fast but lacks the visual aspect that Simulink adds to the simulation. Nevertheless, this approach allows system models to be developed from legacy code to speed development. The models in RPCSIM use both the visual models and C code. Once the code and links have been added to the SIMULINK™ models to form a simulation, the connection with MatLab™ allows for easy plotting, manipulation, and analysis of the output data. Simulink allows simulations to run for limited time periods or indefinitely, thus allowing specific scenarios to be looked at, and exploration of reactions to real-time user input.

2.6.3 Dynamic Model Description and Assumptions for a Liquid Metal Cooled Reactor and a Gas Cooled Reactor

Figure 2-35 and Figure 2-36 show the top level RPCSIM block diagram for a lithium-cooled reactor and for a Gas Cooled Reactor (GCR). Both reactors are coupled to a closed-Brayton-cycle. The Liquid Metal cooled Reactor (LMR) is connected to the Brayton loop via an intermediate LM (Liquid Metal) to gas heat exchanger. The GCR is coupled directly to the Brayton cycle without using an intermediate heat exchanger. The schematics are arranged to look similar to the typical CBC block diagrams. The dark heavy lines in the schematics represent the flow paths for the coolants. These paths contain values for the temperature, the mass flow rate, and the pressure entering or leaving each component. The subscripts o1 - o6 identify the coolant stations and follow the same numbering scheme that was used before. The thin lines represent scalar data flow such as shaft speed (rpm), or inserted reactivity. Gold colored boxes represent control subsystems, thin gray rectangles represent the ducting, and the blue box is a monitor that contains a number of prearranged plots.

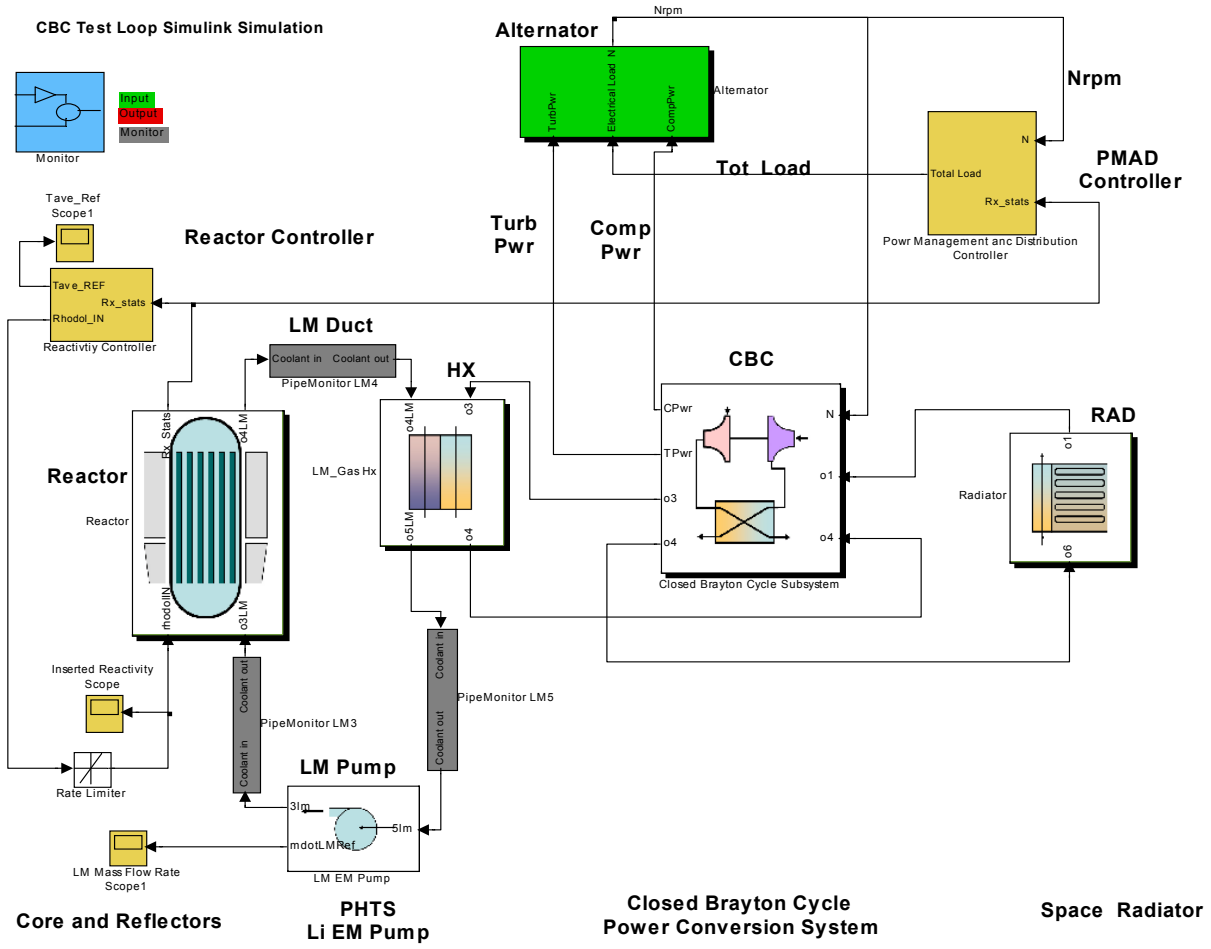

Figure 2-35: Simulink™ schematic of a liquid metal cooled reactor (LMR).

The main assumption used in RPCSIM is that the mass flow is constant around the loop. This assumption (as well as other assumptions) was selected because it permits fast running code. A list of the system model simplifications and assumptions follows:

1) The mass flow rate is constant around the loop.
2) The coolants are pure liquid or vapor at all temperatures (no freezing or thawing is modeled).
3) For liquid metals or water, the coolant is circulated or pumped at a user prescribed flow rate.
4) For gas flow, the characteristic flow equations and the state variables of the CBC loop determine the flow rate.
5) All coolants have constant heat capacity in this version, though the viscosity, thermal conductivity and densities are functions of temperature. The constant heat capacity restriction was removed for subsequent projects.
6) The heat exchangers are assumed to be counter flow, but the coolants in each leg can be different, and can have different flow rates.

7) The gas coolant is normally a mixture of He and Xe with a He mole fraction of 63.5 atom%, though other gases or gas mixtures can be used simply by changing the gas constant, the viscosity, thermal conductivity, heat capacity, and ratio of specific heat $Cp/Cv = \gamma$.
8) The reactor uses a single average fuel pin with a user specified axial power distribution. The fuel pin can have any number of axial nodes. Heat transfer from the reactor coolant is coupled to other structural materials such as core blocks and the pressure vessel so that other feedback effects can be incorporated. The average fuel temperature is used to determine the fuel temperature feedback effects, while the temperature of other structures may be used to determine other feedback phenomena.
9) The reactor uses the point kinetics model with 6 delayed neutron groups. Currently the user can specify up to three reactivity feedback terms that depend on the average fuel temperature, the core block (or coolant) temperature and the reactor pressure vessel temperature. The initial reactor power and reactivity are selected by the user. In this paper the reactor power starts with a neutron source(currently 10^7 neutrons/s) and with an initial reactivity of zero. It is easy to change the source strength or to change the initial reactivity so that the startup can begin from a sub-critical configuration.
10) The space radiator assumes that heat is transferred from the gas to the radiator panel structure through a heat exchanger that has a user specified heat transfer area, hydraulic diameter, and structural mass. The temperature drop across the heat exchanger structure is calculated at each node along the coolant flow path. Each radiator panel node radiates thermal power to space at a constant temperature that equals the structure temperature. Any number of nodes can be used to simulate the space radiator.
11) The initial temperature for all components can be selected by the user. For near-earth space startup scenarios we have selected the initial temperature to be 225 K.
12) The heat exchangers, ducts, and radiator can have any number of nodes. As in the radiator model, heat is transferred to the structure by user defined flow areas, heat transfer areas, hydraulic diameters, and mass of the structure.
13) The turbine and compressor characteristic flow curves are calculated from multivariate polynomial fits to the mean line flow analysis characteristic flow curves. These curves can be generated by the NASA codes for compressible rotating machinery (Galvas 1973 and Wasserbauer 1975) and described by Japikse (1996 and 1997) as described earlier, or they can be provided by turbo-machinery vendors.
14) Incompressible flow is assumed around the loop in all components except for the turbine and compressor where compressible flow is accounted for. For the other components density variations are computed.
15) Pressure drop and gas velocities are determined in each component by quasi-steady state flow laws. The design and dimensions of all components, except for the turbomachinery, is arranged so that the gas velocity is kept to less than 10% of the sonic speed.
16) The gas loop contains a fixed quantity of gas specified by the user; however, the gas inventory can be made to be a function of time to simulate inventory control.
17) The thermal lag due to the capacitance of the coolant is neglected.

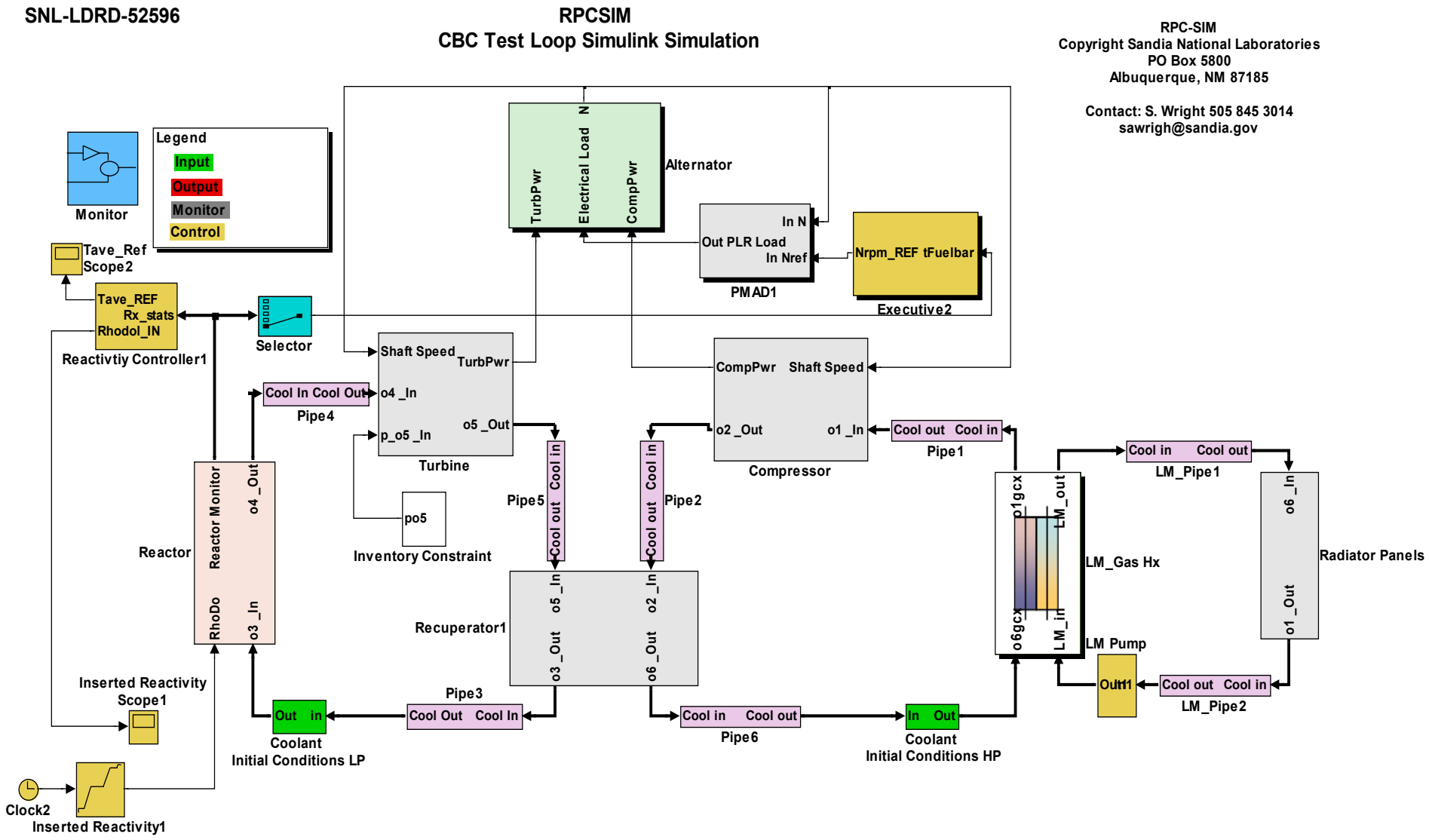

Figure 2-36: Simulink™ schematic of a gas cooled reactor (GCR).

2.6.4 Gas Cooled Reactor Description and CBC Overview

Complete Simulink system models for gas cooled reactors and liquid metal reactors that drive closed Brayton loops and models of electrically heated gas Brayton loops have been created. This section provides an in depth description of one possible configuration for a gas cooled reactor. This version was modeled in Simulink for this report. This reactor concept is described in (Wright and Lipinski, 2003). This configuration was provided to NASA and Naval Reactors as an example of a GCR space reactor concept as part of their reactor assessment during the Prometheus Project. The reactor is nominally a 400 kW_t reactor that uses 313 fuel pins.

A conceptual layout of the Gas Cooled Reactor and closed Brayton power conversion system is shown in Figure 2-37. The reactor is below the shield and has one inlet duct and one outlet duct. Note that there is no heat exchanger. The gas that flows through the CBC system also flows through the reactor. The system is designed to keep all pressure boundaries cool (~900 K). The inlet duct carries a He/Xe gas mixture that is about 900 K, which cools the reactor pressure vessel to keep it at about the same temperature as the gas. The outlet duct has gas temperatures that are at 1150 K to 1200 K. However, the pressure boundary to this duct is cooled by radiation, and the hot duct pressure boundary is insulated from the 1150 K gas by a liner and a thermal insulator. In this manner the pressure boundary for the hot gas is kept to about 900 K which permits the use of super-alloy metals (Inconel-718, Hastelloy X, etc). These metals are readily available, can be easily welded, are very insensitive to corrosion, have well known material properties, and are widely used in the reactor industry.

The reactor itself uses refractory metal cladding on the fuel, (Nb1Zr Re-lined), but these are simple tubes that can be welded in well-controlled vacuum systems. Due to their simplicity, they can also be easily inspected and QA'd. They do not require the welding and manufacture of complicated refractory metal components for which the commercial industry has limited capability. Furthermore, the use of Nb1Zr cladding is common to many space reactor systems being considered.

In addition to the major benefits of cool structure and exclusive use of superalloy materials for the pressure boundaries, the gas-cooled reactor also avoids a number of challenging design issues. The challenges avoided by using the gas-cooled reactor approach are:

- No high temperature heat exchanger
- No transition joint from refractory metal to superalloy
- No high temperature liquid metal pumps
- No auxiliary radiator for pump thermoelectrics
- No thaw system for the liquid metal or volume accumulators
- No freeze-thaw concerns
- No liquid metal compatibility (solubility) or ES&H concerns
- No gas separators for helium or hydrogen generated by Li
- No exposed refractory metal and 10^{-8} Torr testing difficulties

Programmatically the two design features: 1) superalloy pressure boundary and 2) cool structure, together with the avoidance of the challenging design issues, permits the GCR Nuclear Sub-System to minimize cost, schedule, and risk for developing a Nuclear Electric Propulsion System.

The use of superalloys accelerates the development schedule because these alloys are widely used to manufacture the required components such as pressure vessels, heat exchangers, ducts, turbines, etc., it also permits competition as dozens of vendors are capable of manufacturing components from superalloys, and it increases reliability because the materials have well known fabrication and QA processes. In addition the material properties including irradiation behavior are well known.

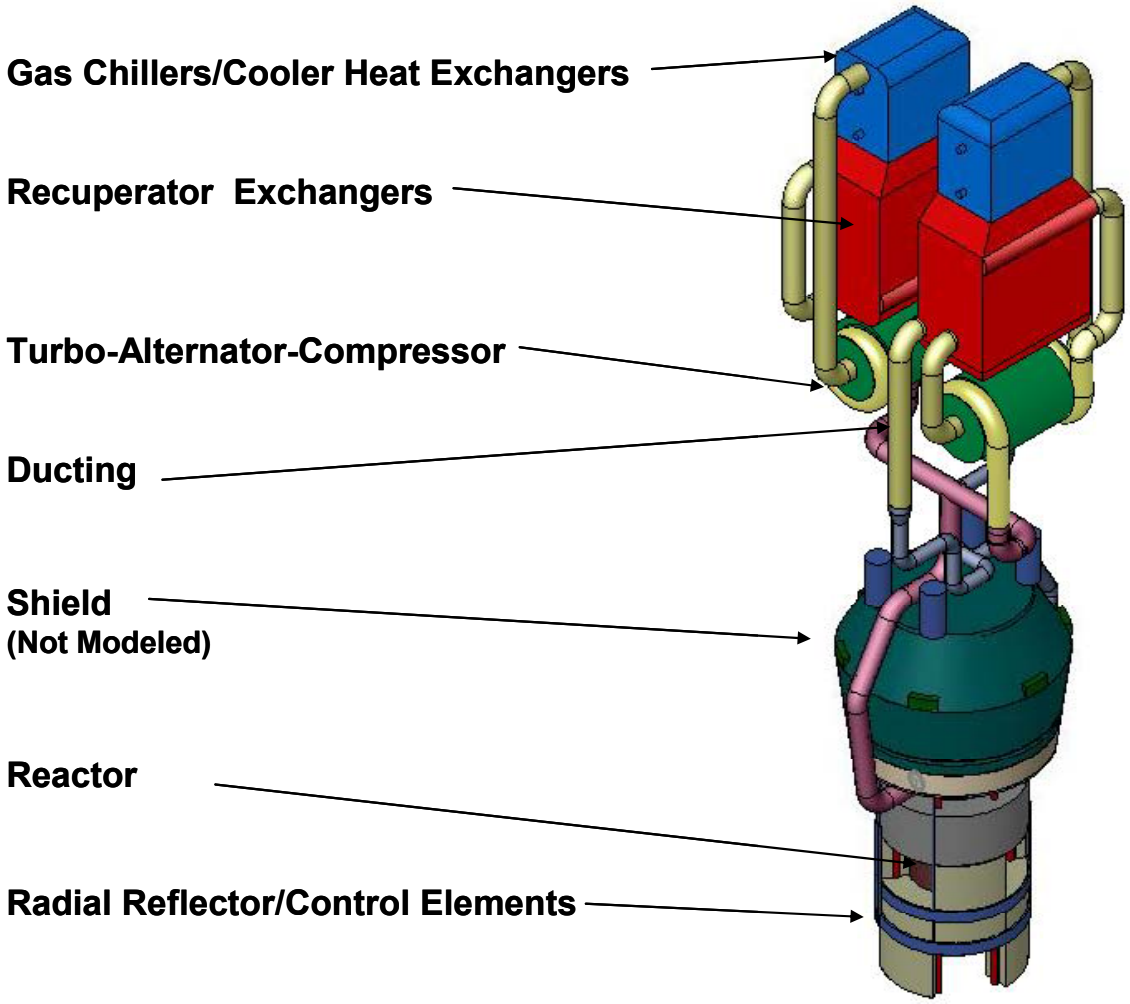

Figure 2-37: Conceptual layout for a direct gas cooled reactor coupled to two Brayton systems. Only one CBC loop is modeled in the present version of RPCSIM.

The use of cool structural materials (at about 900 K) means that a wider selection of materials can be used to fabricate necessary components such as bearings, motors, clutches, fasteners, insulator, slip joints. The lower temperatures generally make it easier to meet lifetime

requirements, will generally lower the thermal expansion accommodation requirements, and will provide a lower thermal load to the shield.

The avoidance of challenging issues such as freeze thaw, hydrogen and helium generation, fluid volume expansion, etc. means that time, money, and effort does not need to be dedicated to designing, fabricating and testing complicated components to operate at 1350 K in lithium, and with refractor metals. These complicated devices include gas separators, and Thermoelectric Modules (TEM), or Annular Linear Induction Pumps (ALIP), volume accumulators, and freeze thaw mechanisms. The SP100 program developed a number of designs for these systems and even fabricated portions of them; however none of these devices has ever been built and operated in lithium, at 1350 K and with refractory metals.

Thus overall the GCR concept provides a number of simple engineering solutions to difficult design issues compared to the HPR(Heat Pipe Reactor) and LMR concepts that require high temperature core structures (~1300 K) and refractory metal components.

Finally the developers of the nuclear sub-system must take a systems approach to the design. The reactor and shield comprise just one portion of a much larger spacecraft. An example of one systems issue that must be resolved for CBC systems is the selection of materials. The turbine, nozzles, wheels, and ducting for CBC systems use superalloy metals (such as Inconels and Hastelloy). Thus, the system design must join the ducts coming from the reactor or heat exchanger to the CBC ducting. For the GCR, these are the same materials (for the design presented here) and the joint can be easily welded and inspected. However for the LMR and the HPR the joint must transition from a refractory metal to a superalloy. Even if this joint can be manufactured reliably, the determination of acceptable reliability over the lifetime of the mission is problematic. This example illustrates how the GCR concept easily accommodates the system level requirements, while the other approaches impose additional technology development requirements.

The gas-cooled reactor NEP(Nuclear Electric Propulsion) power system uses a gas-cooled, UN-fueled, pin-type reactor to heat He/Xe gas that goes directly into a recuperated Brayton system to produce electricity. Heat is rejected to space via a thermal radiator that unfolds in space. The reference system that will be described here in detail produces 100 kWe but it is scalable from 10 kWe to 10 MWe.

The space reactor power system (excluding radiators) was shown in Figure 2-37. The power system (in addition to the reactor and shield) includes the Brayton rotating units. In the concept shown in the figure the reactor is connected to two independent Brayton rotating units, however the modeling presented here limits the analysis by assuming that only one Brayton loop will be operational at a given moment. Some development has gone into modeling and fabricating dual Brayton loops (Mason, 2005, Fuller 2005) that are coupled to a single reactor or electrical heater but the results of this modeling and hardware validation are not currently available. The closed Brayton Cycle machinery uses a configuration provided by Glenn Research Center. It consists of two 100% power rotating units including turbine, compressor, alternator, recuperator and a waste heat exchanger. The dual units are shown to illustrate how redundancy can be provided for the rotating units in a gas cooled reactor system. The units will be sized to operate at 100% power, but during normal operation they can operate at either 50% power, or individually at 100% power.

Figure 2-38 illustrates the approximate state points of the reactor and power conversion concept as proposed by the Sandia National Laboratories GCR team. These results were generated by two Sandia codes (FEPSIM and RxPwrSys) which are detailed design tools that keep track of system mass, pressure drops, mass flow rates, thermal losses, and many other useful parameters. These codes greatly aid in our understanding of the overall system and guide our design.

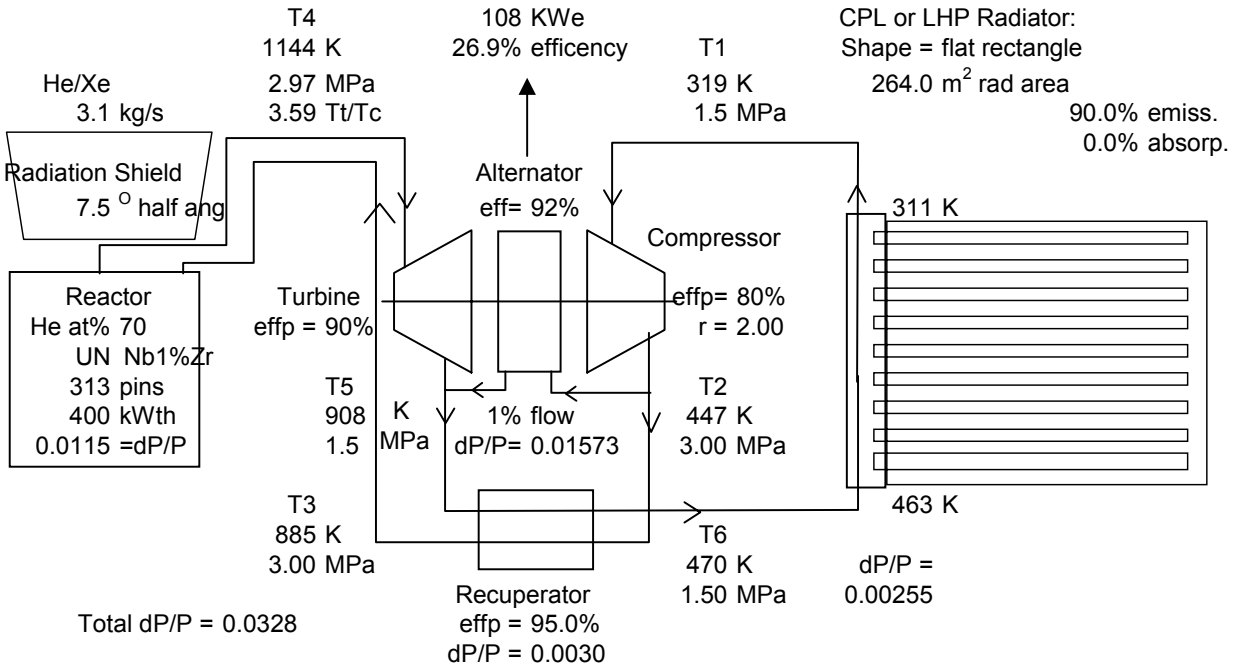

Figure 2-38: Approximate state points for the Closed Brayton Cycle System.

The turbo-machinery shown in Figure 2-37 is oriented parallel the axis of the boom of an electric propulsion spacecraft. However, if the rotating units are oriented perpendicular to the boom (as are the electric thrusters), then the angular momentum of changes caused by changing the speed of the turbo-machinery and drag (which would cause the spacecraft to spin about the center of mass); can be easily removed by powering one thruster more that another for awhile. This perpendicular orientation is the layout preferred by SNL. The size, rotational speeds, and angular momentum of the turbomachinery are very similar to that used in current day momentum wheels, thus engineering solutions to space craft having angular momentum components are well developed. We are assuming a single rotating unit at this time, contingent on being able to prove the case for reliability. Additional units will be added if necessary and the illustration provided in Figure 2-37 indicates how this would be accomplished.

The reactor is very compact and contains approximately 159 kg of 93.15 % enriched UN in 313 fuel pins. The reactor pressure vessel is 0.334 m in diameter and the dome-to-dome length at the tip is a little over 1 m in this current configuration. The radial reflectors are 11 cm thick. The overall length of the shield is about 0.6 m and the shield has a 7.5 degree cone half angle. The mass of the reactor and reflectors is about 694 kg, and the shield mass is about 600 kg.

2.6.4.1 Nuclear Reactor Core and Reflectors Description

A cross sectional view of the Gas-Cooled Reactor concept is shown in Figure 2-39 and a more detailed view in Figure 2-40. Flow of cool inlet gas along the pressure vessel wall keeps the gas cool. The hot outlet gas pressure boundary is kept cool by thermal radiation to space. (Nested flow of the hot duct inside the cold duct is another option that is not shown.) The use of cool pressure boundaries everywhere permits the use of super-alloy metals for all pressure boundaries. The only use of refractory metal is the cladding and liner of the fuel. This configuration of the GCR shows a reactor with a separate inlet and outlet duct. The inlet duct is on one side of the shield (top of the illustration) while the outlet duct is rotated 180 degrees.

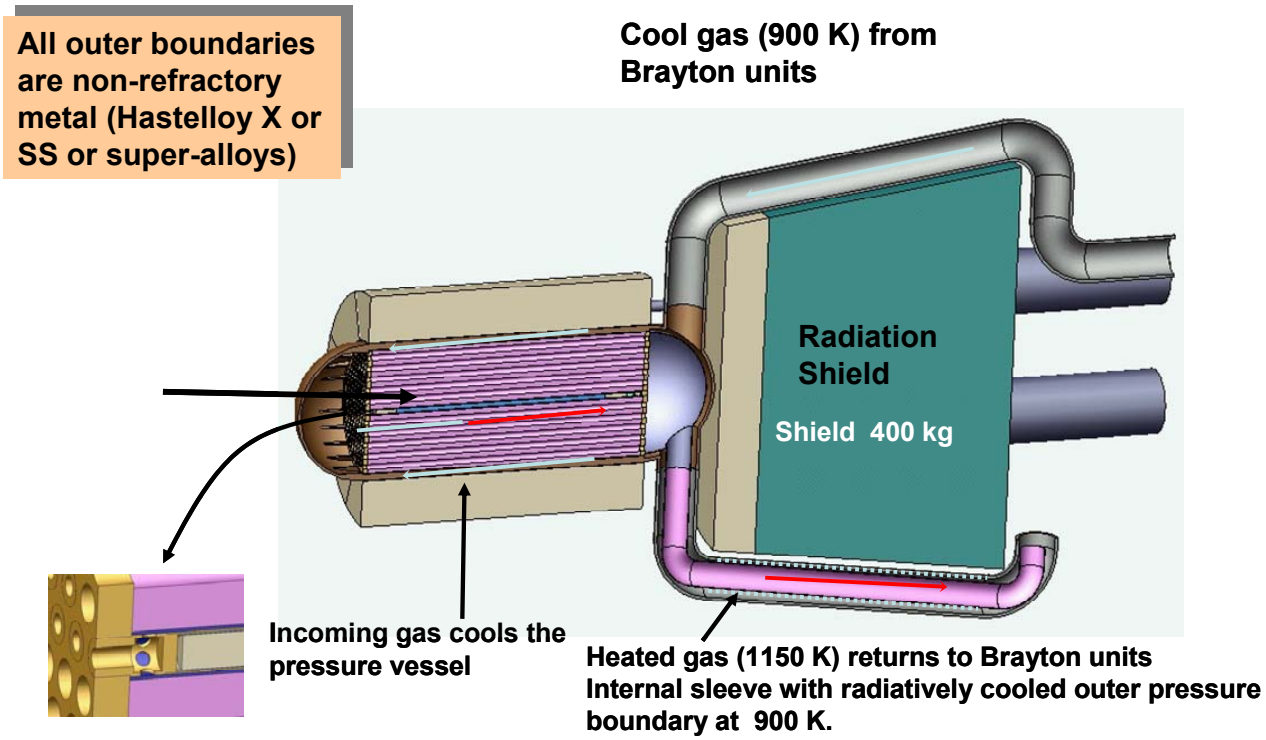

Figure 2-39: Nominal direct drive Gas-Cooled Reactor (GCR) ~400 kW_t showing the reactor, shield, inlet and outlet ducts, bypass flow, and radial reflectors (gray).

The reactor is compact and contains approximately 159 kg of 93.15 % enriched UN in 313 fuel pins. The fuel is 93.15% enriched UN that is clad with rhenium-lined Nb-1Zr. The reactor contains sufficient rhenium (a neutron poison) to make the reactor subcritical under water immersion accidents without the use of internal shutdown rods.

The reactor pressure vessel is 0.328 m in diameter, and the dome-to-dome length at the tip is a little over 1 m. The pin assembly consists of the fuel pin placed in a core block (sometimes referred to as a "matrix" or "prism") to form an annular flow passage (including a Re ribbon-wrap spacer). The length of the shield is about 0.6 m and the shield has a 7.5 degree ½ cone angle. The mass of the reactor and reflectors is about 691 kg, and the shield mass is about 600 kg.

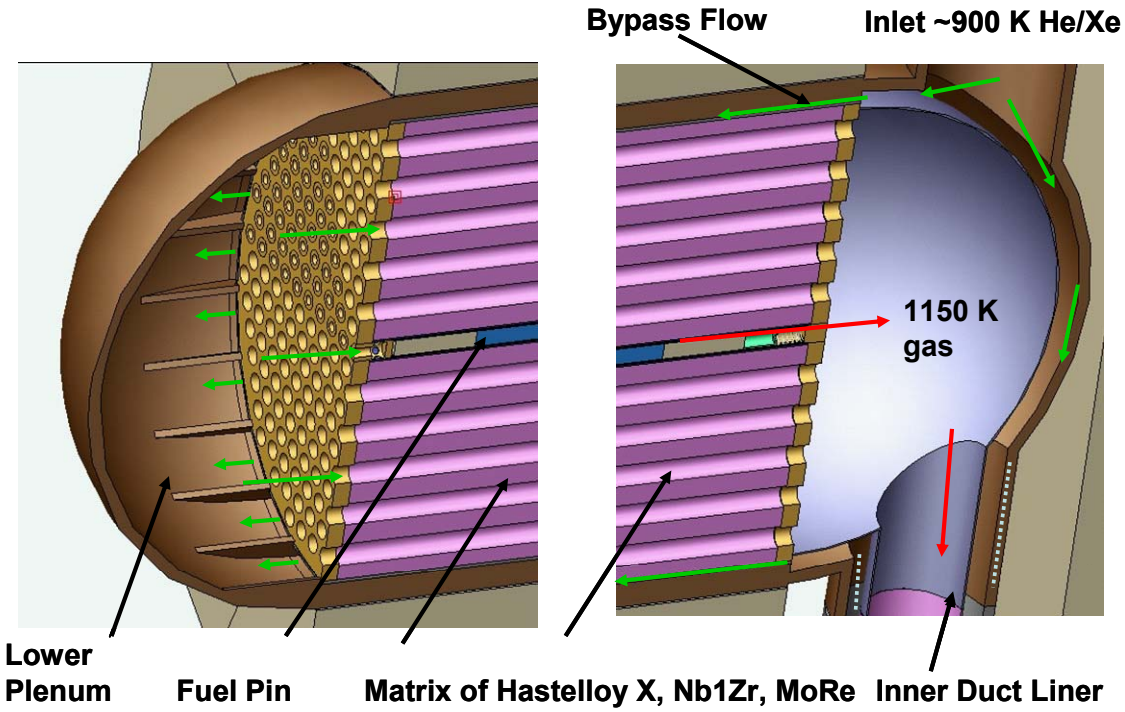

Figure 2-40: Close-up of Flow Through inlet nozzle, bypass, lower plenum, fuel pin flow annulus, and exit plenum and exit duct.

The gas flow through the system is a mixture of He/Xe. Current designs are based on a helium mole fraction of about 63.5%, which has a thermal conductivity of about ¼ that of water. The fraction of He and its pressure are being considered as variables that can be used to improve performance or thermal margin if needed. The baseline design presented in this report assumes that the gas pressure is 1.5 MPa (at the compressor inlet). A detailed description of the thermo-physical properties for mixed gases was already presented.

The reactor inlet gas temperature is approximately 900 K, and the inlet gas flows into a thin dome shaped flow region between the exit plenum and the pressure vessel head. This flow keeps the pressure vessel head at about the 900 K temperature. The inlet gas then flows along an annular flow region along the pressure vessel wall. Again this flow keeps the pressure vessel wall cool. At the bottom (left end of illustration) the inlet gas flows into the bottom plenum. The gas then flows back through the grid plate along each of the fuel pins (left to right). The flow along each fuel pin is in an annular flow passage that is defined by the fuel pin and by a core block. At the entrance to each pin is an orifice that is used to match the power to flow for each pin. This results in the same temperature rise for each channel throughout the core. In the upper plenum the gas flows into the outlet duct. The outlet duct has gas temperatures that are at 1170 K to 1200 K. However, the pressure boundary to this duct is cooled by radiation. The hot duct pressure boundary is insulated from the 1170 K gas by a liner and a layer of stagnant gas. Thermal insulator is simple a stagnant layer of gas at the same pressure as the gas in the flow channel. In this manner the pressure boundary for the hot gas is kept to about 900 K which permits the use of super-alloy metals (Inconel-718, Hastelloy X, etc). At a surface temperature of 900 K the ducts will loose about 20 kW of power.

The reactor is shut down by sliding the radial reflectors to open a gap near the center-plane, similar to one of the methods proposed for SP-100 control. Other options for controlling the reactor are angled radial reflector elements (petals), sliding elements, and rotating drums. The design presented in this report uses sliders; however the final selection of the type of control element will be based further analysis including evaluation of the safety merits of the various control methods. During full power operation with the Be radial reflectors fully closed, the Be reflectors operate at about 640 K, and they radiate about 5 kW_t to space. With the reflectors open, the pressure vessel is capable of radiating an additional 4-5 kW_t to space. These parasitic losses are capable of providing adequate decay heat removal.

Under normal operating conditions, heat is removed by the turbo-machinery, which will continue to move the gas through the reactor without a load down to about 4-20% of full flow at reduced turbo-compressor rpm (revolutions per minute) and reduced turbine inlet temperatures. The reactor and turbo-machinery will be controlled in manner that permits three modes of operation, 1) normal operation, 2) a reduced power mode (20-25% thermal power), and 3) a "safe-standby" mode at reduced thermal and electrical power and reduced reactor temperature (about 700 K). The dimensions of the fuel pin and other core components are listed in Table 2-25 and Table 2-26. These values are presented so that other researchers can model a GCR with similar characteristics.

Table 2-25: Design Dimensions of GCR Fuel Pin

Major dimensions of the fuel pin design for the Gas-Cooled Space Reactor		
Component	Dimension	Comment
Fuel Diameter and Height	ϕ=10 mm L=45 cm	37.7% fraction of core vol.
Gap	65 μm	0.988%
Re liner (thickness)	700 μm	11.4%
Nb1Zr Cladding	0.508 mm	9.2%
Coolant Gap	0.9 mm	16.7%
Ribbon Wrap (Re)	1.8 mm x 0.9 mm (2x)	1.6%
Fuel Pin Pitch	15.5 mm	
Fuel Enrichment	93.15%	SP-100 used 97%
Theoretical Density	14.32 gm/cc	@93.15% enriched
Density of UN	97.19%	Same as SP-100
Length of BeO Axial Refl.	50 mm	Both Upper and Lower
Fission Gas Plenum Length	40 mm	Variable to be determined
Total Pin Length	0.624 m	Subject to small changes
Gap for Axial TE diff	~1 mm	Delta between Fuel & Clad

Table 2-26: Major dimensions and components of the GCR.

Major dimensions of the components in the Gas-Cooled Space Reactor		
Component	Dimension	Comment
Fuel Diameter and Height	ϕ=10 mm L=52 cm	37.7% fraction of core vol.
Gap	65 μm	0.988%
Re liner (thickness)	700 μm	11.4%
Nb1Zr Cladding	0.508 mm	9.2%
Coolant Gap	0.9 mm	16.7%
Ribbon Wrap (Re)	1.8 mm x 0.9 mm (2x)	1.6%
Fuel Pin Pitch	15.5 mm	
Core Prism (OD) (Hastelloy X)	302 mm	22.3%
Pressure Vessel ID and OD	ϕ_{in}=314 mm, ϕ_{out}=328 mm	
Radial Reflector ID and OD	ϕ_{in}=330 mm, ϕ_{out}=550 mm	

There is a strong similarity with the space version of the GCR presented in this DDP and the High Temperature Test Reactor operating in JAERI, Japan. (Saito, 1994). The HTTR reactor reached a gas exit temperatures of 1223 K in FY03. The configuration used for the space version of the Gas-Cooled Reactor is a pin-type-reactor cooled with an inert gas flowing in an annular flow passage that is defined by a core block. This is exactly the same configuration that is being used by HTTR. The HTTR reactor uses a Cr-Mo steel pressure boundary and pin type fuel. The fuel pins are carbide based TRISO coated fuel particles embedded in a pyrolitic graphite matrix and clad with pyrolitic graphite. The core block is graphite. The fact that an existing reactor using similar design concepts as proposed here for the gas-cooled space reactor and operating at the desired gas exit temperature is strong evidence that GCR concept as proposed here is valid and has a high likelihood of being developed in a cost effective and timely manner. Note, the carbide based fuel types were considered for the GCR concept, but for the space reactor applications they were rejected because the Uranium density is very low (about 7-10% of UN), and this requires a much larger reactor than if UN fuel is used.

2.6.4.2 Reactor Simulink Module

Given this detailed description of the GCR it is now possible to begin to summarize in more depth the characteristics of the Simulink RPCSIM GCR model. The GCR reactor module consists of three subsystems. One Simulink subsystem solves the reactor point kinetics equations (Keepin 1965, and Hetrick 1971). The reactor model currently contains three thermal feedback effects that depend on structural component temperatures for the fuel, core block, and the pressure vessel. A second Simulink subsystem determines the coolant pressure drop through the reactor (and other thermal hydraulic parameters), and the third subsystem solves the heat transport equations for each component modeled. The pressure drop model and the heat transfer models have already been described.

The Simulink heat transport module and pressure drop module is very modular. These modules can be inserted almost anywhere in the coolant path, and provided the user specifies the correct structural, mass, heat transfer area, flow area, and heat capacitance, then the correct structural temperatures for that component are updated for each time step as are the coolant temperatures. In addition each component can have any number of nodes along the length of

the component. For the GCR RPCSIM model the reactor was divided into 10 axial sections as shown in Figure 2-41. The model has three heat transport paths, one path transports heat from the fuel pin to the gas coolant, another transports heat from the coolant to the core block/prism, and the third path transports heat from the annular bypass flow to the pressure vessel. At the time of writing of this report, we have omitted the coupling of the bypass flow gas to the core prism. This coupling should be small because a thin insulator will be placed between the core block and the bypass flow region.

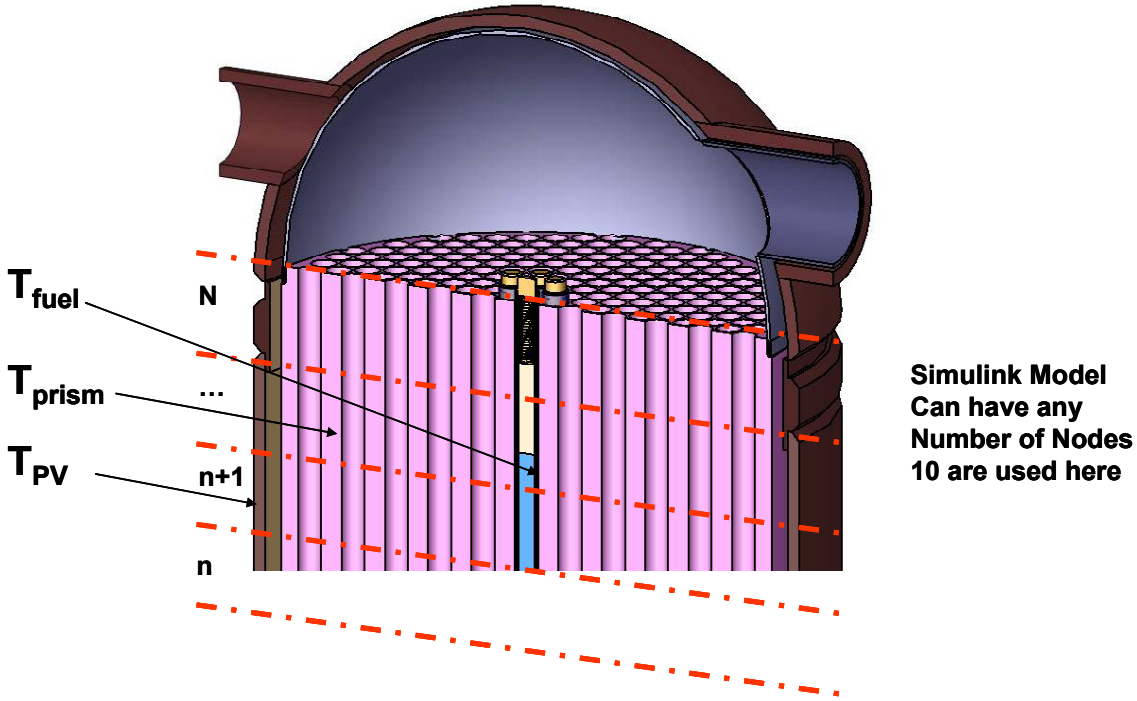

Figure 2-41: Axial flow paths in bypass flow channel and fuel channel with temperature distributions calculated in fuel, prism/block, and pressure vessel

2.6.4.2.1 Point Kinetics Reactor Model

The point kinetics equations are the same as before, but now the initial source strength (S_o) is considered. These equations are listed in equations 2-40 through 2-43.

$$\frac{d}{dt}P_{Rx} = \frac{\rho-\beta}{\Lambda}P_{Rx} + \sum_{i=1}^{6}\lambda_i C_i + S_o \quad , \qquad \textbf{2-40}$$

$$\frac{d}{dt}C_i = \frac{\beta_i}{\Lambda}P_{Rx} - \lambda_i C_i , \qquad \textbf{2-41}$$

$$\beta = \sum_{i=1}^{6}\beta_i , \qquad \textbf{2-42}$$

$$\rho = \rho_{in}(t) + \sum_{k=1}^{3} \alpha_{T,k}\cdot(T_k - T_o) \qquad \textbf{2-43}$$

where T_k is the temperature of the k^{th} structural component within the reactor, that include the fuel, the core block and the pressure vessel. The heat transfer equations were described in Section 2.6.4. The neutron generation time for the reactor depends very strongly on the amount of rhenium in the fuel and on the thickness of the reflector. We have observed neutron generation values that vary from 10 μs to 1 μs. The GCR RPCSIM model uses Λ=10 μs.

The Simulink point kinetics model (consisting of equations 2-43 through 2-45) is coded in C and is dynamically linked to Simulink through a Simulink library. The decoupling of the reactor point kinetics equations from the heat transport was done because it allows the normal heat transport and pressure drop Simulink modules ("calculators") to be used. In addition the C code reduces the calculation times by almost a factor of two.

2.6.4.2.2 Feedback Mechanisms and Models

Three feedback mechanisms are included in the RPCSIM version of the gas cooled reactor. These mechanisms include the axial expansion, fuel pin lattice expansion, and radial displacement of the BeO radial reflectors. These effects are schematically illustrated in Figure 2-42. The axial fuel expansion is caused by fission heating of the fuel and is considered to be prompt (the fuel motion is really limited by the speed of sound in the fuel but this is fast ~1000m/s). Lattice expansion or spreading of the fuel pins was also estimated. Here we assumed that as the core prism or core block heats it would expand radially and force the spacing between the pins to increase by a small amount. To estimate this effect we used the midline core block temperature to determine the amount spreading of the pins and thus the reactivity changes. The last feedback effect is radial displacement of the reflectors. Here we assumed that the reflectors were attached to the pressure vessel. Therefore as the inlet gas heats or cools the pressure vessel, the pressure vessel diameter moves and subsequently displaces the BeO reflectors by the same amount. This motion results in a reactivity impact.

In all cases the reactivity consequences of these displacements were estimated by running the Monte Carlo Neutron Transport Code MCNP (Breismeister, 1977). Table 2-27 lists some early estimates that we made for the three reactivity effects. The circled column shows the estimated reactivity effect in terms of cents / K. A cent of reactivity is 1% of (dK/(K β), where K is the multiplication constant and is equivalent to the average number of neutrons generated in the next generation over the current generation. The fuel and lattice feedback coefficients are on the order of 0.05 cents/K, while the reflector feedback coefficient is several times larger. For comparison purposes, the same feedback coefficients that were calculated for a similar lithium cooled reactor are shown in Table 2-28. For an LMR the fuel and lattice feedback values are very similar to those for the gas cooled reactor, but the reflector feedback value is not as large as was estimated for the GCR. Because we have not performed an in depth analysis of the feedback coefficients, we have decided to used the values listed in Table 2-29, where the fuel and lattice coefficients are taken to be -0.05 cents/K and the reflector coefficient is taken to be -0.1 cent/K. Some earlier calculations only used the fuel coefficient. When this was done all the individual terms were summed and the total feedback coefficient was estimated to be -0.2 cents/K. By way of comparison, we know the measure coefficients for the Sandia ACRR and the SPR reactor. These measured feedback coefficients vary from -0.15 cents/K to -0.350 for the SPR reactor to -0.35 cents/K for the Annular Core Research Reactor at Sandia.

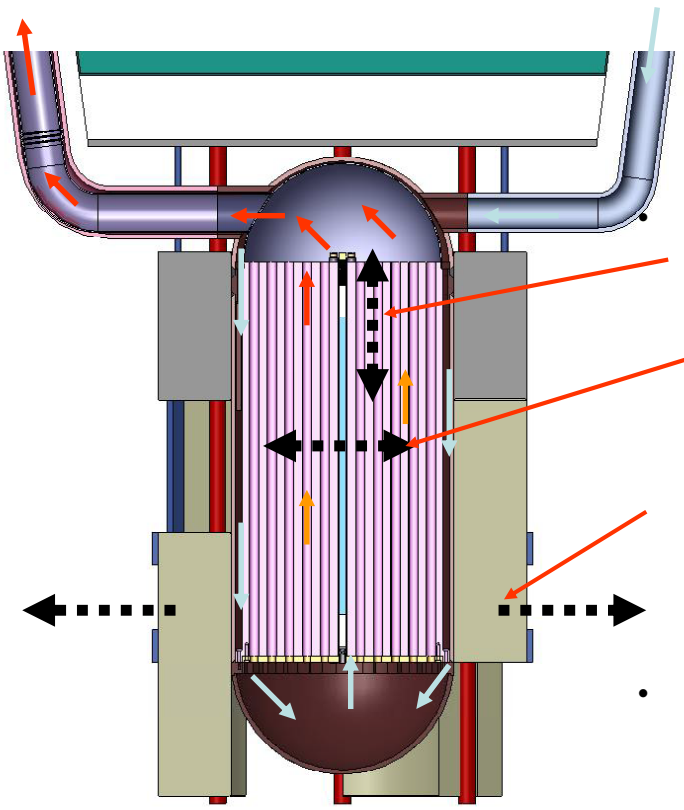

- Reactivity Effects
  - Axial Fuel Expansion
    - Single Average Fuel pin
    - Average Fuel Temp
  - Lattice Expansion
    - Average Lattice/Prism Temperature
  - Radial Expansion of Pressure Vessel Mounts to BeO
    - Average Pressure Vessel Temp
    - Assumes Refl. Mounted to PV
- Pressure drop calculated in all flow channels

Figure 2-42: Feedback Depends on Temperature of Fuel, Prism and Pressure Vessel (& Mounting Methods)

Table 2-27: Estimates of feedback coefficients for the GCR/

Component	Feedback Coefficient	$T_{component}-T_o$	dT	dK
Fuel	-0.048 cents/K	$T_{fuel}-T_o$	1125K - 300K	-0.254 %dK
Lattice	-0.067 cents/K	$T_{cool}-T_o$	1050K - 300K	-0.32 %dK
Beryllium Ref	-0.212 cents/K	$T_{Be}-T_o$	700K - 300K	-0.54 % dK
Total				-1.1% dK
Neutron Generation Time			1.48 usec	
Delayed Neutron Constant			0.0064	

Table 2-28: Estimates of feedback coefficients for an LMR/

Feedback Coefficients and Burnup Reactivity Decrement *Keff at BOL and EOL with and w/o one stuck Control Element*				
			K-eff	K-eff
Cold Excess Critical			1.05408	1.04012
Fuel Expansion	Cents / K	-0.05		
Fuel Doppler	Cents / K	0.01		
Lattice Expansion	Cents / K	-0.07		
Coolant Expansion	Cents / K	-0.05		
BeO Radial Refl. Exp	Cents / K	-0.06		
Total Feedback	Cents / K	-0.22	-0.013	-0.013
Burnup Decrement BU=2.8 a%	dK (estimate only)		-0.024	-0.024
EOL Hot Critical	Cents / K	-0.22	1.017	1.003

Table 2-29: Summary of feedback model used for the Simulink GCR.

$$\rho_{total} = \rho_{insert} + \alpha_{Fuel}(T_{Fuel} - T_{Init}) + \alpha_{Lattice}(T_{Lattice} - T_{Init}) + \alpha_{BeO}(T_{BeO} - T_{Init})$$

Single feedback coefficient model

$$\alpha_{Fuel} = -0.2 \quad cents/K$$

Three feedback coefficient model

$$\alpha_{Fuel} = -0.05 \quad cents/K$$
$$\alpha_{Lattice} = -0.05 \quad cents/K$$
$$\alpha_{BeO} = -0.1 \quad cents/K$$

2.6.4.2.3 RPCSIM Gas Cooled Reactor Simulink Module

The RPCSIM gas cooled reactor model is shown in Figure 2-43. It consists of five major subsystems. The first subsystem (lavender) is the point kinetics model which outputs the reactor power given total reactivity (inserted plus feedback effects). The second subsystem (orange) calculates the pressure vessel wall temperature and all other thermal hydraulic data for the bypass flow region. It uses the method described in Section 2.6.5.1. The third subsystem (orange) calculates the fuel pin temperature and the core block/prism temperature, in addition to the gas coolant temperatures. These two heat transport routines for the fuel pin and the core prism are included in the same subsystem because they have a common coolant flow path and two separate structural regions. The internals of this subsystem is based entirely on the gas calculator module and the heat transport gas calculator module described in Section 2.6.5.1. The fourth block (magenta) calculates the total reactivity given the structural temperature arrays, and just solves the top or total feedback equation in Table 2-29. A detail of this subsystem is shown in Figure 2-44: Simulink feedback model.. In this subsystem the structural temperature arrays are first averaged to find the mean temperature. Then they are multiplied by their respective feedback coefficients and summed together with the inserted reactivity to determine the total reactivity. The last subsystem in the GCR RPCSIM module simply collects a lot of the reactor data (fission power, thermal power, average fuel

temperature, mass flow rate, inlet and outlet temperatures and total reactivity) and puts them in a common array to facilitate plotting and other data handling requirements.

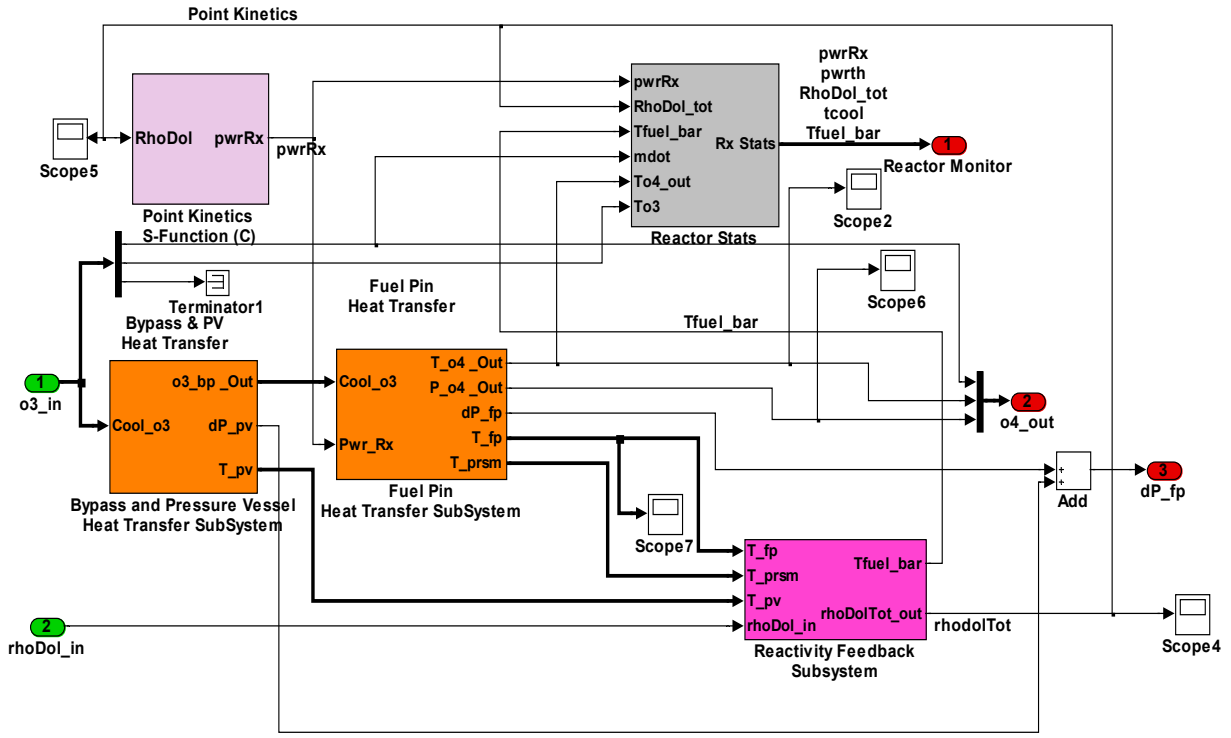

Figure 2-43: Simulink block diagram of GCR model.

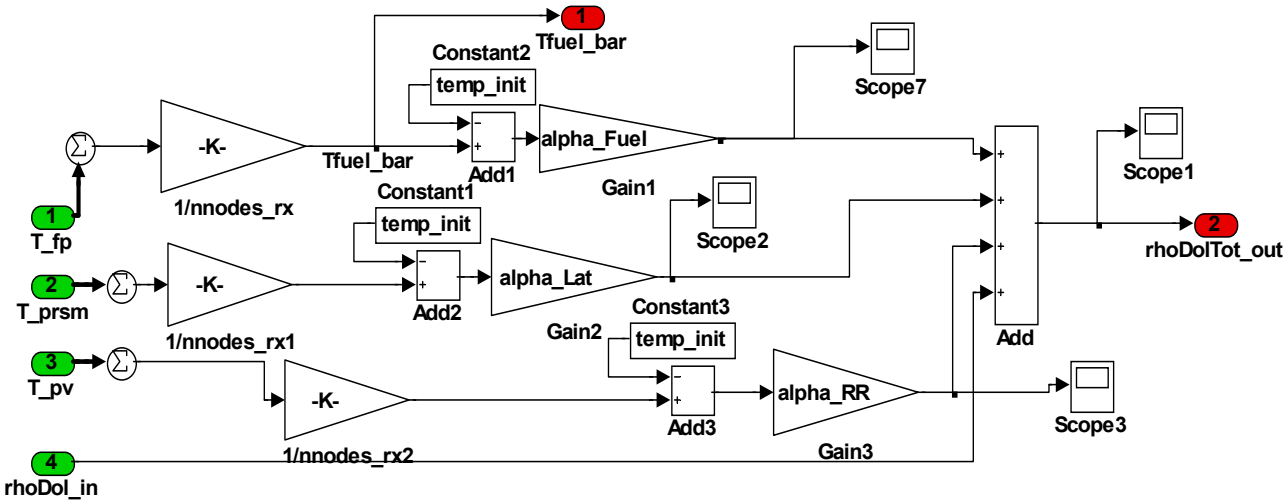

Figure 2-44: Simulink feedback model.

2.6.4.3 Turbine-Alternator-Compressor (TAC) Simulink Model

The turbo-alternator-compressor (TAC) model used in Simulink is virtually identical to the dynamic model equations described in Table 2-24. The differences are minor and they were made primarily to simplify the solution methods and to ease convergence criterion. As before the TAC model relates the rate of change of the shaft speed (N_{rpm} or N) or more precisely the rate of change of angular momentum times the moment of inertia, ($I_{tc} \cdot 2\pi \, {}^{d N_{rpm}}\!/_{dt}$), to the torque ($\tau = {}^{P_{tc\_X}}\!/_{2\pi N_{rpm}} - b' \cdot 2\pi N_{rpm}$). Here τ is the torque and b' is the coefficient of drag which is small, and we normally set it to zero. The other terms have already been introduced. In addition N_{rpm} = N which is shaft speed and has units of revolutions per second, though we sometimes express it as revolutions per minute. $P_{tc\_X} = P_X$ is the excess power on the TAC shaft and was described in Section 2.4.6.3 , Stability Analysis. It is the power generated by the turbine, less the power consumed by the compressor and alternator. As mentioned before, the TAC shaft has very little inertia, therefore small misbalances in P_{tac_X} will result in rapid changes in the shaft speed. This has the advantage that it means that a small dynamically controlled load perturbation can keep the shaft speed on the dynamically unstable steady state operating point. Overall the equations used for the TAC are:

$$\frac{d}{dt} N_{rpm} = \frac{P_{tc\_X}}{I_{tc} \cdot N_{rpm} \; 4\pi^2 \cdot} - b \cdot N_{rpm} \quad , \tag{2-44}$$

$$P_{tc\_X} = mdot \cdot Cp \cdot (T_{o4} - T_{o5}) - mdot \cdot Cp \cdot (T_{o2} - T_{o1}) - P_{load} \, . \tag{2-45}$$

$$P_{turb} = mdot \cdot Cp \cdot (T_{o4} - T_{o5}) \tag{2-46}$$

$$P_{comp} = mdot \cdot Cp \cdot (T_{o2} - T_{o1}) \tag{2-47}$$

Observe that the power in the compressor and turbine are related to the mass flow rate and the total temperature changes through these rotating machines. The temperatures and the mass flow rate are obtained from the characteristic flow curves. The equations for these curves give the turbine and compressor temperature and pressure ratio as a function of inlet temperature and pressure and as a function of mass flow rate (mdot) and shaft speed (N_{rpm}). The turbine and compressor characteristic flow equations are identified in equations 11 through 14.

$$\frac{p_{o2}}{p_{o1}} = f_{prC}(T_{o1}, p_{o1}, mdot, N_{rpm}) \, , \tag{2-48}$$

$$\frac{p_{o4}}{p_{o5}} = f_{prT}(T_{o4}, p_{o4}, mdot, N_{rpm}) \;\Leftrightarrow\; mdot = f_{mprT}(T_{o4}.P_{o4}, P_{o5}, N_{rpm}) \, , \tag{2-49}$$

$$\frac{T_{o2}}{T_{o1}} = f_{TrC}(T_{o1}, p_{o1}, mdot, N_{rpm}) \, , \tag{2-50}$$

$$\frac{T_{o4}}{T_{o5}} = f_{TrT}(T_{o4}, p_{o4}, mdot, N_{rpm}) \;\Leftrightarrow\; T_{o5} = f_{mtrT}(T_{o4}, P_{o4}, P_{o5}, N_{rpm}) \, . \tag{2-51}$$

As before we use multivariate polynomial fits to define these functions, though lookup tables can also be used.

Figure 2-45 shows the Simulink compressor model. This model uses the mass flow rate, the inlet temperature, the shaft speed, and the pressure as input parameters. The heat capacity of the fluid is required and is also shown as an input. The outputs of the model are just the outlet temperature and pressure, but also the power consumed by the compressor. This is exactly the formulation used in all previously described models. The two subsystems tComp and pComp simply compute the temperature and pressure ratios using the multivariate polynomial fits. The detailed programming of the polynomials is not shown.

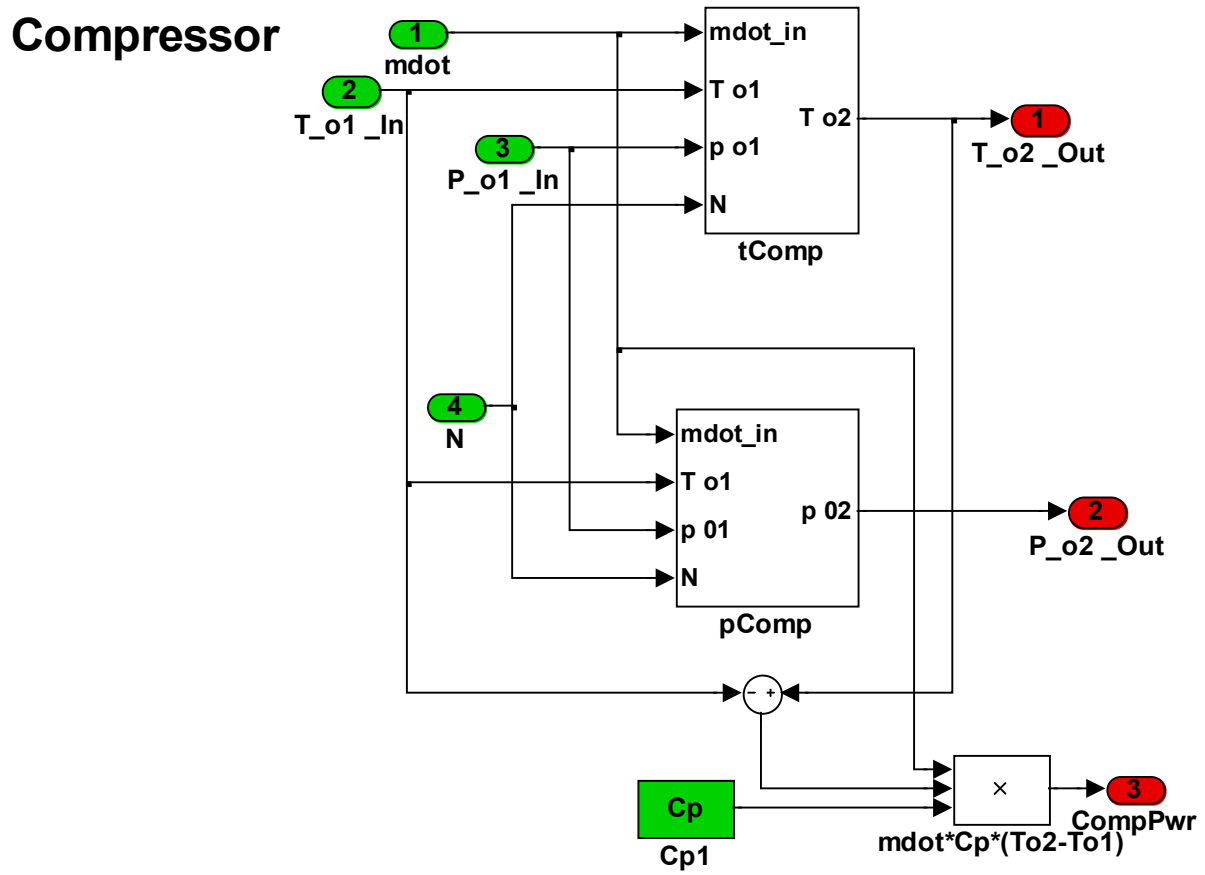

Figure 2-45: Simulink compressor model.

Figure 2-46 shows the corresponding Simulink model for the turbine. In essence it uses the same formalism as for the compressor except that equation 2-49 is replaced with an equivalent formalism that solves for the mass flow rate given the inlet temperature, inlet pressure, outlet pressure and shaft speed. Likewise equation 2-51 is replaced with its equivalent form that solves for outlet temperature given the inlet and outlet pressures, the inlet temperature, and the shaft speed. These equivalent forms for the multivariate polynomial characteristic flow curves

are used, because they directly provide the flow rate and the outlet turbine temperature, T_{o5}. This was done to ease the convergence requirements of the iterative nonlinear solver. We have used both the original form of the turbine characteristic curves and these equivalent forms and they both work, however the later formulism seems to converge quicker, and it is easier to debug. The reader will note, that some of the plots for the turbine were shown as a function of pressure ratio, which is consistent with the alternative solution method described here. Again one of the outputs of the Simulink turbine module is the turbine power.

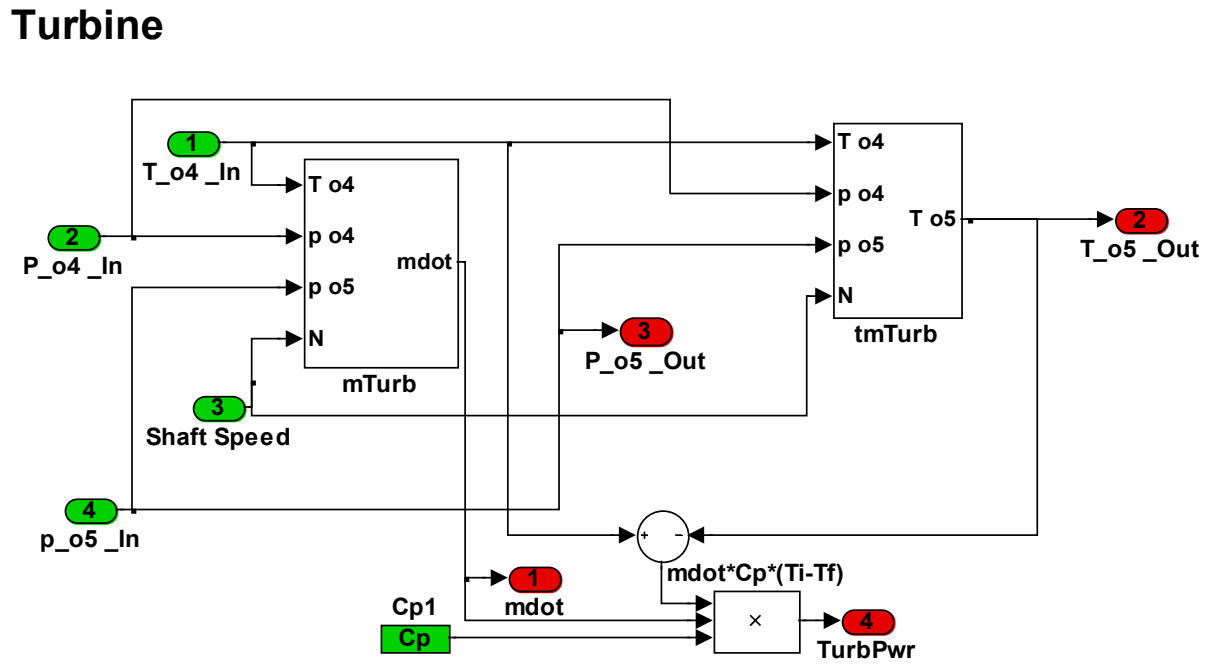

Figure 2-46: Simulink turbine model.

We have found it useful to think of the compressor as determining the pressure difference or pressure ratio in the loop, while the turbine determines the mass flow rate, and the absolute pressure is determined by the inventory constraint.

2.6.4.4 Heat Exchanger and Recuperator Simulink Module

The Simulink module for the recuperator or gas-gas heat exchanger and liquid metal to gas heat exchanger uses two sub-modules, one for each fluid leg. The Simulink block diagram is shown in Figure 2-47. Within each fluid leg the fluid transport properties are determined by a separate submodule and the energy balance equations are determined in its own submodule. The fluid transport properties are determined by fluid (gas or liquid) hydraulic calculator that determines the outlet pressure given the inlet flow conditions. This fluid hydraulic submodule is the "gas calculator" and is the same submodule that is described in Simulink Fluid Thermal Hydraulics Models, Section 2.6.5.1. The energy balance sub-module is a thermal heat transport module that determines the energy transfer from the specific coolant leg to the structure for each node used in the model which was described in the same section. These equations are listed in Table 2-34Table 2-34: Simulink sub-module and equation set for the

heat transport calculator. Because the heat exchanger is a counter flow heat exchanger it is necessary to reverse the numbering sequence of the nodes within each leg of the recuperator, and this is done in cyan colored submodules label U U(E) or U(E) U within Figure 2-47.

The recuperator/heat-exchanger module can be used for ducts, radiators, and liquid metal heat exchangers and for mixed fluid (liquid metal to gas) heat exchangers simply by changing the material properties and correlations used to determine the heat transfer coefficients. The user must supply the correct flow area, the hydraulic diameter, the heat transfer area, the material properties, and identify which the type of heat transfer correlation to use. Four correlations are built into the fluid hydraulic sub-module, the Dittus Boelter equations for coolant heating and cooling, the Martinelli liquid metal heat transfer correlation, as well as the heat transfer correlation for annular flow around a fuel pin (Chapman, 1967).

Table 2-30: Recuperator design dimensions and other properties

Recuperator Dimensions and Design Properties	
M_rcp = Mass of recuperator (kg)	136 kg
Ahp_rcp = Alp_rcp= heat transfer area of high pressure & low pressure leg	50 m^2
lHP = lLP = length of high and low pressure legs	0.4 m
twall_rcp = Wall thickness	0.4 mm
tgap_rcp = coolant channel flow spacing thickness/gap	1.0 mm
Nnodes_rcp = number of nodes in recuperator	25
Material Type for Structure	In718

2.6.4.5 Radiator Simulink Module

The Simulink module for the radiator uses the same components as is used in one leg of the recuperator (see equations HT(1) and HT(2) and are listed in equations 2-52, 2-53. The difference between heat exchanger model and the radiator model is that the structure temperature's heat loss to space is determined by the T^4 law of thermal radiation to space rather than convection. It therefore requires an additional heat loss mechanism or submodule which is shown in Figure 2-48. Again the pressure drop is determined by the frictional drag as listed in Table 2-33 and in equation 2-54. As before, the user must provide a radiator area, mass, and effective emissivity, as well as the coolant flow area, the heat transfer area from the coolant to the structure, material properties and other thermal fluid values. These values can be provided directly to the model or in an input file. The equations used for the radiator are

$$m_{rad_n} \cdot Cp_{rad_n} \cdot \frac{d}{dt} T_{rad_n} = h_{rad} \cdot A_{cs} \cdot (|T_n| - T_{rad_n}) - \sigma \cdot A_{rad} \cdot \varepsilon_{rad} \cdot (T_{rad_n}{}^4 - T_{space}{}^4) \qquad 2\text{-}52$$

$$0 = mdot \cdot Cp \cdot (T_{n-1} - T_n) - h_{rad} \cdot A_{cs\,rad} \cdot (|T_n| - T_{rad_n}) \text{ ,} \qquad \textbf{2-53}$$

$$p_{out} = p_{in} - \sum_{i=i\max} \frac{1}{2} \rho_{gas,i} v_i{}^2 \cdot \frac{4}{D_h} \cdot L_i \cdot f_i \text{ .} \qquad 2\text{-}54\textbf{.}$$

Recuperator

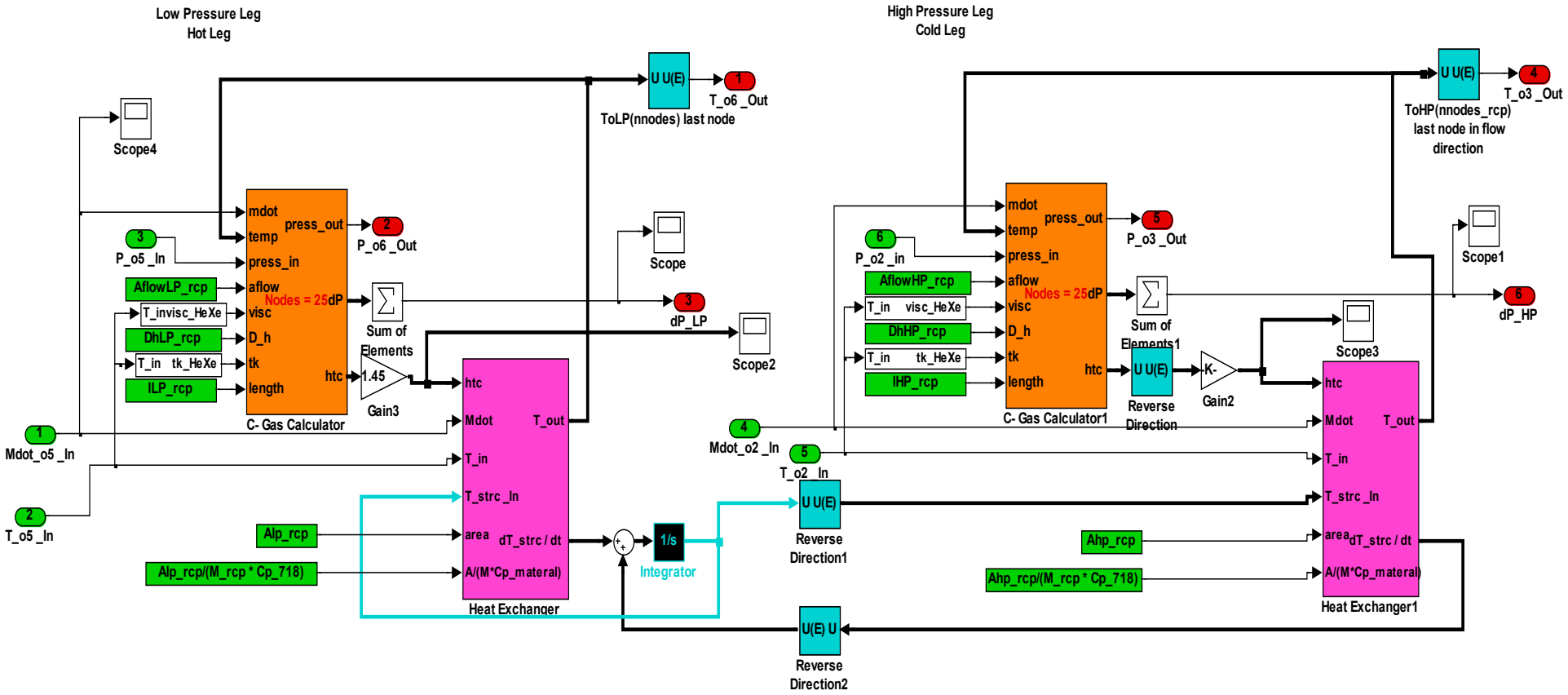

Figure 2-47: Simulink recuperator module for RPCSIM. The model uses has a low pressure leg and a high pressure leg. Each leg uses a gas calculator and a heat transport calculator to determine the pressure drop through the system and the gas and structural temperatures in the recuperator. The model assumes a counter flow recuperator, and the above programming reverses the direction of the node numbers to simulate the counter flow characteristics of the recuperator.

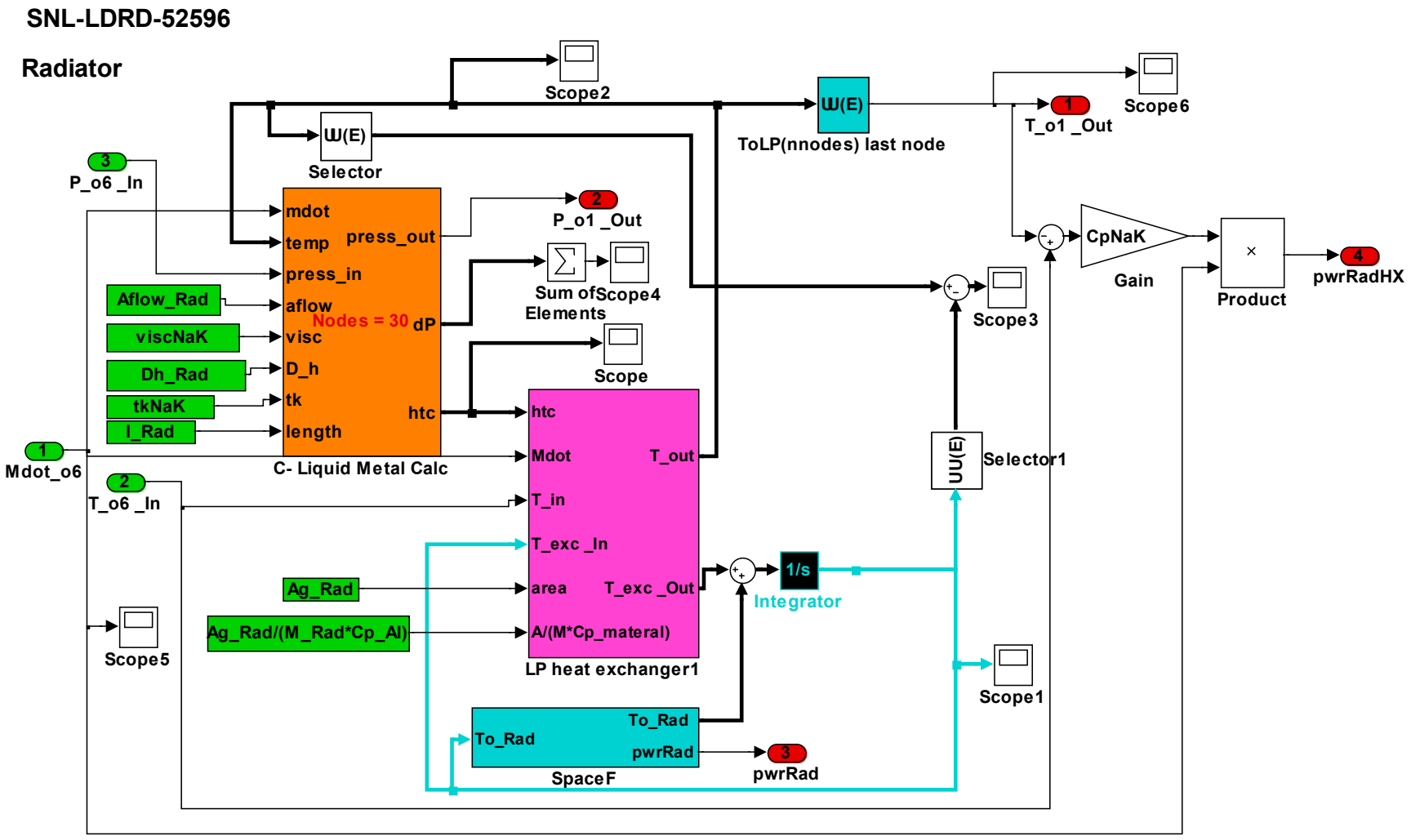

Figure 2-48: Simulink Model for a NaK cooled space radiator. An additional submodule (cyan) is added to the standard heat transport module to account for radiation losses to space.

The Simulink model for the space based radiator is shown in and in Figure 2-36 and in Figure 2-48. The radiator subsystem consists of a gas to liquid metal (NaK)heat exchanger which transports heat to the radiator panels. The NaK is pumped at a user prescribed rate via the pump model, and the radiator model transfers heat from the NaK to the radiator structure or panels that in turn radiation their heat to space. Any number of nodes can be selected for the radiator. The model here uses 30 nodes or radiator panels that are assumed to be at the structure temperature. The design dimensions and other parameters for the radiator are list in

Table 2-31: Radiator design dimensions and other properties

Radiator Dimensions and Design Properties	
M_Rad = Mass of radiator (kg)	438 kg
A_Rad = Radiating area of radiator	232 m^2
Ag_rRad = heat transfer area of LM to radiator panel structure	20.2 m^2
l_Rad = length of gas flow passage in radiator HX	1.0 m
Dh_Rad = Hydraulic diameter of gas in radiator HX	4. mm
eps_Rad =Emissivity of radiator panels	0.9
Nnodes_Rad = number of nodes in Radiator	30
Material Type for Structure	Al
Approximate NaK mass flow rate	1.9 kg/s

2.6.4.6 Gas Coolant Mass Constraint

One last constraint must be used to complete the set of equations and that is the gas inventory constraint. The total mass of the coolant in the flow volume is fixed, thus the sum of the mass in all components (subscript i) equals the initial fill mass.

$$\sum_i \frac{p_i \cdot V_i}{R_o \cdot T_i} = m_{fill} \quad . \qquad 2\text{-}55$$

This is shown as the po5 Inventory constraint submodule in Figure 2-36 and the Simulink details of the constraint are shown in Figure 2-49. The constraint assumes that the gas is an ideal gas and that the total mass in the system equals the fill mass. The fill mass can be a function of time which is input as a lookup table within Figure 2-49. The ducting volumes, lengths, duct mass and hydraulic diameters used by the Simulink model are listed in Table 2-32 and are combined using equation 2-55 in Figure 2-49. Simulink has a built in module called the algebraic constraint that was used to keep the fill mass at the specified level. Algebraic constraints seem to be difficult for Simulink to use. We found that the convergence was better maintained when we multiplied the constraint output by 1000 so that the constraint converged on the units of kPa rather than Pa.

Table 2-32: Table of GCR ducting component volume, length, diameter or and mass. In some cases the reactor, recuperator or radiator or gas chiller heat exchanger data must be used.

Duct or Component ID		Volume (liter)	Length (m)	Hydraulic Diameter (m)	Mass (kg)
V_{11}	Compressor Inlet Duct	10.1 liter	2.0 m	.08 m	20.662
V_{22}	Compressor Outlet Duct	2.5 liter	0.5 m	.08 m	5.1654
V_{23}	High Pressure leg of Recuperator	30.0 liter	0.4	rcp	136.0/2
V_{33}	Reactor Inlet Duct	19.6 liter	2.5 m	.08 m	30.992
V_{34}	Reactor Coolant Volume or Length	25.2 liter	0.644 m	rx	---
V_{44}	Reactor Outlet Duct Volume	19.6 liter	2.5 m	.10 m	30.992
V_{55}	Turbine Outlet Duct	3.9 liter	0.5 m	.10 m	6.1985
V_{56}	Low Pressure leg of Recuperator	30.0 liter	0.4 m	rcp	136.0/2
V_{66}	Gas Chiller Inlet Duct	10.1 liter	2.0 m	.08 m	20.662
V_{61}	Gas Chiller	1.4 liter	0.36 m	rad/gcx	53

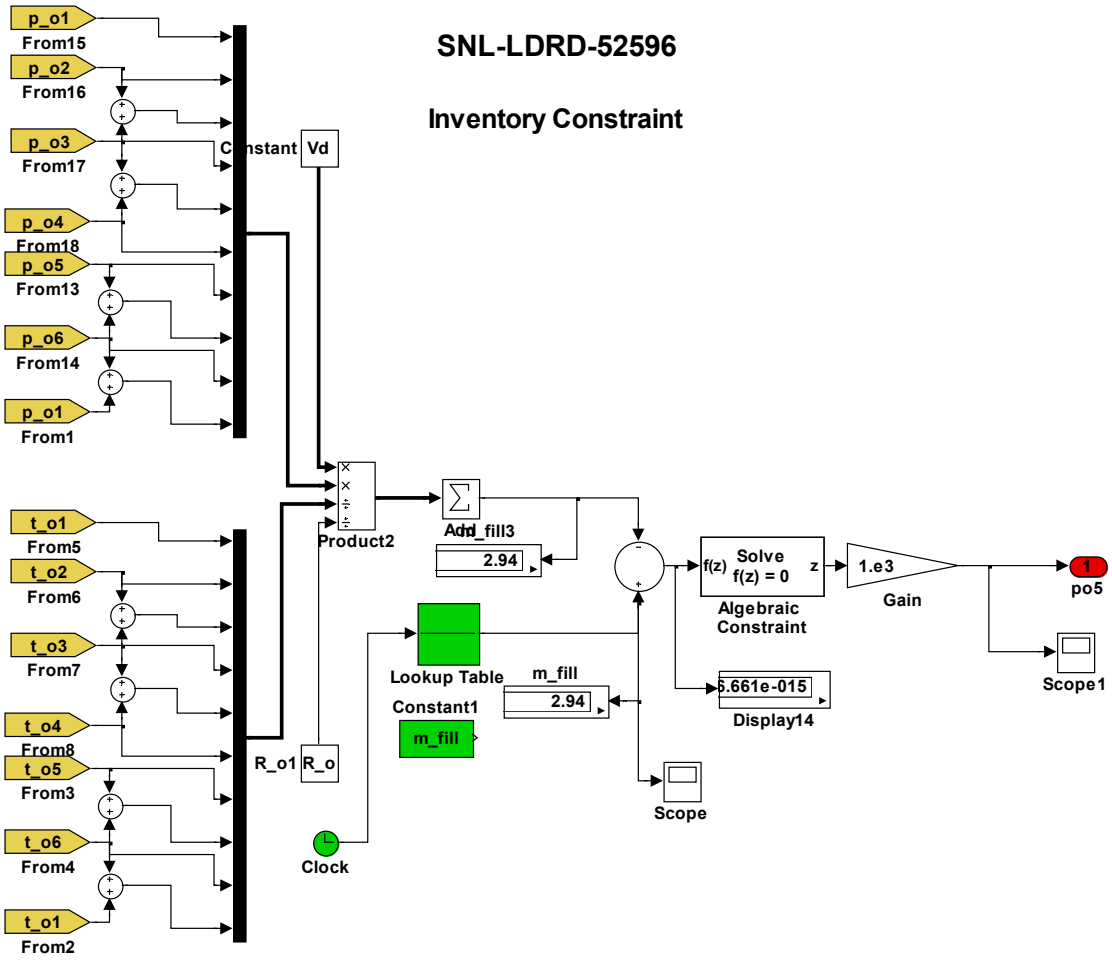

Figure 2-49: GCR Inventory Constraint to determine po5.

2.6.4.7 Feedback Control Loops

Two feedback control loops are used in the GCR CBC model, and they are indicated by the gold colored submodules as illustrated in Figure 2-36. One feedback loop controls the reactor by adjusting the reactivity to provide the requested reference reactor temperature profile. It is called the reactivity controller. The reactivity controller is shown, but it is not connected in this version of the model. Instead the reactivity is inserted via a look up table that is a function of time. The second feedback loop controls the turbo-machinery by adjusting the parasitic load seen by the alternator to provide the requested shaft speed. It is called the PMAD Power

Management and Distribution controller. Each of these feedback loops is briefly described in more detail below.

2.6.4.7.1 Reactor Controller

The reactor controller assumes that one or more instruments are able to provide an estimate of the average reactor coolant temperature T_{ave}. T_{ave} is the average of the inlet and outlet reactor coolant temperature (T_{o3} and T_{o4}), and it is a good approximation of the average fuel temperature. A feedback PID controller is used to adjust the inserted reactivity to follow a user prescribed reference fuel temperature profile. In this version of the controller, this feedback loop becomes active when T_{ave} exceeds 325K (This value is user specified.) Below this temperature the reactor power level is so low that no significant heating effects are observed in the timescale of interest (seconds to 1000's of seconds). In the current version of the reactor controller and during the low power and low temperature phase of startup, the reactor power is controlled by a user prescribed inserted reactivity profile. During this phase the reactivity is simply inserted as a step reactivity insertion of 12 cents, which puts the reactor on an exponential power increase with a period of about 93 seconds. (Again this is user specified.) In future versions of the reactor control loop, we will likely use a PID controller to follow a reference reactor period provided instruments are available that can provide and accurate estimate of the reactor period. Table 2-19 lists the relevant reactor kinetics parameters used in the model for a standard set of delayed neutron constants (Keepin, 1965). Clearly the reactor controller must be coordinated with the turbo-machinery controller and with the mission profile. The level of coordination is essentially the level of autonomous behavior that is desired.

2.6.4.7.2 PMAD or Turbo-Alternator-Compressor Controller

The Power Management and Distribution Controller consists of a reference shaft speed generator and a PID feedback loop that adjusts the value of a parasitic load resistor to force the measured shaft speed to follow the reference speed. The PMAD controller is very simple in this version of the code and assumes that all the power is going through the load resistor. More sophisticated models will be required that model the power converters, the voltage regulation, and partition the electrical power between the load resistor and the power bus. Other logic (not shown) is provided in these models that specify that the reference shaft speed should only startup if and only if T_{ave} (the estimator for the fuel temperature) exceeds a specified value. Depending on the startup scenario, it could take an hour or more for the reactor to exceed the startup set-point temperature. It will take much longer if the reactor is a lithium cooled reactor because a substantial amount of time and control mechanisms will be required to melt the lithium both in the reactor and in the primary heat transport system. The designer may want to selected a reactor startup temperature that is sufficiently large that the turbo-machine will maintain a self-sustaining shaft speed of at least 40% of the full power shaft speed. Alternatively, other startup procedures can be implemented that first start the turbo-machinery and motor the alternator. Once coolant flow has been started then the reactor can be started. Both startup transients will be examined in the following sections.

2.6.5 Simulink System Model and Equations

A brief summary of the system model and equations used by Simulink is provided here. The essence of the solution is as follows. Because the mass flow rate is assumed to be constant around the loop, every component must determine the outlet temperature and pressure of the

coolant or fluid given the initial inlet temperature, pressure and mass flow rate. A nonlinear stiff differential equation solver is used to iteratively solve for a consistent set of temperatures, pressures, and the temperature derivative terms for all components in the CBC loop with the constraint that the total gas inventory remains constant throughout the loop.

The over all equation set includes other (non thermo-hydraulic) models and equations sets to determine the reactor power, given inserted reactivity, and inlet flow conditions, and to model electrical systems such as the alternator, rectifier, and voltage regulator. The electrical components are modeled in a heuristic manner and only include terms such as efficiency and simple linear relationships between speed, voltage and simple electrical loss terms. Complete electrical simulations of these components are not currently included in the model. The turbo alternator compressor (TAC) model is coupled to the shaft speed (and therefore gas flow) by way of the electrical load/torque, rectifier, voltage regulator and power management and distribution system (PMAD).

The current set of equations used by RPCSIM ignores the inertia of the coolant mass. This assumption limits the applicability of the flow rate to time scales that are greater than the time it takes to accelerate the fluid. We estimate this to be less than 0.1 second. Furthermore, because the reactor and CBC components are relatively massive, the thermal behavior of the combined system changes very slowly (1000's of seconds). Therefore the thermal transients are not greatly affected by neglecting the inertia of the fluids within the model. The great benefit of these assumptions is that the transient behavior of the complete CBC system can be rapidly calculated even for time scales that last for many ten's of thousands of seconds to days, but still provide a high level of accuracy for rapid transients that may be as short as a few $1/10^{th}$'s of a second.

2.6.5.1 Simulink Fluid Thermal Hydraulics Models

The conservation equations (or approximations of them) for mass, momentum and energy equations must be satisfied within each component in the coolant loop. The mass conservation equation is satisfied because the mass flow rate around the loop is considered to be everywhere a constant, though it does change with time. The momentum equation is also greatly simplified because the model assumes that the quasi-steady-state pressure drop, as determined by frictional drag, is calculated within each component. The goal of the Simulink program is to develop a generic set of modules that are capable of determining the outlet temperature and pressure of the coolant or fluid given the initial inlet temperature, pressure and mass flow rate. Because the mass flow rate is continuous and because of the simplifying assumptions, all of the thermal hydraulic equations can be included into two modules. These two modules

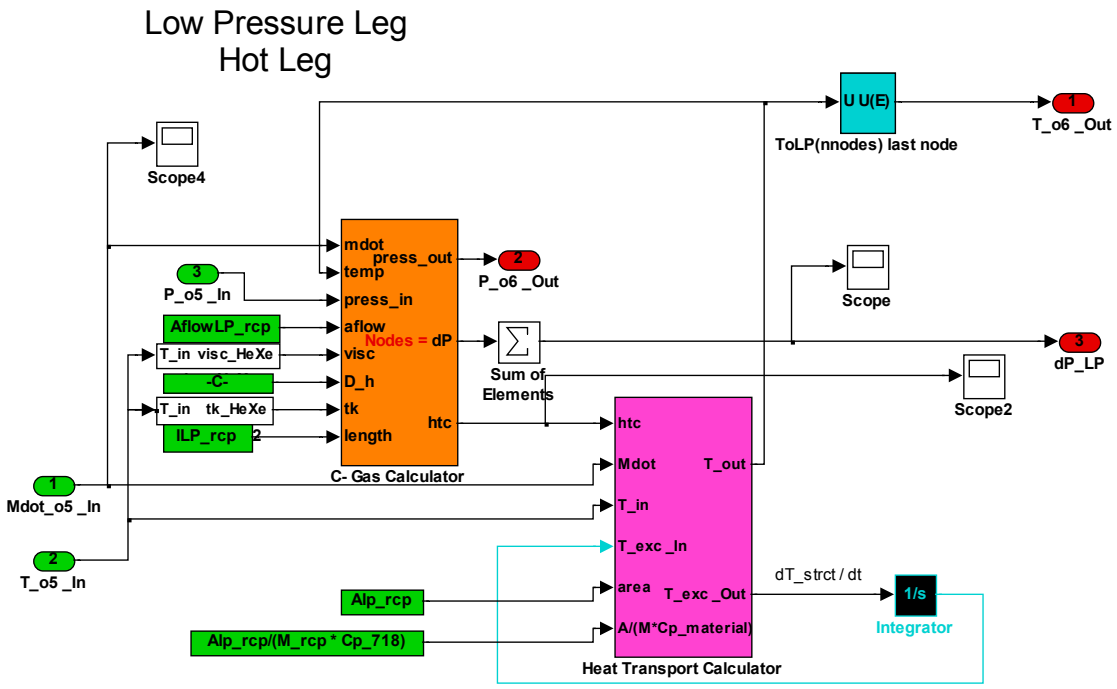

Figure 2-50: RPCSIM thermal hydraulic models for coolant pressure drop (momentum) and heat transport (energy). The gas calculator determines the outlet pressure given the inlet flow rate, temperature and pressure and given the coolant hydraulic flow parameters such as hydraulic diameter, flow area, and flow length as well as the coolant material properties. Likewise the gas outlet temperature and the time rate of change of the structural temperatures are determined by the heat transport module (heat exchanger). Again material properties and design geometries are required.

are shown in Figure 2-50 and consist of the Gas Calculator and the Heat Transport Calculator. The Gas Calculator (orange module) determines the outlet pressure given the inlet conditions (flow rate, temperature and pressure) and given the coolant hydraulic flow parameters such as hydraulic diameter, flow area, and flow length as well as the coolant material properties. For convenience it also calculates a heat transfer coefficient using the Dittus Boelter heat transfer correlation or other correlations. The gas calculator is written in C (though Simulink modules are also available). The Heat Transport Calculator (magenta module) determines the gas outlet temperature and the time rate of change of the structural temperatures (dT_strct / dt) as well. In addition to knowing the inlet conditions (temperature and mass flow) the heat transport calculator needs the heat transfer coefficient, as well as the heat transport area, the mass of the structure, and the thermal capacitance of the structure. The derivatives for structure temperature are integrated (in the 1/s Integrator module, which includes the initial conditions) for each time step to determine the structural temperature at every node in the component and for each coolant node. Simulink has its own internal routines to automatically determine the time step.

In addition the temperature dependence of the viscosity and thermal conductivity are illustrated in Figure 2-50 by small clear modules that output the viscosity and thermal conductivity given the gas temperature. At the current time the coolant heat capacity and other gas properties such as the gas constant is buried within the module and it is not a function temperature.

Figure 2-50 shows these two modules for the low pressure leg of the recuperator. The subscript _rcp stands for the recuperator, LP or lp identifies the low pressure leg. The gas calculator module and the heat transport modules are described in more detail in the following paragraphs.

Table 2-33 shows a detail of the Simulink module for the gas calculator (visual Simulink module, not the C version). This module is very similar to the C code version except that in the C code, the Prandtl number Pr is not passed to the module but is determined from the thermal conductivity, viscosity and heat capacitance of the gas. Note that within the gas calculator that submodules or subsystems are used to calculate the gas density, velocity, Reynolds number, as well as the fanning friction factor, the heat transfer coefficient and outlet pressure. Simulink modules can work with scalars or arrays, thus if an array of inlet conditions and geometries are submitted as input then the module outputs an array of outlet pressures, node pressure drops, and heat transfer coefficients. The C version of the gas calculator module is set up to output the outlet pressure of the last node so that the outlet pressure is passed to the next module. Also note, that the heat transfer coefficient is coded for the Dittus Boelter correlation for gas heating. The C routines contains a parameter that lets the user selected among the Dittus Boelter heating or cooling correlations or to use the High Temperature Test Reactor (HTTR) correlation, (Takase, 1996). Other heat transfer correlations can be easily added. Also observe that the submodules that were used to calculate all the various thermal hydraulic diameter, density, velocity, etc are implemented as a library within Simulink so that they can easily be reused.

Table 2-33: Simulink gas calculator and equations used within the module. The gas calculator internal model calculates the gas density, the gas velocity, the Reynolds number, the friction factor, the heat transfer coefficient, and the node-to-node pressure drop. Green ovals represent input values to the module and red ovals represent the outputs.

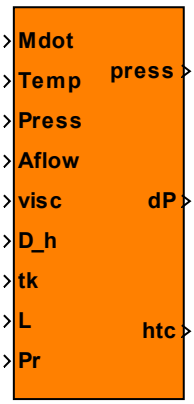	$\rho = T/(p \cdot R_o)$ where ρ is the density, T is temperature, p is pressure and R_o is the gas constant $v = \dot{m}/(\rho \cdot A_{flow})$ where v is the velocity, $\dot{m}$ is the mass flow rate, A_{flow} is the flow area $\mathrm{Re} = (\rho \cdot v \cdot D_h)/visc$ where Re is the Reynolds number, D_h is the hydraulic diameter, and visc is the coolant viscosity $ff = MAX((16/\mathrm{Re}),,(0.0791/\mathrm{Re}^{0.25}))$ where ff is the fanning friction factor $h = 0.023\ \mathrm{Re}^{0.8}\ \mathrm{Pr}^{0.4}\ k\ /D_h$ where h is the heat transfer coefficient, and Pr is the Prandtl number $p_{out\ j} = p_{in\ j} - \frac{1}{2}\rho_{gas,j}\ v_j^{\ 2} \cdot \frac{4}{D_h} \cdot L_j \cdot ff_j$ where j is the j^{th} node, L_j is the length of the j^{th} node

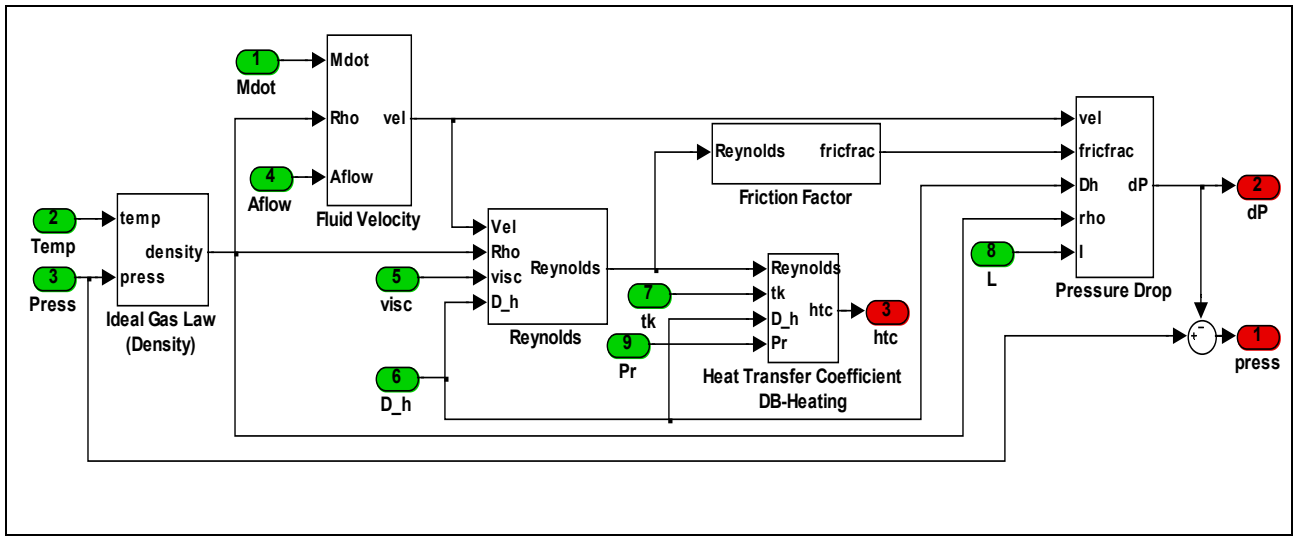

A detail of the heat transport sub-module is shown in Table 2-34. For input this module requires the heat transfer coefficient (htc), the mass flow rate (Mdot), the inlet temperature array for each node, the structure temperature structure array for each node (T_strc_In), the heat transfer area (area), and the ratio of the heat transfer area to the product of the structural mass and the heat capacitance of the structure (Cp_material). The module then outputs the outlet gas/coolant temperature array (T_out) and the time rate of change of the structure (dT_strc/dt). As shown in Figure 2-50, the rate of change of the structure temperature is integrated and feedback into the inlet structure array to complete or close the equation set. The conservation of energy equations that are used in the module are described in HT(1) and HT(2). HT(1) simply states that the energy increase in gas temperature is equal to energy loss from the structure to the gas. Equation HT(2), then equates the energy loss/increase of the structure to the rate of change of the temperature, which is ultimately integrated to give the final structural temperature. The Simulink internals of the heat transfer module are not shown.

Table 2-34: Simulink sub-module and equation set for the heat transport calculator.

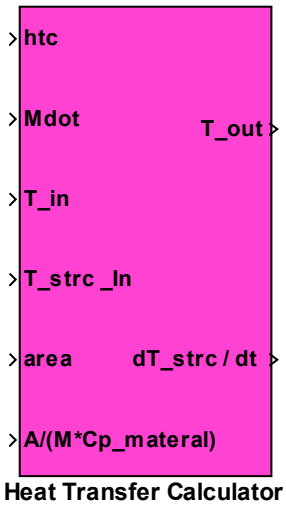

$$0 = mdot \cdot Cp \cdot (T_{n-1} - T_n) - h \cdot A_{cs} \cdot (T_n - T_{strct_n}) \qquad \text{HT(1)}$$

$$m_{strct_n} \cdot Cp_{strct_n} \cdot \frac{d}{dt} T_{strct_n} = \sum_{legs} h \cdot A_{cs} \cdot (T_n - T_{strct_n}) \qquad \text{HT(2)}$$

These two "calculator" modules are very general and can be reused to approximate the solution to a wide variety of problems. By simply changing the design constants (flow and heat transport areas, hydraulic diameters and lengths) as well as making minor modifications to account for additional heat loss mechanisms, due to other structures, we have been able to represent fuel pins, counter flow heat exchangers, radiators, ducts, pressure vessels and core blocks. The method used to simulate these other components is shown in the next section.

2.7 Startup Transients for Reactor Driven Brayton Cycles

In this section the Reactor Power and Control SIMulator program (RPCSIM)) will be used to illustrate a variety of startup transients. The transients will focus mainly on reactor driven closed Brayton cycles for gas cooled reactors, but some results for Liquid Metal Reactor LMR's will also be presented. The goal of this section is to point out general operational behavior of a reactor driven closed Brayton cycle system and its response to effects such as reactivity increases, rpm increases, fill inventory changes, radiator coolant flow perturbations, changes in feedback phenomena, and shaft speed control effects.

For a GCR the startup transient can proceed in two ways. In the first method the reactor is started first, followed by the CBC machinery. In the second method the turbo machinery is started first followed by the startup of the reactor. The first method minimizes the motor power to the alternator which has definite benefits for space applications. The second method minimizes the thermal effects and is similar to startup of systems on earth. Startup transients that used both methods will be presented.

For lithium and sodium cooled space power LMR systems, the reactor power is needed to melt the liquid metal due to the lack of large amounts of auxiliary power, thus the turbo machinery can only be started once the reactor and liquid metal coolant is molten and sufficiently hot that is will not refreeze when the liquid metal pumps and turbo-machinery start. Thus there is no option to start the circulation pumps prior to starting the reactor. Liquid metal systems that use NaK as the coolant may be able to avoid liquid metal freezing, therefore for these systems, reactor startup may begin after startup of the liquid metal pumps.

Often LMR advocates claim that because of the liquid metal to gas heat exchanger, that the LMR is not as tightly coupled to the be behavior of the Brayton system, thus the transient effects will be less. The results presented here show that this is **not** the case and that transient effects for similar startup up transients generally have more and larger transients than seen in the gas cooled reactors. These effects and more will be illustrated in the following sections.

2.7.1 GCR Startup Transient with One Feedback Term

The first startup transient for a Gas Cooled Reactor (GCR) is illustrated in Figure 2-51 through Figure 2-55. The reactor description was provided in Section 2.6.4. A single feedback term was used for the fuel having a value of -0.2 cents/K. The overall transient used here is the basis from which all the other transients that will be presented in this report were built from. It consists of several phases that take the reactor from zero power (which initially is at fractions of a milliwatt) through sensible heat, to turbo-machinery startup. RPCSIM is programmed to initiate the Brayton loop (start motoring the turbo-machinery) when the average fuel temperature exceeds the initial temperature by a specified value (which is 300 K above the initial temperature =225K in this transient). (Options within RPC also allow the startup to occur at any user specified time.) Once the reactor and turbo-machinery are started the total system is then allowed to reach steady state conditions at low shaft speeds and at low reactor temperatures. Because the reactor and turbo-machinery are at low temperatures and shaft speeds the electrical power and reactor power levels will also be low, see Figure 2-32. This low power phase is intended to be a checkout phase with sufficient thermal power that positive electrical power can be produced by the reactor driven loop and connected to the space bus to fully checkout the spacecraft. This commissioning phase may in reality take weeks, but in the transients presented here it is limited to about 3,000 seconds. Next the system transitions over a period of 2000 seconds to full temperature, full shaft speed, and full power by simultaneously increasing the reactor fuel temperature and the TAC shaft speed. Once the full reactivity insertion and shaft speed have been reached these values are kept steady and the complete system is allowed to reach steady state levels. In all cases the PMAD controller uses a feedback loop to adjust the alternator load to provide the specified RPM. The PMAD will then distribute this load to the ion engines, to the scientific instruments, and to the parasitic load resistor according to the mission plan and state of the spacecraft. As mentioned before, the current version of RPCSIM does not include a detailed model for the PMAD.

All of the transients that are presented have been given abbreviated names so that they can be recognized. The first transient is Tinit+300,1FB which indicates that the CBC unit starts at the initial temperature + 300K, and that the reactor has only one feedback term. Subsequent transients have similar names. The results and details of this transient will be presented in some detail because it is the basis from which all the other transients were derived.

The reactor and CBC input values are shown for transient Tinit+300,1FB in Figure 2-51. The reactor power and Brayton power responses to these inputs are shown in Figure 2-52. The gas station pressures and temperatures are shown in Figure 2-53 and Figure 2-54 respectively. RPCSIM outputs large amounts of data that can be viewed from within Simulink, MatLab, or in Excel. In this report only limited reporting of the output variables is provided. A detailed description of the startup follows.

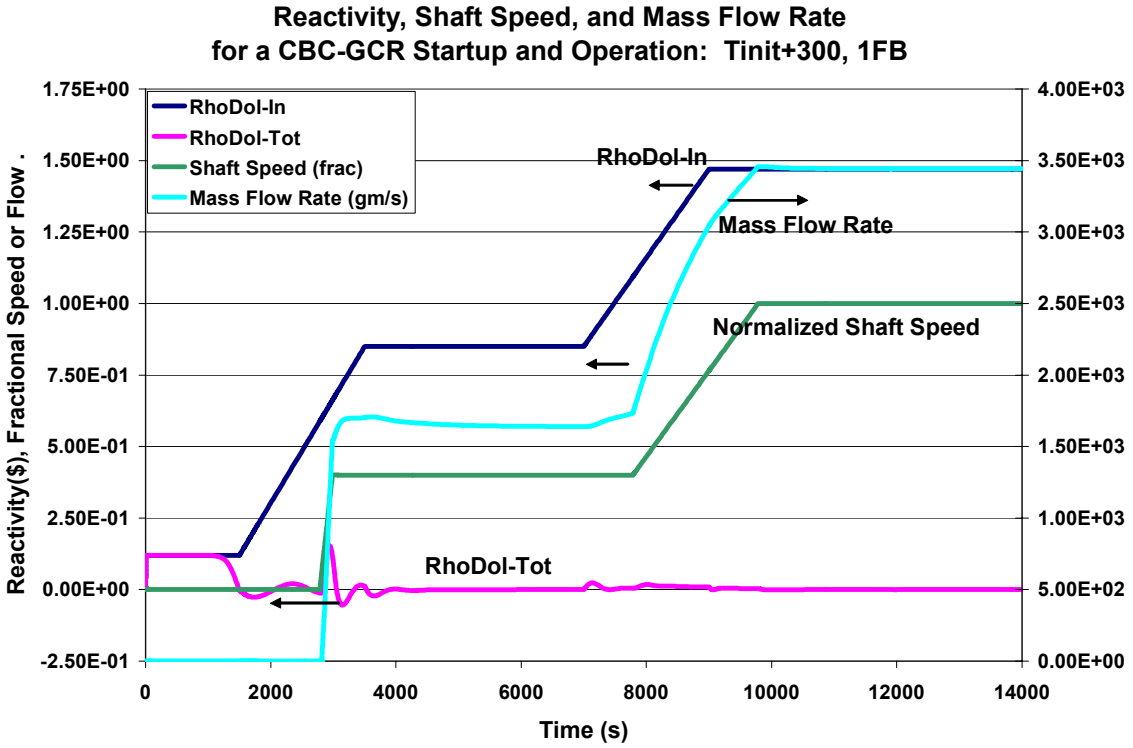

Figure 2-51: Input values for transient Tinit+300,1FB. The plot shows the inserted reactivity (Rho-Dol-In), the TAC shaft speed (Normalized Shaft Speed), the mass flow rate (Mass Flow Rate) and the total reactivity which is the sum of the inserted and feedback terms (Rho-Dol-Tot). The reactivity is given in dollars.

Phase 1: Zero power startup (0 – 1500 seconds).

At the beginning of this phase the reactor starts out at an initial power level that is about 0.2 mW . The reactor is assumed to be shut down with a reactivity level of -7.00 dollars of reactivity. A core neutron source strength of 10^6 neutrons per second is assumed. The initial power, source strength and reactivity can be related to the equation $\rho = -\Lambda \cdot S / P_{rx}$, where S is the source strength W/s (which can be related to the initial neutron source strength by assuming that every fission results in ν fission neutrons), Λ is the neutron generation time (10 μsec), and P_{rx} is the fission power level (W). At time t=0 seconds a step of reactivity is added of 12 cents. This puts the reactor on a positive period of about 80 seconds. The power grows at this exponential period until sensible heating occurs, at which time the reactor fuel temperature becomes sufficiently large that thermal feedback effects are starting to become important. This occurs at about 1300

seconds when the power level is in the kW level. Shortly after this time the feedback effects become sufficiently large to terminate the exponential power increase which results in a power spike at 1500 seconds. The peak power reaches a modest peak power level of 18 kW. The average fuel temperature has increased from 225 K to about 280 K by this time.

Phase 2: Reactivity Insertion Ramp (1500s – 3500 seconds).

During the next phase the inserted reactivity was inserted at a constant rate to increase the fuel temperatures to values that would be sufficiently large that we could attempt to start the turbo-machinery. The insertion rate was set to 0.0365 cents/second which amounts to 73 cents of reactivity inserted over a period of 2000 seconds. At the end of the time period, 3500 seconds, the total inserted reactivity was 85 cents.

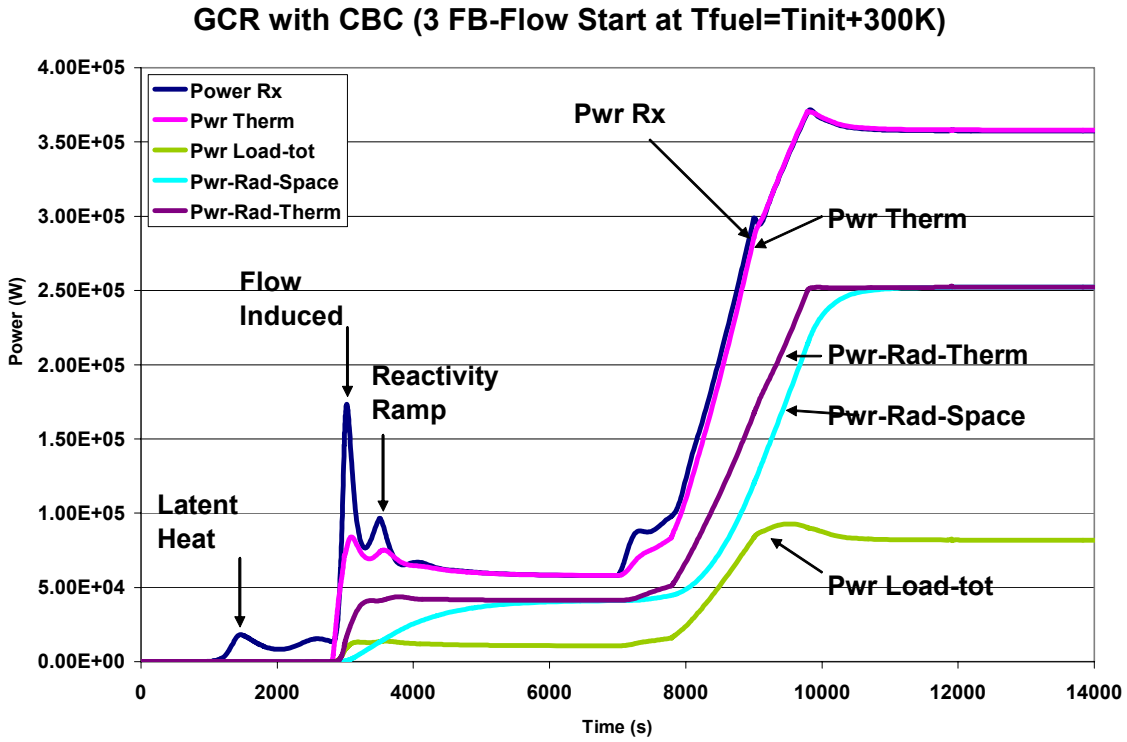

Figure 2-52: Reactor and CBC power levels for transient Tinit+300,1FB. The plot shows the fission power or reactor power, the thermal power transferred to the gas coolant, the power transferred from the coolant to the radiator structure (Pwr-Rad-Therm), the power radiated to space (Pwr-Rad-Space) and the alternator load or electrical power (Pwr-Load-tot).

For a reactor with a single negative feedback term, a slow ramp insertion of reactivity results in an increase in the temperature trace that almost follows the reactivity insertion. The difference is that the reactor power produces small power pulses that occur at regular intervals. A small power pulse of 15 kW is observed in Figure 2-52 at 2600 seconds, just before the large spike. The ramp increase in reactor fuel temperature can be seen in Figure 2-54 which shows the Rx outlet temperature as a function of time. Even though this is not the average fuel temperature, when there is no coolant flow, the reactor outlet

temperature is set to the average of the last fuel temperature node and the core prism node. Therefore the shape of the TIT is similar to the fuel temperature. This curves shows a temperature ramp that increases from 225K to 350 K from 1500 seconds to 2800 seconds.

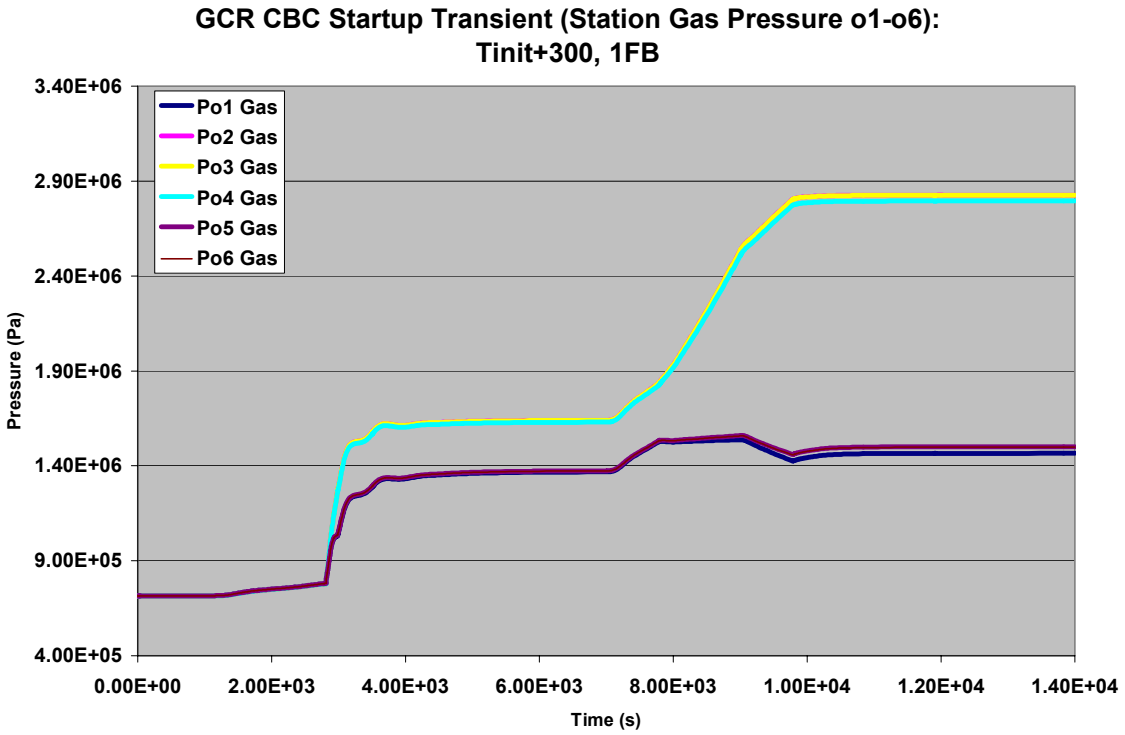

Figure 2-53: Pressure values for transient Tinit+300,1FB. The plot shows the pressure at each station around the loop, but as can be seen the pressures really show the time dependent values of the low pressure leg and the high pressure leg. Pressure drop effects are observable, but they are small.

At 2800 seconds, the average fuel temperature reaches the set point of 300 K above the initial temperature. Once the average fuel temperature reaches its set point (Tinit + 300 K), the PMAD controller schedules the rpm to follow a prescribed reference curve. The curve in Figure 2-51 (Normalized Shaft Speed) is the shaft speed in kilo-revolutions/second and it is scheduled to increase its speed in a ramp from 0 rpm to 400 rev/s which is about 40% of its design value (design rpm is 60,000 rpm = 1000 rev/s). The same figure shows that the mass flow rate curve has the same general shape as the rpm curve.

Because the TAC is likely to use gas bearings, the shaft speed must reach relatively high values very quickly. In the Capstone-C30 system the TAC shaft increases to 25,000 rpm in less than one second. Such a rapid increase in mass flow can cause difficulties for the solvers in Simulink, so we have slowed the startup transient down. In this transient the shaft speed increases to 40% of it design speed in 200 seconds. Typically they startup in about 100-200 seconds, but startup times as short at 2 seconds have been used. Clearly the rate at which the turbo-machinery starts also affects the flow rate and the power

required to motor the alternator. More information on this will be presented in a few paragraphs.

When the CBC starts that the flow increases rapidly and a reactor power spikes to 180 kW is observed at 3000 seconds. This spike occurs because the flow is pushing cool gas into the reactor and the average fuel temperature drops by about (50 K). This temperature reduction is best seen by the rapid increase in the total reactivity at this time. It is also observed as an average fuel temperature decrease within RPCSIM, but the plot for this data is not included in this report. The peak of the power spike happens to occur when the shaft speed ramp has reached is maximum setpoint (40% full rpm). Presumably, if the rpm were ramped to an even higher value the peak would be greater, likewise if we shorten the ramp the peak will occur sooner and will be larger. We have tested these perturbations, and the behavior does indeed occur as hypothesized. In summary, the power spike is flow induced and its peak magnitude depends on the shaft speed ramp rate, and on the maximum speed attained. The peak of the pulse occurs when the full speed is attained.

After the power spike, the reactivity ramp continues to increase the average fuel temperature, and another mild power spike is observed at about 3500 seconds when the reactivity ramp is terminated. This power spike is caused by the reactivity ramp as no drop in fuel temperature is observed within RPCSIM.

The PMAD controller adjusts the alternator load in a Proportional Integral PI feedback loop to produce a real shaft speed that follows the reference rpm. As it turns out, the PI feedback loop is very good, so the reference rpm and the actual rpm are nearly identical. The curve in Figure 2-51 (Normalized Shaft Speed) is the actual shaft speed in kilo-revolutions/second, not the reference shaft speed. The rpm is scheduled to increase its speed in a ramp from 0 rpm to 400 rev/s which is about 40% of its design value (design rpm is 60,000 rpm = 1000 rev/s).

To spin the TAC shaft, the PMAD adjusts the alternator load or power. The power produced by the alternator is shown in Figure 2-55. Negative powers mean that the alternator is motoring, while positive values mean that power is being produced. Because of the inertia of the shaft, the alternator power has a negative spike which first gets the shaft spinning, then more gradual powers are applied to motor the alternator to keep it moving. The peak of the negative spike is about -0.5 kW, while the remainder of the motor curve requires a gradual pulse of 100 W. The alternator must be motored for about 1 minute before positive power is produced, meaning self-sustaining operations. If we shorten the shaft speed ramp period from 200 seconds to 2 seconds both the magnitude of the motor spike and its maximum value also increase. Similarly it takes less time before the system is self-sustaining.

The alternator model is not very sophisticated at this time, but we believe that the overall trend and shapes, and time durations are correct. Note that the turbine inlet temperature (see Figure 2-54) increases its temperature very rapidly to about 650K. Based on the operational map shown in Figure 2-28 self sustaining operations require that the average fuel temperature (which is close to the fuel temperature) must be > 600 K at 40,000 rpm.

Thus, this transient's self-sustaining behavior predicted by the RPCSIM dynamic model confirms the steady state behavior predicted in Figure 2-28.

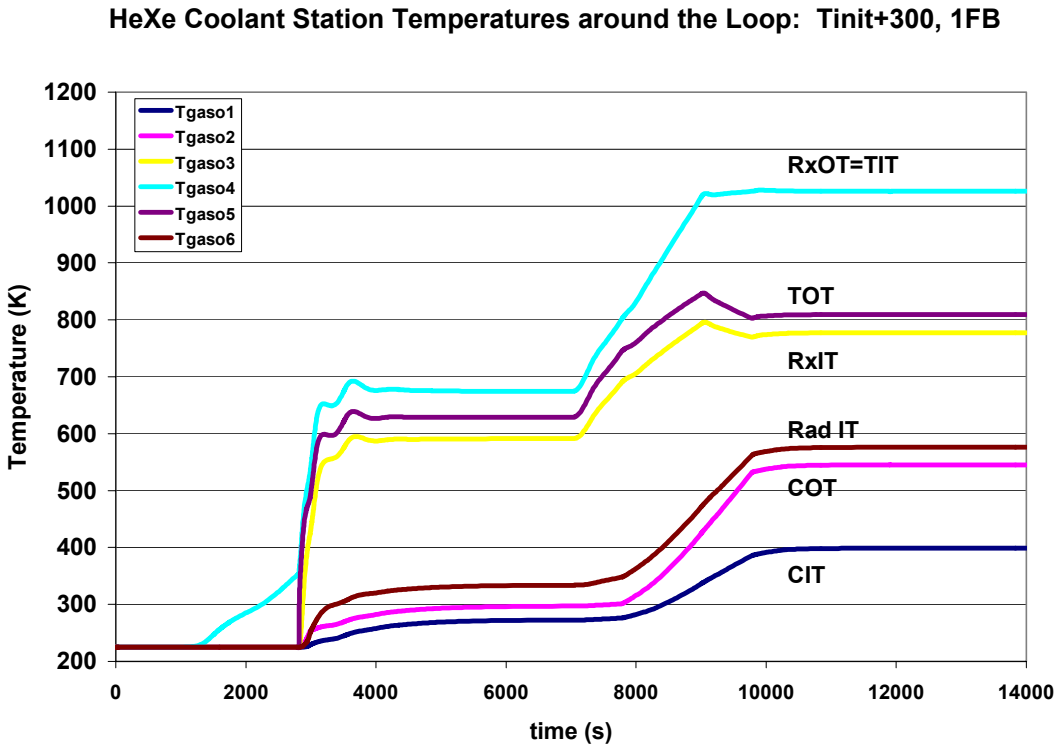

Figure 2-54: Station temperatures for transient Tinit+300,1FB. This plot shows the temperatures for the reactor outlet or turbine inlet (RxOT=TIT), the turbine outlet (TOT), the reactor inlet (RxIT), the radiator inlet (Rad IT), the compressor outlet (COT), and the compressor inlet (CIT).

At 3500 second the inserted reactivity ramp stops and the reactivity is held constant. Another mild power spike is observed. This power spike is caused by the reactivity ramp which is still continuing while the turbo-machinery starts. Again we know that this small spike is reactivity ramp related as no decrease in fuel temperature is observed within RPCSIM.

The reactor power spikes produce step-like increases in the gas coolant temperature. These steps in temperature are illustrated in Figure 2-54 which shows the gas station temperatures around the loop. RPCSIM shows that the average coolant temperature increase from about 300 K to 600 K in about 400 seconds, while the average fuel temperature increases from 470 K to 620 K in about 200 seconds. This results in a rate of temperature increase of about 0.75 K/s. Again as mentioned before, if the shaft speed ramp is faster, then the temperature increase rate is also quicker. The designer will have to develop a maximum acceptable ramp rate that can be tolerated.

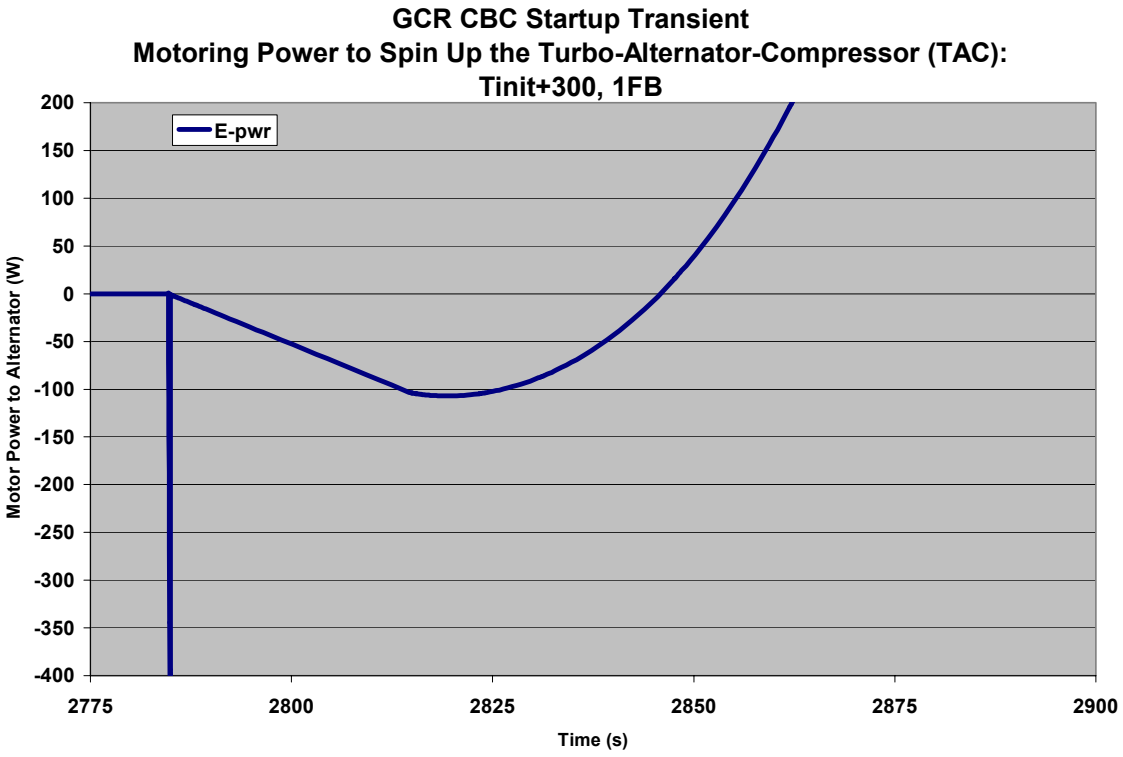

Figure 2-55: Alternator power for transient Tinit+300;1FB. The time scale and power levels show the power required to motor the alternator. Self sustaining operations occur at 2850 seconds.

Phase 3: Low Power Steady State (3500s – 7500 seconds)

At 3500 seconds both the shaft speed and the reactivity are held constant, and the rest of the system is allowed to reach its equilibrium conditions. At around 6000 seconds, the reactor power level and all other power level appear to be approaching their steady state conditions. Also observe (see Figure 2-54) that the higher temperature locations in the loop appear to reach steady state quicker than the lower temperature values. The rate limiting component is the space radiator. This is clearly seen in Figure 2-52 where the radiating power (Pwr-Rad-Space) has the longest time constant. Thus, overall we see that the shaft speed can change its values very quickly and therefore the mass flow rates can change rapidly as well, therefore the thermal response has two components, one that is rapid and depends on the rapid changes in speed or mass flow rate, the next is a slow thermal response that occurs while all the mass and structure (tones) slowly reach their equilibrium values.

At the end of this phase the reactor fission power and the thermal power are identical indicating that steady state has been achieved, and the reactor power level is about 58 kW_t., or about 14-50% of its design value (400 kWt). The radiator is radiating about 42 kW_t to space, and the alternator is producing about 11 kW_e. RPCSIM has thermal radiation loss terms in the model to simulate losses from the ducting, which are designed to have heat losses to control the wall temperatures of the double ducting. These losses

are about 5 kW_t. The average fuel temperature is about 650 K. These values seem sufficiently low and had large margins from the maximum limits of the space reactor power system. Therefore, this low power domain is a good place to check out the complete space craft to assure that all systems are working, and to determine if the system can approach full power, or if minor medications need to be imposed prior to transitioning to full power.

Phase 4: Transition to Full Power (7,500 - 9,780 seconds)

The fourth phase of transient Tinit+300,1FB increases both the reactivity and the shaft rpm. The ramps are staggered. The reactivity ramp increases from 83 cents to $1.47 from 7500 seconds to 9000 seconds. The shaft speed starts its increase at 7800 seconds and reaches 1000 rev/s (full design shaft speed) at 9780 seconds. The staggering was done so that the effects of the reactivity ramp and shaft speed ramp alone could be assessed. The response of the system behaves as expected, showing a relatively smooth increase in reactor power level and alternator power produced.

Phase 5: Full Power Steady State (9,780 – 14,000 seconds)

The fifth phase allows the reactor and CBC system to achieve its steady state levels. For this transient the maximum reactivity insertion was $1.47, and the peak TIT achieved was 1026 K, which is not the GCR design TIT of 1150 K. Nevertheless the peak reactor power level achieved was 358 kW_t, the electrical power is 82 kW_t and the radiator power is 252. kW_t. The total cycle efficiency is 22.9 %, but this does not include losses from the PMAD and other components. In general the sum of the electrical power plus the radiated power plus the losses must sum to the total reactor power produced. The ducting and other parasitic losses amount to 24 kWt. The expected losses from just the hot ducts alone is on the order of 16-20 kW, so this amount of loss appears to be on the correct order of magnitude.

If the same transient is repeated, but with $1.70 of total reactivity insertion, then the turbine inlet temperature reaches 1151 K, which is about the design temperature. For these conditions, the total reactor power was 430 kW_t, the electrical power produced was 117 kWe (for an efficiency of 27.2%). These values are very close to the expected design values predicted from the standard thermodynamic cycle equations, see Figure 2-38.

One figure not discussed much above is the gas pressure in the CBC loop, see Figure 2-53. Initially the fill gas pressure was about 0.7 MPa. When the reactor begins its heating phase, a slight internal pressurization occurs within the system. However when the turbo-machinery starts the compressor does its job and increases the compressor outlet pressure. However, now because the gas is circulating the entire volume of the gas is heated which further increase the system pressure. The inlet pressure rises because of the gas heat up that occurs in the reactor. If the reactor remained off, the compressor inlet pressure would decrease, not increase. By the time the reactor CBC system reaches the low power steady state phase of the startup transient the pressure compressor inlet pressure has doubled to 1.4 MPa, and the compressor outlet pressure is even higher at 1.6 MPa. At the end of the startup transient at full power, temperature and shaft speed, the high pressure leg is at 2.8 MPa and the low pressure leg is at 1.5 MPa. This corresponds to the a pressure ratio of 1.86 which is very near the design point shown in the CBC

schematics of Figure 2-4 and Figure 2-38, and very near the optimum value for a highly recuperated CBC system as illustrated in Figure 2-6. Of course the actual pressure changes depend on the respective volumes in the reactor, ducting and other components, but it is interesting that the low pressure leg operating pressure is about twice the initial fill pressure. As described above, and shown in the validation effort, the fill pressure can be used as a control mechanism. Increasing the pressure effectively increases the flow rate for the same shaft speed. If the reactor coolant outlet temperature is to remain the same, then the reactor power level must increase. Because the pressure ratios and temperature ratios in the turbomachinery remain the same, but with increased flow, then the total power produced will also be increased.

This is very convenient, because it means that if the system design misses the desired power level, than simply by adding or by removing gas to fill mass, it will be possible to "dial" in the desired power level, provided the system design can withstand the additional pressure.

2.7.2 GCR Startup Transient with Three Feedback Terms

The proceeding section described a basic startup transient and was used to illustrate some of the issues of startup for space reactors. These issues addressed power pulses, thermal transients, rate of reactivity insertion, time of startup and amount of motor power required to start the system. In this section the goal was to evaluate a similar set of startup transients but using a more realistic reactivity feedback model. In addition we wanted to explore some variations in the startup especially with respect to when the turbocompressor was started. As a consequence we have examined three different startup scenarios. The first startup is the same as described in the previous study but the more realisctic feedback effects are considered. In the second startup scenario the turbocompressor start time was moved up in time so that it started at a lower reactor temperature (10 K greater than the intial ambient temperature rather than 300 K. In the third scenario the turbocompressor was started prior to reactor heating. Overal these three startup scenarios begin to cover the general options available for startup.

For all three startup scenarios the model used three feedback terms. This model is considered to be more realistic than the single feedback term because it takes into account the temperature and thermal lag associated with other reactor components that will contribute to the reactivity feedback. In this model the temperatures for the fuel, the grid plate, and the radial reflector which is made of BeO are all considered. The fuel feedback coefficient is now -0.05 cents/K rather than -0.2 cents/K, and there are two additional terms, one for the lattice coefficient at -0.05 cents/K and -0.1 cents/K for the BeO radial reflector. Note that the sum of the reactivity feedback terms is equal to that used in the previous transient. All other transient input values, such as neutron generation time, fraction of delayed neutrons were kept the same.

2.7.2.1 GCR Startup Transient with 3 Feedback Terms and Flow Starting well after Reactor Startup (Tinit + 300 K)

This startup transient that was examined is for the same GCR and is virtually identical to that described in the previous section. The only difference is that the reactor has three feedback terms, as described in Table 2-29. The PMAD controller starts the CBC flow at the same initial condition. Startup occurs when the average fuel temperature exceeds the initial temperature by

300 K. Likewise the inserted reactivity and the scheduled shaft rpm are identical. As before the total inserted reactivity is $1.47.

The same four plots of power, input reactivity and flow, pressure, and temperature for this transient, Tinit+300,3FB is shown in Figure 2-56, Figure 2-57, Figure 2-58, and Figure 2-59. As before the reactor is started first followed by the CBC startup, the low power steady state phase, followed by the ramp to full power and the full power steady state. Because the basic startup transient (Tinit+300,1FB) was described in detail, only the highlights and significant differences for this transient will be described.

First observe that because of the smaller fuel feedback coefficient, the latent heat power spike is larger in transient three feedback model. The peak power in the single feed back model was 18 kW and now the transient pulse rises to about 80 kW in the 3FB case. However, the flow induced transient is smaller, 100 kW_t for the 3FB case versus 180 kW_t in the 1FB case. Actually, the flow induced pulse seems to be caused more by a combination of the reactivity ramp and the flow startup, because RPCSIM shows no decrease in the fuel temperature even though there is a leveling off of the fuel temperature heat up when the flow starts.

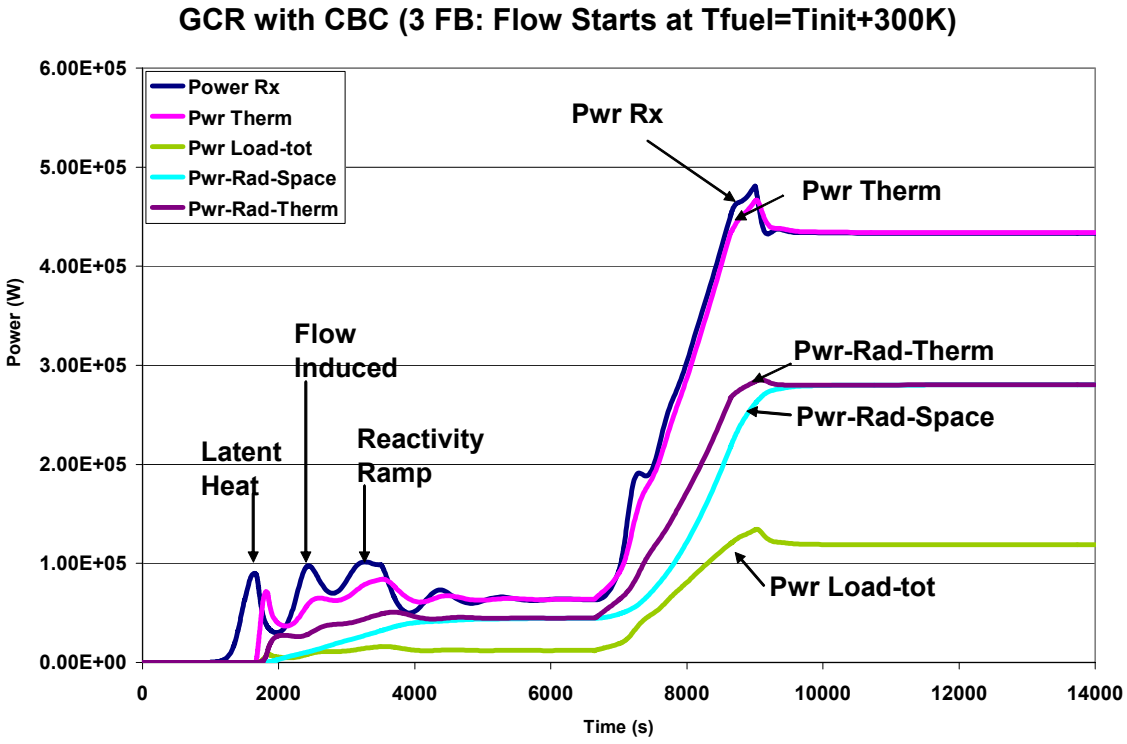

Figure 2-56: Reactor and CBC power levels for transient Tinit+300,3FB. The plot shows the fission power or reactor power (Pwr Rx), the thermal power transferred to the gas coolant (Pwr Therm), the power transferred from the coolant to the radiator structure (Pwr-Rad-Therm), the power radiated to space (Pwr-Rad-Space) and the alternator load or electrical power (Pwr-Load-tot).

Also because of the lower prompt fuel feedback coefficient the 3FB model low power steady state value is a little higher than in the single feedback model 64 kW_t versus 54 kW_t. During the

transition to full power the reactivity and shaft speed almost occur simultaneously, but still the 3FB model has an addition small reactivity ramp induced pulse that occurs at about 7400 seconds. Finally, again because of the lower prompt fuel feedback coefficient in the 3FB model, the final power level is about 435 kW_t, while the electrical power level produced is 119 kWe, and the turbine inlet temperature is 1159. The cycle efficiency is about 27.4%.

The gas pressure curves look very similar in the two cases, but the gas temperatures show some differences. Comparing Figure 2-59 , the 3FB with Figure 2-54 the 1FB model, the gas temperatures increase more rapidly for the latent heat pulse but slower for the flow induced spikes. The final temperatures achieved are larger in the 3FB model, but if the same average fuel temperature were to be desired, the final fuel and coolant temperatures for the two cases would be about the same. This means that the motion of the control elements (BeO reflectors) will be less in the 3FB model. For design purposes, it is going to be desirable to be able to have some margin in the amount of swing in the control elements as the final feedback coefficient model will not be fully known until the system is built and operated in space.

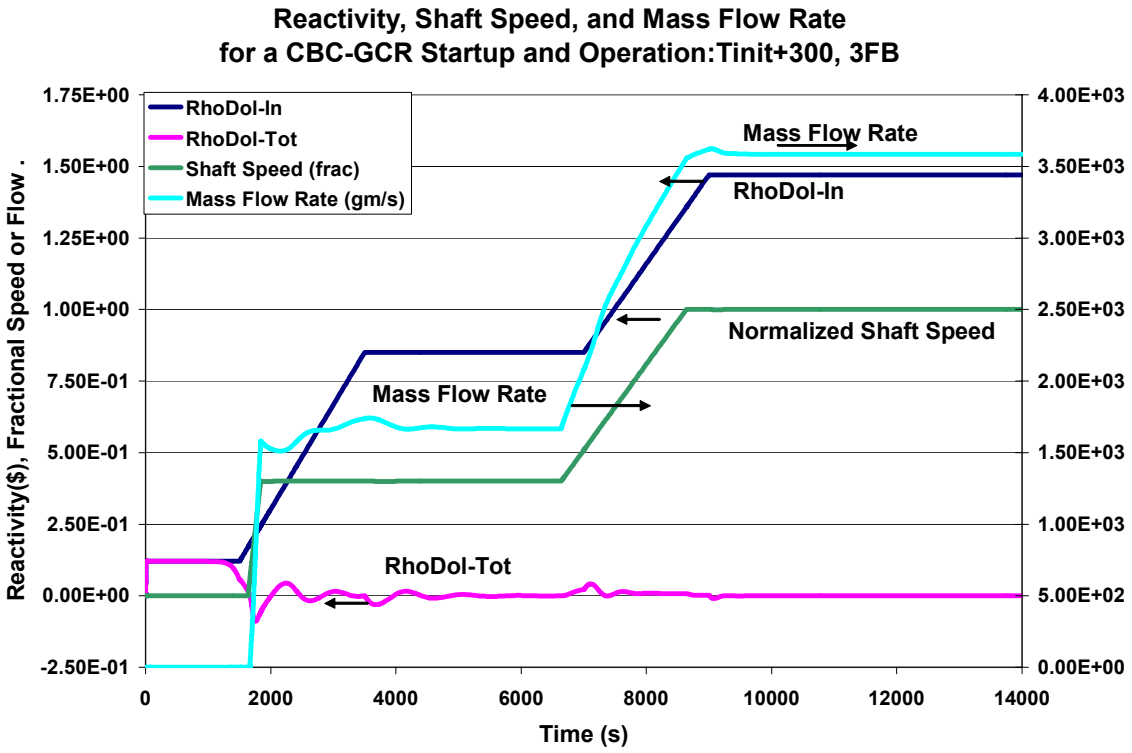

Figure 2-57: Input values for transient Tinit+300,3FB. The plot shows the inserted reactivity (Rho-Dol-In), the TAC shaft speed (Normalized Shaft Speed), the mass flow rate (Mass Flow Rate) and the total reactivity which is the sum of the inserted and feedback terms (Rho-Dol-Tot). The reactivity is given in dollars.

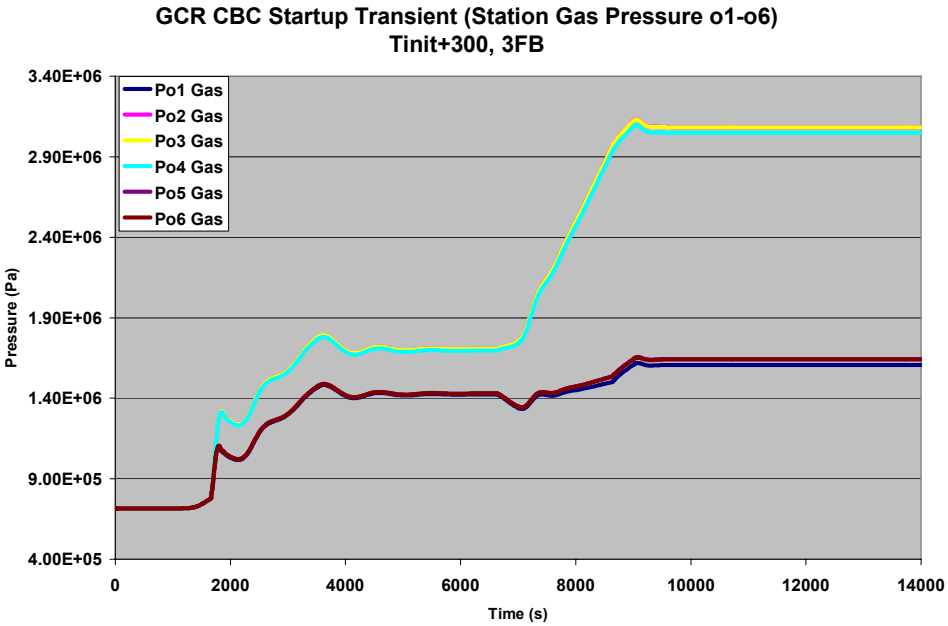

Figure 2-58: Pressure values for transient Tinit+300,3FB. The plot shows the pressure at each station around the loop, but as can be seen the pressures really show the time dependent values of the low pressure leg and the high pressure leg. Pressure drop effects are observable, but they are small.

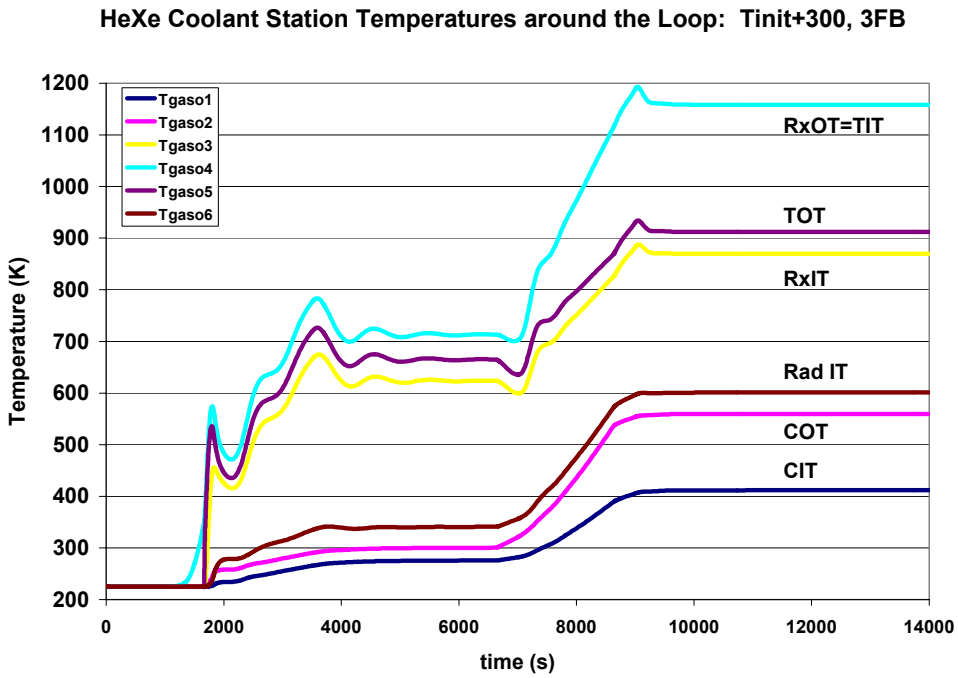

Figure 2-59: Station temperatures for transient Tinit+300,3FB. This plot shows the temperatures for the reactor outlet or turbine inlet (RxOT=TIT), the turbine outlet (TOT), the reactor inlet (RxIT), the radiator inlet (Rad IT), the compressor outlet (COT), and the compressor inlet (CIT).

2.7.2.2 GCR Startup Transient with 3 Feedback Terms but with Flow Startup at 10 K above the Initial Temperature

We also used RPCSIM to analyze a transient that used the same 3 feedback terms as just described, but with the turbo-machinery starting up at 10 K above the initial temperature of 22K. The predicted reactor power levels and other power terms are shown in Figure 2-60, and the predicted temperatures are shown in Figure 2-61. Overall the power trace for this model Tinit+10,3FB looks very similar to Tinit+300,3FB except that the thermal anre reactor power spikes or transients are reduced in the case when the flow starts up earlier.

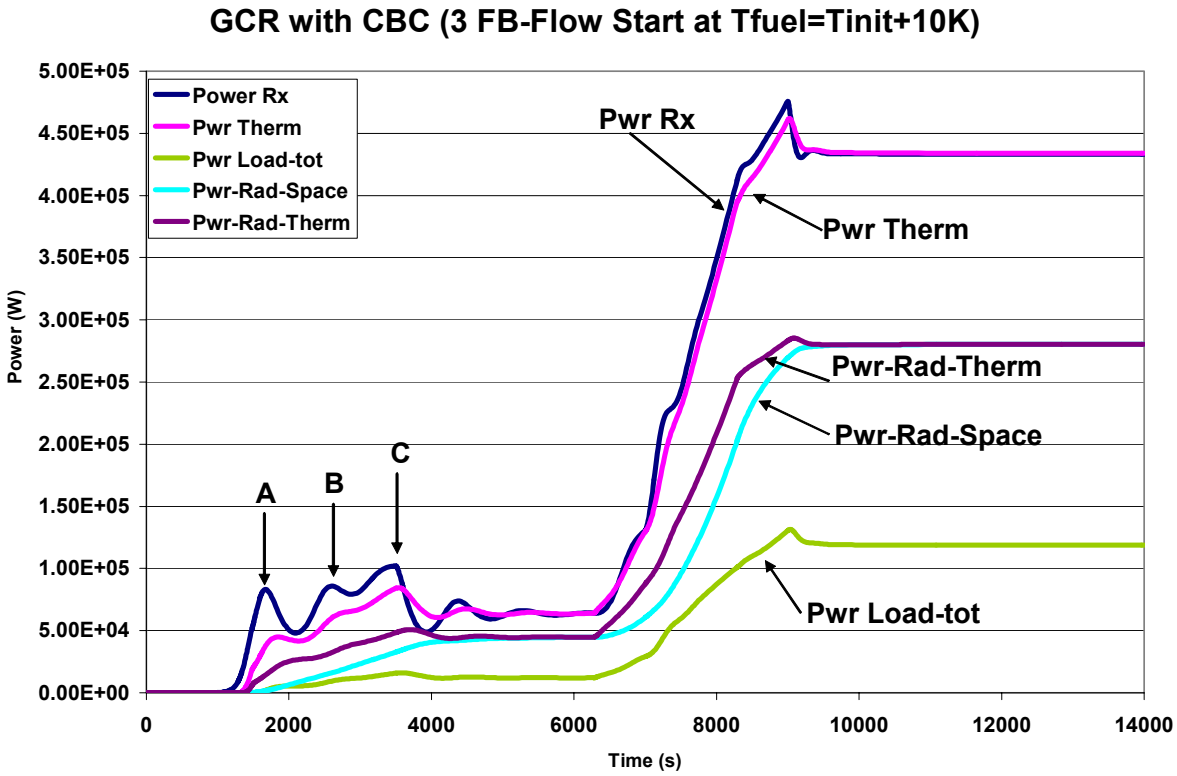

Figure 2-60: Reactor and CBC power levels for transient Tinit+10,3FB. The plot shows the fission power or reactor power (Pwr Rx), the thermal power transferred to the gas coolant (Pwr Therm), the power transferred from the coolant to the radiator structure (Pwr-Rad-Therm), the power radiated to space (Pwr-Rad-Space) and the alternator load or electrical power (Pwr-Load-tot). The power pulse at A is caused by the latent heat effect, at B by the startup of coolant flow, and at C by the reactivity ramp.

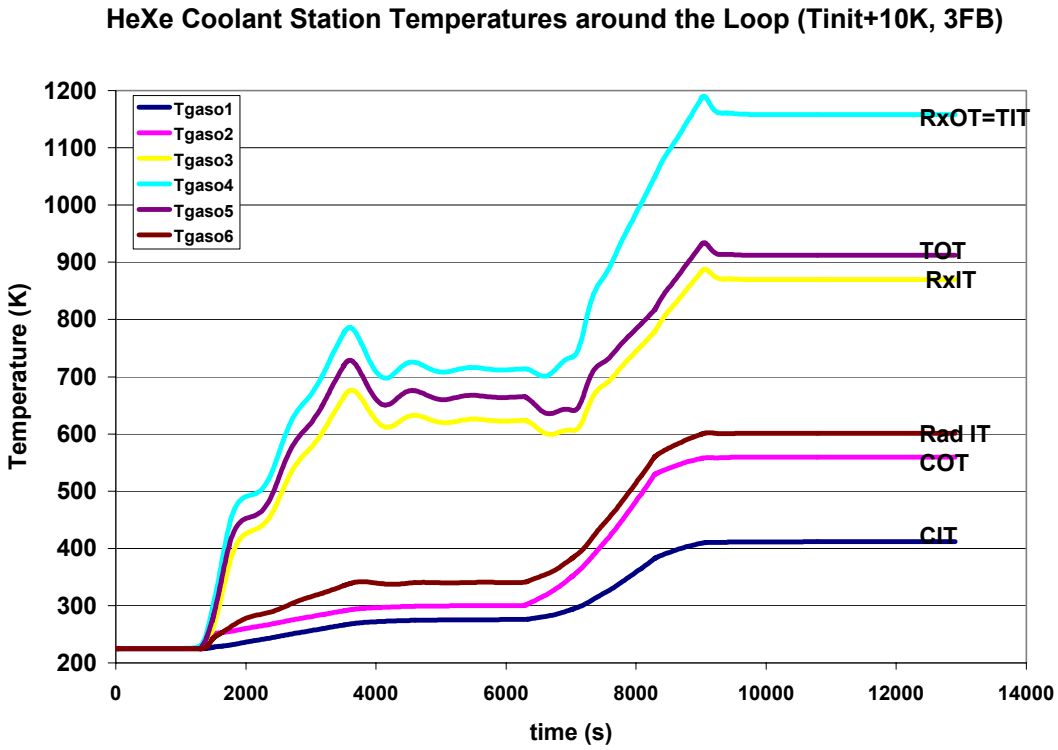

Figure 2-61: Station temperatures for transient Tinit+10,3FB, This plot shows the temperatures for the reactor outlet or turbine inlet (RxOT=TIT), the turbine outlet (TOT), the reactor inlet (RxIT), the radiator inlet (Rad IT), the compressor outlet (COT), and the compressor inlet (CIT). All conditions are the same as in Figure 2-59 but the flow starts sooner, at the initial temperature + 10K.

2.7.2.3 GCR Startup Transient with Flow Startup Prior to Reactor Startup: Reactor has 3 Feedback Terms

To fully explore the startup scenarios, the startup transient in this section starts the turbo-machinery prior to the reactor startup. This was done by changing motoring the turbo-machinery at 500 seconds rather than waiting until the fuel temperature exceeds its initial temperature by 300 K. As before, the reactor has three feedback terms. This transient is call Time+500,3FB. The transient uses the exact same reactivity insertion values used in Tinit+300,3FB and Tinit+10,1FB. It also uses the same scheduled increase in shaft speed. The three plots of power, inserted reactivity and shaft speed, and gas station temperatures are shown in Figure 2-62 (power), Figure 2-63 (input reactivity and flow), and Figure 2-64 (gas temperatures).

Because the reactivity transient starts with a step insertion of 12 cents, the reactor is on a positive period when the flow starts. The reactor power is about 0.2 W, but because no heating has occurred there are no active feedback terms. Starting the turbomachinery earlier would only require motoring the TAC for a longer period of time. At about 1300 seconds, (600 –700 seconds after flow starts) the power levels are sufficiently high that thermal feedback effects are beginning to heat the fuel and impact the power level through the feedback mechanisms. At

1450 seconds the first power spike occurs due to step insertion of reactivity and terminated by the latent heating. The peak of the latent heat spike is about 80 kW_t, which is about the same value as observed in the transient Tinit+300,3FB. In terms of the reactor power there are no large differences in the two startup scenarios; however there are temperature differences that may be important.

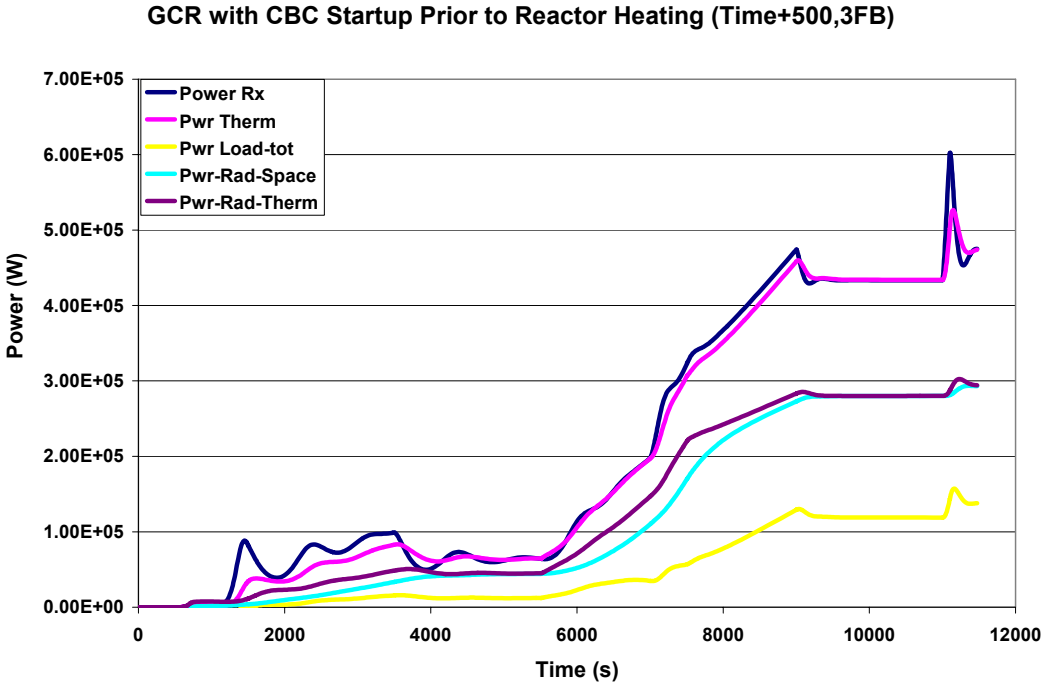

Figure 2-62: Reactor and CBC power levels for transient Time500,3FB. The plot shows the fission power or reactor power (Pwr Rx), the thermal power transferred to the gas coolant (Pwr Therm), the power transferred from the coolant to the radiator structure (Pwr-Rad-Therm), the power radiated to space (Pwr-Rad-Space) and the alternator load or electrical power (Pwr-Load-tot). In this transient the CBC flow starts after reactor heating.

The gas station temperatures are illustrated in Figure 2-64. First note that when the flow starts, the hot leg of the loop decreases in temperature and actually cools below the initial temperatures by as much as 20 K. This cooling occurs because the reactor is at its initial temperature (about 225 K), and when the gas expands in the turbine it cools. The cool turbine exit gas lowers the reactor inlet temperature. The slightly warmer reactor heats the inlet gas by a few degrees, but still the reactor outlet temperature or turbine inlet temperatures drop. This cooling effect is slightly unusual, but is not likely to introduce significant design issues.

The major thermal effect of starting the reactor first is that the reactor fuel gas temperatures are gradually increased over a long period of time, about 40 minutes (from 1500 s to 3500 s for this transient). In this startup transient the turbine inlet temperature increases from 225 K to about 800 K over a period of 40 minutes and the temperature increase is more gradual than shown in the transients that start the reactor prior to starting the flow. (The time period of heating is easily controlled by the rate of reactivity insertion.)

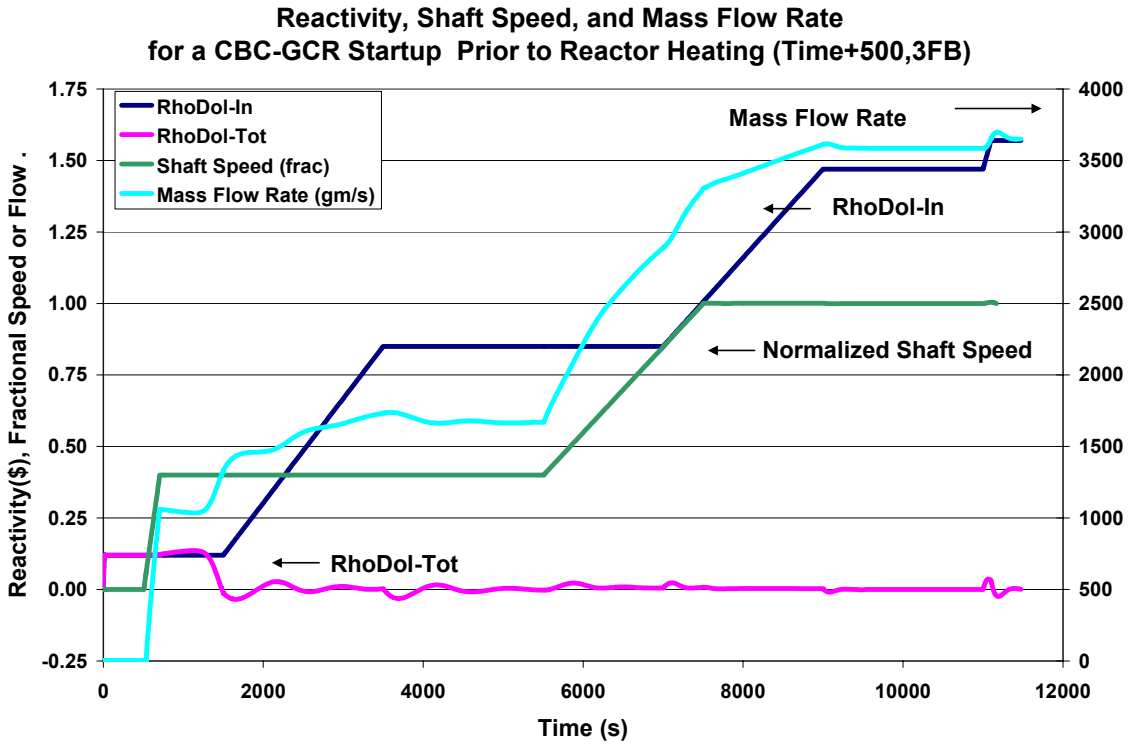

Figure 2-63: Input values for transient Time500,3FB. The plot shows the inserted reactivity (Rho-Dol-In), the TAC shaft speed (Normalized Shaft Speed), the mass flow rate (Mass Flow Rate) and the total reactivity which is the sum of the inserted and feedback terms (Rho-Dol-Tot). The reactivity is given in dollars. Note that the rpm and flow start at 500 seconds.

Another important difference between this transient and the others is that the power to motor the alternator is larger and must be supplied for a much longer period of time. Figure 2-65 shows a plot of the alternator power during the startup phase (Time500,3FB), which can be compared to the alternator motoring power required when the reactor starts prior to the flow, see Figure 2-55 (transient Tinit+300,1FB). In the case when the flow starts prior to the reactor, the alternator motoring power levels are higher (~5 kW, versus a few hundred watts) and the length of time that the motoring is needed is much longer (10 minutes versus 1 minute). Nevertheless, for the transient shown here (Time500,3FB) the energy required to motor the alternator is still only 600s*5 kW = 3 MJ of energy storage. This value is still easily within the range of current batteries, so other things such as efficiency of power conversion and conditioning will likely be important issues with respect to startup circuitry design approaches.

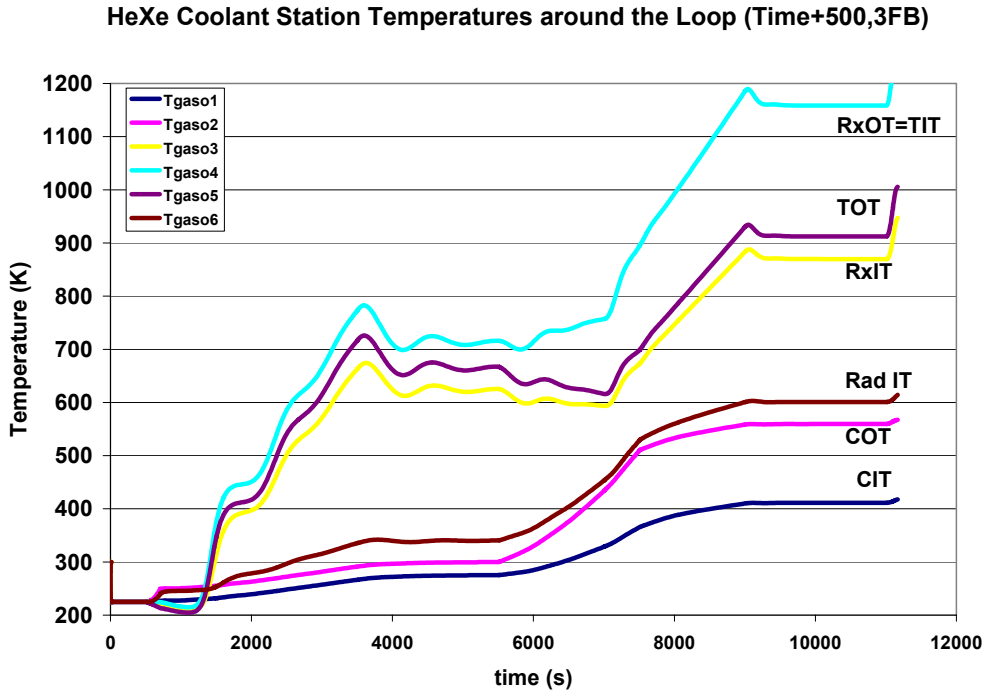

Figure 2-64: Station temperatures for transient Time500,3FB, This plot shows the temperatures for the reactor outlet or turbine inlet (RxOT=TIT), the turbine outlet (TOT), the reactor inlet (RxIT), the radiator inlet (Rad IT), the compressor outlet (COT), and the compressor inlet (CIT). All conditions are the same as in Figure 2-59 but the flow starts at 500 seconds which is prior to reactor heating.

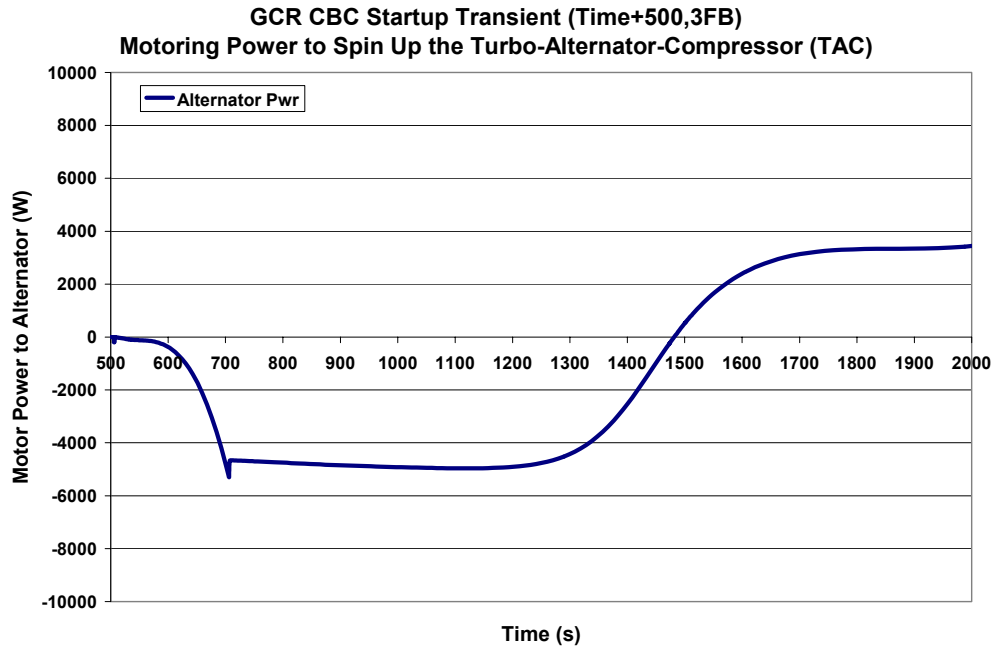

Figure 2-65: GCR startup transient Time500,3FB, showing alternator power as a function

of time. This transient starts the CBC flow prior to reactor heat up and thus the motoring power (negative alternator powers) of almost 5 kW must be supplied for over 10 minutes before self-sustaining operations are observed.

The power spike and thermal steps observed at the end of transient Time500,3FB are the result of a 10cent step increase of reactivity. This perturbation and other perturbations like it will be discussed in the next section.

2.7.2.4 Summary of the Three Startup Scenarios

Overall the thermal and reactor power transients for the three startup scenarios are relatively similar. They do exhibit a few differences. We first observe that the three feedback terms generally results in milder reactor power pulses. This is because the small fuel feedback term minimizes the feedback effects due to start up of the coolant. We also observed that starting the coolant flow at an earlier time further reduce the magnitude of the reactor and thermal spikes. The last run started the coolant flow up prior to the reactor startup, however even in this case the thermal and reactor spikes were evident and of the same magnitude as in the previous runs. The major difference in this case was that the motor power required to start the system up was substantially larger ~1 kWhr than when flow startup occurred after the reactor had heated by 300 K (0.1 kWhr). However in either case these startup power levels are small and easily delivered by batteries.

2.7.3 Dynamic Stability

Section 2.4.6.3 used the lumped parameter model to evaluate the dynamic stability of the reactor driven closed Brayton cycle. The lumped parameter model results showed that there are two steady state solutions, meaning that if the alternator load is set to a fixed value, then for a fixed average fuel temperature, two solutions are predicted that have different shaft speeds/flow and different reactor powers even though the alternator power was kept constant and even with the average fuel temperature kept constant. The early section of the report also used curves for the excess torque or power on the shaft as a function of rpm to show that only the higher speed result was dynamically stable. In this section of the report, we discuss these results more thoroughly and use the Simulink RCPSIM dynamic model to verify the same behavior but with a more sophisticated model. In addition the Chapter 4 of this report uses operates the Sandia Brayton Loop made from the Capstone C-30 gas turbine power generator (which is described in Chapter 3) to validate this behavior.

In Section 2.4.6.3 the lumped parameter steady state model was used to develop an operational curve for the reactor driven CBC system. This plot, Figure 2-28, plotted the electrical load or alternator load developed as a function of shaft speed for various fixed fuel temperatures. Now, RPCSIM is used to make the same plots which are shown in Figure 2-33 and in Figure 2-34. These curves were made by running RPCSIM with the RPM controller (which is sometime called the PMAD controller) operational. The RPM-Controller uses a proportional integral feedback loop to dynamically adjust (force) the load to follow a user specified shaft speed or reference rpm time history. The RPM-Controller does this so well that on the scales that we are plotting the shaft speed that there is no discernable difference between the reference rpm and the actual rpm. Figure 2-66 shows the Simulink PI feedback controller. Note that the input looks at the difference between the true shaft speed and the reference shaft speed, and the output is just the parasitic load (PLR is the parasitic load resistance). Figure 2-36 shows that the PMAD

controller (PMAD1) is in a feedback loop with the alternator, and that the executive controller (Executive 2) sets the user specified reference shaft speed (reference RPM). The PI feedback controller shown in Figure 2-66 is just a sub-module of the PMAD1 controller. The other parts of the PMAD1 control consist of logic telling the simulation when to turn it on, as it cannot be used when the turbo-machinery is not running.

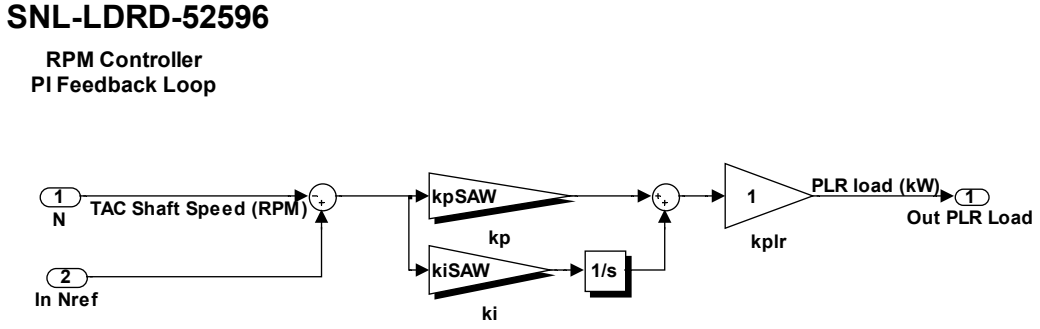

Figure 2-66: RPM-Controller Simulink sub-module within Module PMAD1 (see Figure 2-36) . The RPM controller uses a proportional-integral feedback loop to dynamical keep the true shaft speed very close to the user defined reference shaft speed.

Figure 2-67 shows a plot of the alternator power (at steady state) for a fixed amount of reactivity insertion as a function of shaft speed. Note that fixing the inserted reactivity is equivalent to fixing the average fuel temperature. The RPCSIM model used the 313 pin Gas Cooled Reactor model, but with only one feedback coefficient for the fuel (-0.2 cents/K). The curves were generated by running the RPCSIM model at a fixed user specified rpm and then waiting until steady state was reached, then the rpm was increase and a new data set was take at the new steady state. The two curves in Figure 2-67 show the alternator load versus rpm for two values of inserted reactivity ($1.12, and $1.65). Figure 2-68 shows the same data but the reactor power level curves are also plotted. Note that at high levels of shaft speed that the alternator power curve turns over, meaning that if the load were fixed at this value, that the shaft can operate at two shaft speeds (1000 rev/s and 1280 rev/s). Both of these speeds have the same load and same average fuel temperature, but they have different reactor power levels because the mass flow rate is different at the two conditions.

But which one is real? It turns out that both points are, but the method of control determines where one can operate. With the RPM-Controller which continuously dithers (or dynamically) modifies the load on the alternator to force the true shaft speed to run at or very near the user specified shaft speed, then every point on the curve is stable. However, if the RPM-Controller is turned off, then only the solution with the negative slope is dynamically stable. Turning off

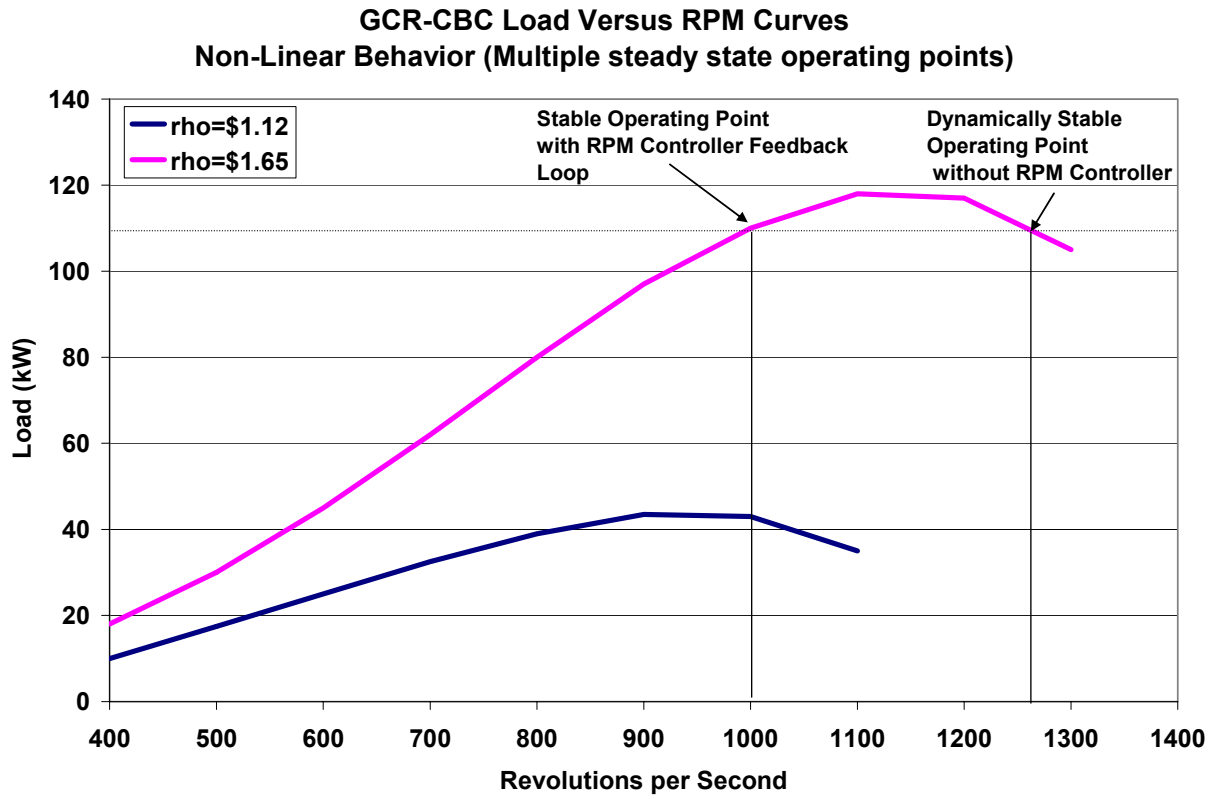

Figure 2-67: RPCSIM predicted steady state alternator power level shown as a function of shaft speed for two values of inserted reactivity ($1.65 and $1.12). Note that there are two shaft speeds that give the same alternator power level.

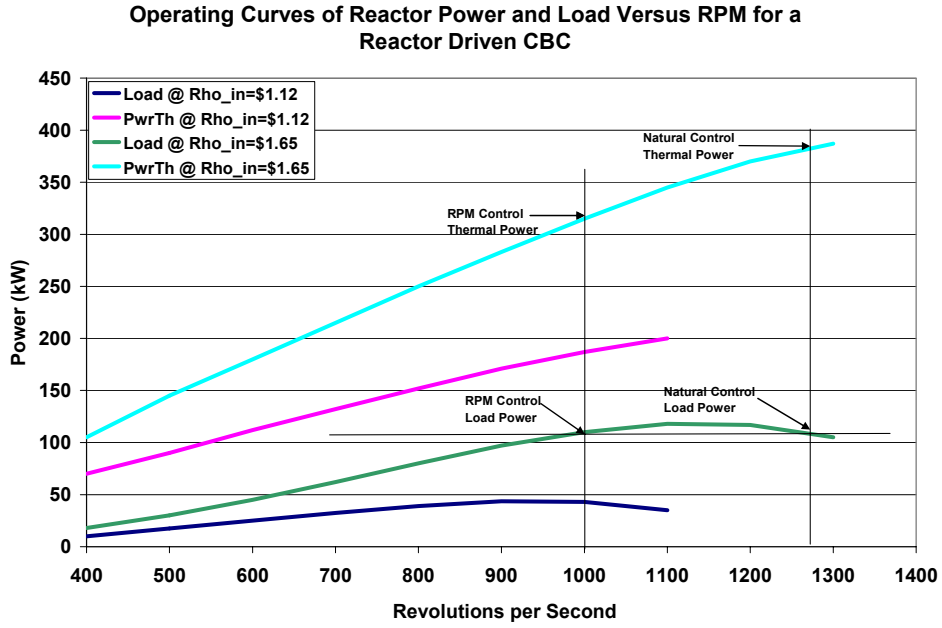

Figure 2-68: Steady state alternator and reactor power levels as a function of shaft speed.

the RPM controller is equivalent to specifying a fixed alternator load. This effect is illustrated in Figure 2-69 through Figure 2-71.

The transient simulation is shown in Figure 2-69 through Figure 2-71 which show the reactor and alternator power levels, the inserted/reference shaft speed and reactivity, and the gas coolant temperatures. The transient is very similar to the ones described previously which go through a startup of the reactor followed by startup of the turbo-machinery through a low power steady state operation and ending with full power steady state. The difference is that once steady state full power conditions were achieved, the RPM-Controller was turned off, which means that the alternator power was just set to a constant. Thus, for this transient at 11,000 seconds the PI feedback controller circuit was bypassed and the load was set to hold

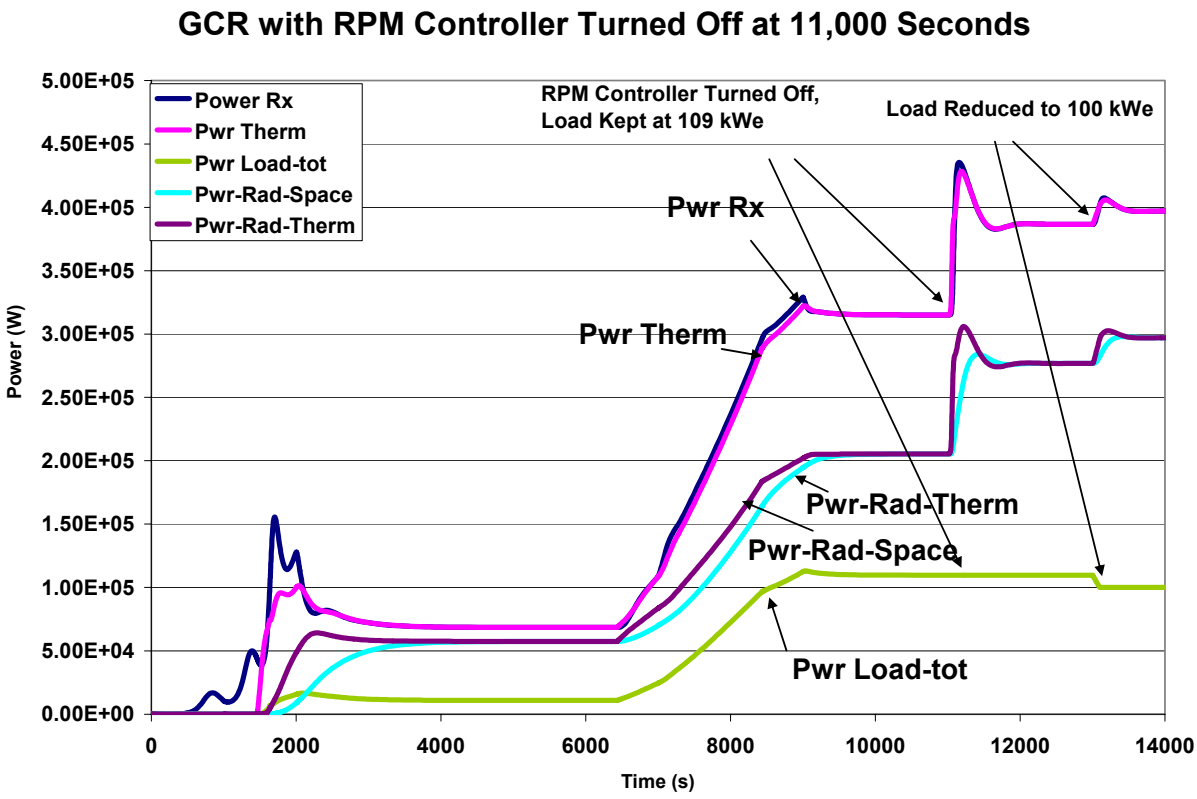

Figure 2-69: Plot of reactor power and alternator power to demonstrate that the lower shaft speed solution is dynamically unstable. At 11,000 seconds the RPM-Controller was turned off, which caused the shaft speed and reactor power level to increase. At 13,000 seconds the alternator load was decreaseed which caused an increase in reactor power and shaft speed.

steady at109 kWe. When the controller was turned off, the shaft speed rapidly increased (see Figure 2-70). This resulted in an increased in flow. The additional flow causes a spike in reactor due to its increased cooling capability, but eventually the reactor power level, the gas temperatures, and the shaft speed all reach new steady state values, but now at higher flow rates. Note that after the RPM-Controller was turned off the new shaft speed is increased from 1000 rev/s to 1280 rev/s which is just the value predicted by the operational curve shown in Figure

2-67. The reactor power level is higher also, but the alternator power or electrical power produced has not changed. This is exactly the behavior predicted by the lumped parameter model and initially reported in (Wright, 2003).

As a further test of stable operations, the RPCSIM simulation transient perturbed the alternator load by reducing it to 100 kWe at 13,000 seconds. Note that this "reduction" in power (from 109 kWe to 100 kWe) resulted in an increase in speed and therefore an increase in the reactor thermal power, but the perturbation was stable.

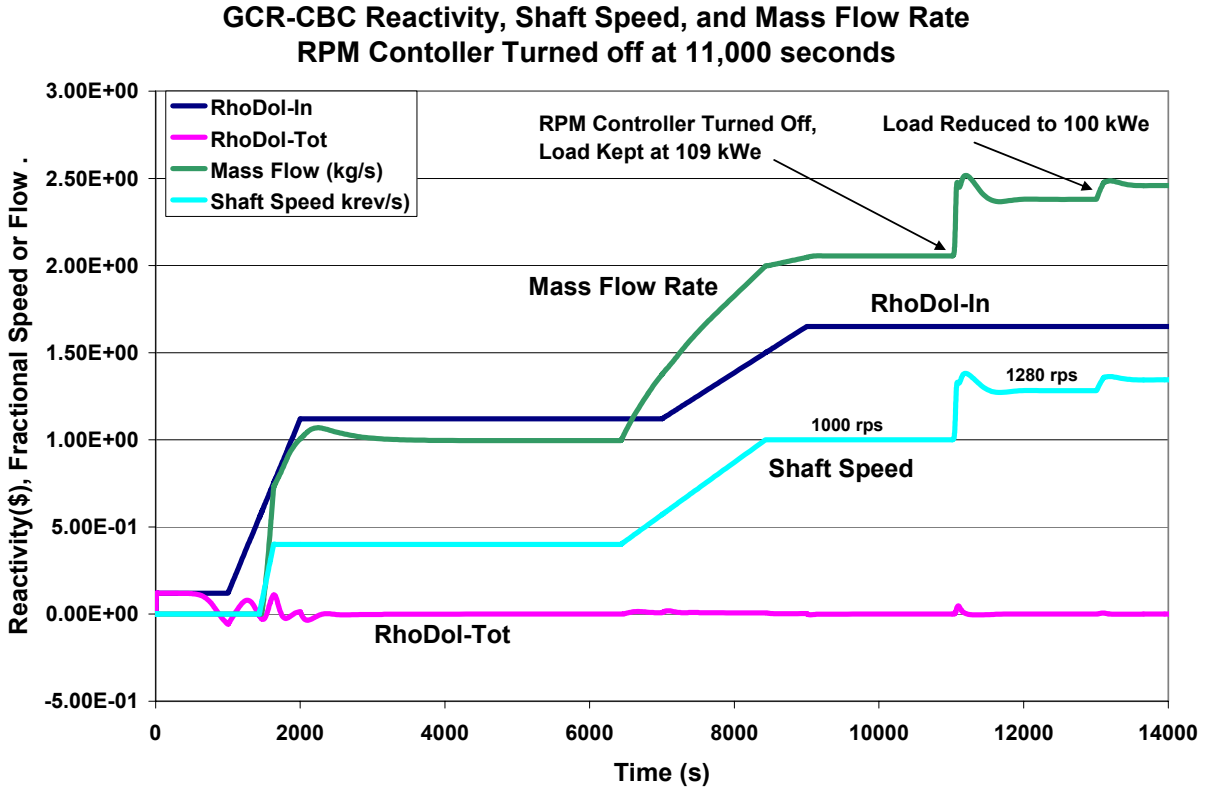

Figure 2-70: Input values for reactivity, shaft speed, and mass flow rate for the dynamic stability demonstration transient. At 11,000 seconds the RPM-Controller is turned off, and the jump in rpm from 1000 rev/s to 1280 rev/s illustrates that the reactor CBC system goes through a transient to reach the dynamically stable point at 1280 rev/s. At 13,000 seconds the load is further decreased which causes an increase in shaft speed and flow rate, which in turn results in a reactor power level increase even though the load decreased.

In spite of the fact that this type of operation is stable it is counter intuitive (decreases in electrical load result in increases in reactor power) and it is less efficient than the lower rpm solution. It is not how one would wish to operate a reactor driven CBC system. Some type of dynamic control will be required to operate on the positive sloped portion of the operating power-versus-rpm curves. RPCSIM uses dynamic load control to force the true rpm to follow a user specified value. This method of control has the advantage that it is fast, and can accurately control the shaft rpm, and it is thermo-dynamically efficient. Also the dynamic variations in power required to keep the power at the steady state point are very small compared to the total

power being produced. Based on our observations of the Sandia Brayton Loop, these power fluctuations are on the order of 0.1% of the total power. Nevertheless, to load follow it requires changing the shaft rpm if the reactor temperature is to stay constant.

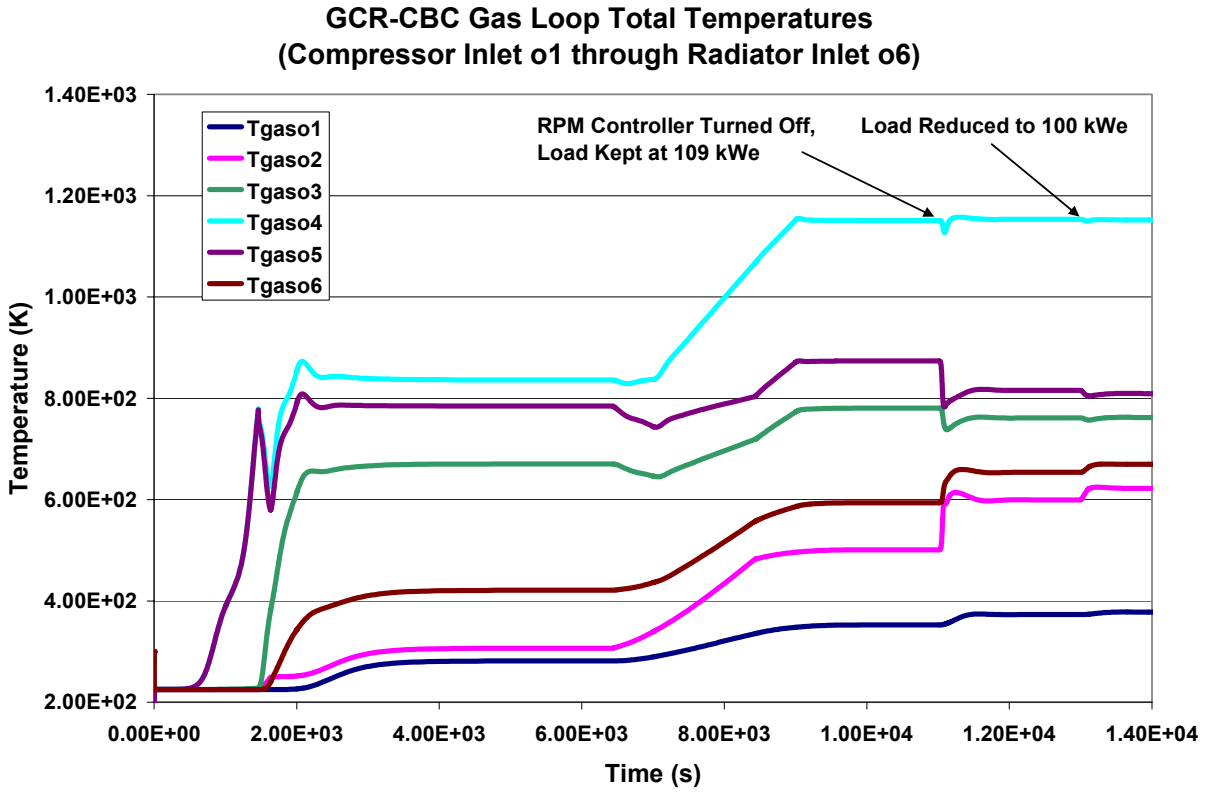

Figure 2-71: Gas station temperature for the dynamic stability demonstration transient. Note that turbine inlet temperature(Tgas04) remains constant for the dynamically stable operating points, but the radiator temperature increases (Tgas06 and Tgas01 are the radiator inlet and outlet temperatures respectively) meaning that the thermodynamic cycle efficiency has decreased.

As mentioned before, other types of control are possible such as inventory control, bypass valves, or throttle valves. RPCSIM can currently model inventory control or throttle valves, but bypass valves have not been installed into the model to date. Future efforts will focus on developing control strategies and methods consistent with the mission and application (space, planetary, or terrestrial).

2.7.4 Consequences of Various Perturbations

RPCSIM is a very useful tool to answer "what if" questions. Three questions of this nature often come up and we have used RPCSIM to look at the results. The curves and plots are not presented here, but their analysis will likely be the focus of future publications. Three what if questions that are frequently asked are: What happens if the system pressure is increased/decreased, what happens if the flow in the gas chiller is increased or decreased?, and

how long can the system run if the reactor power is turned off. A brief paragraph summarizing the results of the simulations is presented for these three questions.

2.7.4.1 What happens if the system pressure is increased?

When the system pressure is increased, the mass flow rate increases for the same shaft speed. The increased mass flow cools the reactor which means that the reactor must produce more power to bring the average fuel temperature back to its original value. (This is done either automatically via the negative thermal feedback coefficient, or by adjusting the external neutron reflectors). With the same average fuel temperature the turbine inlet temperature is very close to its original value and so are all the other temperatures because the temperature and pressure ratios have not changed much. This means that more electrical power or alternator power can be produced because the mass flow rate is higher while the temperatures are all very close to their original values. It is this concept that is used for inventory control, and also provides a way for the engineers to fine tune the operating conditions to assure that the system will meet its design conditions.

2.7.4.2 What happens if the flow in the gas chiller is increased?

If the flow rate in the liquid coolant used within the gas chiller is increased, the compressor inlet temperature is lowered. Lowering the inlet temperature, while keeping the reactor average fuel temperature (and thus the turbine inlet temperature nearly constant) constant, results in more power being produced and at a better efficiency. In general, because the thermo-dynamic efficiency of the system is near 30%, lowering the compressor inlet temperature by 1 K has the same effect (in terms of increasing the efficiency) as increasing the turbine inlet temperature by 3 K.

2.7.4.3 How long can the system run if the reactor power is turned off?

In general this is the question addressed in the validation section of this report (Section 4.5). We will see that the system can operate for over 1 hour provided the shaft speed is decreased to values that are sufficiently low that little load is put on the system. The Sandia Brayton Loop which uses the Capstone-C30 gas turbine was operated for over 1 hour with the rpm adjusted to keep the load at about 100 W while the shaft speed ran at no less than 25% of the design rpm. The RPCSIM code produces very similar results, but because of inaccuracies in the flow curves at low rpm and low flow, the results currently do not predict such extended operations as observed. Nevertheless, the basic behavior is predicted correctly, and has the fortunate result that the Brayton machinery can be used to remove the decay heat from a reactor driven CBC system sufficiently long that the decay heat can decay to 1% or less than the nominal operating power of the system.

2.7.5 Liquid Metal Reactor Startup Transients

A liquid metal reactor version of RPC was also developed used to assess the response of LMR reactor driven CBC power conversion systems. The reactor model is virtually identical to the gas cooled reactor but use lithium as the coolant rather than He/Xe. The block diagram of the LMR CBC concept is shown in Figure 2-35. In this model, regardless of temperature, the lithium was always assumed to be molten.

Figure 2-35 shows the top level diagram of the LMR model, and the results of the Simulink dynamic model are illustrated in Figure 2-72 through Figure 2-75 . The transient presented was

designed to test the model and to take the Space Reactor Power system through a complete startup transient. The transient that was modeled is simply one of many and represents only one approach to startup. To aid in overall comparisons, the LMR transient is very similar to the GCR transient. The reactivity feedback model is very simple and includes effects for the average fuel temperature only. It uses a single fuel temperature feedback coefficient of -0.2 cents/K just as the GCR single feedback model does. The reactor thermal model has only one node for the fuel temperature.

The startup transient performs a variety of activities, such as increasing reactor temperature, ramping the TAC shaft speed to a desired set point, increasing reactor temperature, or permitting the system to approach equilibrium. In addition to examining the startup of the CBC and reactor, the response to a severe off-normal transient was also explored. The off-normal transient consisted of a turbine coast-down over a period of ~100 seconds. The abnormal transient was used to illustrate the ability of the control system and the reactor to withstand such severe behaviors without damaging the system.

The overall transient consisted of eight phases, labeled A through H. These phase take the reactor and CBC system from zero power cold critical conditions through heat up to low speed operations (at low temperatures and power levels) to full temperature, full shaft speed, and full power. Near the end of the transient simulation the last phase (H) simulates the response to a turbine coast-down. For each phase the time and duration is indicated in each Figure. Figure 2-72 shows the reactor fission power, the thermal power transferred to the lithium, the radiator power, and the electrical power produced. Figure 2-73 shows the inserted and total reactivity. Figure 2-74 shows the lithium and HeXe mass flow rate as well as the shaft speed. Figure 2-75 shows the reactor coolant inlet, outlet, and average coolant temperature as well as the fuel temperature. A brief description of each phase follows.

Phase A: Zero power startup.

During this phase the reactor increases from its initial power level (1 W) to power levels that produce latent heat effects (typically kWs) where thermal feedback is significant. We have assumed that initially the reactor is at 1 W (to shorten the run time of the Simulink Code) and that the reactivity is zero. In reality startup will begin from a deeply shut down case and at power near 1 milliwatt (Sitton, 2004). The initial temperature was assumed to be 225 K which (depending on the design of the system) will be the earth orbit space equilibrium temperature of the reactor at startup. During phase A the lithium flow was increased linearly from zero to 1 kg/s (see Figure 2-74). The lithium was assumed to be liquid even though its temperature is below the freezing point. (The models for thawing the lithium have not been converted to Simulink at this time.) The reactor controller is scheduled to insert $0.12 of reactivity into the reactor (Figure 2-73). This results in an exponential increase in power with a period of about 93 seconds. At about 700 seconds there is sufficient latent heat, that thermal feedback effects are adequate to terminate the exponential power increase. This results in a small reactor power peak of about 20 kW (Figure 2-72). At this time the reactor fuel temperatures are beginning to increase. When the temperature reaches 325K the reactor controller is switched on (Figure 2-75). This transition starts phase B.

Phase B: Reactor Controller Initiation

The reactor controller uses a feedback loop to force Tave (the average coolant temperature) to follow a user prescribed transient (see TLM_cool Ave in Figure 2-75). The prescribed transient used for this report linearly increases the temperature from 325 K to 800 K (over ~2000 s). It then holds the temperature at 800 K through phases C, D, and E. (up to 10,000 s). Figure 2-72 shows the reactor power that was required to produce this linear temperature increase. Because there are no parasitic heat losses (in this model) during phase B, the reactor power level stays constant except during the hand-off from phase A to B. The inserted reactivity is shown in Figure 2-73. When the coolant average temperature exceeds 700 K the rotating machinery is initiated and the PMAD controller becomes active.

Phase C: Turbo-Machinery Startup with PMAD Controller Active

At about 2700 s the coolant average temperature starts to exceed 700K (Figure 2-75) which triggers the startup of the CBC system. The TAC controller (PMAD) adjusts the load to force the shaft speed to follow the user specified rpm which increases to 40% full speed in about 100 seconds. (See Rev. per Sec. in Figure 2-74.) During this early portion of phase C the electrical load is negative (not shown) which just means that the TAC is being motored. In this startup scenario, the motor power peaks at about 150 W with a duration of about 60 seconds. After this time span the CBC is self-sustaining, and it is capable of producing useful power. Once the gas coolant flow starts, the reactor controller adds sufficient reactivity to continue the linear increase in temperature at the same rate until 800 K is reached (Figure 2-75). This causes a slow peak in power to (110 kW_t) which then reduces to about 50 kW_t (Figure 2-72). At the end of phase C the CBC shaft speed is 40% of its full speed (Figure 3), Tave=800K (Figure 2-75), the reactor power level is 50 kWth (Figure 2), the parasitic load power (electrical load) is 10kWe (Figure 2-72) and the gas flow rate through the CBC loop is about 1kg/s (Figure 2-74). Note that the thermal power and the reactor power are equal indicating the approach to equilibrium at the end of phase C. This phase could represent a "Safe Standby" power producing mode of operation because of the low power levels and low thermal temperatures. In this mode the temperatures and power levels are sufficiently low that a lot of time (1000's of seconds) is available to the autonomous control system to diagnose problems and correct them. Also in this mode the margins for stress, creep, and other life limiting issues are very large.

Phase D: Ramp Shaft Speed to 100%

This phase ramps the shaft speed from 40% to 100% speed (1000 rev/s = 60,000 rpm) (see Figure 2-74: Rev per Sec). All other conditions are kept constant except for the lithium flow rate which has little effect on the system. The lithium coolant flow rate was ramped from 1 kg/s to 1.5 kg/ s during phases C and D. Note that Tave=800 K for both the 40% and 100% rpm shaft speed and that the electrical power produces increases from 9.4 kWe to 24 kWe. Similarly the thermal power increases from 60 kWth to 150 kWth. These power ratios reveal that for constant Tave, the reactor power and the electrical power are very nearly proportional rpm or shaft speed.

Phase E: Equilibrate to 100% shaft speed at reduced temperature

Phase E lets the complete system reach its steady state or equilibrium conditions at 100% shaft speed but with the reactor Tave temperature limited to 800 K. At the end of phase

E the thermal power is 150 kWth, the radiator is radiating about 126 kWth to space, the alternator produces about 24 kWe. This operating mode could represent the reduced power mode during the coast phase of the transit to outer planet missions, where approximately 20% power demand is required. Because the fuel temperatures are much lower than the full power design conditions the lifetime of the system could be extended because less thermal creep would occur at these lower temperatures and because the burnup would be reduce by a factor of three compared to running the reactor at full temperature and power. Another characteristic behavior to note in this phase is that it is essentially the same as in phase C except that the rpm and He/Xe gas flow rate are increased. The larger flow rate results in a higher reactor power without increasing the reactor temperature. To first order, for a fixed reactor fuel temperature, the reactor power is proportional to the gas coolant flow rate which in turn is roughly proportional to the shaft speed. Also note that because the fuel temperature is held constant the net reactivity insertion is also kept constant.

Phase F: Ramp to 100% Operating Temperature

Phase F consists of a linear increase in reactor fuel or coolant average temperature along with the corresponding increase in reactivity (as determined by the reactor control loop). The temperature was increased from 800 K to its full operating temperature of 1150 K (see Figure 2-75). Because the fuel temperature has increased, more power is available to the turbo-machinery. The PMAD or TAC feedback automatically increases the electrical load to keep the rpm constant, however, because the temperature differences are larger, the gas coolant mass flow rate increases. Both the increased temperatures and mass flow rates result in reactor power increases. There is a slight overshoot in reactor power (to 325 kWth) before the final steady state thermal conditions are established at the end of the next phase.

Phase G: Equilibrate to100% Shaft Speed at Full Temperature

Phase G lets the CBC loop come to its equilibrium temperature, flow, and power levels. It starts at about 11,000 s and we allowed about 3,000 seconds for the system to reach equilibrium. At these full power and thermal levels the time constant to approach equilibrium appears to be on the order of 500-1000 seconds and is dominated by the thermal inertia of the space radiator (see the power level of the radiator in Figure 2-74). At the end of the transient the Lithium coolant outlet temperature is about 1160-1180 K, the reactor thermal power is 285 kWth, the electrical power is approximately 100 kWe (Figure 2-72). Note that the sum of the electrical power and the space radiator power equals the thermal power. An important observation is that the final increase in temperature from 800 K to 1150 K increases the electrical power from 20-25 kWe to ~100 kWe. This is just an observation that for fixed shaft speed there is a temperature (estimated to be about 650-700K for 100% shaft speed in this example) below which the CBC cannot sustain power production. This is the system level stall point that was briefly described and discussed in AIAA paper (Wright, 2003). Essentially this analysis shows that for a given fuel temperature and for a given shaft speed there is one stable power level. The PMAD control loop automatically adjusts the parasitic load to the value required to run at the requested shaft speed. If the PMAD controller were not used, then the shaft rpm would adjust its value to be consistent with the applied parasitic load. The end points for these two cases are the same; however, the path to get this state point is different. The first method adjusts the load to match the rpm, while the other adjusts the

rpm to match the load (for a given fuel temperature). The later control approach describes the natural stability of the reactor/CBC system, and provides a beneficial property to reactor driven CBC systems because can provide control redundancy (at least over a range of operating conditions).

Phase H: Turbo-Compressor Coast-down

The off-normal transient was included in the analysis to test the operational behavior of the system to a severe transient. The transient consisted of reducing the flow from 100% to 10% over a period of 100 seconds. The flow was not taken fully to zero, because the current version of the dynamic model has components and modules that produced undefined results at zero flow. The major response is that the control system reduces the reactor power levels to very low power levels (~8 kWth, see Figure 2-74), but keeps the coolant average temperature Tave equal to the specified input level of 1150K (see Figure 2-75). Note that there is no fuel temperature or shaft speed over-shoot observed in Figure 2-74 or Figure 2-75, because the reactor controller keeps the temperature in the preprogrammed range. Thus, proper action by the autonomous controller should be able to deal with a variety of off-normal conditions including turbine coast-down.

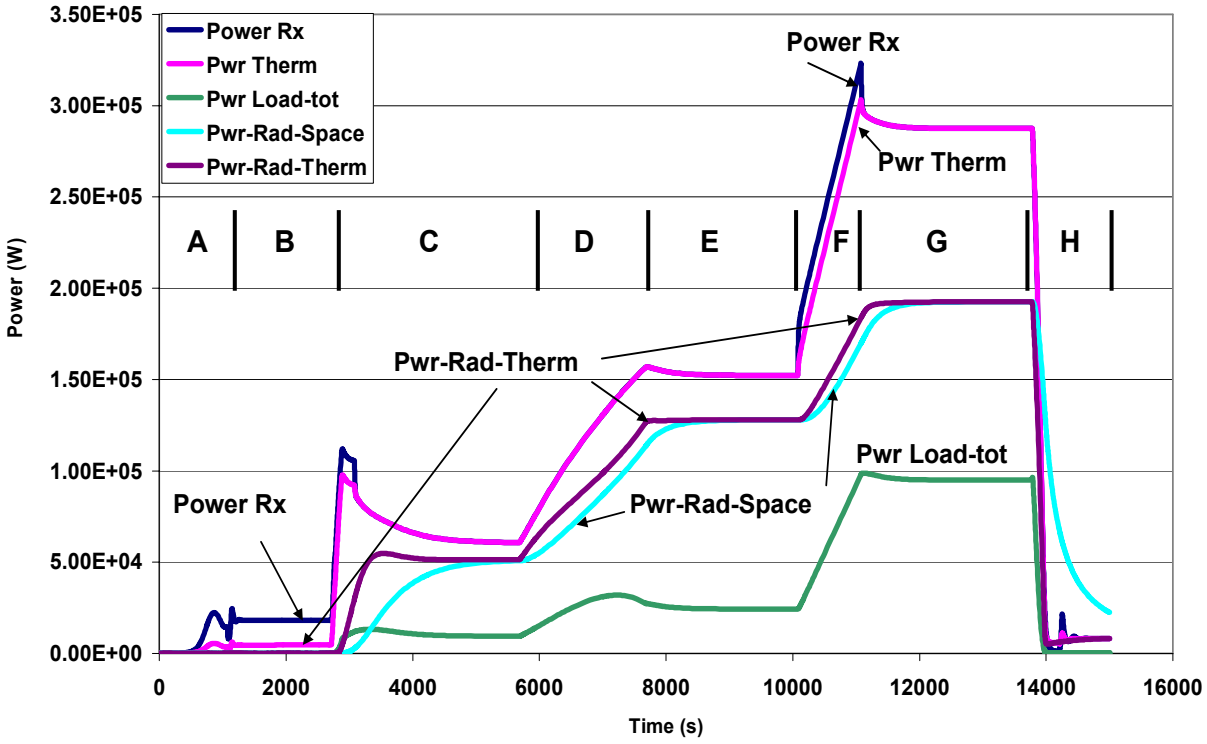

Figure 2-72: Startup transient showing reactor, radiator, and electrical power including the response to a turbine-coast-down transient.

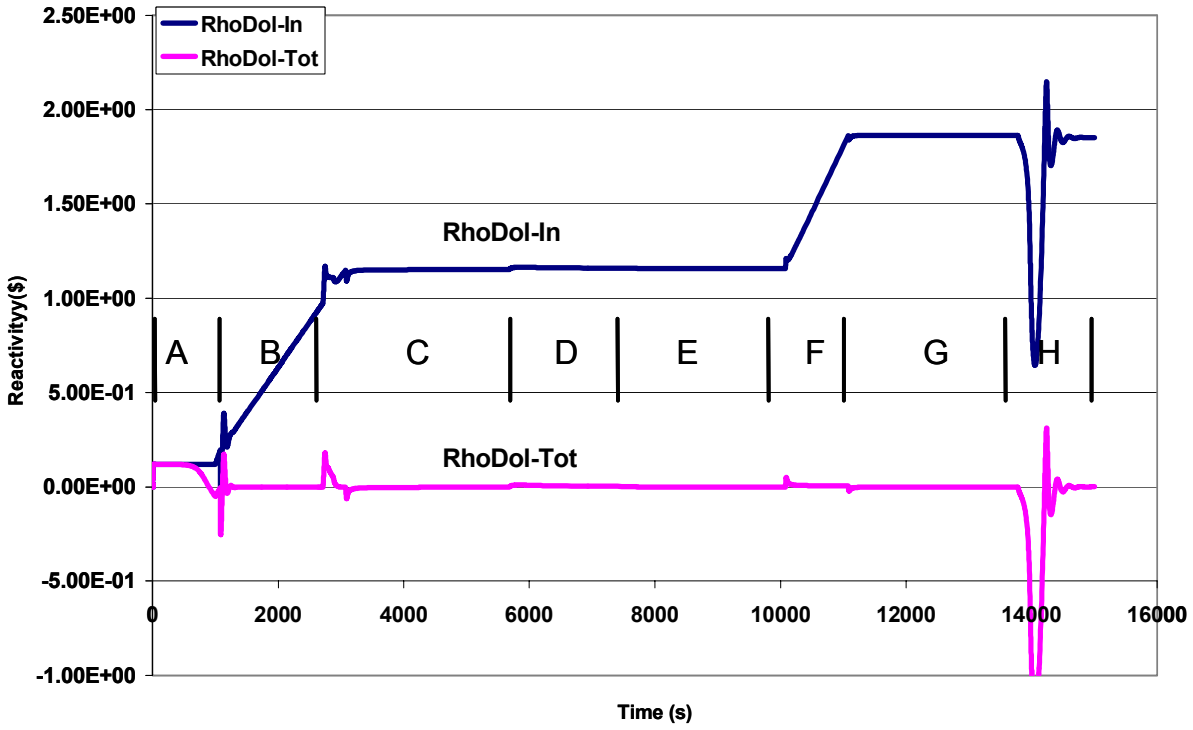

Figure 2-73: Inserted and total reactivity for the startup and turbine-coast-down transient.

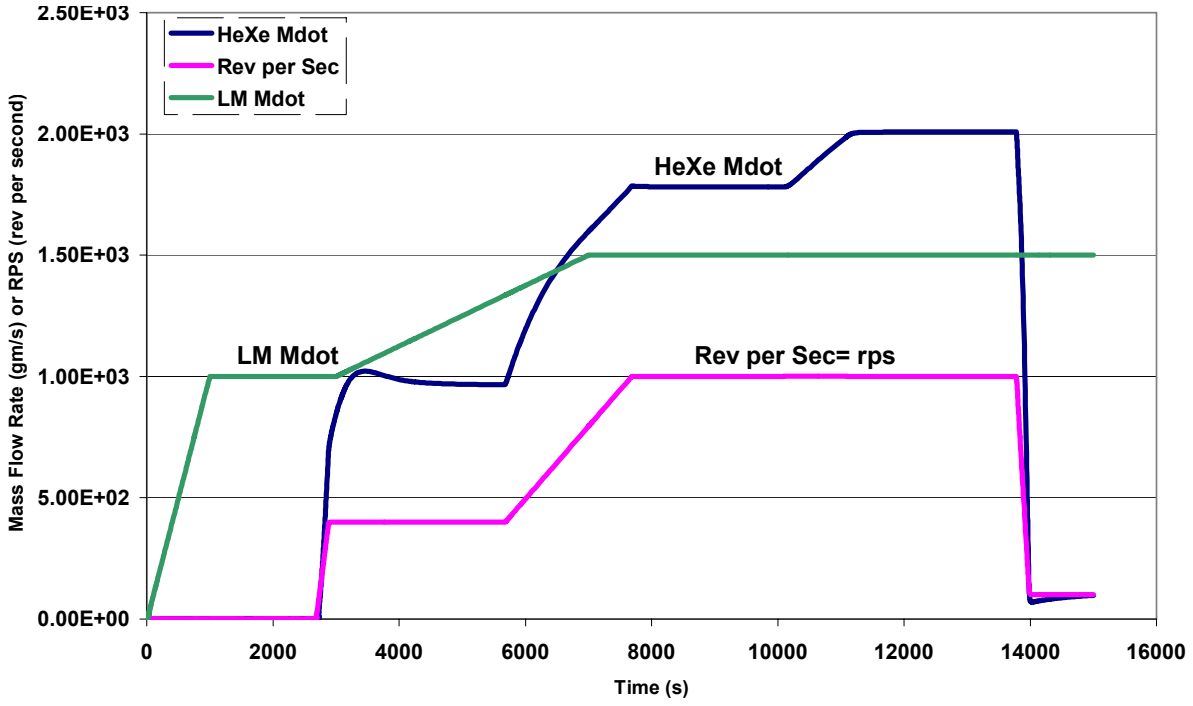

Figure 2-74: Shaft speed (rev per second) , lithium and HeXe flow rate (gm/s) for the LMR startup and turbine coast-down.

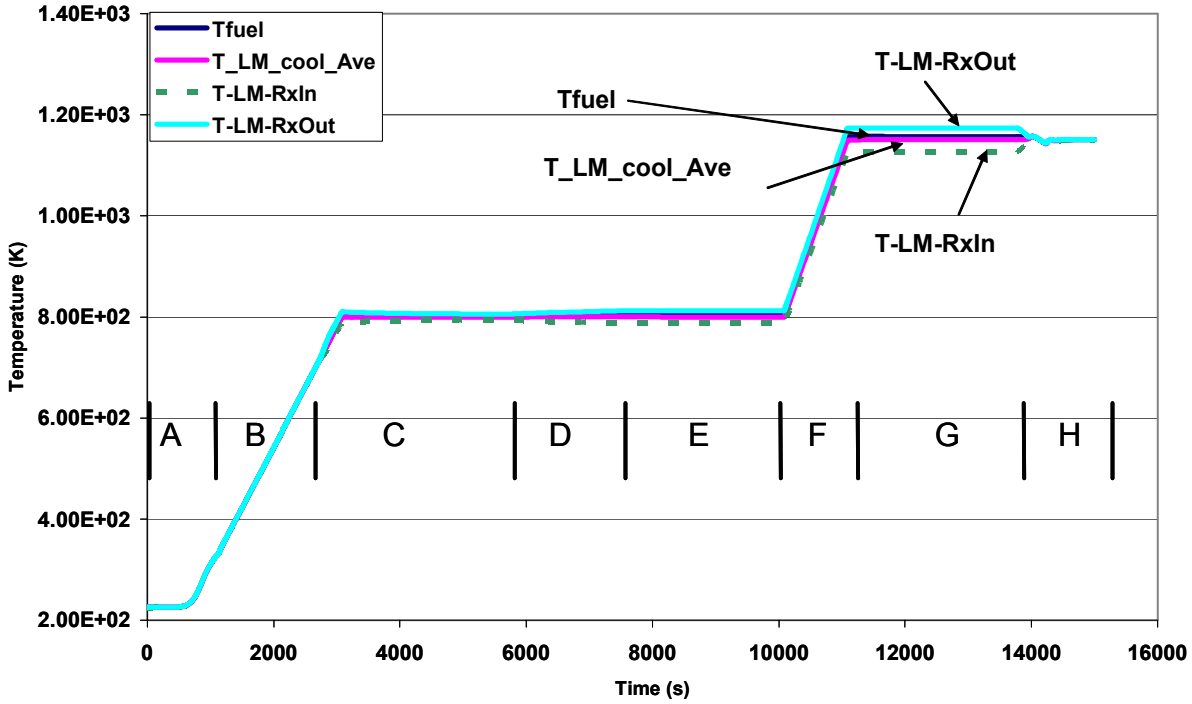

Figure 2-75: Temperatures of the LMR reactor inlet, outlet, fuel, and average lithium coolant temperature for the startup and turbine coast-down.

3 Sandia Brayton Test Loop Description

Because of the limited experience in operating reactor driven closed Brayton cycle systems (and indeed operating just closed Brayton systems) we decided that the best way to validate the models was to build an electrically heated closed Brayton loop. We would then use a reactor simulator controller to operate the electrical heater as a reactor using air or nitrogen as the working fluid. Our goal was to manufacture a closed Brayton loop by modifying available commercial turbo-machinery. To accomplish this task, Sandia issued a Request for Quote to evaluate the possibilities of manufacturing an inexpensive closed Brayton loop. Barber-Nichols Incorporated (Barber-Nichols, 2005,) responded to the request and developed an approach that could be accomplished within the time constraints and budget available to this project. The result is the 30 kWe Sandia Brayton Loop (SBL-30) that it described here.

We provide a detailed description of the Sandia Brayton Loop in this section of the report. We first describe the Capstone C-30 open cycle gas turbine upon which the Sandia closed Brayton loop is based. The modifications to the Capstone C-30 system are described next, and some time is spent describing the modifications to the turbo-alternator compressor and the flow path through it, because it is quite complicated, and it impacted the design modifications that were required. The flow path is difficult to follow because is consists of flow through a series of nested annular "cans". A number of photos of the modifications are provided, along with photos of the assembled unit at the Barber-Nichols site and now at Sandia. These sections are then followed by a description of the electrical heater, the gas chiller, and then an overview of the ducting and instrumentation are described. Within these sections, information regarding size, mass, flow volume, heat transfer areas, and hydraulic diameters of the various components is provided to support other modeling efforts. In addition a brief description of the pressure safety issues is summarized.

A description of the Controller software is also provided which uses a real time National Instruments LabView^{TM} computer and field point data acquisition system to communicate with the Capstone controller and with the Watlow Heater controller. The LabView^{TM} hardware and software were assembled and developed in a contract to PrimeCore Corporation (contract number 334766). The Real Time CBC LabView^{TM} controller performs two functions. First it communicates with the Capstone controller via an RS-232 port to send commands to initialize the communication protocols, to idle, startup, change speed, to shutdown and to receive operational information such as shaft speed, as wells as rectifier and inverter voltage and current information. In addition, the CBC Real Time controller records a variety of signals that measure temperatures, pressure and flow rate. A separate LabView^{TM} monitor program CBC_Monitor communicates with the real time LabView^{TM} controller via an Ethernet connection to display the acquired data and to send operational commands to the Real Time controller. This architectural style of data acquisition is used by Sandia National Laboratories to control the Annular Core Research Reactor (ACRR), and it could form the basis for terrestrial and space based autonomous reactor power systems. A brief summary of these controllers and how they operate is provided. In addition some of the early data that was recorded is also presented.

Note that the hardware and control systems were designed using the conventional US units of degrees F, ft, psia, and psig (pounds per square inch absolute/grade). As such, the figures and tables in this section will often use mixed units. In addition the SBL-30 is installed and operating at Sandia, but our test series are only beginning, and the results that are presented here only

cover a limited range of the tests that we are planning. Some tests that are not presented but are being planned or under consideration, include using different gases as the working fluid, different fill gas pressures, adding electronic control to the heater to make it look like a reactor, use of inventory control, use of throttle control and bypass control. For the tests that use different gases, we first intend to use inert gases with higher and then lower molecular weights that in air or nitrogen. We also intend to use CO_2 as with working fluid, which will serve as a precursor test for a super-critical CO_2 Brayton cycle. A very interesting test that is under consideration is the use of gases that decompose at elevated temperature such as N_2O_4 or N_2O. Simple thermodynamic models of these systems that assume equilibrium decomposition indicate that substantial improvements to the cycle efficiency can be obtained for the same turbine inlet temperature. In addition the loop can be used to develop control methods and approaches for various types of rectification and voltage regulation methods. Tests that use higher power and higher temperature heaters are being considered as well as tests that study autonomy issues, response to instrumentation failures, and accident conditions can also be examined.

Clearly, this list of potential future tests is incomplete and more tests will be thought of once as we accrue data and experience with the loop.

3.1 Closed Brayton Cycle Test-Loop Description

Sandia contracted Barber-Nichols Inc. to design, fabricate, and assemble an electrically heated CBC system. The system design is based on modifying a commercially available micro-turbine power plant. This approach was taken because it was the most cost effective among a number of approaches considered because all the rotating components, the recuperator, the gas bearings, and the control components could be reused. Other methods of designing and fabrication a closed loop Brayton cycle that were examined included modifying an automobile turbo-charger and possibly using an auxiliary power unit (APU). The modification of the Capstone open cycle gas turbine system was selected largely because it only required modifying the housing to permit the attachment of an electric heater and a water cooled gas chiller. This approach therefore allowed the reused of all the other components including the alternator and associated rectification electronics and control hardware. The Sandia Brayton test loop uses a 30 kWe Capstone C-30 gas-micro-turbine generator that normally operates at 1144 K turbine inlet temperature (TIT) with a shaft speed of 96,000 rpm (Capstone, 2005).

An early conceptual layout of the Capstone gas micro-turbine modifications shown as block diagram modules for the heater, gas cooler, and load bank is illustrated in Figure 3-1. In addition to the turbo-compressor-recuperator-alternator unit, the hardware consists of an electrical heater, a water chiller to cool the waste heat in the gas, and an external electrical load that can be used to control the shaft rpm and gas flow rate through the system. As shown on the diagram the alternator, compressor and turbine are all mounted to the same shaft. Gas bearings are used for the turbo-compressor wheels and in the alternator. The recuperator is a counter flow recuperator and is shaped into an annulus that surrounds the compressor and turbine. The cool inlet gas flows over the alternator to control its temperature. Not shown on the diagram is the power converter and control unit. This power converter/inverter produces 480 V 3 phase power at 60 Hz, regardless of shaft operating speed. This power can be routed to the electrical grid or transferred to a resistive load bank. Because we purchased the grid connected version of the Capstone C-30 unit, it allowed us to connect the power converter/inverter to the grid rather than use a separate load bank as shown in Figure 3-1. Because the electrical grid is used for the load,

most of this power goes right back into the heater. Thus, in effect the heater provides the load, and we did not have to purchase a separate load bank for our system. The Capstone internal controller (power inverter) adjusts the phase difference between the power inverter and the grid to control the power draw by the grid. This is the actual method used by the Capstone controller to regulate/control the shaft speed or rpm. Furthermore, the grid power can also be used as a power source to "motor" the alternator to start the gas turbine. All of these control mechanisms are provided by the Capstone controller, eliminating the need for us to design, fabricate and purchase electronics to provide these functions.

The CBC test-loop hardware is currently configured with a heater that is designed to ~80 kW_t with an outlet temperature of 1000 K. Other heater systems that better simulate the thermal hydraulics of nuclear reactors and that are capable of providing higher temperatures and more power can be attached in the future. At the present time the heater is limited to 63 kW and 900 K outlet temperatures. The chiller is capable of rejecting up to 90 kW_t and has a water flow rate of 68 liters/min of chilled water at 285 K=56 F. The Sandia house water supply is at 56 F. The heater power is controlled by a 4-20 mA current source by a Sandia provided National Instruments controller. The water flow rate is not directly controlled at this time. Some minor modifications to the Sandia facilities were required to provide 122 kW of electrical power at 480 V 3 phase, and the chilled water.

Early testing of the open cycle C-30 turbo-alternator-compressor was used to partially calibrate/validate our initial models for the CBC test-loop and to help determine the size of the heaters and chillers. These tests were performed in air with the unmodified C-30 unit. The results of these open air tests are summarized in Table 3-1 and in Figure 3-2 Summary results of this open cycle testing are shown in the second column Table 3-1. Columns three and four show the results of modeling (based on the models describe in the previous chapters). This data predicts that if the closed unit operates at a TIT near 1000 K, and at a shaft speed of 96,300 rpm, and at compressor inlet pressure of 0.083 MPa, the test-loop will produce about 15.6 kW of electrical power, and that the heater will require ~76 kW_t of power. The gas chiller will be required to reject up to 54 kW_t. The alternator will produce about 15.6 kWe of total power, but after the efficiency of the alternator and power converter are considered the total net electrical power produced will be ~14.8 kW_e. This information was used to size the heater, heater controller, and gas chiller.

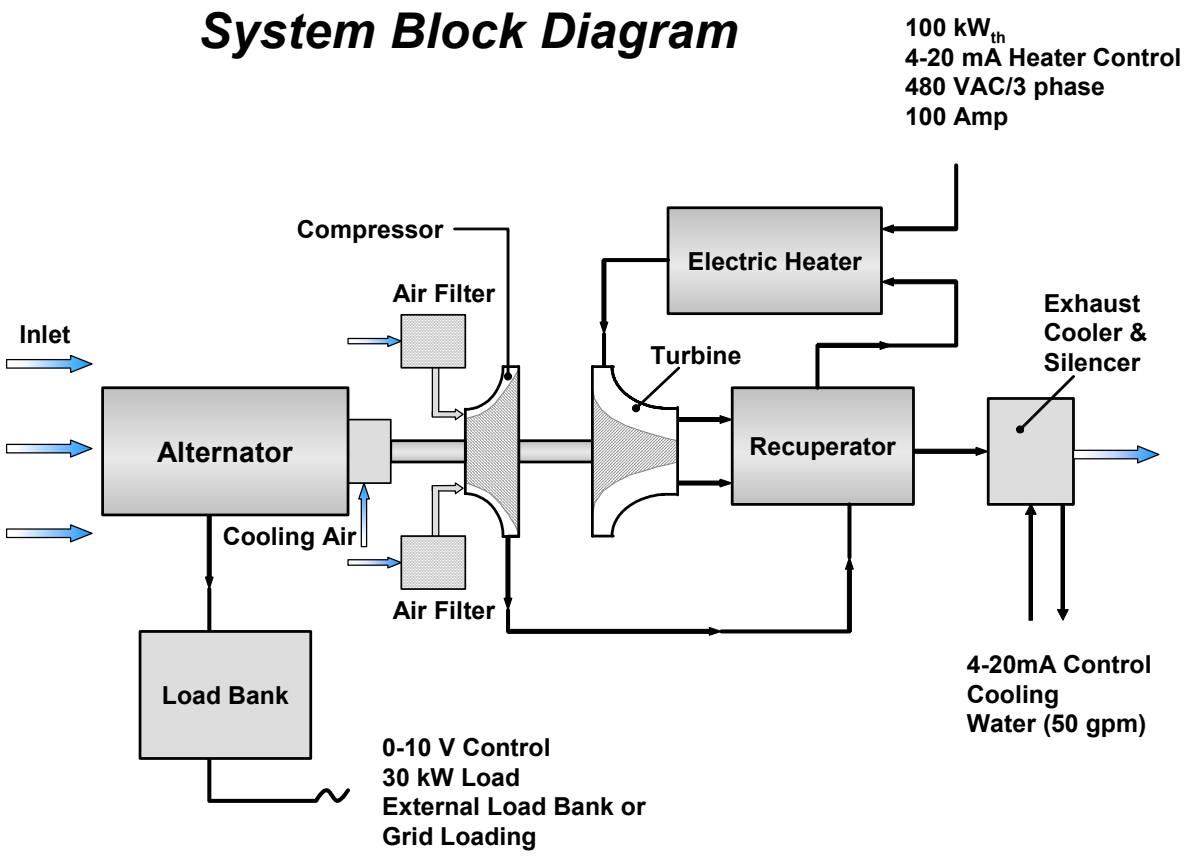

Figure 3-1: Block Diagram of the Closed-Brayton Cycle Test Loop. Cooler Exhaust Connects to the Inlet.

More detailed measurements of the open cycle gas turbine measured net power (and predicted) as a function of shaft speed, for fixed turbine inlet temperatures if 1144 K, and 1000 K are provided in Figure 3-2. These measurements (for the 1144 K turbine inlet temperature) were made while the Capstone unit operated using it predefined schedule of fuel versus rpm. We believe that fuel is scheduled at a rate so that at varying shaft speeds, the "head coefficient" (the ratio of the gas turbine wheel tip speed to the "spouting velocity" $c_o = \sqrt{2\ g\ H_{ad}}$, where H_{ad} is the adiabatic head or ideal enthalpy change as measured in distance) is kept near 70%. This roughly keeps the turbine efficiency near its optimum value regardless of speed. (The coefficient g is the acceleration of gravity.)

Table 3-1: Measured operating conditions of the open cycle C-30 gas-micro-turbine (Column 2) and expected operating conditions of the CBC test loop (columns 3 & 4) at 1000 K and 1144 K with a compressor inlet pressure of .0825 MPa.

Component	Orig. Capstone Unit	CBC Test-Loop (1000K)	CBC Test-Loop (1144 K)
Heater	~120 kW_t (propane)	76 kW_t	107 kW_t
Chiller	-	61 kW_t	79 kW_t
Total Alternator Load	30 kW	15.6kW	30 kW
Net Electrical Power	26.6 kWe	14.8 kWe	26.6 kWe
Turbine Inlet Temp (TIT)	1144 K	1000 K	1144 K
Shaft Rpm	96300 rpm	96,300 rpm	96,300 rpm
Compressor Inlet Temp	283 K	300 K	283 K
Working Fluid (Coolant)	Air	Air	Air

Figure 3-2 shows our first comparison of the dynamic model with measured data, even though it was made for the open gas turbine system. As can be seen the measured data (magenta triangles) agree very well with the predicted net power produced by the Capstone C-30 micro-turbine unit (dark blue line). Given this level of agreement between measurements and predictions for the open cycle system, we felt confident that the closed version of the model would be able to

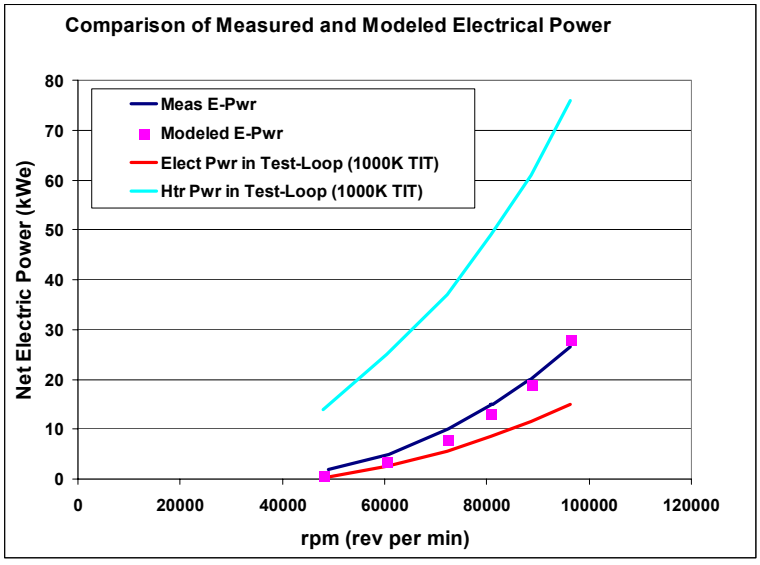

Figure 3-2: Measured (dark blue) and predicted (magenta squares) net electrical power as a function of shaft speed (rpm) at 1144 K. The measurements were made using the open cycle gas turbine operating conditions. The 1000K model predictions are colored red (Net electrical power) and cyan (total thermal power).

predict the expected net electrical power levels as a function of turbine inlet temperature and shaft speed. Figure 3-3 shows the predicted results of our dynamic models for the closed Brayton loop using the C-30 micro-turbine in air. As will be shown later, these plots are very close to what we have actually observed.

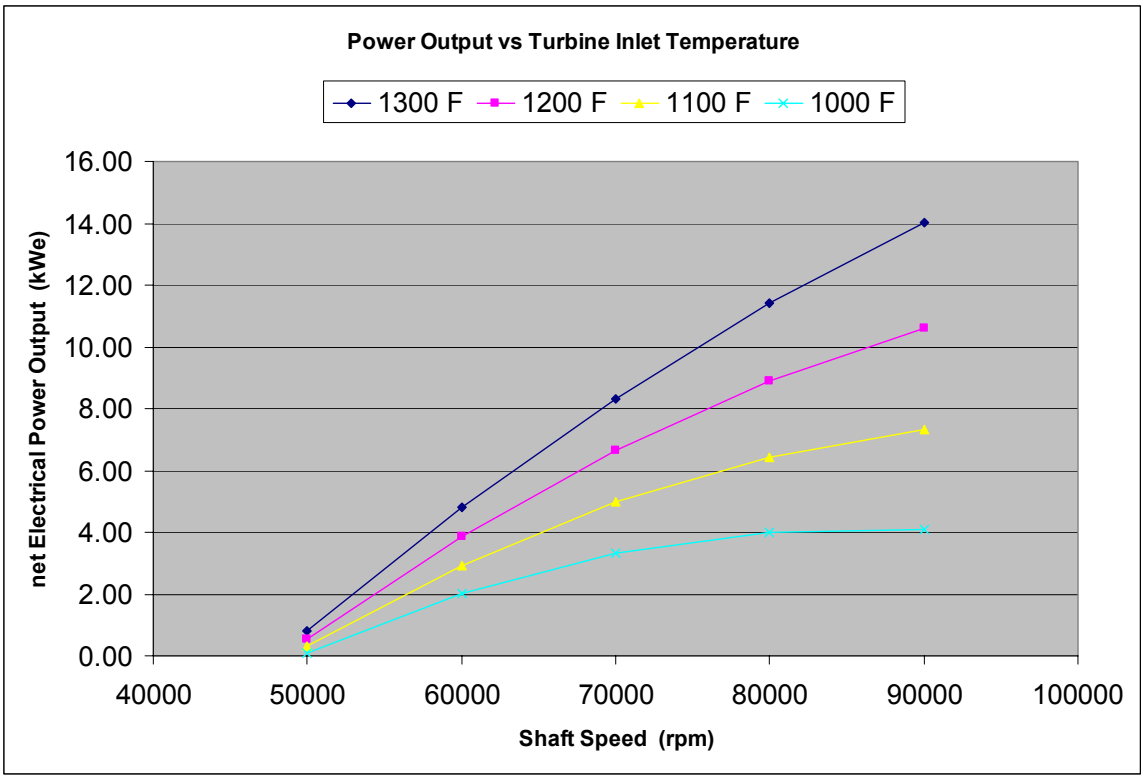

Figure 3-3: Predicted closed Brayton test loop power levels as a function of shaft speed for various turbine inlet temperatures. At 1100 F turbine inlet temperature the expected net power produced is about 7 kWe at 90,000 rpm.

3.2 Capstone Turbo-Alternator-Compressor Modifications

A schematic drawing of the unmodified C-30 micro-turbine unit as an open air gas turbine is shown in Figure 3-4. In this configuration the C-30 micro-turbine uses natural gas fuel to heat the. The original path of the gases and temperatures is indicated by the arrows and colors. The flow path is quite convoluted and flows through several annular regions. The blue lines show that the gas inlet passes along the alternator housing to directly cool it. This gas then flows through the compressor and passes into the recuperator (the gas is colored yellow at this point). After exiting the recuperator (orange) it flows axially and radial around and internal annulus and then flows into the combustor region from both sides of a baffle. The combusted gases (red) then flow (to the left in the drawing) into the radial turbine and then exit the turbine axially (orange). The turbine exit gases then reverse direction while flowing around the combustor region and then flows axially (to the left) back into the recuperator. The gas exiting the recuperator (yellow) and then flows into a plenum and exit to the atmosphere.

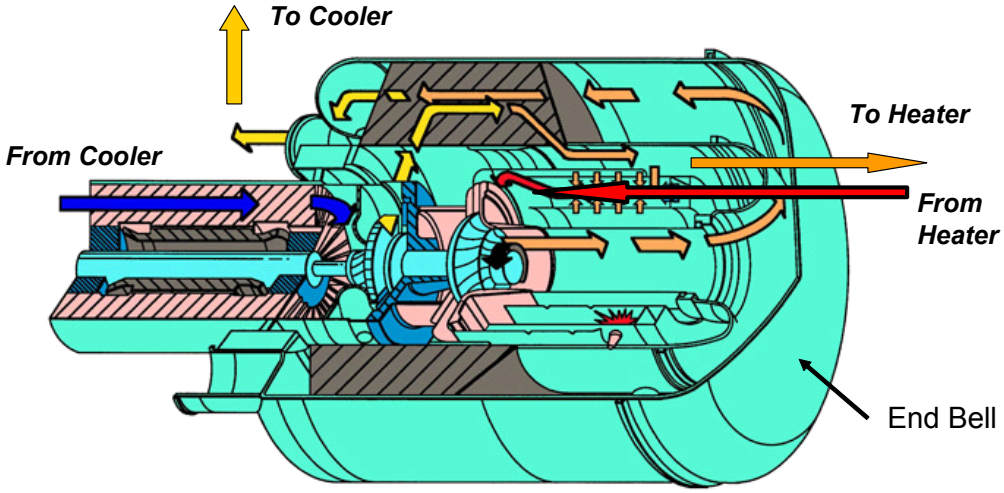

Figure 3-4: Schematic of the unmodified C-30 with arrows illustrating the gas flow path and proposed housing modifications.

On the hot end of the unit, (illustrated in Figure 3-4) the two long straight arrows indicate the modified flow paths that are required to connect the gas from the recuperator to the heater (orange) and from the heater to the turbine (red). The arrow that points to the left shows the flow path of the gas from the heater to the turbine inlet. . The design modifications used the six tubes to transport the hot gas from the heater into the "combustor" annulus. Photos of the interior of the hot head of the unit are shown in Figure 3-5 with the top "End Bell" removed. A close up view of the recuperator exit and the turbine exit are shown in Figure 3-6. The gas injector and igniter passages were used to connect to a heater inlet manifold as shown in Figure 3-6 and Figure 3-7.

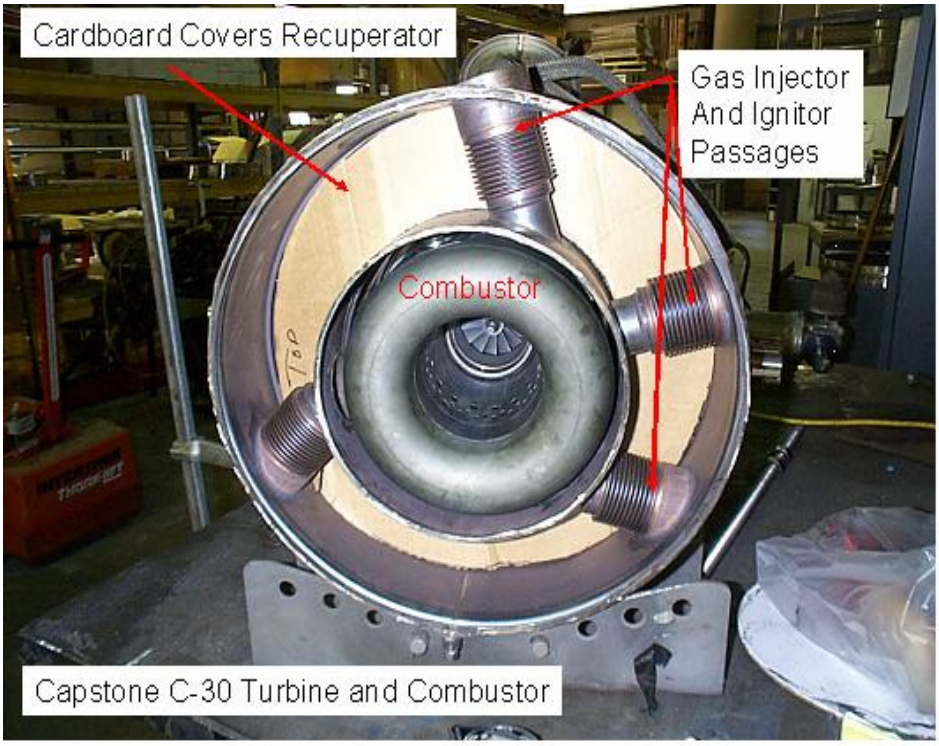

Figure 3-5: "Hot End" of the Capstone C-30 micro-turbine showing the turbine wheel, the combustor annulus, and the gas injector passages.

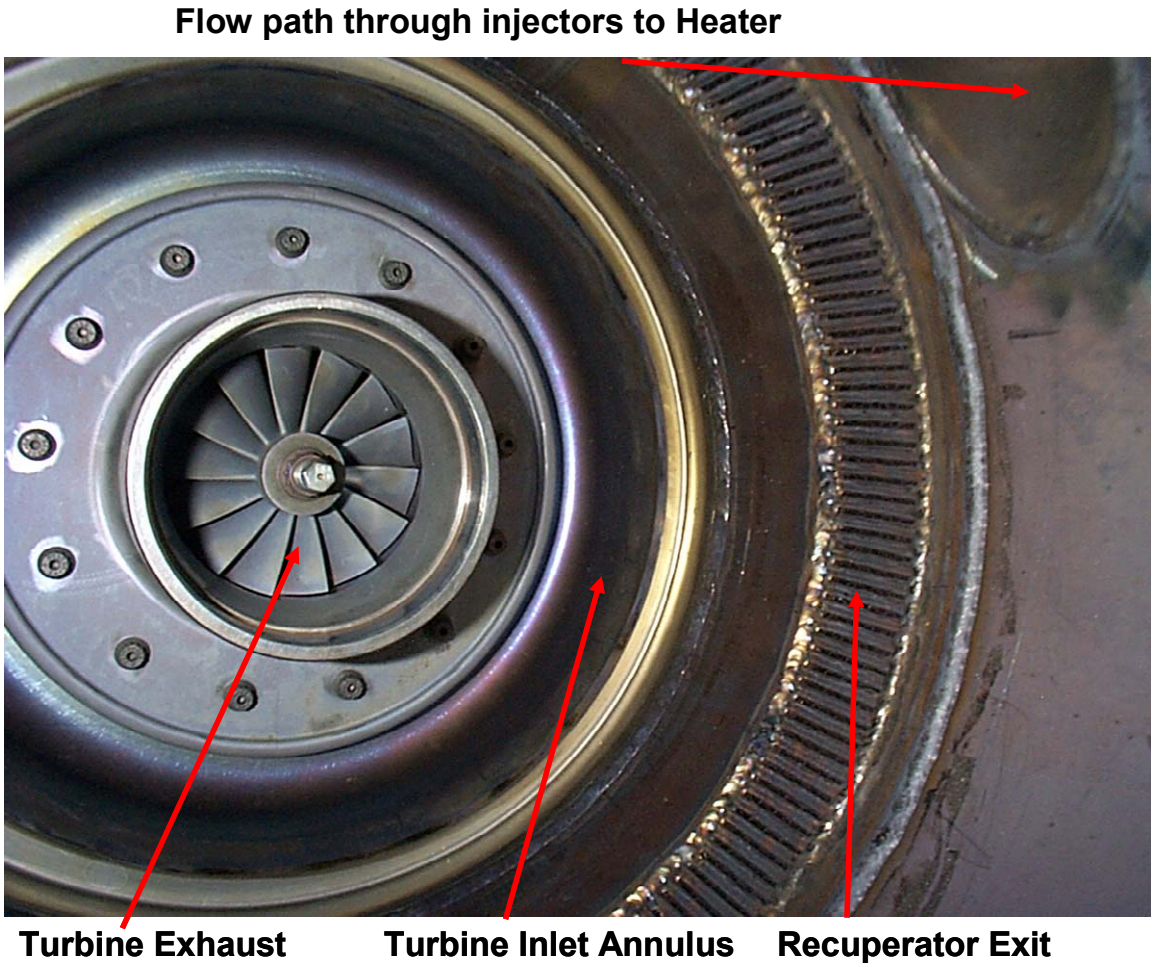

Figure 3-6: Photo of the 14 turbine exit blades, the turbine inlet annulus, and the high pressure recuperator exit. An annular shaped "combustor can" is slipped into the turbine inlet annulus to direct the gas exiting the recuperator through the injector ports to the heater.

Figure 3-7: "Hot" end of the connection flow paths between the injector ports and the heat inlet duct manifold for the C-30 Capstone Micro-Turbine assembly.

To connect the heater outlet gas to the turbine inlet passage, six tubes were used to penetrate the three cover domes or housings as shown in design drawing of Figure 3-8 and in the photo of the hardware illustrated in Figure 3-9. The tubes first penetrate the turbine exit bell housing, next they penetrate through the combustor outer housing annulus and also through the turbine exit inner housing dome shaped annulus. These design modifications use the six tubes to transport the hot gas from the heater into the "combustor" annulus. Figure 3-10 provides further details from a cut-away drawing of the turbo-compressor unit illustrating how the injector and igniter passages are connected to a common manifold that supplies gas to the heater. The flow passages are also shown as well.

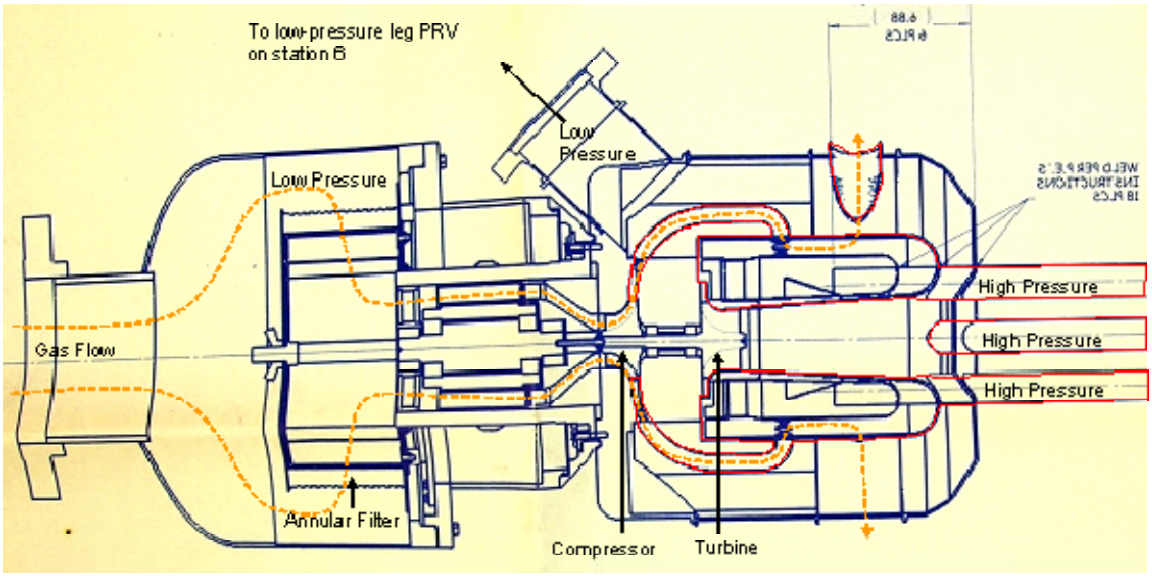

Figure 3-8: Capstone C-30 turbo-alternator-compressor cutaway with high-pressure zone highlighted.

Figure 3-9: Six tubes penetrating through the turbine exit dome, through the combustor dome shaped annulus (middle "dome"), and through the turbine inlet dome (smaller bottom dome shaped annulus) .

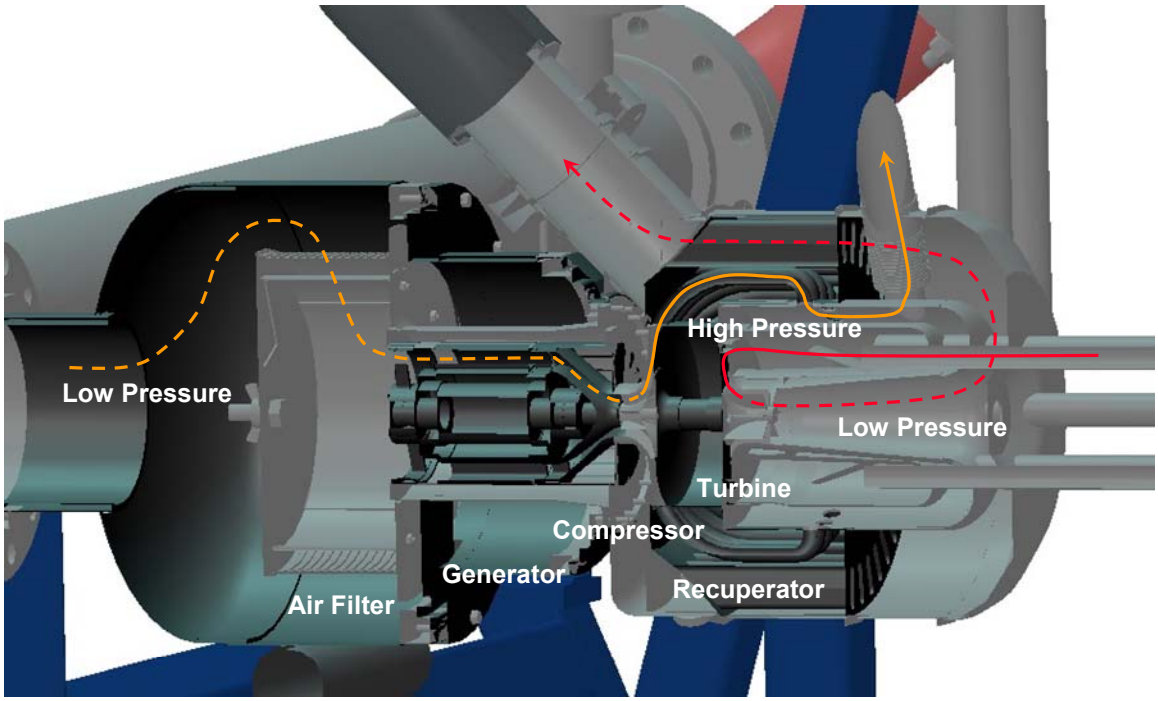

Figure 3-10: Capstone C-30 turbo-alternator-compressor engineering drawing cutaway showing the gas flow path. Orange lines show the flow path through the compressor and recuperator, red lines show the flow path through the turbine and recuperator.

A photo of the cold end of the turbo-alternator-compressor is shown in Figure 3-11. This photo clearly shows the inlet flow passage past the alternator, it also shows the low pressure gas exit leg from the recuperator. The spiral shaped annular flow passages from the recuperator are clearly visible in this image. We have been able to make estimates of the heat transfer areas, and hydraulic diameters for the recuperator based on images like this.

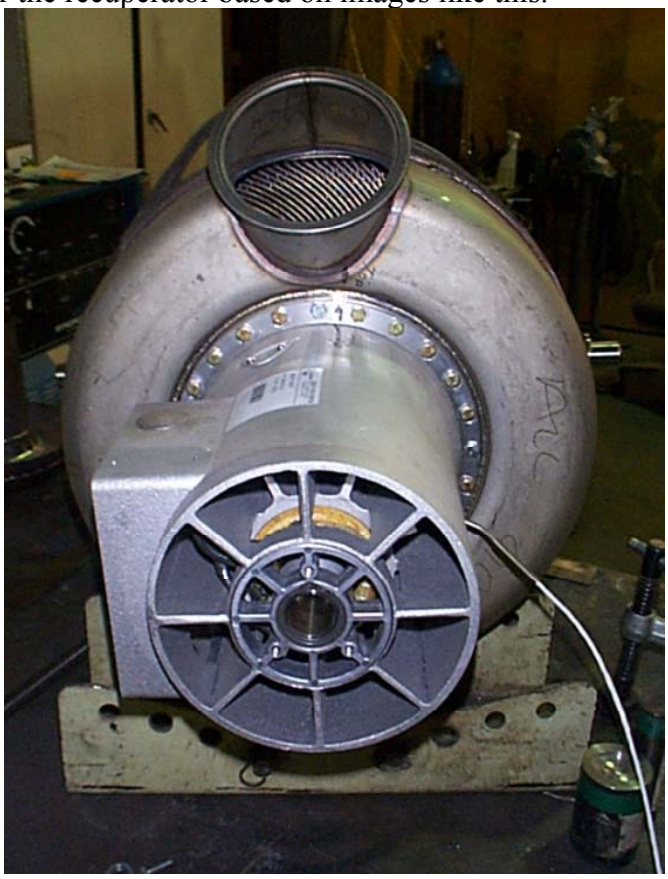

Figure 3-11: "Cold End" of the Capstone C-30 micro-turbine illustrating the spiral recuperator, the alternator, and the inlet cooling passages along the alternator.

The electrical heater and the gas chiller were then connected to the turbo-alternator-compressor as shown in Figure 3-12 which shows a complete assembly drawing of the entire closed Brayton cycle. Note that the system design used a "U" shaped configuration so that it would fit into the laboratory. This configuration easily accommodates thermal expansion by use of the ducting bellows at the ends of the legs. In addition the heater and chiller are mounted on pedestals, while the turbo-alternator compressor set stands on wheels to allow for some motion during heating. The photo in Figure 3-13 shows the fully assembled and operational Brayton loop at Barber Nichols Inc. These photos show the system without thermal insulation, as permanent insulation was only installed on the system after shipping the unit to Sandia.

Photos of the un-insulated Sandia Brayton Loop, as installed at Sandia, are shown in Figure 3-14 and in Figure 3-15. Figure 3-16 shows a photo of the Sandia Brayton Loop with insulation and as installed and operational.

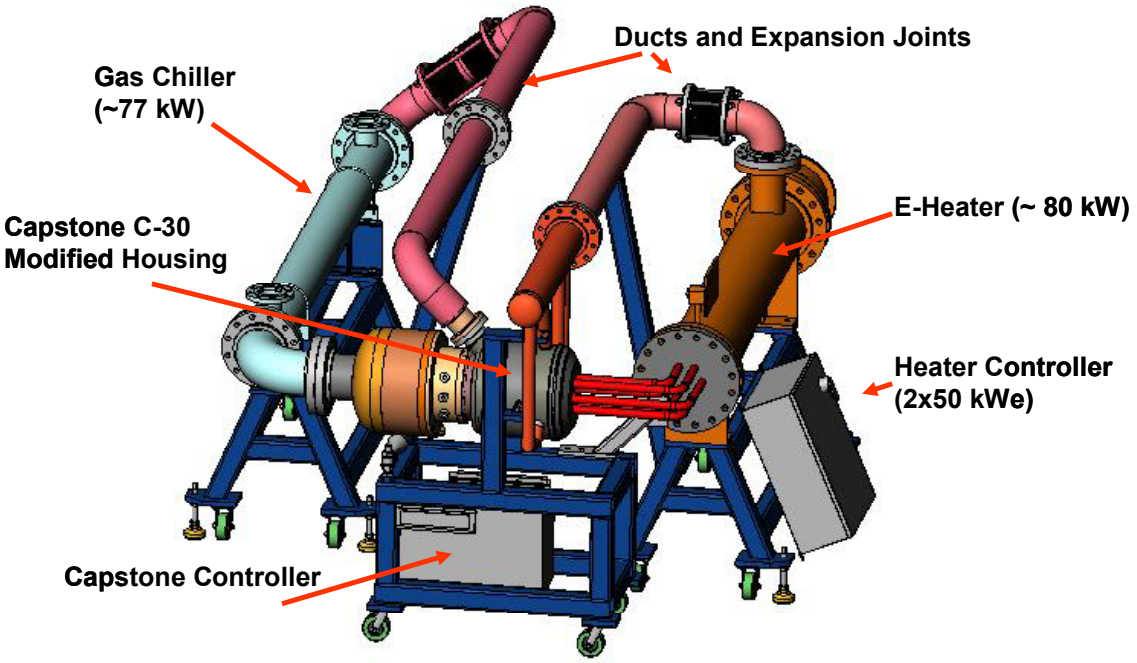

Figure 3-12: Assembly drawing of the Sandia closed-Brayton-cycle test-Loop (SBL-30).

Figure 3-13: . Fully modified and assembled Capstone C-30 closed-Brayton loop as assembled at the manufactures (Barber-Nichols Inc.) is illustrated. The gas chiller is in the fore ground and the heater is on the left side of the image.

Figure 3-14: Sandia Brayton Loop as installed at Sandia. The loop is un-insulated in this figure. The heater is on the left, the gas chiller on the right, and the TAC in the middle.

Figure 3-15 Overview of the Sandia Brayton loop as viewed from the compressor inlet.

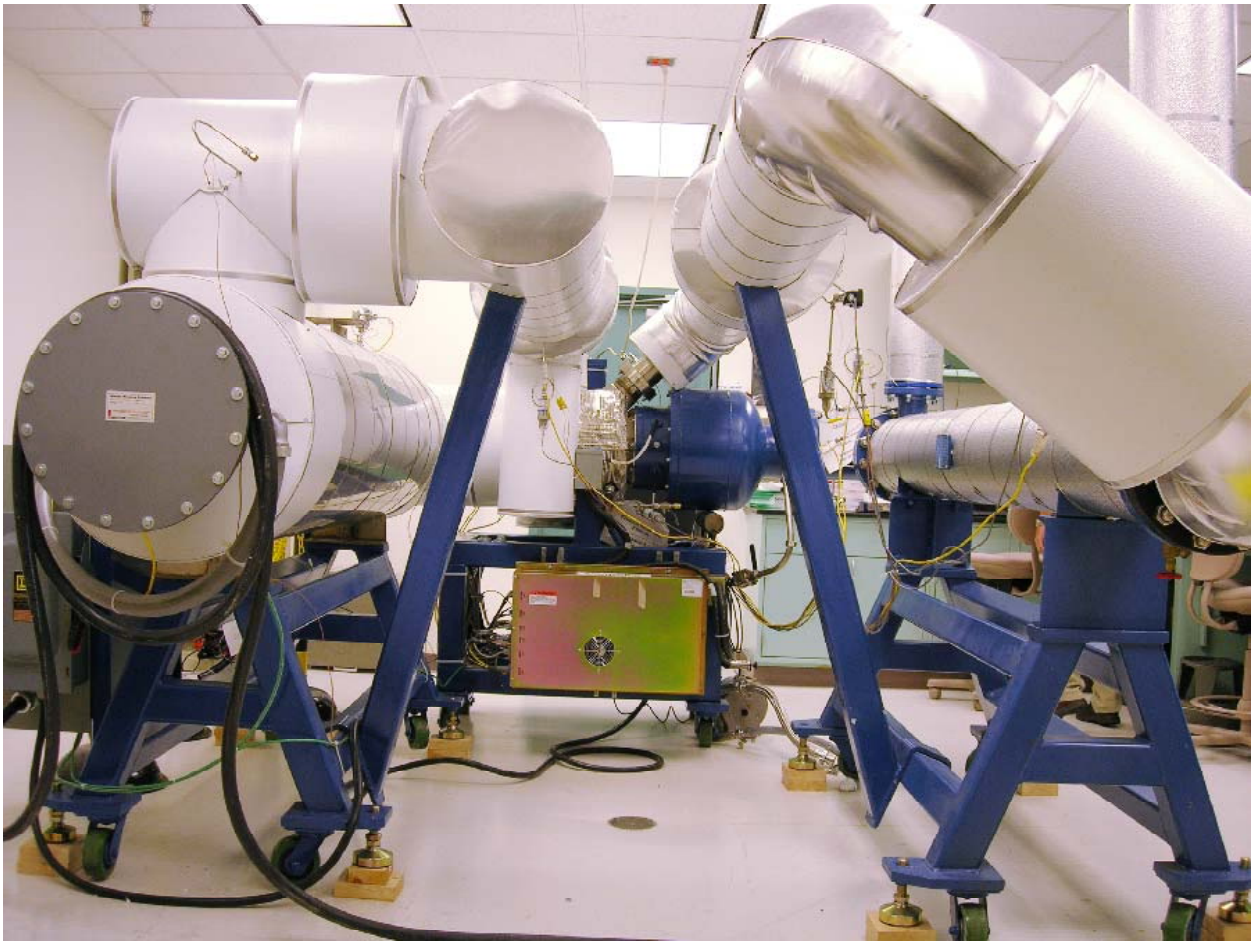

Figure 3-16: Fully installed and insulated Sandia Brayton Loop.

3.3 Gas Heater Description

The Brayton loop gas heater was designed to add about 80 kW of thermal power to the gas which would heat the flowing nitrogen or air to about 1000 K for a flow rate of about 0.25 kg/s. The heater and controller were designed and fabricated by Watlow Inc., Wright City, Mo. A photo of the heater and controller is shown in Figure 3-17 and in many of the other photos already shown. In general the heater consists of a horizontal 12" diameter schedule 300 304 stainless steel vessel through which 54 "U" shaped heater elements are placed. The heater elements are 0.430" inches in diameter and have a leg length of 71" (see Figure 3-18). The gas flows in an "L" shaped fashion through the heater, but 7 baffles force the gas flow into a serpentine path the crosses the heater elements. The inlet flow is downward, and the exit flow is horizontal. The heater element power density is about 5 Watt/in^2 and requires a supply voltage of 480 V 3 phase. The heaters are wired into two banks of three phase resistance bridges with each leg of the resistance bridge having a resistance that varies from 10.55 – 12.22 ohms. The vessel is designed to ASME specifications and it was designed for a fill gas pressure of up to 42 psia at a vessel temperature of 1425 K. The vessel was hydrostatically pressure tested to 474 pisg. Detailed engineering design specifications for the vessel and for the heater elements are listed in Table

3-3 and Table 3-4. The design drawings for these two components are provided in Table 3-2 and in Figure 3-19.

Figure 3-17: Watlow 80 kW Brayton loop gas heater and controller.

Figure 3-18: "U" shaped heater elements used in the Watlow heater. The photo shows the heater elements, the grid spacer wires, the baffle, and the gas exit thermocouple (vertical rod).

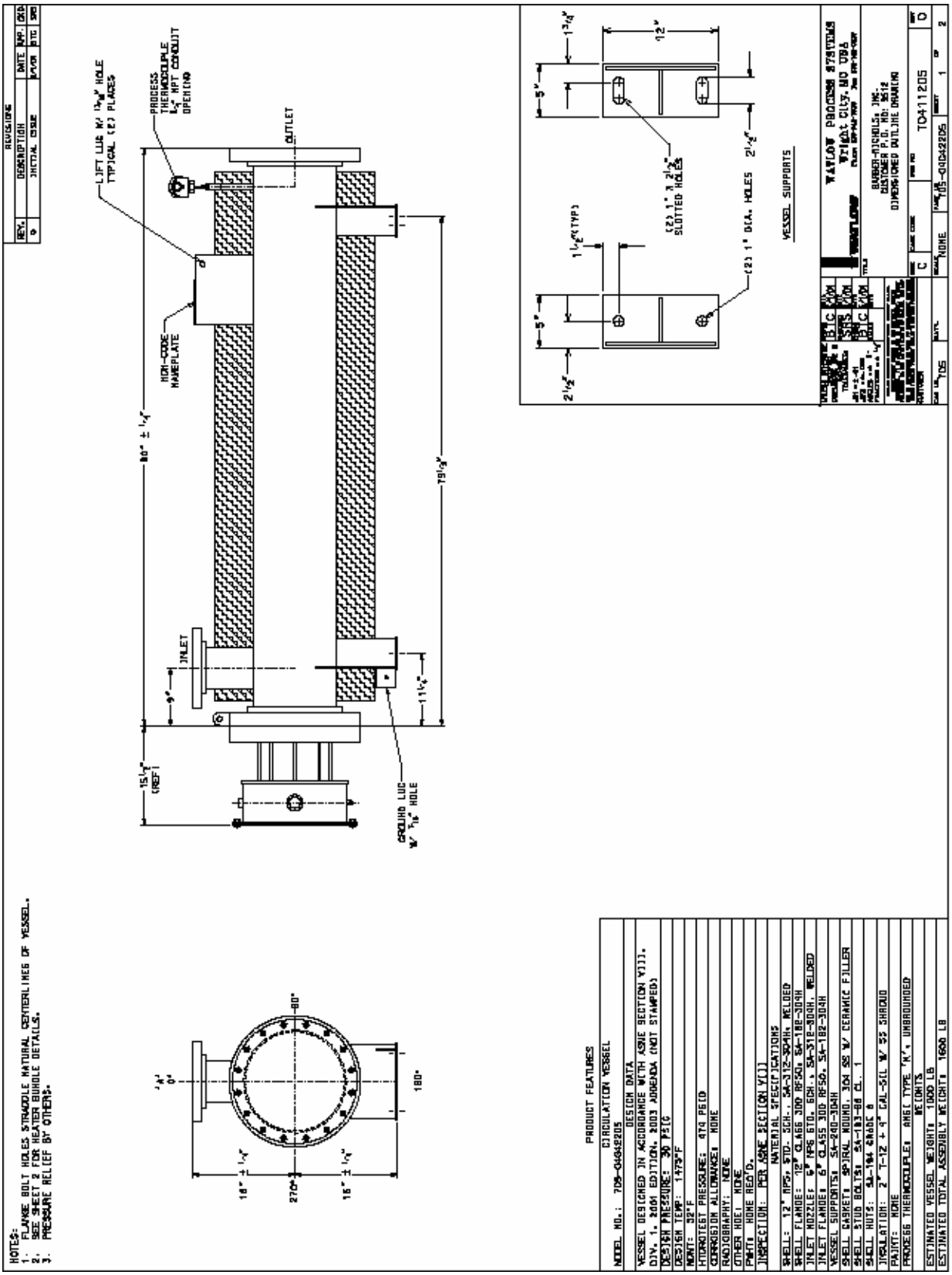

Table 3-3: Watlow 80 kW gas heater vessel product specifications.

The RPCSIM dynamic model for the Sandia Brayton loop uses the reactor model for the electrical heater. However new input parameters are used to simulate the heater elements, the wall, and other design parameters. The RPCSIM core prism model is used for the wall, and the fuel pin model is used for the heater elements. The data that were used to determine the model input parameters were obtained from the tables and figures presented here and summarized in

Table 3-5. The heat transfer coefficient uses the Dittus-Boelter model for gas heating. Thirty axial nodes are used along the length of the heater.

Table 3-4: Watlow gas heat product specifications for the immersion heaters and their material specifications.

PRODUCT FEATURES
CIRCULATION VESSEL
MODEL NO.: 705-D4G42205
DESIGN DATA
VESSEL DESIGNED IN ACCORDANCE WITH ASME SECTION VIII, DIV. 1, 2001 EDITION, 2003 ADDENDA (NOT STAMPED)
DESIGN PRESSURE: 30 PSIG
DESIGN TEMP: 1475°F
MDMT: 32°F
HYDROTEST PRESSURE: 474 PSIG
CORROSION ALLOWANCE: NONE
RADIOGRAPHY: NONE
OTHER NDE: NONE
PWHT: NONE REQ'D.
INSPECTION: PER ASME SECTION VIII
MATERIAL SPECIFICATIONS
SHELL: 12" NPS, STD. SCH., SA-312-304H, WELDED
SHELL FLANGE: 12" CLASS 300 RFSO, SA-182-304H
INLET NOZZLE: 6" NPS STD. SCH., SA-312-304H, WELDED
INLET FLANGE: 6" CLASS 300 RFSO, SA-182-304H
VESSEL SUPPORTS: SA-240-304H
SHELL GASKET: SPIRAL WOUND, 304 SS W/ CERAMIC FILLER
SHELL STUD BOLTS: SA-193-B8 CL. 1
SHELL NUTS: SA-194 GRADE 8
INSULATION: 2" T-12 + 4" CAL-SIL W/ SS SHROUD
PAINT: NONE
PROCESS THERMOCOUPLE: ANSI TYPE 'K', UNGROUNDED
WEIGHTS
ESTIMATED VESSEL WEIGHT: 1000 LB
ESTIMATED TOTAL ASSEMBLY WEIGHT: 1600 LB

Table 3-5: Fluid hydraulic and heat transfer properties used in the RPCSIM for the Sandia Brayton Loop SBL-30.

Heat Transfer to Coolant from Heater Elements		Heat Transfer from Coolant Vessel Wall	
Radius of element	4.953 mm	Wall inner radius	0.1492 m
L of element	1.727 m	Wall Length	2.235 m
Element Heat transfer Area	6.3988m^2	Wall heat transfer Area	2.0952
Flow Area	0.598 m^2		
Hydraulic Diameter	5.15 mm		
Element Inverse Thermal Capacitance (κ, kappa)	0.0016 K/J	Mass of Wall	221 kg
Number of effective pin or elements	108		

Table 3-6 Watlow gas heater vessel design drawings and specifications.

PRODUCT FEATURES

IMMERSION HEATER
MODEL NO: T01-04GD2205
ELECTRICAL DATA
DUTY: 79KW, 480 VAC, 3 PH
ELECTRICAL CLASSIFICATION: NON-HAZARDOUS
ELECTRICAL ENCLOSURE: NEMA 12
MAX. ANTICIPATED HOUSING TEMP: 142°F
ELECTRICAL CONNECTION(S): (2) 3 PH CKTS., #2 AWG MAX.
PROCESS DATA
MEDIUM: NITROGEN
NOMINAL FLOW RATE: 2000 LB/HR
OPERATING PRESS: 21 PSIG
INLET TEMP: 960°F
OUTLET TEMP: 1350°F
ESTIMATED SHEATH TEMPERATURE: 1500°F
RECOMMENDED SHEATH LIMIT TEMPERATURE: 1700°F
DESIGN DATA
VESSEL DESIGNED AND MANUFACTURED IN ACCORDANCE WITH ASME SECTION VIII, DIV. 1, 2001 EDITION, 2003 ADDENDA (NOT STAMPED)
DESIGN PRESSURE: 30 PSIG
DESIGN TEMP: 1475°F
MDMT: 32°F
TEST PRESSURE: 474 PSIG
NDE: DYE PENETRANT
POST WELD HEAT TREAT: NONE
CORROSION ALLOWANCE: NONE
MATERIAL SPECIFICATIONS
TUBESHEET: 12" CLASS 300 RF BLIND, SA-182-304H PER ASME B16.5-1996 EXCEPT 2 5/8" THK.
HEATING ELEMENTS: ALLOY 600 OVER STEEL
ELEMENT SUPPORTS/BAFFLES: 304 SS
ELECTRICAL ENCLOSURE: CARBON STEEL
ENCLOSURE HARDWARE: ZINC PLATED
ENCLOSURE PAINT: VENDOR STANDARD GRAY
ELEMENT END SEAL: EPOXY
HEATER SPECIFICATIONS
QTY & SIZE OF ELEMENTS: (54) 0.430" DIAMETER
WATT DENSITY/HEAT FLUX: 8 WPSI
IMMERSED LENGTH (BUNDLE REMOVAL DIST.): 77"
LIMIT SENSOR: (1) ANSI TYPE 'K' THERMOCOUPLE, UNGROUNDED
WEIGHTS
ESTIMATED HEATER BUNDLE WEIGHT: 600 LB

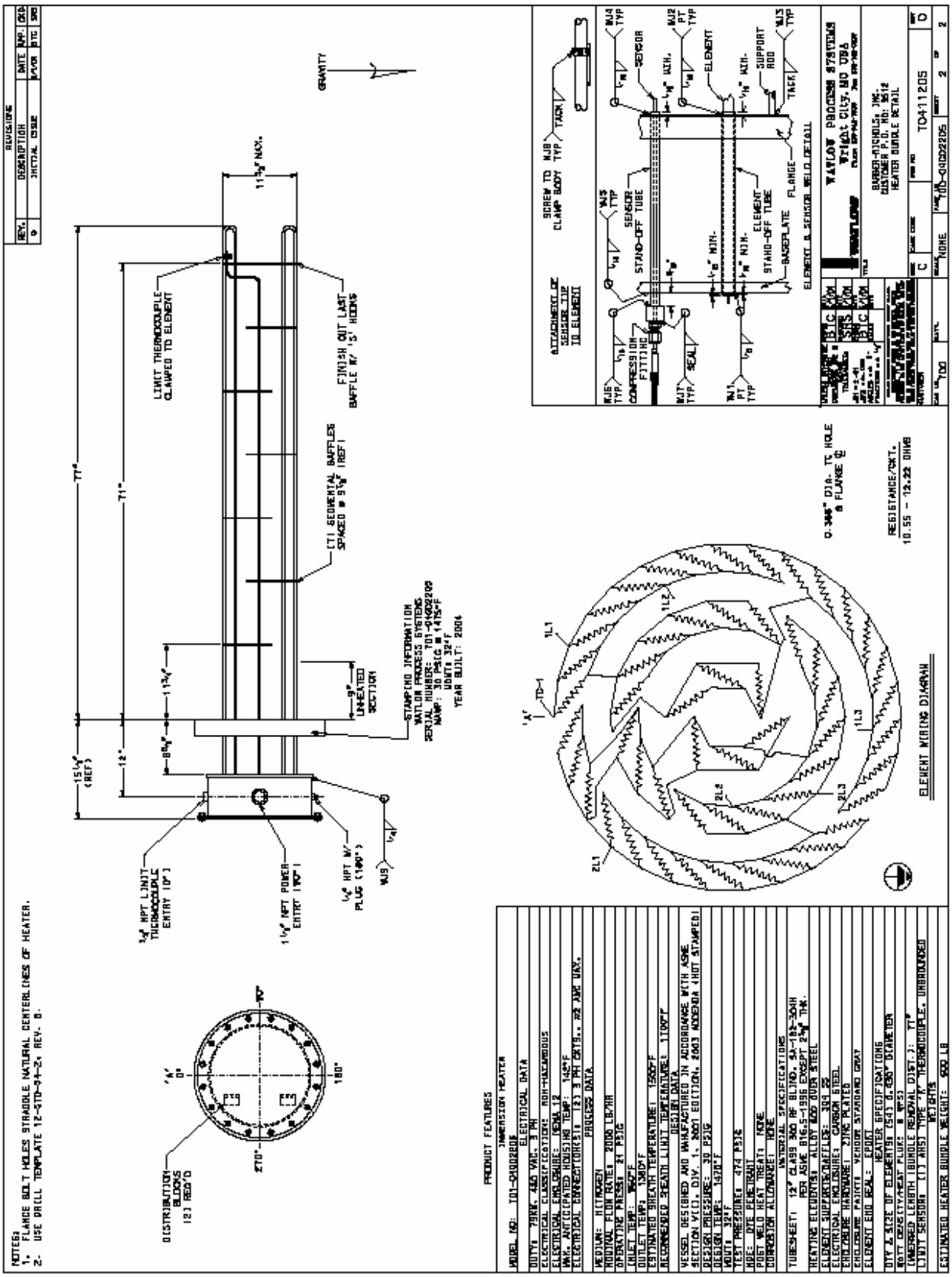

Figure 3-19 Watlow 80 kW gas heater element design drawings and specifications.

3.3.1 Electrical Power Description

Electrical power is required to run both the Watlow heater and the Capstone Power Management Controller. Both circuits require 480 V 3 phase power. The Capstone Power Management Controller is a grid connected controller and is designed to power the electronics in the controller, the inverter circuitry and the motor/alternator. As such, it can draw power from the grid to "motor" the permanent magnet alternator, or it can put power back on the grid which in the Sandia Brayton test loop goes to powering the heater. The Model 330 electrical output can accommodate 3 phase, 400-480 VAC, and 45-65 Hz. Both voltage and frequency are determined by the grid.

Table 3-7 shows the maximum and typical power draw conditions expected from the Capstone Power Management Controller during various phases of operation. The facility power in the laboratory was increased to 100 amperes from 60 amperes (480 Volt) to accommodate the power draw and the supply to the grid and heater. Figure 3-21 shows the approximate layout of the hardware as located in Sandia building 6585 room 2504. The laboratory was designed to supply these levels power and cooling water, but minor modifications were required to connect the water to fill and drainage system, and to increase the amperage. These modifications were made by Sandia facilities.

Table 3-7: Maximum and Typical Power Draws/ Supply form Capstone Power Management Circuitry

	Max	Typical	Duration
Motor Power	3.5 kWe	2 kWe	Minutes
Electrical Pwr Management	2-3 kWe	2-3 kWe	Continuous
Electrical Pwr to Grid	30 kWe	10.5 kWe	Hours to Continuous
Power Draw/Supply	5.5 kWe/30 kWe	5.5kWe/10.5 kWe	
Notes	*Limited to 15 kWe based on maximum design temp of Heater*	*This is the maximum power to grid measured to date*	

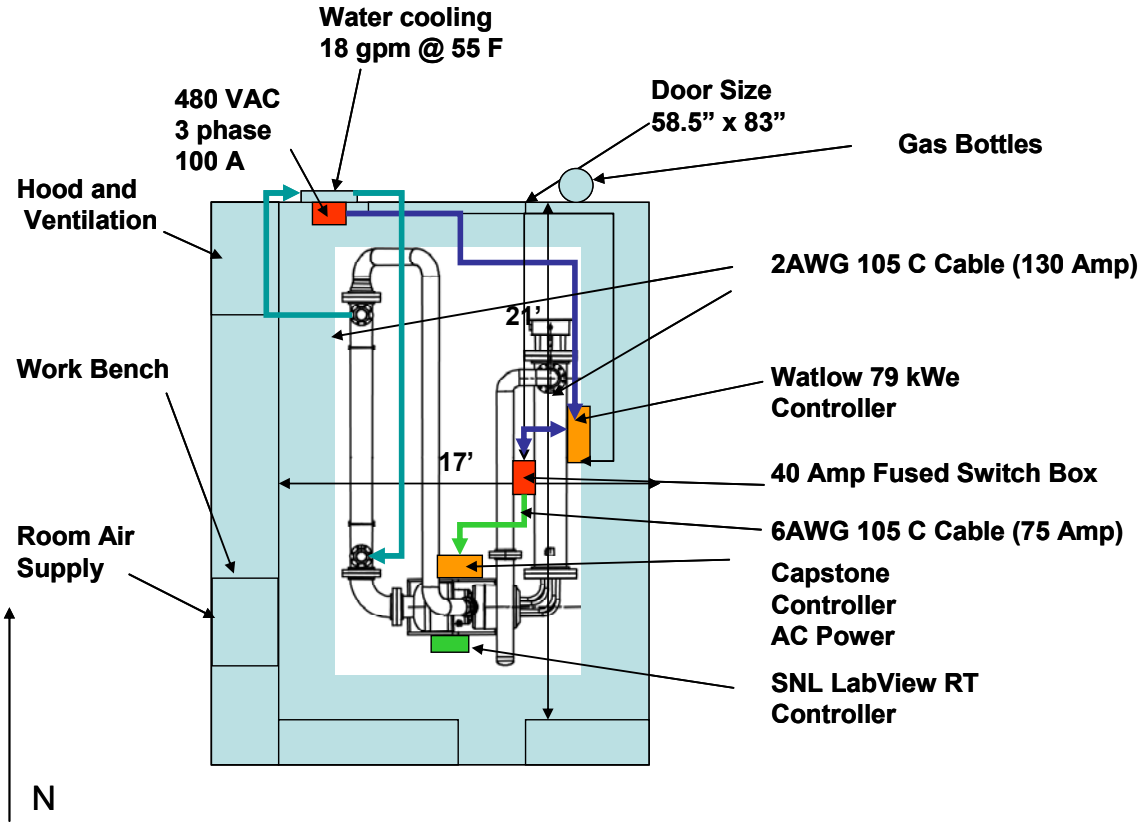

Figure 3-20: Electrical connection and cooling water supply for the SBL-30 as located in building 6585 room 2504. All power is supplied by the 480 3phase 100 amp service from the wall. The cooling water is provided by the building facilities manager.

The electrical circuit for the Watlow heater controller that was purchased from Watlow, and it is shown in Figure 3-21. The Watlow heater control box is interlocked through the door to remove electrical service power to the heater when the service box door is open, it also has a manual switch that must be turned to off before the door can be opened. The circuitry within the heater box then splits into two 50 kWe Dynamite DC2T-60F0-0000 SCR controllers. The SCR controllers switch at the zero crossing intervals and the fractional power is determined by dwell time when no current is allowed to flow. For 50% power, the SCR switches the current on for 3 cycles of the 60 Hz power supply, and then off for 3 cycles. Similarly 25% power uses a dwell time of 6 cycles for the off mode and 3 for the on. The amount of power draw is controlled by a 4-20mA current loop that is set by the RT_CBC_Controller. The internals of the box was wired and provided by Watlow and the electrical circuit for this controller is shown in Figure 3-21. Two thermocouple high temperature limit circuitry interrupts the current draw if the heater element temperatures exceed their maximum temperature limits. One thermocouple is connected to the heater element at the hot outlet side of the heater and is set to a value at or below 1450 F = (1061K), and the other thermocouple measures the gas exit temperature and is set to a value below 1350 F = 1005 K. These thermocouples are also monitored by the RT_CBC_Controller.

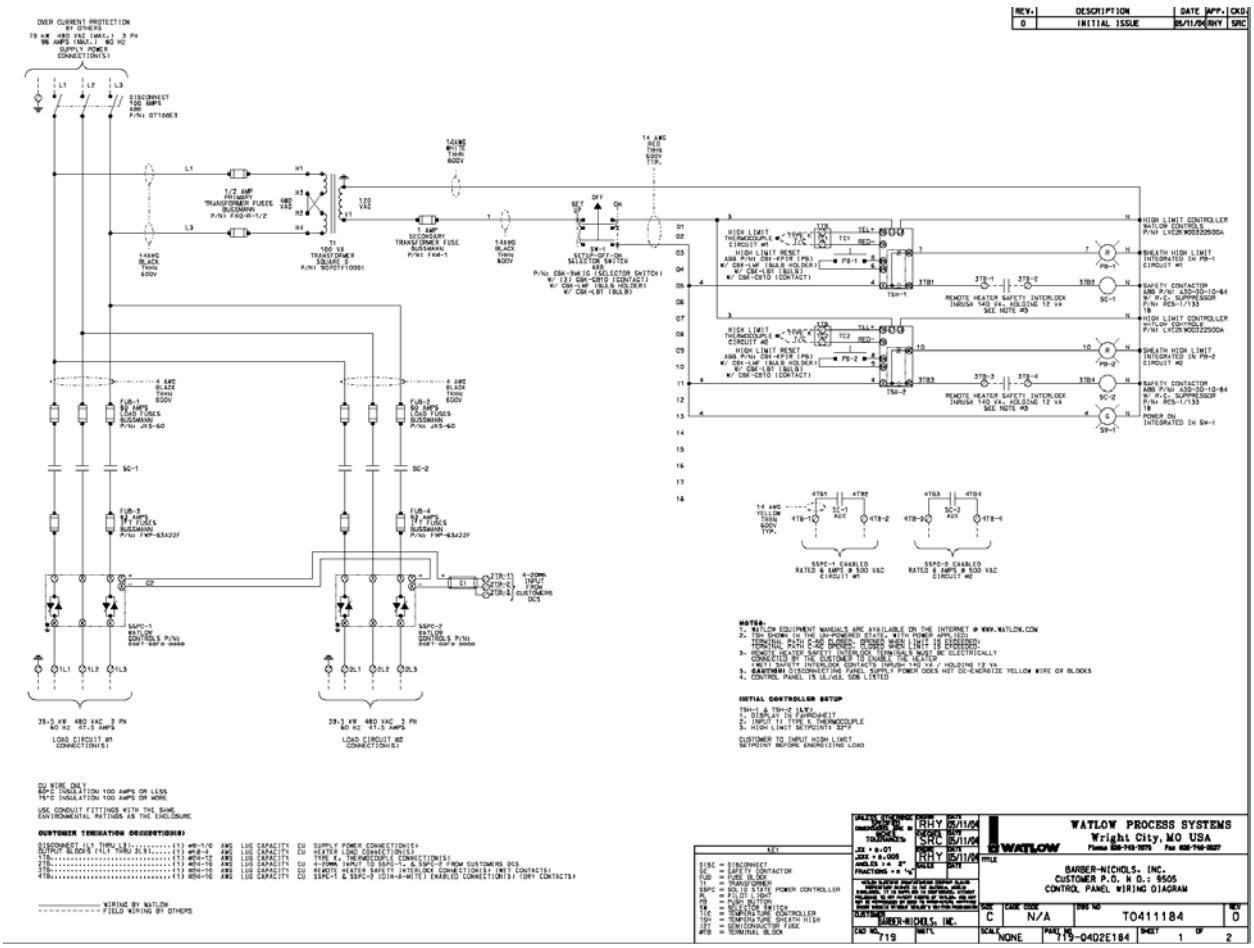

Figure 3-21: Electrical Power circuit for the heater provided by Watlow.

3.4 Gas Cooler Description

The gas cooler provides waste heat rejection capability for the Sandia Brayton Loop. It uses a Basco/Whitlock, Buffalo, NY, shell and tube counter flow heat exchanger. Water flows in the shell portion and the gas/nitrogen flowing in the tubes. It was designed to reject 68.9 kW of heat for a water flow rate of 18 gallons per minute (1.089 kg/s) with a water temperature difference of 15.1 K. The design can accommodate even higher flow rates, up to 50 gallons per minute, thus if we upgrade the power capability of the heater, we can still use the same gas chiller as it is oversized for our nominal operations. Photos of the chiller and the gas inlet passages are shown in Figure 3-22 and Figure 3-23. The cooling water available within laboratory 6585/2504 provides 18 gallons per minute of cooling water at 55 F.

Table 3-8: Basco/Whitlock gas chiller hydraulic and heat transfer properties used in the RPCSIM model for the Sandia Brayton Loop

Hydraulic and Heat Transfer Properties of the Gas Cooler Heat Exchanger	
Mass of Heat Exchanger	114 kg
Area of Water Flow Leg in Heat Exchanger	10.109 m^2
Area of Gas leg in Heat Exchanger	8.0870 m^2
Length of Wtr leg in Heat Exchanger	2.896 m
Length of Gas Leg in Heat Exchanger	2.896 m
Effective Wall thickness of Heat Exchanger	1.587 mm
Hydraulic Diameter of Water Leg	21.3 mm
Hydraulic Diameter of Gas Heat Exchanger leg	25.4 cm
Flow area in HP Heat Exchanger Leg	.019 m^2
Flow area in LP Heat Exchanger Leg	.008867 m^2

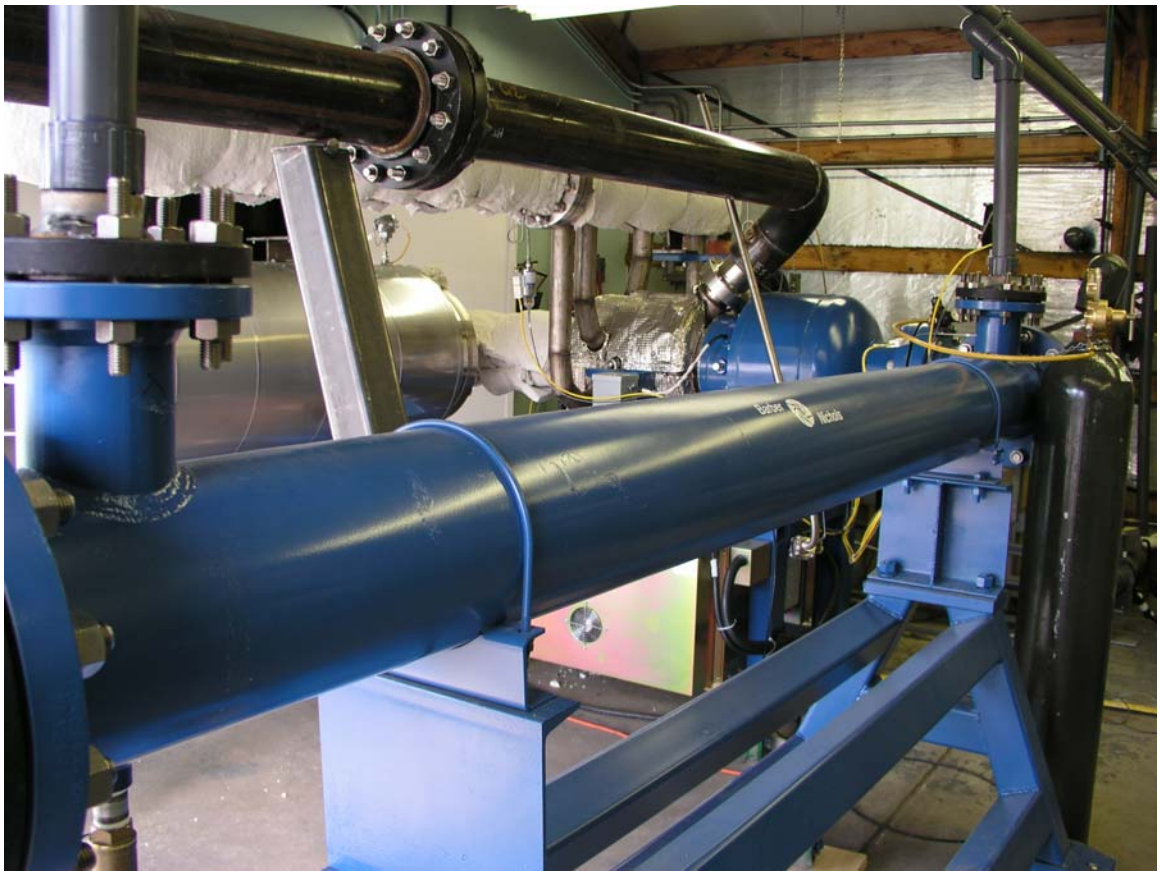

Figure 3-22: Image of the Basco/Whitlock shell and tube gas chiller. Inlet water flows from the upper right side of the image to the lower left, while gas flows in the opposite direction.

Figure 3-23: View of the Basco/Whitlock shell and tube heat exchanger gas inlet flange, showing the stainless steel tubes.

API Heat Transfer

Basco/Whitlock Shell and Tube Heat Exchanger

					JOB NO.	
	CUSTOMER	BARBER NICHOLS			REFERENCE NO.	
	ADDRESS				PROPOSAL NO.	JHB03-16980
	PLANT LOCATION				DATE	06 MAY 2004
	SERVICE OF UNIT	NITROGEN COOLER			ITEM NO.	101 REVISION 02
	SIZE	08-114	TYPE	"-EM"	(HORIZ.) (VERT.)	CONNECTED IN
	SQ.FT.SURF/UNIT (GROSS) (EFF.)	107.3	SHELLS/UNIT	ONE	SQ.FT.SURF/SHELL (GROSS) (EFF.)	107.3
	PERFORMANCE OF ONE UNIT					
			SHELL SIDE		TUBE SIDE	
	FLUID CIRCULATED		WATER		NITROGEN	
	TOTAL FLUID ENTERING	LB/HR	24750		2088	
	VAPOR	LB/HR				
	LIQUID	LB/HR	24750			
	STEAM	LB/HR				
	NON-CONDENSABLES	LB/HR			2088	
	FLUID VAPORIZED OR CONDENSED	LB/HR				
	STEAM CONDENSED	LB/HR				
	SPECIFIC GRAVITY					
	VISCOSITY @ TEMP	cP @ °F	@		@	
	MOLECULAR WEIGHT					
	SPECIFIC HEAT	BTU/LB-°F				
	THERMAL CONDUCTIVITY	BTU/HR-FT-°F				
	LATENT HEAT	BTU/LB				
	TEMPERATURE IN	°F	70.0		540.0	
	TEMPERATURE OUT	°F	79.5		95.0	
	OPERATING PRESSURE	PSIA			35.0	
	NO. PASSES PER SHELL		ONE		ONE	
	VELOCITY	FT/SEC				
	PRESSURE DROP	PSI	2.5		0.2	
	FOULING RESISTANCE (Min)	°F-FT²-HR/BTU	0.001		0.001	
	HEAT EXCHANGED 235500	BTU/HR	MTD CORRECTED	149		°F
	TRANSFER RATE - SERVICE 14.9		CLEAN			BTU/HR-FT²-°F
	CONSTRUCTION OF ONE SHELL					
	DESIGN PRESSURE	PSIG	150		150	
	TEST PRESSURE	PSIG	Per Code		Per Code	
	DESIGN TEMPERATURE (Max/Min)	°F	500 / +20		600 / +20	
	TUBES 304SS SA249	NO. 70	OD 0.625"	BWG 18	LENGTH 9'-6"	PITCH 0.78125" Tri
	SHELL Carbon Steel	ID	OD 8.625"	SHELL COVER		(INTEG)(REMOV)
	BONNET/CHANNEL			CHANNEL COVER		
	TUBESHEET-STATIONARY 304 SS			TUBESHEET-FLOATING		
	BAFFLES-CROSS Carbon Steel	TYPE		FLOATING HEAD COVER		
	BAFFLES-LONG	TYPE		IMPINGEMENT PROTECTION	No	
	TUBE SUPPORTS					
	TUBE TO TUBESHEET JOINT	Mechanically Rolled & Double Grooved				
	GASKETS			PACKING		
	CONNECTIONS-SHELL SIDE	IN 4"	OUT 4"	RATING 150# RFSO		
	BONNET/CHANNEL SIDE	IN 8" Axial	OUT 8" Axial	RATING 300# RF		
	CORROSION ALLOWANCE - SHELL SIDE	1/16" on C. Steel	TUBE SIDE None			
	CODE REQUIREMENTS	ASME Sec. VIII, Div. 1 (Latest Addenda)		TEMA CLASS "C"		
	OTHER					
	REMARKS					
	Customer's 8" 300# ANSI RF pipe flanges to bolt directly to tubesheets.					
	Cooling water must be the first stream turned on and the last stream turned off.					
	Fixed tubsheet heat exchanger. Do not thermally shock.					

• API Basco • 2777 Walden Avenue, Buffalo, NY 14225 • (716) 684-6700 Fax: (716) 684-2129

• www.apiheattransfer.com

Figure 3-24 Gas cooler specifications (1).

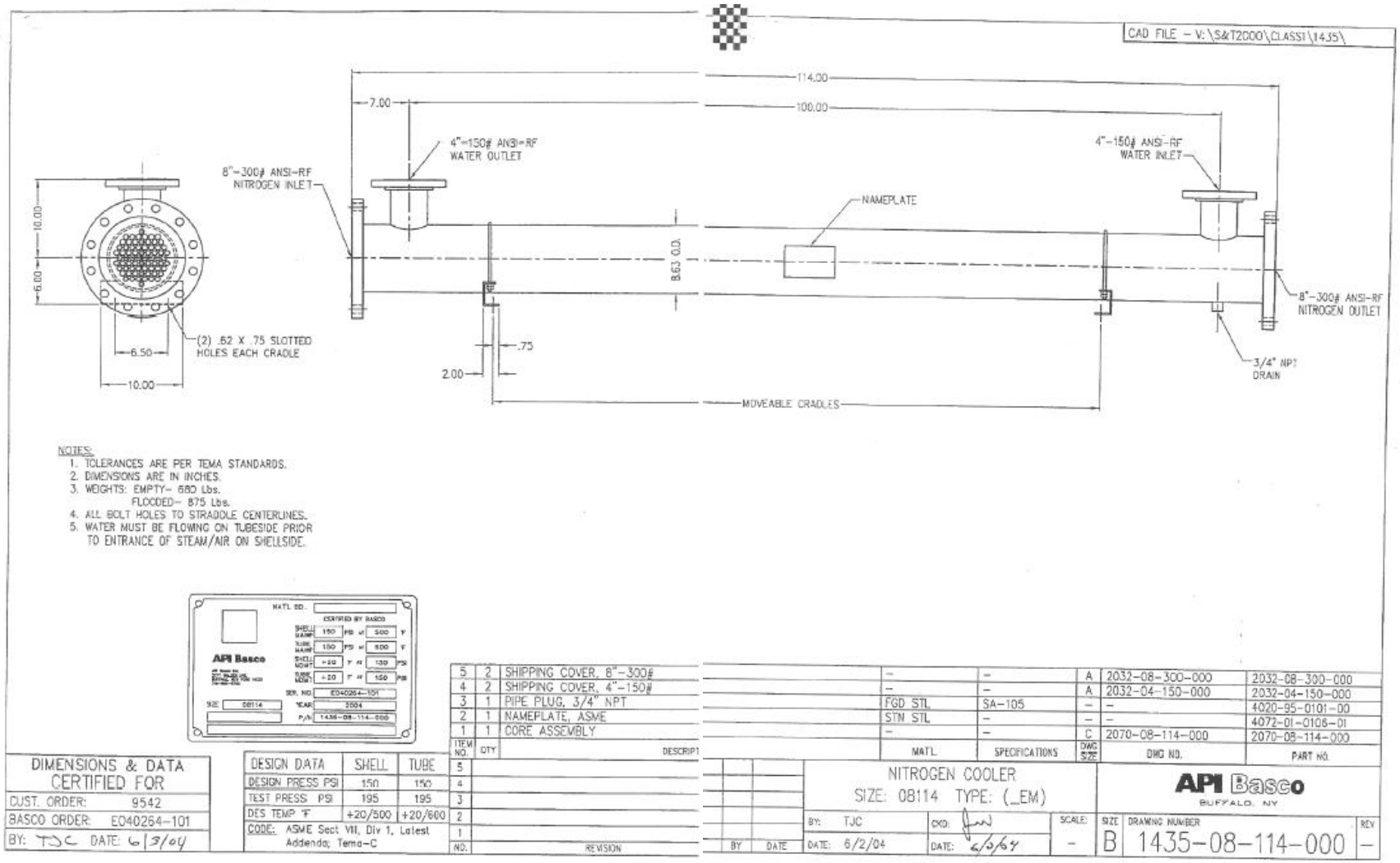

Figure 3-25 Gas cooler design specifications.

3.5 Ducting and Instrumentation Description

A schematic of the Sandia Brayton Loop is shown in Figure 3-26. This figure shows the location of the pressure and temperature sensors used in the loop. Since the time of writing of this report a few addition sensors have been added. The major sensors consist of temperature and pressure measurements at either the entrance or exit of every major component. The stations are labeled 1-6 by using the same nomenclature as described earlier. The manufacturer used a different numbering scheme when installing the instrumentation. This nomenclature starts with 100 (at the turbine inlet) and then progresses around the loop in increments of 100. The loop also contains a flow orifice at station 6B. The orifice is has a diameter of ½ the ducting inside diameter and the pressure taps are at ½ and 1 times the diameter of the ducting. The ½ diameter tap is located down stream of the orifice. For the gas temperature we use the temperature sensor located at station 6. The flow is calculated using the methods described in ASME MFC-3M-1989. In all cases type K thermocouples are used. For the gas temperature measurements the thermocouples are 1/8" diameter ungrounded sheathed thermocouples. Other pressure tapes not shown in the diagram are located on the inlet and outlet flange of the Watlow heater. Similarly a number of thermocouples were added to provide measurements of hot duct wall temperatures.

Pressure Taps, Temperature Taps, and other Hardware

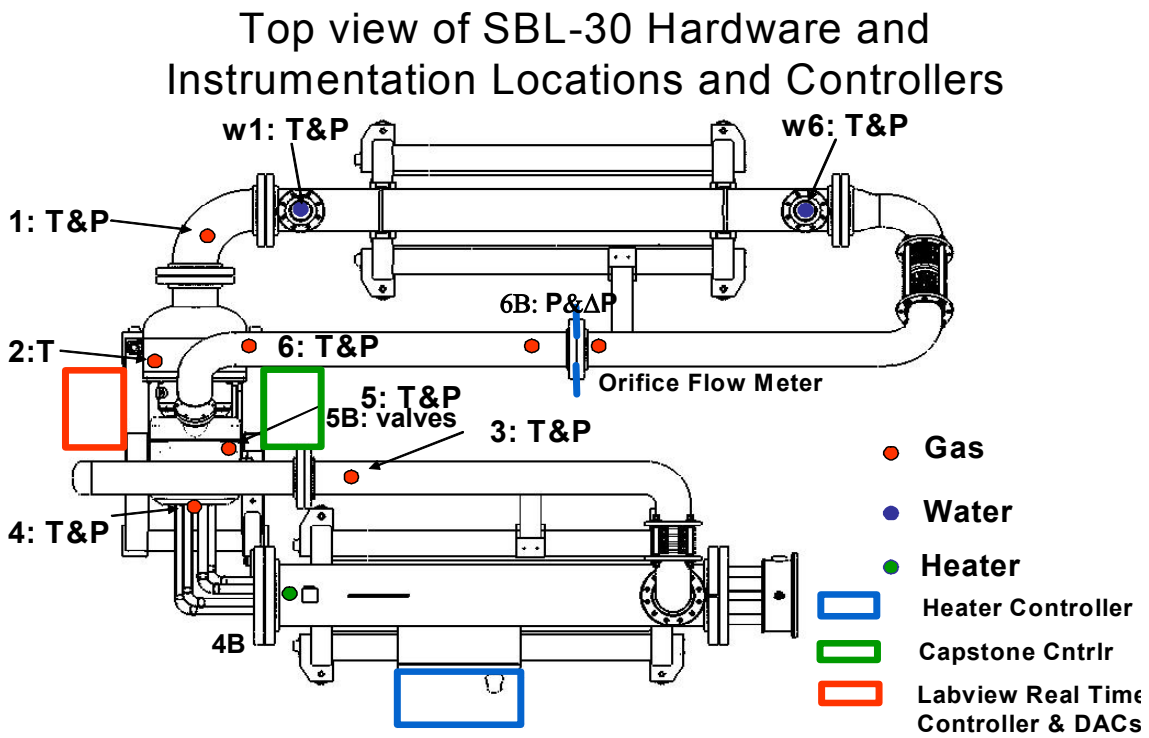

Figure 3-26: Top view schematic of Sandia Brayton Loop and location of major temperature and pressure sensors, and the controllers.

Table 3-9: Description of instrumentation, feedthroughs, and connectors at each station identified in Figure 3-26.

1. TC, Type K on SS Swagelok, T400
   PT on SS Swagelok hardware, Setra Systems, C280E, 1277375, 0-25 psia, P400

2. PT on SS Swagelok hardware, Setra Systems, C280E, 2369046, 0-100 psig, P500
   5B ¾" pipe, steel flange, ¾" cast iron nipple, 3/4"-1" elbow, brass adaptor, rubber vacuum hose with hose clamps, CC Valve (100 psi, electric), ¾" steel tube, manual valve (Whitey, SS-65TSW16P 2200 psi CF3M), ¾" steel tube; tee off ¾" pipe to PT 2373889, 0-25 psig, P200

3. TC, Type K on SS Swagelok, T601
   PT on SS Swagelok hardware, Setra Systems, C280E, 2369045, 0-100 psig, P601

4. TC, Type K on SS Swagelok, T100
   PT on SS Swagelok hardware, Setra Systems, C280E, 2373889, 0-25 psig, P200
   4B TC, Type K on SS Swagelok, TC, Type K on SS Swagelok

5. TC, Type K on SS Swagelok, T200 on housing dome
6. TC, Type K on SS Swagelok, T300
   PT on SS Swagelok hardware, Setra Systems, C280E, x297734, 0-25 psia,
   6B PT on SS Swagelok hardware, Setra Systems, C280E, 1277377, 0-25 psia
   ΔPT, Setra, 2301001PD2F11B, 0-1 psid
   W1 TC, Type K on SS Swagelok, T700
   W2 TC, Type K on SS Swagelok, T701; PT 2372251, 0-50 psig, P701

Two photos of the instrumentation and the feed through ports are shown in Figure 3-27 and in Figure 3-28. Figure 3-27 shows the turbine inlet temperature port and the pressure port. Both measurements are made on one of the six heater outlet tubes. Also, if one looks closely, the turbine exit temperature and pressure ports can also be seen. They are mounted directly to the bell housing near the center of the dome. Figure 3-28 shows the temperature and pressure feed through used for the compressor inlet. Also shown in this figure is the inlet gas feed through which the system is filled.

Table 3-10 Volumes on the components in the gas loop.

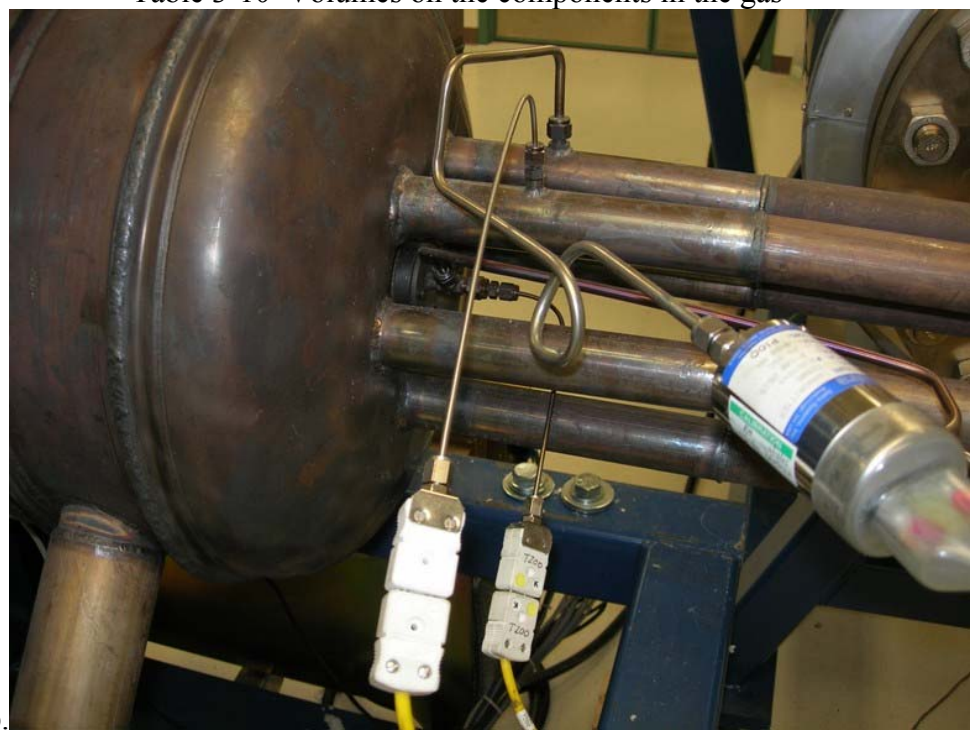

Figure 3-27: Turbine inlet temperature and pressure sensors and their feed through ports. Note that these instruments measure the gas temperature and pressure in one of the six heater exit tubes.

Figure 3-28 Compressor inlet temperature and pressure feed through port and sensors.

An important parameter that is used in the dynamic model is the volume and mass of each duct and component. The volume of the components in the high and low pressure legs are given in Table 3-10. Stainless steel was used for all hot ducts and carbon steel was used for the low temperature ducts which consist of the Gas cooler inlet ducting and the compressor inlet ducting. The summed volumes and the resulting stored energy are given in Table 3-11. The differential pressure (absolute minus ambient) is used in these calculations. The total stored energy in the gas loop at the values of the respective pressure relief valve settings is 0.163 MJ. The total volume of the gas loop is 0.57 m^3(20 cf). For comparison, the volume of the room that the unit is in is about 97 m^3 (3400 cf).a

Table 3-10 Volumes on the components in the gas loop.

Component: Pipes & Ducts	Inner Diam (in)	Inner Diam (m)	Length (m)	Vol (m3)
Low-Pressure Leg				
Turbine Housing	17.760	0.451	0.480	0.077
Recup-to-Gas-Cooler Small Pipe	4.760	0.121	0.130	0.001
Gas-Cooler Inlet First Elbow	6.352	0.161	0.380	0.008
Gas-Cooler Inlet Line	6.352	0.161	3.250	0.066
Gas-Cooler Inlet Second Elbow	6.352	0.161	0.380	0.008
Cooler Inlet Bellows	6.625	0.168	0.410	0.009
Gas-Cooler Inlet Elbow	6.352	0.161	0.740	0.015
Gas Cooler Tubes	0.527	0.013	189.0	0.027
Compressor Inlet Elbow	7.9810	0.203	0.5100	0.016
Compressor Inlet Pipe	7.9810	0.203	0.2000	0.006
Filter Housing	20.000	0.508	0.470	0.095
Generator Housing	13.500	0.343	0.200	0.018
High-Pressure Leg				
Recup-to-Heater Small Pipes	2.635	0.067	2.500	0.009
Recup-to-Heater Manifold	5.761	0.146	1.120	0.019
Heater Inlet Large Pipe	6.060	0.154	1.500	0.028
Heater Inlet First Elbow	6.060	0.154	0.380	0.007
Heater Inlet Bellows	6.625	0.168	0.230	0.005
Heater Inlet Second Elbow	6.060	0.154	0.300	0.006
Gas Heater Inlet Pipe	6.352	0.161	0.180	0.004
Gas Heater Shell	11.380	0.289	2.300	0.151
Gas Heater Element Tubes	0.430	0.011	-124.2	-0.012
Turbine Inlet Pipes	1.402	0.036	4.860	0.005
Turbine Inlet Elbows	1.402	0.036	0.120	0.000

Table 3-11 Total volume gas loop.

Low-Pressure Leg Total Vol (m3)	0.348
Low-Pressure Leg Pressure (MPa_g)	0.206
Low-Pressure Leg Energy (MJ)	0.036
High-Pressure Leg Total Vol (m3)	0.221
High-Pressure Leg Pressure (MPag)	0.413
High-Pressure Leg Energy (MJ)	0.046
Total loop volume (m3)	0.569

Table 3-12: Duct and component volumes, mass, length, and hydraulic diameter.

Duct or Component ID		Volume (liter)	Length (m)	Hydraulic Diameter (m)	Mass (kg)
V_{11}	Compressor Inlet Duct	127 liter	0.662 m	..4048 m	60.748
V_{22}	Compressor Outlet Duct	3 liter	0.10 m	0.4 m	0.252
V_{23}	High Pressure leg of Recuperator	20 liter	0.25 m	rcp	250
V_{33}	Heater Inlet Duct	77 liter	4,239 m	0.307 m	121.78
V_{34}	Reactor Coolant Volume or Length	139 liter	2.235 m	rx	---
V_{44}	Heater Outlet Duct Volume	5 liter	1.067	..0696 m	9.6769
V_{55}	Turbine Outlet Duct	3 liter	0.1 m	.4 m	0.25196
V_{56}	Low Pressure leg of Recuperator	20 liter	0.25 m	rcp	250
V_{66}	Gas Chiller Inlet Duct	108 liter	5.004 m	0.3226 m	70.425
V_{61}	Gas Chiller	27 liter	2.5 m	gcx	114

3.5.1 Pressure Safety Overview

The Sandia Brayton Loop is an OEM (Barber-Nichols Inc.) designed and fabricated closed loop in which nitrogen, air, an inert gas, or a mixture of those flows from an electrical heater, through a turbo-compressor, and then through a gas-cooler. The system is filled prior to operation from a gas cylinder. When the turbo-compressor is spun up, the gas circulates and is redistributed so that the pressure increases in half the loop and decreases in the other half. When the gas is heated (by the electrical heater) all system pressures increase. The pressure safety analysis therefore takes into consideration the pressures in the high pressure leg and low pressure leg separately. The specific pressure safety hazard considerations included evaluations for pressure sources where the Maximum Allowable Working Pressure MAWP is defined as the ultimate tensile strength of the component UTS/ MAWP = 3.5. For the low-pressure leg the MAWP is based on compressor housing bolts. For the high pressure leg the MAWP is based/limited by the heater stamp.

Under normal operation, the high pressure in the system will not exceed 40 psig because that is the maximum pressure that the original Capstone turbo-machinery can produce at its maximum speed. All components can easily take this pressure at nominal temperatures. Indeed, even the weakest link, the heater inlet bellows, can tolerate this pressure at 1300 F. For the bellows to reach 1300 F would require operation of the heater, lack of water flow in the gas cooler, and operation of the turbomachinery long enough (under these conditions) to heat the gas cooler to high temperatures. These are conditions that could be noted fairly easily or with sensors and interlocks if needed.

Failure of the high-pressure piping would cause a hot gas stream for a limited time as the system depressurized. The high-pressure leg piping is all encased in thick insulation. This will reduce the direct impingement hazard. But consideration of this hazard is included in the operating procedure for the SBL-30. A gas leakage ultimately results in the coolant being replaced with air rather than the fill gas. The loop has been operated with air, thus no damage is expected to occur due to leakages.

Water cooling is needed to remove the waste heat. The CBC controller monitors the water flow rate, temperature and pressure to assure that they are within specified operating ranges. If any these measurements fall outside their expected ranges, the the loop will be automatically shutdown.

3.5.1.1 Pressure Ratings of Vessels and Components

There are two separate pressure systems in the SBL-30:

(1) a gas loop, which includes the turbomachinery unit, and

(2) a water loop, which is the waste-heat rejection system. The analyses of these two systems will be addressed separately.

The SBL-30 is a loop with many separate sections and components. The major sections are labeled in Figure 3-29 below. The arrows show the path the flowing gas takes. Over pressure protection is provided by two pressure relief valves. One PRVs is located on the high pressure leg (set @ 30 psig) and the other is located on low-press line (set @ 10 psig). Another pressure relief valve is located on the house supplied chilled water loop (set by Facilities @ 40 psig). The gases that we can use in the system include air, nitrogen, and inert gases. Except for air, all of the gases are asphyxiants.

3.5.1.2 Ducts and Vessels

The failure pressure was calculated from $P = 2 \sigma t / D$, where σ is the ultimate tensile stress, t is the pipe thickness, and D is the pipe diameter. The pipe-like components along the flow path are listed in Table 3.1 starting at the compressor inlet pipe and following the gas flow around the loop. The table also shows the calculated failure pressure based on ultimate tensile strength. Table 3.2 shows the same thing for 0.2% yield. Carbon steel data are from *Structural Alloys Handbook, 1988 Ed,* Battelle's Columbus Division, Columbus, OH. Stainless steel data are

Table 3-13: SBL-30 components, material, dimensions, and calculated UTS pressure.

Component: Pipes & Ducts	Material	Inner Diam	Outer Diam	Thick-ness	UTS	UTS	UTS	UTS	UTS	Fail Press	Fail Press	Fail Press	Fail Press	Fail Press	MAWP with	ASME MAWP
		(in)	(in)	(in)	(ksi)	(ksi)	(ksi)	(ksi)	(ksi)	(psig)	(psig)	(psig)	(psig)	(psig)	s.f. =	Rating
Temperature (F)					70	800	###	###	1500	70	800	1000	1340	1500	3.5	or
Temperature (K)					294.4	700	811	###	1089	294	700	811	1000	1089	at 70 F	Stamp
Low-Pressure Leg																at 70 F
Turbine Housing			17.750													
Recup-to-Gas-Cooler Small Pipe	4-in?	4.760														
Gas-Cooler Inlet First Elbow	Carb Steel, Sch 40, 6-i	6.065	6.625	0.2800	60	50	30	12	8	5072	4226	2536	1014	676	**1449**	**700**
Gas-Cooler Inlet Line	Carb Steel, Sch 10, 6-i	6.357	6.625	0.1340	60	50	30	12	8	2427	2023	1214	485	324	**693**	**350**
Gas-Cooler Inlet Second Elbow	Carb Steel, Sch 40, 6-i	6.065	6.625	0.2800	60	50	30	12	8	5072	4226	2536	1014	676	**1449**	**700**
Cooler Inlet Bellows Stamp Extrap	SS 304L, SA/A182, 6-i	6.625	8.125		60	50	30	12	8	630	525	315	126	84	**180**	**150**
Gas-Cooler Inlet Elbow	Carb Steel, Sch 40, 6-i	6.065	6.625	0.2800	60	50	30	12	8	5072	4226	2536	1014	676	**1449**	**700**
Gas Cooler Tubes	SS 304 SA249 18 BW(	0.527	0.625	0.0490	60	50	30	12	8	9408	7840	4704	1882	1254	**2688**	**150**
Compressor Inlet Elbow	Carb Steel, Sch 40, 8-i	7.9810	8.6250	0.3220	60	50	30	12	8	4480	3733	2240	896	597	**1280**	**1073**
Compressor Inlet Pipe	Carb Steel, Sch 40, 8-i	7.9810	8.6250	0.3220	60	50	30	12	8	4480	3733	2240	896	597	**1280**	**1073**
Filter Housing	Carb Steel, 14 gauge	19.850	20.000	0.0750	60	50	30	12	8	450	375	225	90	60	**129**	
Generator Housing	Carb Steel, Sch 10, 14	13.500	14.000	0.2500	60	50	30	12	8	2143	1786	1071	429	286	**612**	
High-Pressure Leg															**0**	
Recup-to-Heater Small Pipes	SS 304 Sch 10s, 2.5-i	2.635	2.875	0.1200	75	66	57	36	23	6261	5510	4758	3005	1920	**1789**	**1090**
Recup-to-Heater Manifold	SS 304H Sch 10s, 6-in	6.357	6.625	0.1340	75	66	57	36	23	3034	2670	2306	1456	930	**867**	**620**
Heater Inlet Large Pipe	SS 304H Sch 10s, 6-in	6.357	6.625	0.1340	75	66	57	36	23	3034	2670	2306	1456	930	**867**	**620**
Heater Inlet First Elbow	SS 304H Sch 10s, 6-in	6.357	6.625	0.1340	75	66	57	36	23	3034	2670	2306	1456	930	**867**	**620**
Heater Inlet Bellows Stamp Extrap	SS 304L, SA/A182, 6-i	6.625	8.125							597	525	453	286	183	**170**	
Heater Inlet Second Elbow	SS 304H Sch 10s, 6-in	6.357	6.625	0.1340	75	66	57	36	23	3034	2670	2306	1456	930	**867**	**620**
Gas Heater Inlet Pipe	SS 304 Sch 10s, 6-in	6.357	6.625	0.1340	75	66	57	36	23	3034	2670	2306	1456	930	**867**	**620**
Gas Heater Shell	SS 304H Sch 80s, 12-i	11.750	12.750	0.5000	75	66	57	36	23	5882	5176	4471	2824	1804	**1681**	
Gas Heater Stamp Extrapolation			0.430							380	334	289	182	117	**109**	
Turbine Inlet Pipes	SS 316	1.402	1.500	0.0490	82.4	71	68	37	24	5383	4639	4443	2417	1568	**1538**	
Turbine Inlet Elbows	SS 316	1.402	1.500	0.0490	82.4	71	68	37	24	5383	4639	4443	2417	1568	**1538**	

Table 3-14: SBL-30 components, material, dimensions, and calculated yield pressure.

Component: Pipes & Ducts	Material	Inner Diam	Outer Diam	Thick-ness	0.2% Y	0.2% Y	0.2 % Y	0.2 % Y	0.2% Y	Yield Press	Yield Press	Yield Press	Yield Press	Yield Press
		(in)	(in)	(in)	(ksi)	(ksi)	(ksi)	(ksi)	(ksi)	(psig)	(psig)	(psig)	(psig)	(psig)
Temperature (F)					70	800	###	###	1500	70	800	1000	1340	1500
Temperature (K)					294.4	700	811	###	1089	294	700	811	1000	1089
Low-Pressure Leg														
Turbine Housing			17.750											
Recup-to-Gas-Cooler Small Pipe		4.760	?											
Gas-Cooler Inlet First Elbow	Sch 10, 6-in	6.352	6.625	0.1365	35	19	17	14	13	1442	783	701	577	536
Gas-Cooler Inlet Line	Sch 10, 6-in	6.352	6.625	0.1365	35	19	17	14	13	1442	783	701	577	536
Gas-Cooler Inlet Second Elbow	Sch 10, 6-in	6.352	6.625	0.1365	35	19	17	14	13	1442	783	701	577	536
Cooler Inlet Bellows Stamp Extrap	SS 304L, SA/A182, 6-i	6.625	8.125							278	151	135	111	103
Gas-Cooler Inlet Elbow	Sch 10, 6-in	6.352	6.625	0.1365	35	19	17	14	13	1442	783	701	577	536
Gas Cooler Tubes	SS 304 SA249 18 BW(	0.527	0.625	0.0490	35	19	17	14	13	5488	2979	2666	2195	2038
Compressor Inlet Elbow	Carb Steel, Sch 40, 8-i	7.9810	8.6250	0.3220	35	19	17	14	13	2613	1419	1269	1045	971
Compressor Inlet Pipe	Carb Steel, Sch 40, 8-i	7.9810	8.6250	0.3220	35	19	17	14	13	2613	1419	1269	1045	971
Filter Housing	Carbon Steel, 14 gauge	19.850	20.000	0.0750	35	19	17	14	13	262	142	127	105	97
Generator Housing	Carb Steel, Sch 10, 14	13.500	14.000	0.2500	35	19	17	14	13	1250	679	607	500	464
High-Pressure Leg														
Recup-to-Heater Small Pipes	SS 304 Sch 10, 2.5-in	2.635	2.875	0.1200	35	19	17	14	13	2922	1586	1419	1169	1085
Recup-to-Heater Manifold	SS 304 Sch 80, 6-in	5.761	6.625	0.4320	35	19	17	14	13	4565	2478	2217	1826	1695
Heater Inlet Large Pipe	SS 304H Sch 10, 6-in	6.060	6.625	0.2825	35	19	17	14	13	2985	1620	1450	1194	1109
Heater Inlet First Elbow	SS 304H Sch 10, 6-in	6.060	6.625	0.2825	35	19	17	14	13	2985	1620	1450	1194	1109
Heater Inlet Bellows Stamp Extrap	SS 304L, SA/A182, 6-i	6.625	8.125							278	151	135	111	103
Heater Inlet Second Elbow	SS 304H Sch 10, 6-in	6.060	6.625	0.2825	35	19	17	14	13	2985	1620	1450	1194	1109
Gas Heater Inlet Pipe	SS 304 Sch 10, 6-in	6.352	6.625	0.1365	35	19	17	14	13	1442	783	701	577	536
Gas Heater Shell	SS 304H Sch 80, 12-in	11.750	12.750	0.5000	35	19	17	14	13	2745	1490	1333	1098	1020
Gas Heater Stamp Extrapolation				0.430						177	96	86	71	66
Turbine Inlet Pipes	SS 316	1.402	1.500	0.0490	42	26	23	22	21	2744	1699	1503	1437	1372
Turbine Inlet Elbows	SS 316	1.402	1.500	0.0490	42	26	23	22	21	2744	1699	1503	1437	1372

from Sandmeyer Steel Co., Philadelphia, PA. The table shows ASME A53-B and B-31.1 pressure ratings, which are not too far off from the calculated values. More data is provided in the CBC pressure safety data package (Lipinski, Wright, 2005). Most of the components can withstand over 1000 psi, even at high temperature. But the filter housing and the bellows are the weak elements by a large margin. The UTS failure pressure for the filter housing is 558 psig at 70 F and 268 psig at 1340 F. The filter housing is not likely to reach 1500 F (1089 K), or even 1000 F, because the gas passes over the gas cooler just before it enters the alternator chamber. The heater-inlet bellows are hotter under normal conditions (750 F), so this is the limiting component for the high-pressure leg. A summary of the limiting pressures is provided in

Table 3-15: Summary of low pressure leg and high pressure leg limiting MAWP at various operating conditions.

	Low-Pressure Leg				**High-Pressure Leg**			
Condition	Temp (F)	Pressure (psig)	MAWP (psig)	Total safety factor	Temp (F)	Pressure (psig)	MAWP (psig)	Total safety factor
Stagnant, cold	70	0	68	>100	70	0	109	>100
Stagnant, hot	560	10	60	21.0	560	10	100	35.0
Spun-up, cold	70	-6	68	39.7	70	21	109	18.2
Spun-up, hot	530	0	60	>100	1300	28	52	6.5

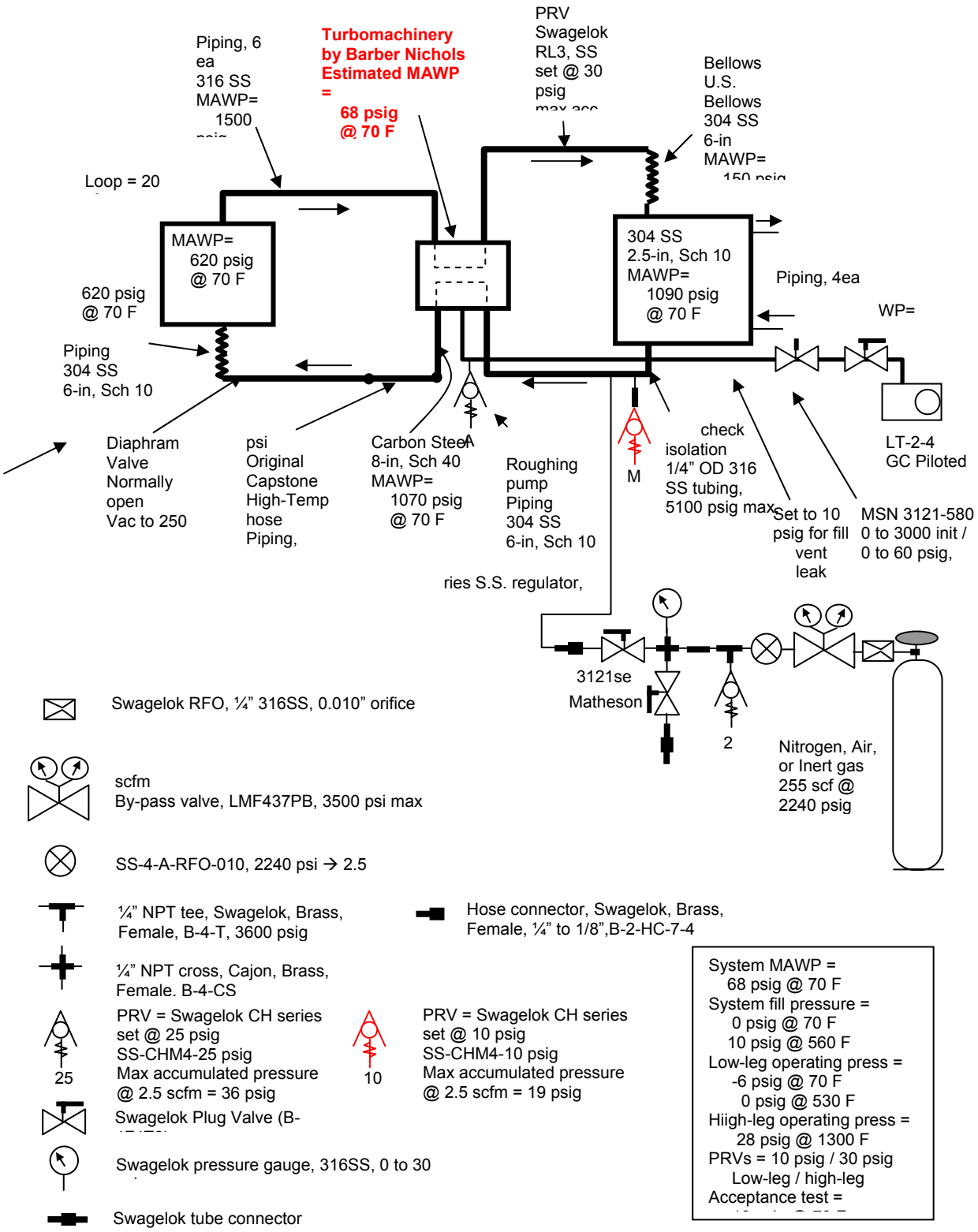

Figure 3-29: Schematic of the gas loop and water loop for the Sandia Brayton Loop. Various pressure safety devices and components are listed here.

3.6 CBC RT Controller Operation Summary

The Sandia Brayton Loop Controller hardware and software uses a real time National Instruments LabView™ computer and field point data acquisition system to communicate with the Capstone controller and with the Watlow Heater controller. The LabView™ hardware and software were assembled and developed in a contract to PrimeCore Corporation (contract number 334766). The Real Time CBC LabView™ controller performs two functions. First it communicates with the Capstone controller via an RS-232 port to send commands to initialize the communication protocols, to idle, startup, change speed, to shutdown and to receive operational information such as shaft speed, as wells as rectifier and inverter voltage and current information. In addition, the CBC Real Time controller records a variety of signals that measure temperatures, pressure and flow rate. A separate LabView™ monitor program CBC_Control Panel communicates with the real time LabView™ controller via an Ethernet connection to display the acquired data and to send operational commands to the Real Time controller. The real time software is imbedded within the CBC_Control Panel software so that it can be down loaded to the real time controller computer. This architectural style of data acquisition by a real time controller with display, monitoring, and control requests issued by a separate program and is used by Sandia National Laboratories to control the Annular Core Research Reactor (ACRR), and it could form the basis for terrestrial and space based autonomous reactor power systems (Wright, 2003). A brief summary of these controllers and how they operate is provided. In addition some of the early data that was recorded is also presented.

1. CBC_RT: This is the RT program that resides in the NI field point computer. The commands that it uses were taken from the proprietary Capstone "Depot" software controller. Now these commands are issued by e CBC_RT controller box. The Sandian CBC_RT controller cabinet is mounted to the Capstone C-30 turbo-alternator-compressor frame and communicates with the Capstone controller through an RS-232 connection. The Capstone controller contains the C-30 hardware which has its own proprietary computer and internal data acquisition. It also contains the active rectifier, the inverter and the starter circuitry, brake circuitry, and other options. It records rpm and a large number of other parameters. Originally, Sandia and Barber-Nichols Inc. used the "Depot" software running on a laptop computer to talk to the C-30 controller. Now we use the CBC_ControlPanel R1_10.llb and executable file to run the Sandia Brayton Loop. The real time National Instruments Visual Interface software has eliminated the need to use the "Depot" software. The communications protocols are now in the CBC_RT controller software. The CBC_RT software also communicates with another display National Instruments Visual Interface program called CBC_ControlPanel_R_10.llb, through a cross-over either net cable. The CBC_ControlPanel_R_10.exe software contains the RT program within its library files and can be down loaded to the RT hardware computer. The ControlPanel program displays the data, and issues commands to the RT Controller which in turn communicates with the Capstone controller and issues the real commands.
2. To operate the CBC_ControlPanel first, connect to the RT computer through the cross over Ethernet cable to the monitor or display panel computer.
3. When connecting through an intranet, just connect the intranet cable to the RT controller T100 connector. Ultimately it will is possible to control the Sandia Brayton

Loop through the internet, however, some work is still required to make this all function correctly.

4. To run the Control Panel program double click the CBC_ControlPanel R_10.exe shortcut. When the program opens up, it will automatically transmit all the passwords, protocol signals for the CBC_RT controller to start talking to the Capstone controller.
5. When the Control Panel opens up, the main screen shows 4 tabs.
    a. Tab 1 is main CBC control panel display.
    b. Tab 2 is CBC Data "Channels",
    c. Tab 3 is CBC "Configuration" ,
    d. Tab 4 is Diagnostics.
6. When running the CBC_ControlPanel R_10.llb program through the LabView software to control the program right click anywhere on the screen and select request control of VI.
7. The Control Panel and RT Controller has several different operating states:
    a. Idle:
        i. Turbine off, heater is powered but PID controller is commanding no heating. (so be careful there still is power to the heater elements)
        ii. Data is being logged and displayed and transmitted via the Ethernet crossover cable.
    b. Startup:
        i. Flow control interlock on the water, there must be at least 5 gpm of flow for the test loop to run.
        ii. Command turbine to spin to 25000 rpm. (this happens fast, within one second)
        iii. When the RT Controller detects spinning at 25000 rpm, then the heater PID loop will be enable to increase power.
            1. If you set the T-100 target temperature, then the PID loop takes over and heats to that temperature. The heater loop looks at the heater dT and if it is over 400 F then heater power is killed.
            2. Or you can turn on manual control, and specify the percent heater power to operate at.
        iv. During speed up, the Real Time controller increments the rpm in steps of 1000 rpm up to the set point rpm (nominally 40,000 rpm) . The alternator is monitored to assure that it doesn't 3 kWe of motor power. (This all limited in time or rate heating rate since the heater is on.)
        v. After 40,000 (target rpm) then we switch to SS running mode again.
    c. Running steady state:
        i. Here you can change the TIT set point T and the rpm set point.
        ii. The controller still limits the rate of rpm increase to steps of 1000 rpm and continues to monitor the alternator power to limit motor power to less than 3 kW.
    d. Running test sweep:
        i. The user can input a table of rpm and Temperatures versus time.
        ii. When the user starts the sweep, then the sweep timer starts and the heater power and rpm are controlled to follow the target sweep.

iii. (Note, PID heater controller is tuned to work best at higher temperatures and powers, it has over shoots and oscillations at low T and power.)
iv. At the end of the sweep, control mode reverts back to SS mode, and holds the last value set.

e. Normal shutdown:
i. When you press shutdown turbine button, the heater power is turned to zero, through the 4-20 mA circuit. Then the controller monitors the (generator power out), normally you'll be producing power, eventually the power turns negative and the alternator is now being motored. The rpm is reduced in 5000 rpm increments to keep the motor power to less than 3 kWe. Typically, the rpm reduces to 40-45000 rpm and with the motor power below 3 kWe. Then the T-100 temperature is monitored, when it gets below the T-100 Shut-off temperature set point (Typically 400 F), then the turbine is shutdown completely. This is done by commanding the cycle to go to 25,000 rpm, waiting a few seconds and then CBC RT Controller sends the final shut down sequence commands to the capstone controller. At zero rpm the capstone controller is rebooted.

f. Exit application:
i. Terminates the CBC_RTVI program.

8. Emergency shut down:
a. ***Don't press this button*** unless it is a real emergency. IT HAS ONLY BEEN TESTED AT LOW TEMPERATURES. It turns off the heater, and then immediately goes through the turbine shutdown sequence very quickly. So it reduces the rpm to 25000 rpm and waits a few seconds, and then sends through the final turbine shutdown command to the capstone controller.
b. One risk here is thermal soak back, i.e. that you could get a gas bearing too hot once the flow is shut off, then the thermal soak back from hotter components could over heat and damage the coatings on the bearings.
9. Tab-1 CBC Control Screen (See Figure 3-30).
a. T-100 shutoff temp is the TIT temp at which the CBC unit spools down in a controlled fashion. All the above applies to this tab.
10. Tab2 is the CBC Data Channels (See Figure 3-33):
a. This tab displays a list of temperatures, pressures, and Turbine/Compressor/Alternator data from the Capstone unit. The turbine Aux Channels allow the user to select reports from the capstone output data. This is from the capstone list, but only contains stuff that gives data. We are not sure that all of them give meaningful data.
11. TAB3 CBC-Configuration (not shown) :
a. This has the calibration tables. These are set up in the display program. The Channel names are fixed, the Label can be anything. Flow is hard coded for now. Slope and offset for other things.
12. TAB4-Diagnostics: (not shown)
a. System errors, PID settings are here, you can change these here. If the system shuts down on a interlock, then the interlock check box is marked.
13. Charts TAB: (See Figure 3-31 and Figure 3-32).

a. These displays show time history plots of the temperature, pressure and user selected data.

14. Cycle times are sample every 0.25 seconds, and transmitted every 1 second. The capstone loop is separate from the data logging. In the SS and Sweep its cycle time is 1 second.

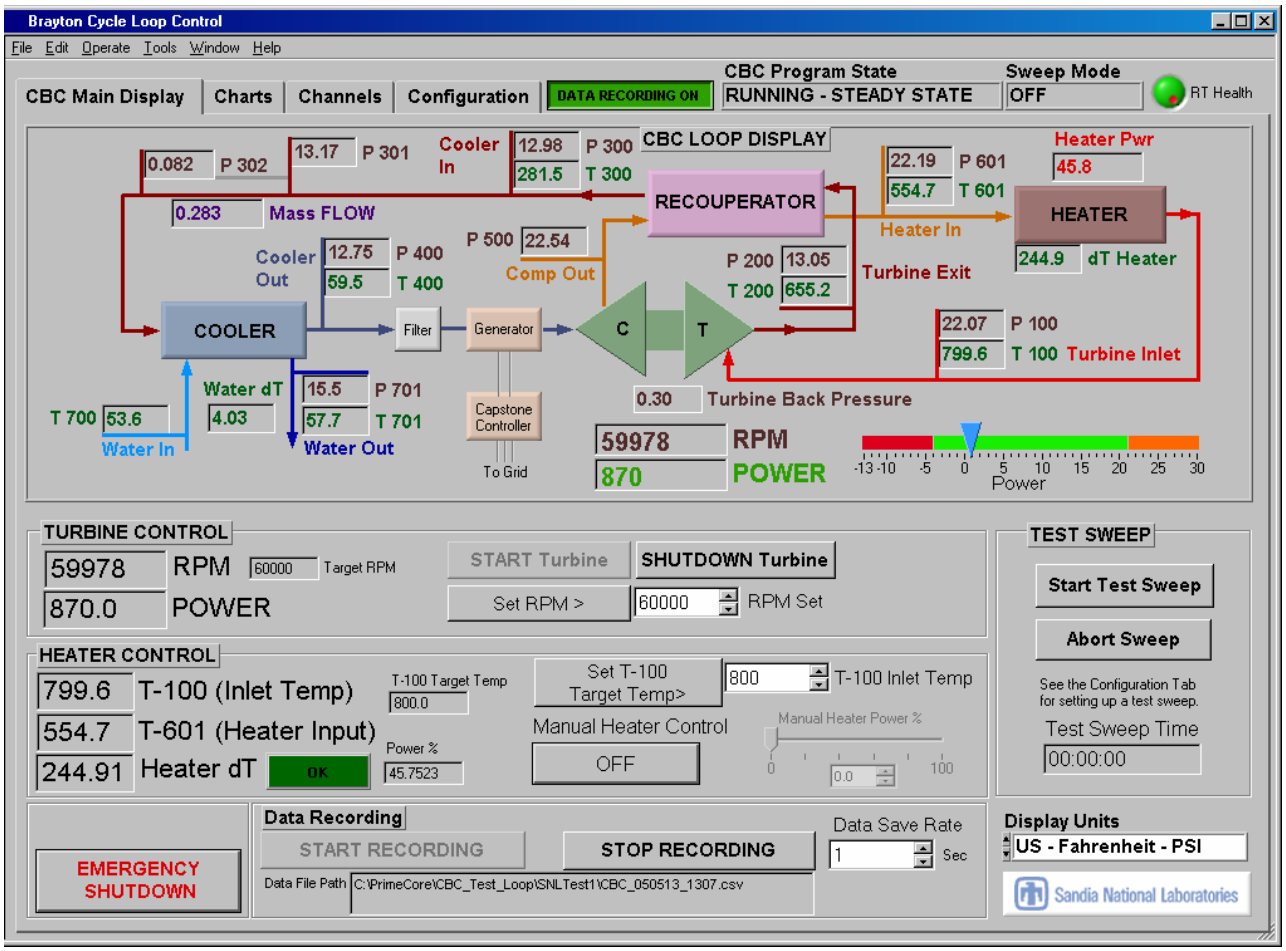

Figure 3-30: This tab shows the main control screen. The top half shows a schematic of the loop with temperature, pressures, flow rates, alternator power, and shaft speed (rpm) displayed. The bottom have shows various control commands that the user can issue.

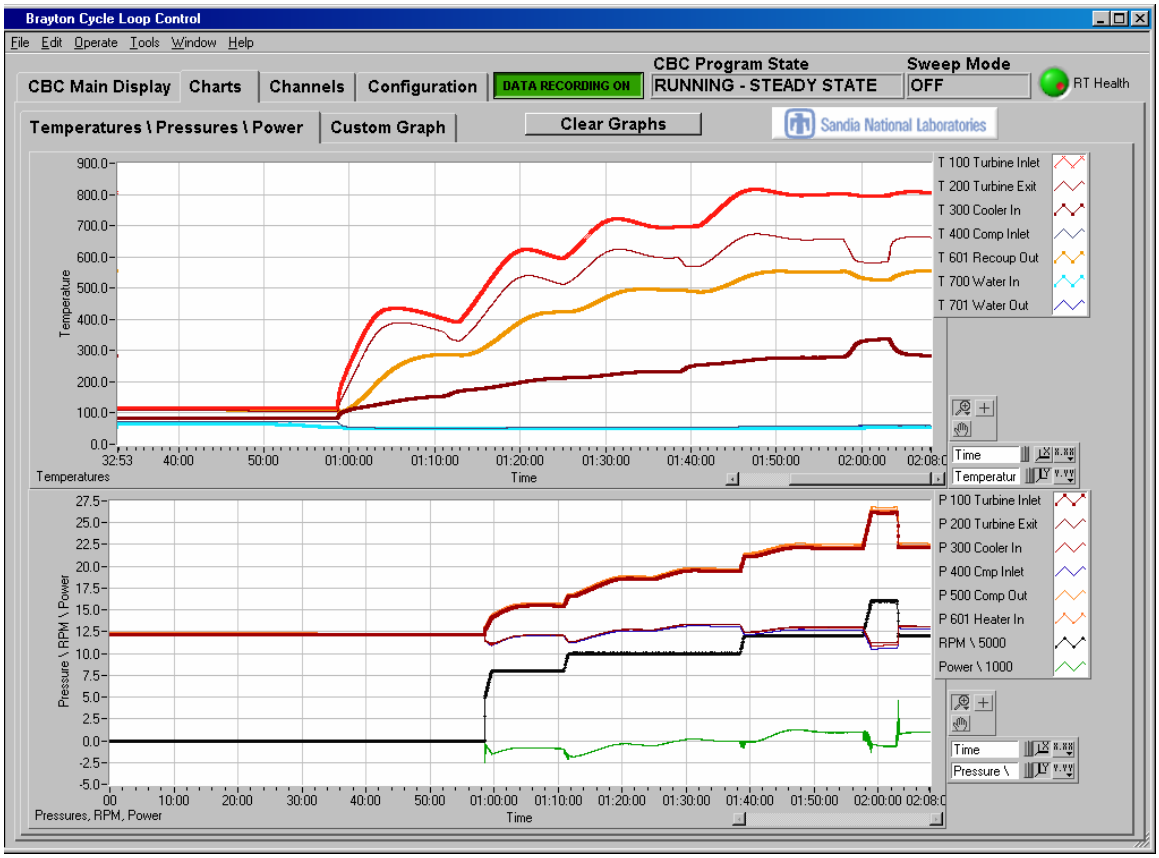

Figure 3-31: Charts tab, shows predefined plots of the gas temperature (top view), while the bottom view shows pressure, rpm and power.

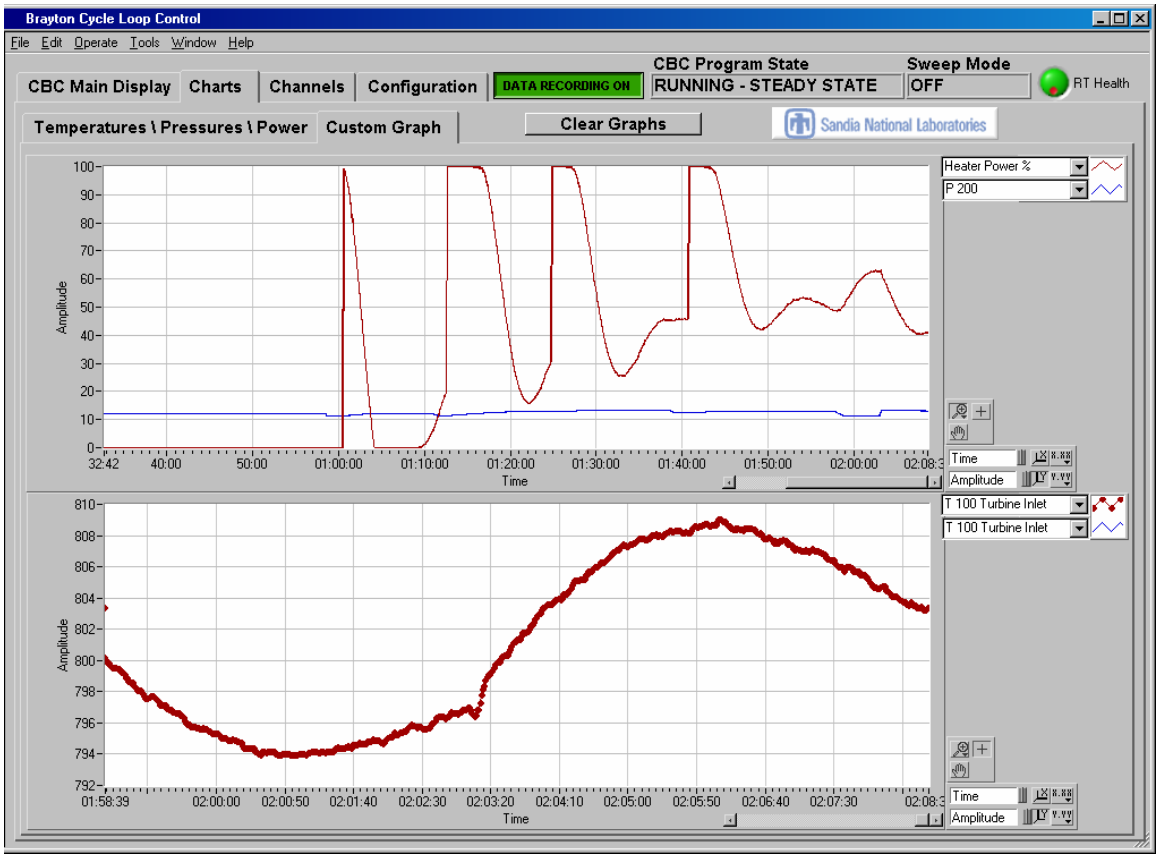

Figure 3-32: Auxiliary charts can display any of the channels available to the system. Here the top chart shows the heater power and turbine exit pressure. The bottom chart shows the turbine inlet temperature.

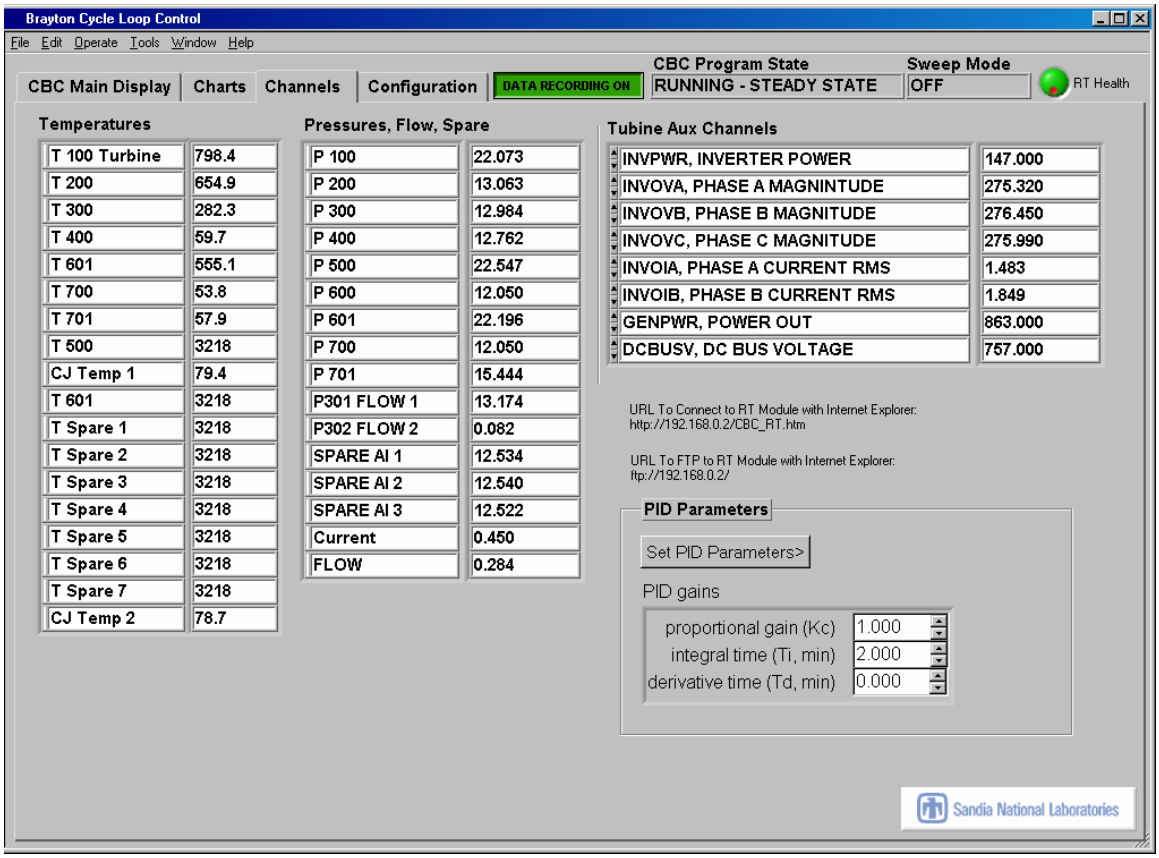

Figure 3-33: This display show the "Channels Tab. It lists all of the data channels being recorded in real time.

3.7 Alternative Working Fluid Gases and Electrical Breakdown in the Gas Cooling the Generator

The working fluid (gas) of the CBC is also used to cool electrical generator. Because there are exposed copper leads (i.e. that are not insulated) there is a potential to spark if the leads are too close for the voltage involved. Because we are considering using other gases for the working fluid care must be exercised prior to operating the system. This section of the report describes the "Paschen" effect and how it impacts our actions.

Friedrich Paschen first quantified this electrical breakdown phenomenon in 1889 (Paschen, 1889). The data can be plotted with breakdown voltage on the vertical axis and gas pressure times electrode separation on the horizontal axis. This curve has become known as the Paschen curve. (To be independent of temperature, the horizontal axis should be plotted as density times separation rather than pressure times separation).

The definitive book on electrical breakdown of gases is by Meek and Craggs (Meek and Craggs, 1978). The chapter in that book by D. T. A. Blair ("Breakdown Voltage Characteristics", 122 pages) provides an excellent summary of Paschen curves from the past century of research.

Figure 3-34 shows a typical set of Paschen curves using selected data for various gases from that reference, with helium data from Postel (Postel, 2000). The data are for 20 ^{o}C between

two flat parallel electrodes made of copper or brass (except for CO2 with platinum electrodes). The horizontal axis is the product of pressure times distance in units of "Torr-cm", which is awkward but conventional. So, for example, with a pressure of 1 atm (i.e. 760 Torr) and a distance of 1 mm between electrodes (i.e., 0.1 cm), the pressure-distance value would be 76 Torr-cm, and the breakdown voltage for air would be about 5000 Volts.

Generators are generally designed with 1-atm, room-temperature air in mind. So one must be cautious in using them for a lower pressure, higher temperature, or a different gas unless there is a re-design, or all the spacings are adequate, or all the electrical components have insulation on them. For example, with pure helium gas at 1-atm and 400 K, the pressure-distance product would be 56 Torr-cm and the breakdown voltage would be 400 V. This might be a difficulty for a 480-VAC generator, depending on the design.

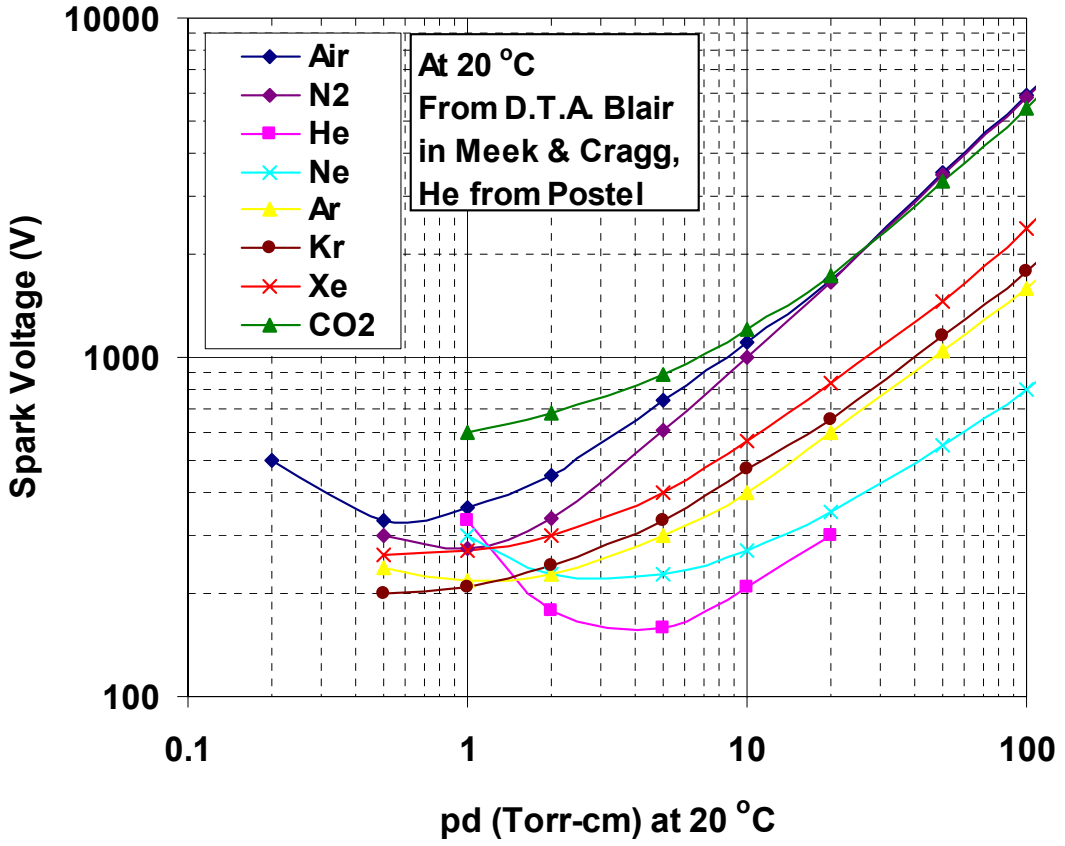

Figure 3-34: Paschen curves for various gases at 20 °C (from Blair).

Figure 3-35 shows curves for various mixtures of He and Xe (O. B. Postel and M. A. Cappelli, 2000). Notice that the breakdown values are not quite the same as in Figure 3-34 for pure xenon. This points out the variability in the breakdown data. Note also that there is a fairly smooth transition from pure helium to pure xenon to the right of the minimum, but the behavior at the minimum is a bit more complicated.

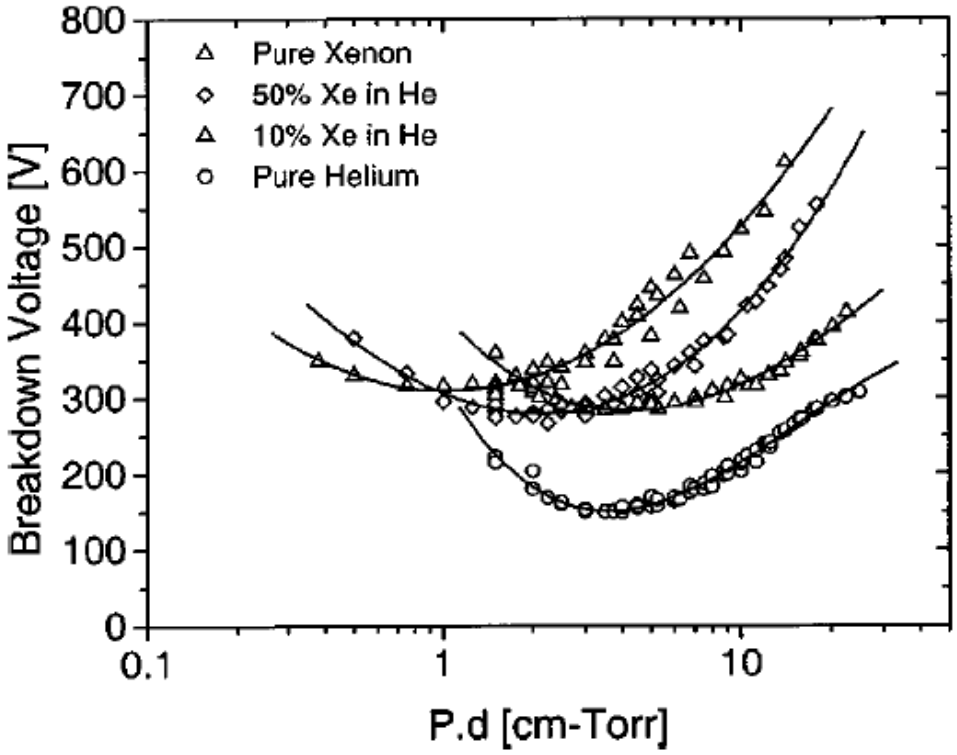

Figure 3-35. Paschen curves for various mixtures of He and Xe.

Figure 3-36 shows how the breakdown voltage is a function of electrode material (Jones, 1939). In addition, it is a function of geometry. Also, there is a glow discharge which initiates at voltages below the spark voltage. So it is important to have some margin in the design. There also can be a synergistic effect in which a mixture of two gases can have a breakdown voltage that is less than either of the constituents if there is a metastable state in one of the components which can ionize the other when it collides with it. Ne and Ar are an example of such a mixture.

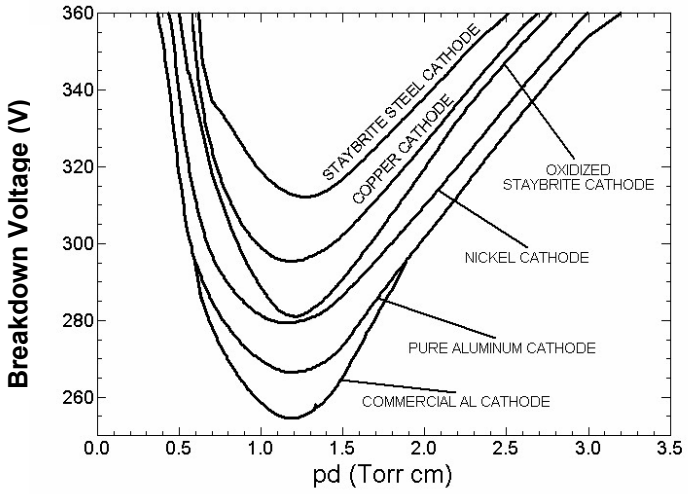

Figure 3-36. Paschen curves for different electrode materials.

The Paschen model for the spark voltage is summed as follows:

$$V_B = \frac{Bpd}{\ln\{\frac{Apd}{\ln(1+\frac{1}{\gamma_i})}\}} \quad \textbf{3-1}$$

where A, B, and γ_i are characteristics of the particular gas. Note that although there are three empirically determined constants in the formula, the formula only has two independent constants in it since it can be rearranged algebraically to be:

$$V_B = \frac{Bpd}{\ln(Cpd)} \quad \textbf{3-2}$$

where

$$C = \frac{A}{\ln(1+\frac{1}{\gamma_i})} \quad \textbf{3-3}$$

Note also that if V_{min} is the voltage at the curve minimum and $(pd)_{min}$ is the pressure times distance value at the curve minimum, then the empirical constants B and C can be obtained from those values:

$$B = \frac{V_{\min}}{(pd)_{\min}} \quad \textbf{3-4}$$

$$C = \frac{e}{(pd)_{\min}} = \frac{2.7183...}{(pd)_{\min}} \quad \textbf{3-5}$$

So once you know the minimum point of the curve, you know the entire curve, and the Paschen formula can be re-written as:

$$V_B = \frac{Bpd}{\ln(Cpd)} = \frac{V_{\min} pd}{(pd)_{\min} \ln\left(\frac{epd}{(pd)_{\min}}\right)} = \frac{\frac{V_{\min} pd}{(pd)_{\min}}}{1+\ln\left(\frac{pd}{(pd)_{\min}}\right)} \quad \textbf{3-6}$$

Figure 3-37 shows curves of this model compared to the data shown previously. The model does well in matching the minimum point (because it was fit explicitly to that point) but it tends to overestimate the breakdown voltage at higher pressure.

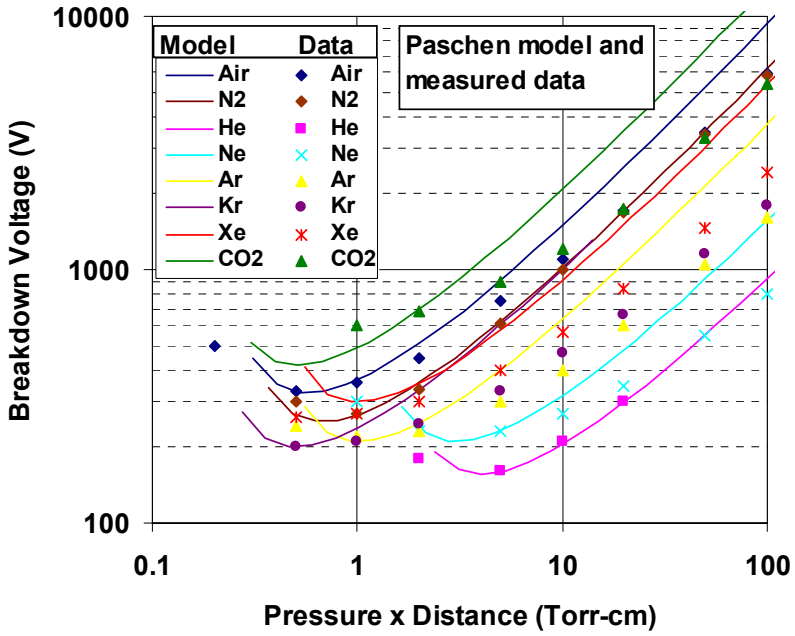

Figure 3-37: Paschen model and data for various materials.

The model can be empirically adjusted so that the breakdown voltage does not scale as rapidly with pressure:

$$V_B = \frac{V_o x^F}{1 + \ln(x)} \qquad \textbf{3-7}$$

where x is a dimensionless variable defined as

$$x = \frac{pd}{pdo} \text{ and} \qquad \textbf{3-8}$$

$$F = 0.85 \qquad \textbf{3-9}$$

Here pdo is an empirical value that is approximately equal to the minimum pressure-distance product and V_o is a also an empirical value that is approximately equal to the minimum breakdown voltage. (The form of the revised formula makes these two values no longer precisely equal to the actual minimum of the curve.)

Table 3-16 shows the constants used in the modified Paschen model described above to better fit the data. Figure 3-38 shows the modified model with the measured data. The agreement is much better. The model with these constants may be used to conveniently determine the expected breakdown voltage.

Table 3-16: Empirically determined constants for the modified Paschen model.

	Air	N2	He	Ne	Ar	Kr	Xe	CO2
pdo	0.5	0.5	2.5	3.2	1.1	0.8	0.8	1.1
Vo	330	300	160	210	210	200	250	600

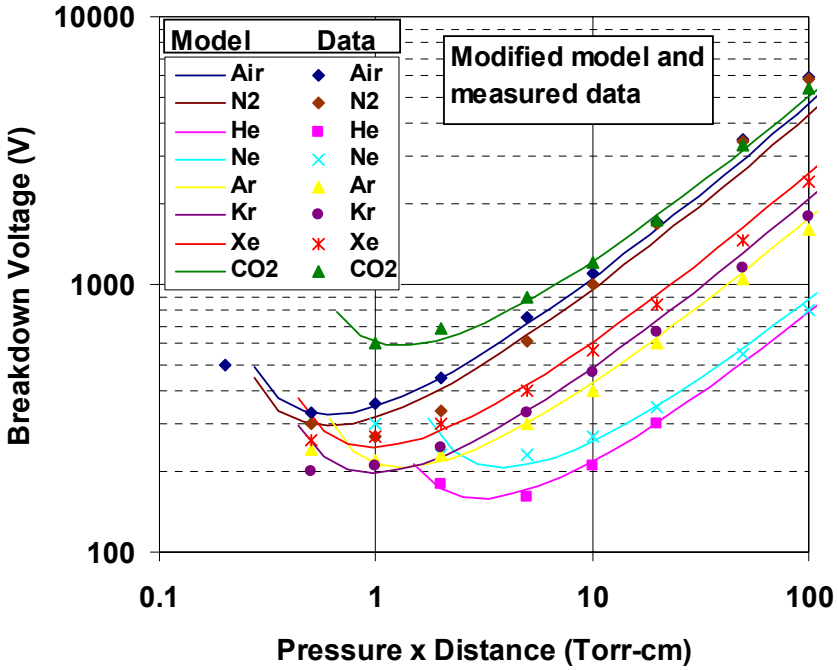

Figure 3-38: Modified Paschen model and data for various materials.

The modified Paschen model was then used to fit the HeXe mixture data from Postel that was shown in Figure 3-35. Those curves do not rise as steeply with the pressure-distance product as the air and nitrogen data do, and it was determined that the modified model fit was better with F=0.75. With this coefficient, a reasonable fit was obtained with the constants shown in Table 3-17. The resulting curves are shown in Figure 3-39. The trend in the coefficients can be fit with lines to obtain an approximate general formula for arbitrary helium fraction. Those trend lines are shown in Figure 3-40 along with their respective equations.

Table 3-17: Modified Paschen model constants for HeXe mixtures using F=0.75

	He	90% He 10% Xe	50% He 50% Xe	Xe	Xe Blair
pdo	2.3	2.6	1.3	1	0.6
Vo	170	270	270	300	260

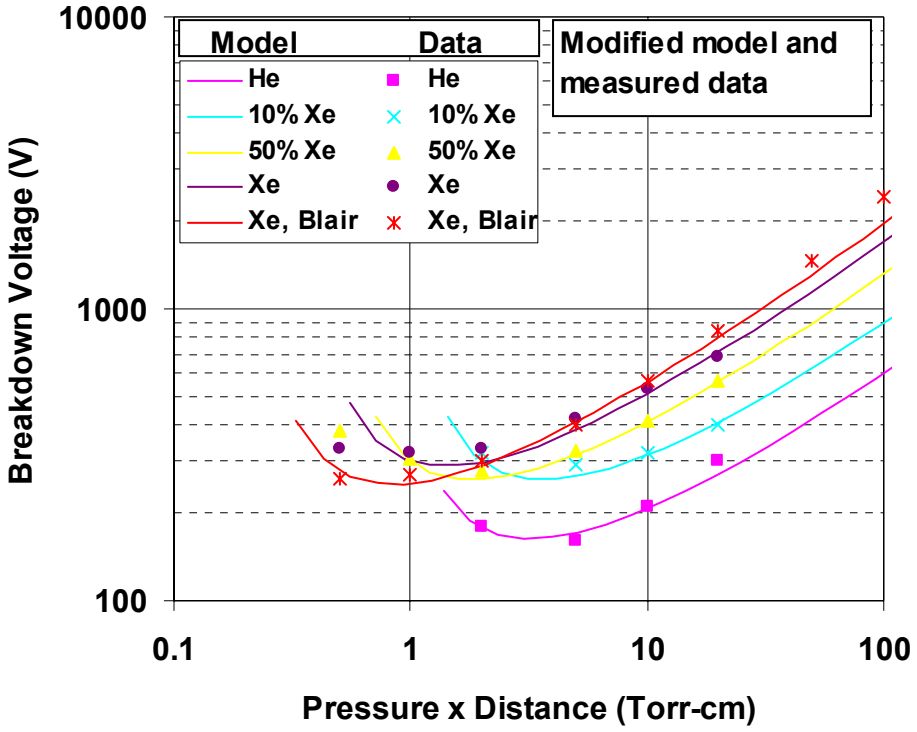

Figure 3-39: Modified Paschen model and data for HeXe mixtures.

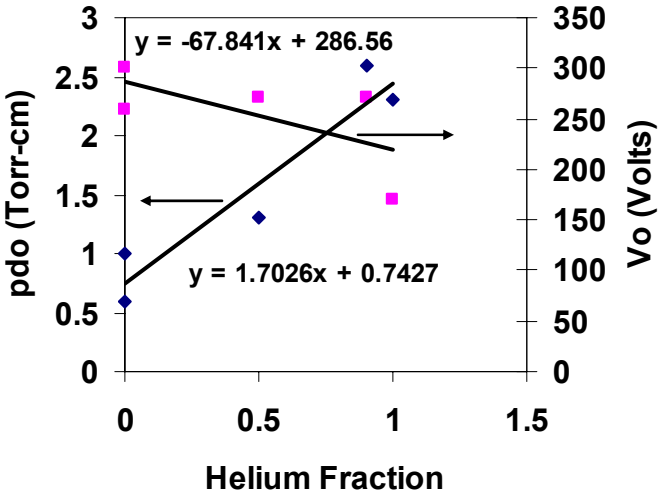

Figure 3-40: Modified Paschen model coefficients vs. helium fraction for HeXe.

3.7.1 Sandia Brayton Loop Paschen Effect Conditions

The Sandia Brayton loop has two locations where bare wires might be exposed to the coolant gas. The first location is at the electrical connection to the alternator, and the second is where these wires feed through the pressure boundary containment. Figure 3-41 shows the wiring connection to the terminal strip that is mounted to the alternator housing. The closest approach

of the phase to phase wires is approximately 1.6 cm. Thus, for this connection the Paschen pressure distance parameter at one atmosphere is 760 torr * 1.6 cm = 1,200 torr-cm. Based on Figure 3-39 even for pure Helium the break down voltage at 1200 torr-cm is approximately 2000 VAC. The rectified alternator voltage is 750 V. If we assume that the maximum alternator AC voltage does not exceed the rectified voltage then break down is unlikely to occur at this electrode even in helium. Some of the future tests that we propose to run will use gas mixtures of helium and nitrogen and helium and argon. As shown in the earlier figure the breakdown voltage for the gas mixture is always larger than the pure helium breakdown voltage. Thus, we feel that with respect to the Paschen effect we can safely use mixtures of helium and nitrogen, carbon dioxide, or argon.

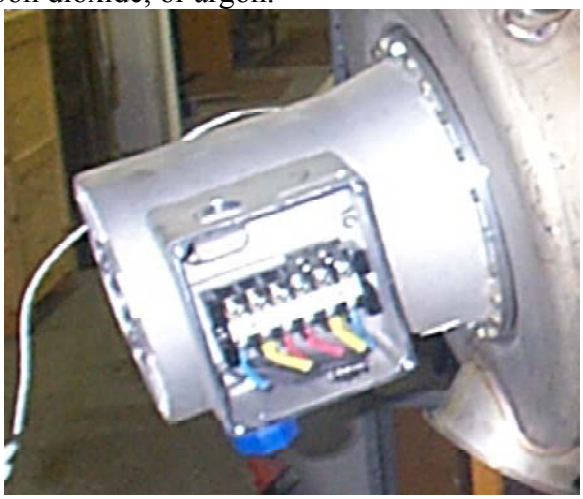

Figure 3-41: Alternator exposed electrical connections. The closest approach of two phase to phase wires is 1.6 cm.

The other potential spot of breakdown is at the pressure boundary feed through. Based on the design drawings and the feedthrough specifications (Pave-1575 feed-thru) this feed through has no exposed bare wires through the penetration. Thus this location should also not be a site of breakdown.

4 Operational Results, Validation, and Comparison of the Dynamic Model with the SBL-30 Operation

The Brayton test loop was installed at Sandia Laboratories during the summer of 2005 and the first operation at Sandia began in August. The initial operations were aimed at getting the system running, debugging instrumentation and software, adding additional instrumentation, measuring the thermal and noise environment in the laboratory and in improving our operating procedures. While these initial tests were being performed we were also upgrading the facility to provide greater amounts of electrical power, and to install insulation (both thermal and sound) on the Sandia Brayton Loop.

The first runs were operated at low power levels with no or with limited amounts of insulation on the ducting. One of these tests (TT4, Transient Test 4) was used to provide data to compare the measured and predicted characteristic flow curves for the turbine and compressor. This comparison is presented in the following section. As would be expected, we observed large heat losses in these un-insulated tests. After the insulation was installed and the facility power levels were increased, two more tests were performed (TT5 and TT6) to provide more data that could be used to compare with the dynamic models.

Each test run was aimed at accomplishing a number of objectives. Test TT5 was fully insulated therefore our goal for this test was aimed measuring the system energy balance at steady-state conditions and at high turbine inlet temperatures (880 K). During this test we also measured the operating performance curve. This curve plots the electrical power produced as a function of rpm for constant turbine inlet temperature (880 K). Also during this test we explored reactor shutdown conditions. Specifically we wanted to observe the length of time that the Brayton loop could generate small but positive power after the heater was turned off. In effect these measurements explored the decay heat removal capability of the closed Brayton system, and its ability to move the heat from the reactor/heater even after the reactor/heater is “turned off”. As a note, it was observed that the turbo-machinery could operate for over one hour after the heater was turned off.

The last test TT6 focused mainly on filling out more data on the operational curves for the CBC loop. In this test the electrical power generated was measured as a function of rpm for turbine inlet temperatures that were kept constant at 600, 650, 700 and 750 K. The results of all these tests are provided in this section and are compared with the models. This data also revealed some undocumented behavior of the Capstone controller.

To date, the data evaluation and validation effort has focused on

1) determining the energy balance with in the loop,
2) comparing the measured and predicted characteristic flow curves,
3) comparing of the measured versus predicted operational curves (operational curves show the power produced versus rpm curves at various turbine inlet temperatures),
4) evaluating the decay heat removal capabilities of the CBC test loop and exploring the implications for space and terrestrial reactors, and finally on
5) comparing the transient behavior of the predictions with the actual measured data.

Detailed descriptions of each of these test series will be presented in separate sections that follow.

4.1 Brief Summary of Measurements from Three Transient Tests using the Sandia Brayton Loop

The operational results from three tests will be presented and discussed in this section. A brief description of these tests is presented first as an introduction to the operation of the Sandia Brayton Loop. Up to sixty channels of data for each test were recorded, at a sampling rate of one sample per second. A test typically lasts for 8-12 hours. Because it takes such a long time for the system to heat up and cool down, the tests usually are arranged so that multiple experiments or behavioral studies are performed within one test. The long duration and the large number of channels, coupled with the one second sampling rate means that a lot of data is recorded for each test. In this report we will examine some of the major behaviors of the loop and its operating characteristics. Other more subtle behaviors will be reserved for subsequent publications. This chapter will present much of measured data (and RPCSIM predicted data) in the form of plots or curves. Each of the curves is associated with a data channel that has a unique identifier consisting of either a display name or a channel name. These names will generally be listed within the legend of the plots. Similar names are used by the dynamic model. Table 4-1 lists the recorded data channels and their associated names.

4.1.1 Introduction and Summary of Test TT4

The first test was performed on August 8, 2005. It is designated as TT4-050812, or TT4 for short. It was the first transient test performed at Sandia, though the first three transient tests were performed at Barber Nichols Inc.. This test (TT4) was performed with no insulation and was used primarily as a system level checkout. The maximum heater power at the time was limited to 50% of full power because the power upgrades to the facilities were not complete. The coolant was 94 mole % nitrogen with the remainder was estimated to be oxygen. The data collected in this test was used to determine measurements of the characteristic flow curves, which were then compared with predicted curves used in the RPCSIM dynamic model.

Figure 4-1 shows a summary plot of the measured data. This curve shows the measured gas temperatures around the loop, the shaft speed, the alternator power, and the heater power. The alternator power is reported by the Capstone controller. Based on the Capstone documentation it is believed to be the raw 3 phase electrical power produced in the alternator; however, recent measurements indicate that at very low shaft speeds additional power is applied to the alternator by the Capstone controller to avoid operating at a shaft resonance. The electrical power is reported as percent full power, and it is the commanded signal to the Watt Low SCR controllers that run the heater elements in the heater. The effective full power of the heater is 62.35 kWe.

The curves in Figure 4-1 show the measured temperatures at various stations around the loop. NOTE THAT THE TEMPERATURES ARE SHOWN IN DEGREES F in this figure. T100 is the turbine inlet temperature; T200 is the turbine exit temperature; and so on around the loop (also see Table 4-1). The numbering scheme follows the convention used by Barber Nichols Inc. and unfortunately differs from that used in the dynamic models because it starts at the turbine inlet rather than the compressor inlet. This transient test is a simulation of one possible

startup transient of a reactor connected directly to a closed Brayton cycle. In this startup transient the alternator power (tan curve) is first motored (shown as negative power produced, approximately -500 W) at 25,000 rpm for a few minutes, then at 40,000 rpm (-2 kW) for a few more minutes. Shortly after the flow is established and the temperature changes caused by compression and expansion are allow to equilibrate with the structure temperatures, the electrical power is turned on. In this transient the heater power is first increased to 40% power for 20 minutes (2500s – 4000s) and then increased to 50% power. Because the facility power was not yet upgraded at this time we did not increase the power levels above 50%. The heater power gradually increases the turbine inlet temperature (TIT), causing the required motoring power to decrease. When the TIT reaches about 700 F then the motoring power is no longer negative and positive power starts to be produced at about 6000 seconds.

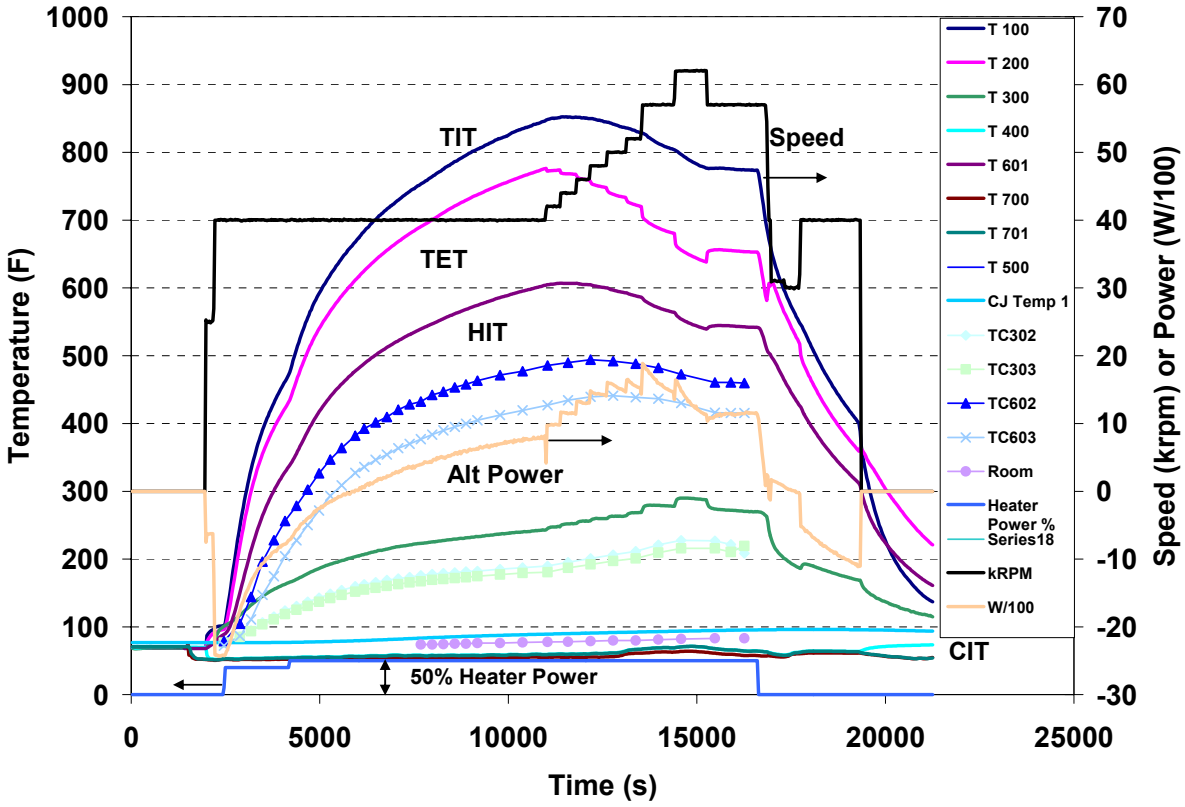

Figure 4-1: Sandia Brayton Loop Transient Test 4 (TT4-050812) performance with no insulation and with the electrical power limited to 50% of full power or about 31 kW of heater power.

The reader should observe that the shaft speed can be changed very quickly (within a fraction of a second) but the gas temperature changes are more constrained. The gas temperatures appear to have two time constants. One time constant is relatively quick (a few seconds) and responds rapidly to the increase flow and change in heat transfer and to the change in pressure. The temperature changes that observed for this faster time constant are limited to 5-20 K. The second gas time constant is slow and follows the thermal lag in the heater, ducting, flanges, and recuperator/ heat exchangers. This slow time constant is on the order of 20-40 minutes for

most of the ducting and components but is as long as several hours for the heater exit flange (details to be shown later).

Table 4-1: List of recorded data channels, providing the channel number, name, display name and a brief description of each recorded channel.

Channel Number	Channel Name	Display Name	Description
1	T 100	T 100 Turb In	Turbine Inlet Temperature
2	T 200	T 200 Turb Out	Turbine Exit Temperature
3	T 300	T 300 GCool In	Recuperator Hot Leg Exit Temperature or Gas Chiller Inlet Temperature
4	T 400	T 400 Comp In	Compressor Inlet Temperature
5	T 601	T 601 Htr In	Heater Inlet Duct Gas Temperature after Manifold
6	T 700	T 700	Water Coolant Inlet Temperature
7	T 701	T 701	Water Coolant Outlet Temperature
8	T 500	T 500 Comp Out	Not Available
9	CJ Temp 1	CJ Temp 1	Cold Junction Temperature in FP NI hardware-1st module
10	T 602	T602 Htr Man Pipe	Heater Inlet Duct Manifold Wall Temperature
11	T 603	T603 Htr In Pipe	Heater Inlet Duct Wall Temperature
12	T 302	T302 Chlr InDuct1	Gas Chiller Inlet Duct Wall Temperature 1
13	T 303	T303 Chlr InDuct2	Gas Chiller Inlet Duct Wall Temperature 2
14	T 101	T 101 Htr Out	Heater Gas Outlet Temperature
15	T 102	T 102 Htr Flng	Heater Outlet Flange Temperature
16	T 604	T 604 Htr In	Heater Gas Inlet Temperature
17	T 103	T 103 Htr Elmt	Heater Element Surface Temperature
18	CJ Temp 2	CJ Temp 2	Cold Junction Temperature in FP NI hardware-2nd module
19	P 100	P 100	Turbine Gas Inlet Pressure
20	P 200	P 200	Turbine Gas Outlet Pressure
21	P 300	P 300	Hot Leg Recuperator Gas Outlet Pressure or Gas Chiller Inlet Pressure near Recuperator
22	P 400	P 400	Compressor Gas Inlet Pressure
23	P 500	P 500	Compressor Gas Outlet Pressure
24	P 600	P 600	Ambient Pressure Measured in NEMA box
25	P 601	P 601	Recuperator Cold Leg Outlet Pressure Heater Inlet Duct Pressure and Recuperator Exit
26	P 700	P 700	Water Inlet Pressure
27	P 701	P 701	Water Outlet Pressure
28	FLOW 1	P301 FLOW P	Orifice Pressure (upstream of Orifice)
29	FLOW 2	P302 FLOW dP	Orifice Pressure Drop (1D 0.5 D)
30	Water Flow	Water Flow (gpm)	Water flow rate Gallons per Minute
31	P 101	P 101	Heater Outlet Pressure at Flange
32	P 604	P 604	Heater Inlet Pressure at Heater Entrance
33	Ambient Pressure	Ambient Pressure	Ambient Pressure Measured in NEMA box (=P600)
34	Mass Flow	FLOW	Mass flow rated based on Orifice Measurements
35	RPM	RPM	Shaft speed (revolutions per minute)
36	POWER	POWER	Alternator Power
37	T Aux 1	INVERTER POWER	Inverter Power
38	T Aux 2	T Aux 2	Auxilliary Data Reported From Capstone Controller
39	T Aux 3	T Aux 3	Auxilliary Data Reported From Capstone Controller
40	T Aux 4	T Aux 4	Auxilliary Data Reported From Capstone Controller
41	T Aux 5	T Aux 5	Auxilliary Data Reported From Capstone Controller
42	T Aux 6	T Aux 6	Auxilliary Data Reported From Capstone Controller
43	T Aux 7	T Aux 7	Auxilliary Data Reported From Capstone Controller
44	T Aux 8	T Aux 8	Auxilliary Data Reported From Capstone Controller
45	CBC State	CBC State	Capstone Controller Error State
46	Sweep Mode	Sweep Mode	Sweep Mode Flag (for power sweeps)
47	Heater Delta T	Heater Delta T	Heater dT (T101-T604)
48	Target Inlet Temp	Target Inlet Temp	Target T100 Temperature
49	Target RPM	Target RPM	Target RPM
50	Heater Power %	Heater Power %	Heater Power in percent (100 % = 62.3 kWe, Nov 9, 2005)
51	OverTemp	OverTemp	Over temperature flag reported by Capstone Controller (?)
52	Sweep Time	Sweep Time	Time within sweep
53	On Time	On Time	Data Time (absolute time)
54	Spare A	Spare A	Spare A
55	Spare B	Spare B	Spare B
56	Spare C	Spare C	Spare C
57	Spare D	Spare D	Spare D

The noise levels around or near the un-insulated hardware were measured during operations. The noise levels at the control station which is located about 6 ft from the turbo-alternator compressor set was generally 70-75 dB and is high frequency (~8000 Hz). There is no perceptible vibration. At some locations, very close (inches) to the hardware, the noise levels loop were measured and found to be <82 dB. Most people's observation is that the loop noise levels are much less than expected and can generally be compared to a shop-vacuum. After the thermal insulation was installed the noise levels were noticeably reduced. In fact most people's comments about the system are how quiet it is.

4.1.2 Introduction and Summary of Test TT5

The second test is designated TT5-050913 and was performed September 13, 2005. The hardware for this test was fully insulated (both thermally and for noise abatement), and the facility upgrades permitted full power electrical heater operations. Also, additional thermocouples were added to measure the heater gas exit temperature and the bulkhead flange temperature. Additional pressure transducers were also installed. There were three major purposes of this test. The first was to make near steady-state measurements of the system energy balance. The second was to measure the electrical power produced by the alternator as a function of rpm for a fixed turbine inlet temperature of 880 K. This curve is called the operational curve. The third goal was to measure the decay removal characteristics of the closed Brayton loop by measuring the amount of time small but positive power could be produced by the loop after the electrical heater was turned off.

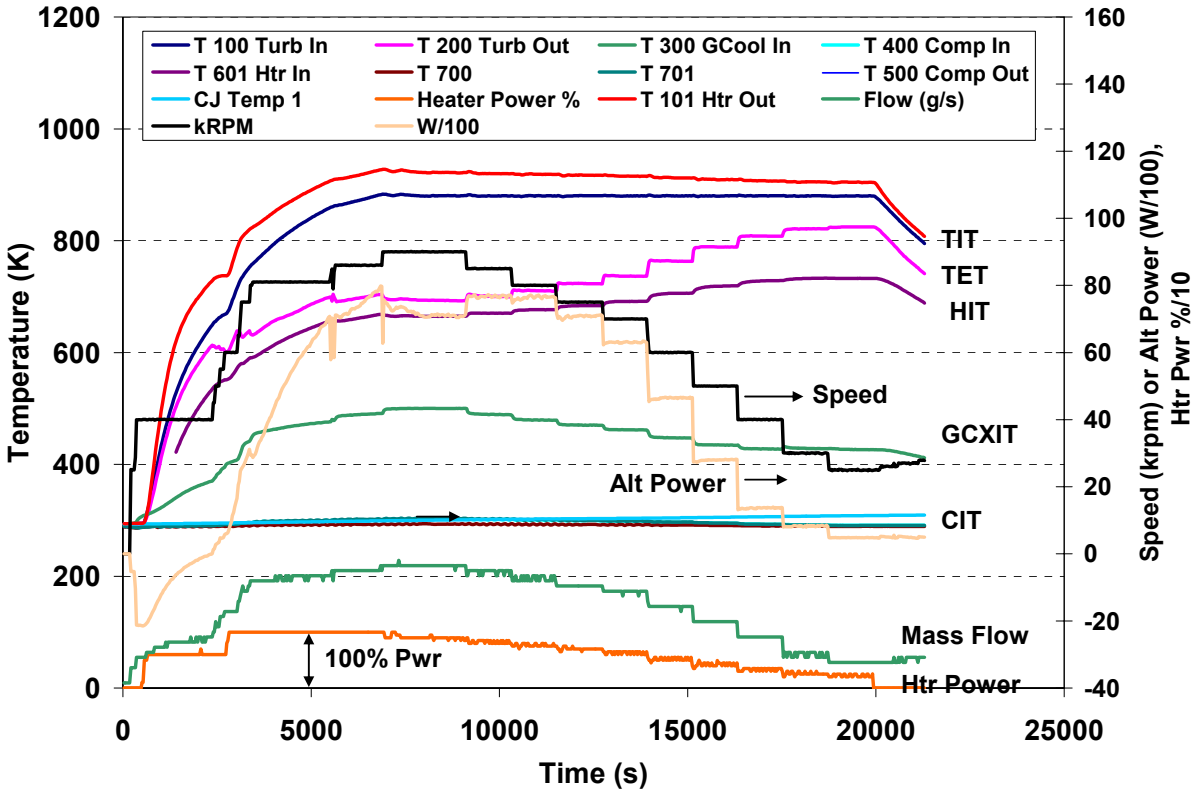

Figure 4-2: Summary data and plot of measured data from Transient Test 5, TT5-050913. This test was fully insulated and aimed at determining the energy balance at

100% power (62.3 kW), measuring the alternator power as a function of speed for fixed turbine inlet temperatures and in measuring decay heat removal capabilities after the heater power was turned off.

To make the steady-state energy balance measurements the test-loop was run at high temperatures for a few hours. The heater input power was known because the supply voltage and heater element resistance were measured. The heater electrical power was then compared to the power transferred to the gas, rejected by the gas chiller, and produced by the permanent magnet alternator. The power in all other components can also be determined by knowing the flow rate and the temperature change within the component. Figure 4-2 shows a summary plot of the measured gas temperatures, the shaft speed, alternator power, and heater power during the transient.

As before, the startup transient consists of first starting (motoring) the turbo-compressor set to initiate flow through the loop (rpm = 40,000). After a few minutes of operation, the heater power is turned on, in this case to 60% of full power. The alternator power crosses zero when the turbine inlet temperature (TIT) reaches about 650 K at 2500 seconds into the run at a speed of 40 krpm. In addition to showing the turbine inlet temperature (TIT), the plot also shows the heater gas exit temperature (see the red curve). The measured gas heater temperature exceeds the TIT by about 40-90 K over most of the test and is an indication that several kJ of heat is lost to the very massive bulkhead on the heater. At about 7,000 seconds into the run, the TIT begins to approach steady-state conditions. The energy balance is based on the temperature measurements and mass flow rate data at this time.

To measure the data for the operational curve we began to decrease the turbo-compressor shaft speed in steps of 5,000 rpm starting at about 7000s. Whenever we varied the shaft speed (rpm) we made heater power adjustments to keep the TIT at 880K. As shown in Figure 4-2 the TIT was kept within 1 K of 880 K for over 4 hours while the shaft speeds were varied from 90,000 rpm down to 25,000 rpm. (See the speed curve from 7,000 s to 20,000 seconds.) The measured alternator power is shown as the tan line in this same figure.

The third goal of this test was to study shut down or decay heat removal capabilities of the closed Brayton loop. This portion of the test began at about 20,000 seconds. Here the heater power was turned off completely and the shaft speed was changed to keep the reported alternator power at 500 W for as long as possible. As shown in Figure 4-2 the shaft speed had to increase slightly from 25,000 rpm to 28,000 rpm over a period of almost one hour while the "reported" alternator power was kept at 500 W. (The actual power produced was 100 W due to a Capstone controller feature, as will be described later). This shows that the CBC can spin or operate for a long time without motoring (auxiliary power required to run the main compressor/pump) provided the main cooling heat sink is available. This has important applications for both space and terrestrial gas cooled reactors because it means that the main turbo-compressor set can run off of the latent heat of the reactor and other structures for a very long time. This means that the heat can be transferred to the main heat sink for a sufficiently long time to allow it to decay to small values (~ 1% of operating power). Of course pumps and power must be supplied to operate the waste heat rejection system, but some of this power may be obtained from the TAC as it is still producing small but positive power. For both space and terrestrial application this means that the reactor can be cooled by the TAC for a sufficiently long time that most of the decay heat can be allowed to decay to sufficient levels that the main compressor can be turned off.

4.1.3 Introduction and Summary of Test TT6

The third test is designated TT6-051017 and was performed October 17, 2005. The hardware for this test was fully insulated and full power electrical heater operations were possible. An additional thermocouple was added to measure the heater element surface temperature at its hottest location. This thermocouple also serves as a safety set point in the Watlow power controller. Figure 4-3 shows a summary plot of the gas temperature measurements, the shaft speed, the input heater power, the measured alternator power, and the mass flow rate. The LabView CBC controller has a feedback controller that adjusts the heater power to maintain a user specified turbine inlet temperature (TIT). This PID (proportional integral differential controller) was used in this test give the desired TIT. In the previous test this function was performed manually by the operators, but in this test we used the automatic feature. The automatic control feature does a good job of keeping the temperature at the set point provided the set point is above 500 K. In this test the actual temperature followed the set point within 1 K.

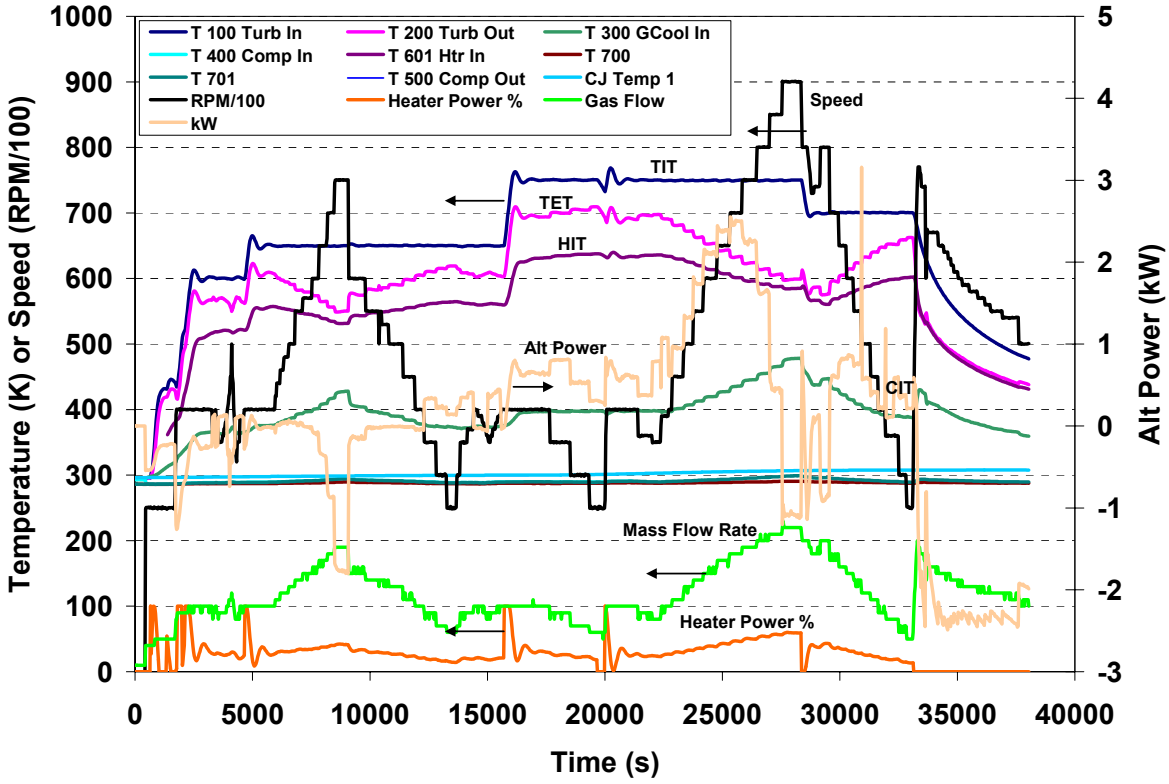

Figure 4-3: Summary data and plot of measured data from Transient Test 6, TT6-051017. This test was fully insulated and used the heater feedback controller to provide a user specified turbine inlet temperature. The test was used to determine curves for the power produced by the alternator as a function of rpm for various turbine inlet temperatures (TIT). The mass flow rate has units of gm/s.

The major goal of this test was to measure the operational curve at more TIT temperatures. An examination of Figure 4-3 shows that operational curves were measured at TIT's of 600K, 650K, 700K, and 750K. The reader will observe that for each TIT temperature the shaft speed was varied over a range. Previous tests had shown anomalous behavior at low shaft speeds, so

we performed a number of measurements in the 25,000-40,000 rpm range. We indeed observed a hysteresis effect in the measured alternator power level as a function of shaft speed.

4.2 Energy Balance

The energy balance data was taken during test TT5, and the summary data for this test was shown in Figure 4-2. This test heated the gas to a turbine inlet temperature of about 880 K for over 15, 000 seconds. The heater power was kept at 100% power for the first 5000 seconds of the high temperature duration and the energy balance data was taken at the end of the 100% power run when the shaft speed was 86,000 rpm (6843 seconds into the transient). The recorded data and calculated energy balance for this test is shown in Table 4-2. It consists of the measured gas temperatures at various locations around the loop and the gas and mass flow rate. Given the flow rate, the heat capacity of the fluid (see Table 4-3), and the temperature change it is possible to estimate the power or heat generated or lost in each component.

Table 4-2: Table of measured gas and water temperatures used to determine the mass balance. The power levels report the power in kW based on the corrected gas flow rate.

T100 Turb In (K)	T101 Htr Out (K)	T604 Htr In (K)	T700 Wtr In (K)	T701 Wtr Out (K)	Corrected Gas Flow gm/s	Gas Flow 1 gm/s	Wtr Flow gpm
882.3	926.7	659.4	292.3	301.6	0.21	0.24	17.88
Q htr	62.8 kW			R1a	12.5 ohm		
Q htr-TIT	52.1 kW			R2a	12.5 ohm		
Qchlr-gas	41.9 kW			R3a	12.5 ohm		
Qchlr-wtr	42.1 kW			R1b	13.4 ohm		
Q-alt	8 kW			R2b	12.5 ohm		
P-htr (V^2/R)	62.4 kW			R3b	13.4 ohm		

Table 4-3: Average nitrogen heat capacity used for the heater and the gas chiller.

Component	T average	Cp(Nitrogen) J/kg*K
Heater	793	1119
Heater-1	770	1114
Chiller	395	1047

The mass flow rate was measured by using a flow orifice plate in the duct that that connects the gas chiller to the high temperature leg of the recuperator (see Figure 3-26). The flow orifice plate has a diameter of ½ the pipe diameter (D) and the pressure taps are located at D and ½ D with the down stream tap located at ½ D. The plate and taps are designed to ASME specifications and the ASME recommended discharge coefficient is used to calculate the flow rate based on ASME MFC-3M-1989 and reaffirmed in 1995 (ASME 1989). The equation used to calculate the flow rate is

$$\dot{m} = C_d S_o \sqrt{\frac{2\rho\, dp}{1-\left(\frac{S_o}{S_1}\right)^2}}\,. \qquad 4\text{-}1$$

where $\dot{m}$ is the mass flow rate, C_d is the discharge coefficient, ρ is the gas density, dp is the pressure drop across the orifice plate, S_1 is the duct flow area, and S_0 is the orifice plate flow area. The orifice plate diameter is 3.725 inches and the duct diameter is 6.357 inches. As currently configured and for the tests reported in this document the gas is always assumed to be nitrogen.

The ASME recommended discharge coefficient for the Brayton loop geometry is $C_d = 0.61$. However based on the energy balance a more consistent value for the discharge coefficient is 0.53. This is best seen by comparing the heat loss in the gas within the gas chiller (41.9 kW) compared to the heat added to the water (42.1 kW). As described below a 12% correction in the gas flow rate (or discharge coefficient) was imposed to make the heat balance for the gas chiller agree in both the nitrogen and water phase legs of the gas chiller. This correction also makes the estimated electrical power to the heater agree with the heat transferred to the gas in the heater. The mass flow rate meter for the water leg in the gas chiller uses a vane type flow meter which is expected to have a high degree of fidelity compared to the gas flow orifice plate.

There are also inaccuracies in the measured data. For example, the differential pressure used to make the gas mass flow rate is taken from D and D/2 pressure taps using a SETRA 1 psid NIST calibrated pressure transducer, and the density was determined from the pressure and temperature measurements made in the duct. The pressure is measured at the inlet to the orifice with a SETRA Model C280E 0-25 psia pressure transducer, and the temperature was made with a type K thermocouple. The thermocouple is located at the exit of the recuperator and not at the orifice plate. An accurate energy balance is obtained if the discharge coefficient is reduced by 12% from the ASME predicted flow rate. Because of the location of the thermocouple and the relative small magnitude of change in measured pressure drop across the orifice plate (approximately 1.9 kPa, at 86,000 rpm) and the fact that the measured signal exhibits bit noise the authors feel that this correction in flow is warranted.

The energy balance (Table 4-2) shows a measured power that is transferred to the gas within the heater (using the corrected flow) of 62.8 kW = $\dot{m}\ Cp\ (T_{101} - T_{604})$ while the predicted electrical power to the heater (at 100%) based on the resistance measurements and known voltage of 480 V. The electrical heater power is 62.4 kW. The multiphase power is calculated from

$$\textbf{Power} = \sqrt{\sum V^2 / R} \qquad \textbf{4-2}$$

Where V is the 480 Volt AC grid signal and R is the resistance values given in Table 4-2 and assuming 480 VAC for the voltage. These two power values (62.8 and 62.4 kW) are within 0.6%, which is further evidence that the correction in flow is required.

As mentioned earlier a substantial amount of power goes into heating the exit flange on the heater. The flange has a mass of 161 kg. At the time that these temperature measurements were made, the flange had not reached its equilibrium temperature, see purple curve in Figure 4-4 which shows that the flange temperature was about 625 K and still heating at a rate of 0.05 K/s which is equivalent to about 4.5 kW of heat loss. However we would expect the heat loss to the flange to be even larger because the flange is 4" thick in some places, thus the heat flux at the center of the flange is only a fraction of the heat flux at the surface. Fortunately, we have

a thermocouple that is located in the gas flow at the turbine inlet ducts (see Figure 3-27). The power/heat transferred to the gas based in the temperature difference between the TIT and the Heater Inlet Temperature (HIT) is 52.1 kW which is almost 10 kW less than the actual heater power. As just mentioned it appears that this difference is almost exclusively due to energy being transferred to the heater exit flange.

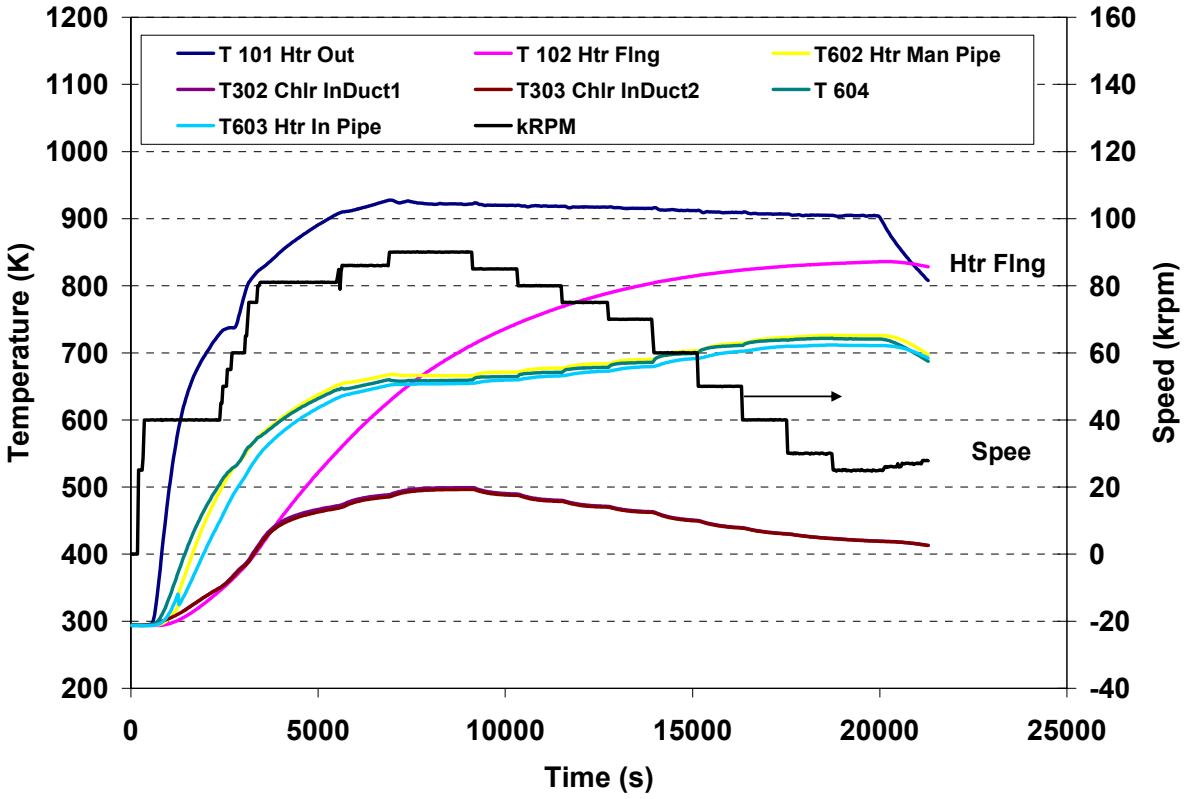

Figure 4-4: Temperature of ducting and flanges for test TT5. The purple curve shows the heater exit flange temperature, and note that at 6800 seconds the flange temperature is not at steady state, though the other duct temperatures are.

The difference in power between the heater power as measured from the heater inlet to the TIT is 52.1 kW and the power rejected from the gas in the gas chiller (41.9 kW, plus other ducting losses) should be equal to the power available to spin the turbo-alternator-compressor shaft or 52.1-41.9= 10.3 kW. The measured alternator power is 8 kW which is close to the 10.3 kW available but not the same value. The alternator is not 100% efficient. For rough calculations one typically expects a 5% loss in efficiency from alternator windage and gas bearing effects. We would also expect another 3-5% loss from the conversion of mechanical energy in the permanent magnet alternator to electrical power. Similarly the rectification and voltage regulation will also have inefficiencies on the order of 2-5% as well. Indeed some of these inefficiencies are probably a function of the shaft speed. Clearly in large terrestrial power plants a lot of design work goes into reducing these efficiencies, however for this small system we would expect the inefficiencies to tend to the larger estimates. As of writing this report we don't have good measures of these inefficiencies largely because we don't have available all of the design information on these components. We hope that future tests, by making more and

better measurements, and engaging in more communications with the Capstone microturbine corporation and its suppliers that we will be able to retire some of these uncertainties. Nevertheless, based on our estimates of inefficiencies it the 8 kWe power generated by the alternator is totally consistent with the 10 kW of torque power available to the TAC set (10 kWe – 15% 8.5 kWe). Further more some additional ducting losses on the order of 0.1 – 0.8 kW must also be considered reasonable. Thus overall we believe that we've been able to account for the energy balance within the Sandia Brayton loop.

4.3 Comparison of Measured and Predicted Characteristic Flow Curves for the C30 Turbo-Compressor Set

Probably the most important validation test is to compare the measured and predicted operational flow curves for the C30 turbo-compressor. This section begins this process by comparing the measured operating states at selected shaft speeds during one of the early validation tests TT4. In section 2.3 we described the use of mean line flow analysis models to predict the of design flow characteristic curves for the C30 turbo-compressor. Figure 4-5 shows the predicted operational curve for air in the C30 compressor inlet temperature of 300 K and for C30 turbine inlet temperature of 1150 K. Because the turbine and compressor must spin at the same speed, the intersection of the pressure ratio curves for the turbine and the compressor define the steady state operational curve (pressure ratio versus mass flow rate) for various rpm, and for fixed CIT and TIT. Thus, during steady state conditions, as the shaft speed increases or decreases (due to changes in the load) the operating point moves up and down the red dotted line.

In transient test TT4 the peak turbine inlet temperature was about 700 K (see Figure 4-1). The operating line at this turbine inlet temperature has different values, thus the operating curve at the shaft speeds of 40, 46, 57, 62 krpm as used in TT4 at 700 K turbine inlet temperature and for 285 K compressor inlet temperature are shown in Figure 4-6. In addition this figure also plots the actual operating points (pressure ratio versus mass flow rate for the same shaft speeds.) These measured operating points are shown as triangles and used the corrected mass flow rate based on the energy balance analysis described above. As shown in Figure 4-6.the measured and predicted operating curve are similar and fairly close to each other but they are not identical. The predicted curves indicate a higher flow rate for the same shaft speed than observed. This difference is probably due to inaccuracies in the models used to develop the characteristic flow curves for both the compressor and turbine. Overall the results are reasonable but further study is warranted. Future efforts and tests will focus on performing tests at fixed shaft speed while varying the fill gas pressure so that the actual observed characteristic flow curves can be measured. Then efforts to improve the mean line flow analysis for off design performance can be made to improve the results.

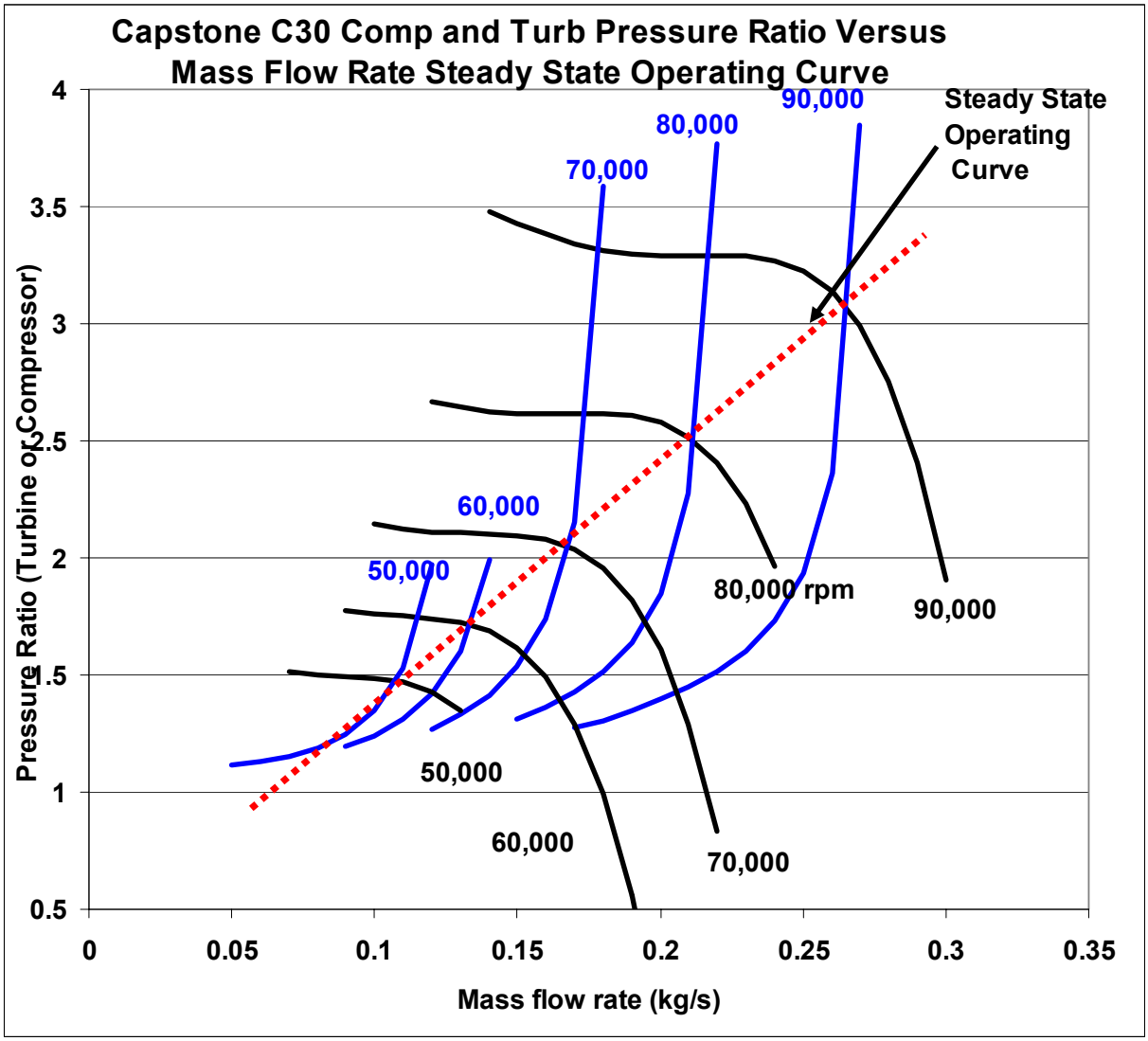

Figure 4-5: Capstone operating curve based on the NASA off design performance curve mean line flow analysis models for the C30 turbine and compressor. The compressor inlet temperature is 300 K and the turbine inlet temperature is 1150 K.

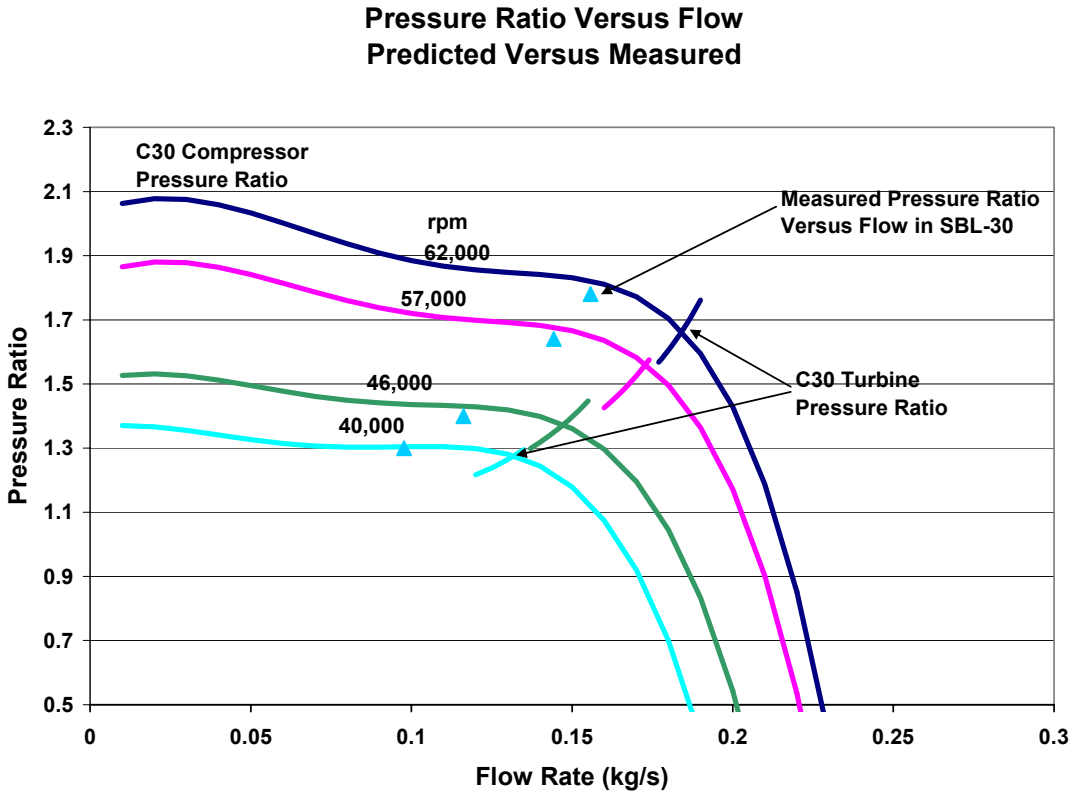

Figure 4-6: Comparison of the measure operating curve (pressure ratio versus flow measured from test TT4) for the Capstone C30 turbine and compressor versus predicted curves (solid lines) based on the mean line flow analysis off-design performance models for a 285 K compressor inlet temperature and a 700 K turbine inlet temperature. The measured data (blue triangles) was corresponds to a shaft speed of 40, 46, 57, and 62 krpm.

4.4 Operations and Test Results of the Sandia Brayton Loop Tests TT5 and TT6

The following section describes tests results from TT5 and TT6. The primary objectives of these two tests were to measure the operational performance curve for the Sandia Brayton Loop and to study the decay heat removal capability of the test loop. Sections 4.4.1 through 4.4.5 describe the operation of the CBC test loop at for fixed turbine inlet temperatures at 880 K, 750 K, 700 K 650 K and 600 K. For each of these turbine inlet temperatures the turbo-compressor shaft speed was varied from as low as 25,000 rpm up to 90,000 rpm and the alternator power was recorded for each combination of speed and TIT. The result of these test measurements provides a curve that gives the measured alternator power as a function of shaft speed for the selected TIT's. As will be described in the following sections these sets of curves can be used to predict the thermal conditions and shaft speed at which positive net power can be produced. Sometimes this is called the self sustaining point. The data can also be used to indicate how much extra power will be produced if the TIT is increased by a certain amount or whether the alternator power will increase or decrease for an incremental change in shaft speed. These curves also confirm the operational behavior predicted in section 2, and it also

confirms the dynamic stability data described in section 2 was well. The next five subsections will describe the results of these tests. The lastly the results of the decay heat removal test will be described.

4.4.1 Power Generated Versus Shaft Speed: Operational Curve

Transient test TT5 was used for a number of purposes. It was the first operation of the Brayton loop at Sandia that had full electrical power capabilities and was fully insulated. Section 4.2 described the energy balance test results, and a subsequent section (Section 4.5) will describe the decay heat removal characteristics of the Brayton loop. This section will describe the results of TT5 and TT6 and how these tests were used to generate the operational curve which plots the alternator power generated as a function of shaft speed.

4.4.1.1 Test TT5 (880-K Turbine Inlet Temperature)

The SBL-30 was operated in a mode to explore the power that can be removed as a function of shaft speed (rpm) for fixed turbine inlet temperatures. The gas fill was estimated to be 99.4% N_2 and 0.5% O_2 (with 0.1% He left over from initial leak testing). The system was heated with full heater power (about 62 kWt) until the turbine inlet temperature was 880 K and the system speed was 90,000 rpm. These conditions were held fixed until steady-state conditions were achieved. Then the speed was reduced in increments and held steady for 20 minutes to achieve a new steady-state condition. At the end of the 20 minute increment the alternator power and shaft speed were used to produce one point on the operational curve. The process was repeated at different shaft speeds to complete a full curve at constant TIT. The data presented in this section describes test TT5 in which the TIT was kept constant at 880 K. Additional data from test TT6 is provided which used the same technique to determine the operational power curve at TIT's of 750 K, 700 K, 650 K, and 600 K.

Figure 4-7 shows the gas temperatures vs. time for this test run which is identical to the data presented in Figure 4-2. The turbine speed and alternator power consumed or generated is also shown. The steps in speed are apparent in the figure. A close examination of the gas temperatures shows that they rapidly reach their new thermal conditions associated with the new speed and have a time constant of about one minute. The data also shows that a longer decay constant is involved as the structural masses slowly find their new equilibrium points. The time constant for the structural masses appears to be about 20 minutes (excluding the massive flange on the exit of the heater).

Figure 4-8 shows how closely the TIT was held to 880 K (within one degree). As described earlier the TIT was kept constant by manually cycling the heater power up and down to keep the TIT near 880 K. This cycling can be seen in the power curve (orange) of Figure 4-7, by the small saw tooth shape of the curve. Figure 4-9 plots the heater gas inlet temperature (T601) and shows that it took around ten minutes or more for some of the gas temperatures to reach within a few degrees of their equilibrium values. This duration was caused by the ducts and flanges taking some time to heat up. Figure 4-10 shows the duct temperatures slowly heating or cooling as the speed and power level changed. Figure 4-11 shows the heater manifold duct temperatures near the recuperator (T602) and near the heater inlet (T603) during a number of step changes. This plot also shows that the duct temperatures were not changing much at the end of the 20 minute increment and thus the data taken at these locations is very nearly at steady-state.

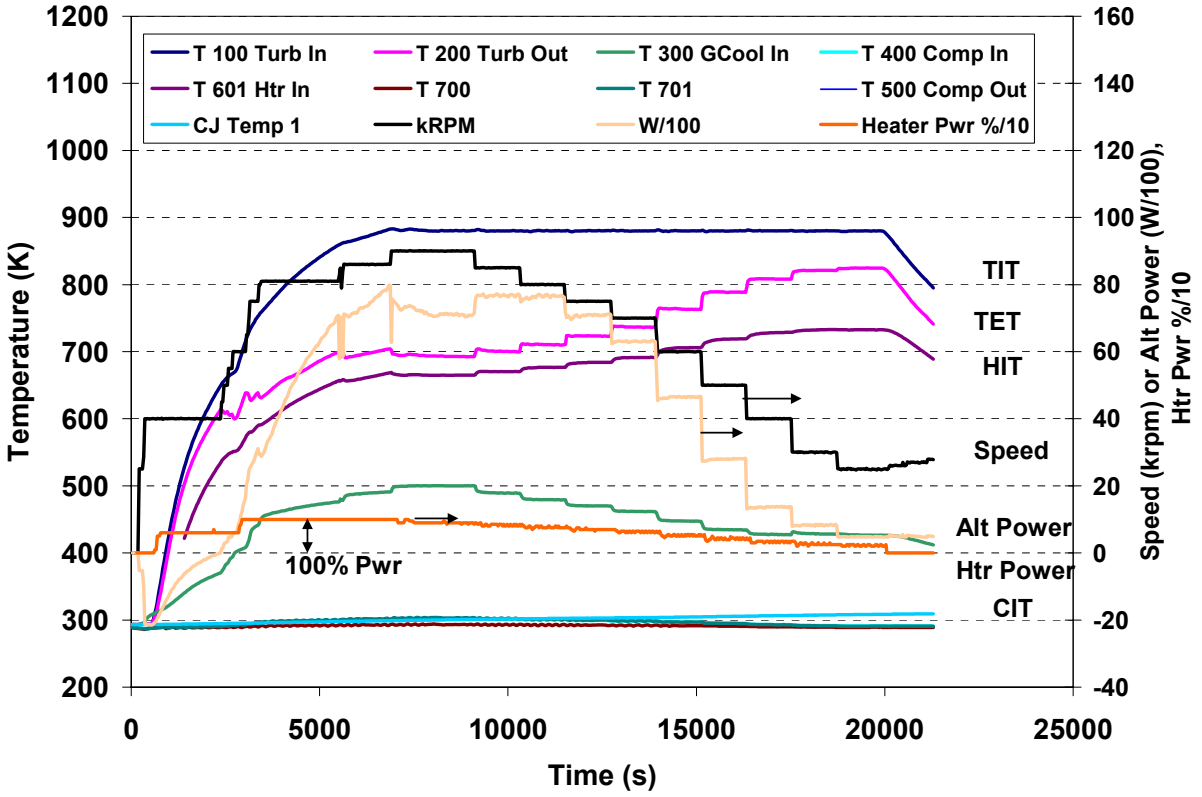

Figure 4-7: Gas temperatures for SBL-30 run TT5-09-13-05 with TIT held at 880 K.

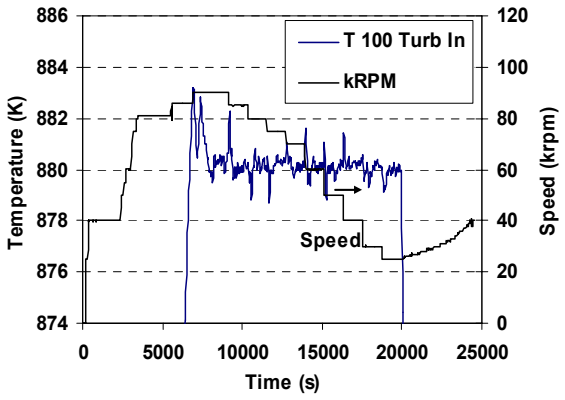

Figure 4-8: TT5 Turbine inlet temperature detail including shaft speed.

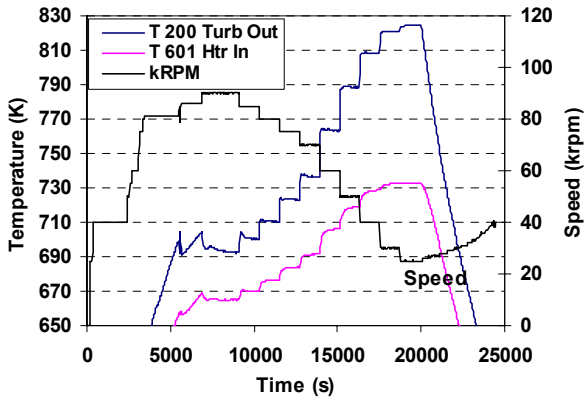

Figure 4-9: TT5Gas temperature details including shaft speed.

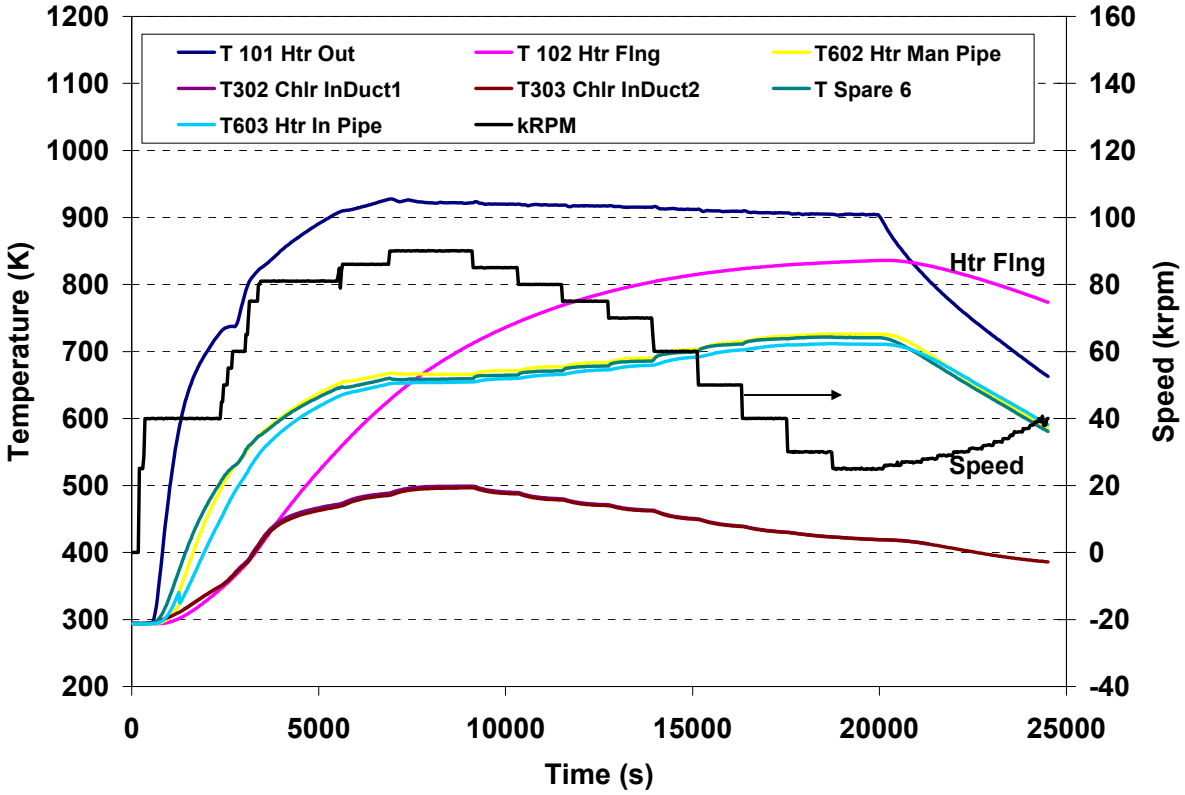

Figure 4-10: Measured Duct and flange temperatures for SBL-30 run TT5 with TIT held at 880 K.

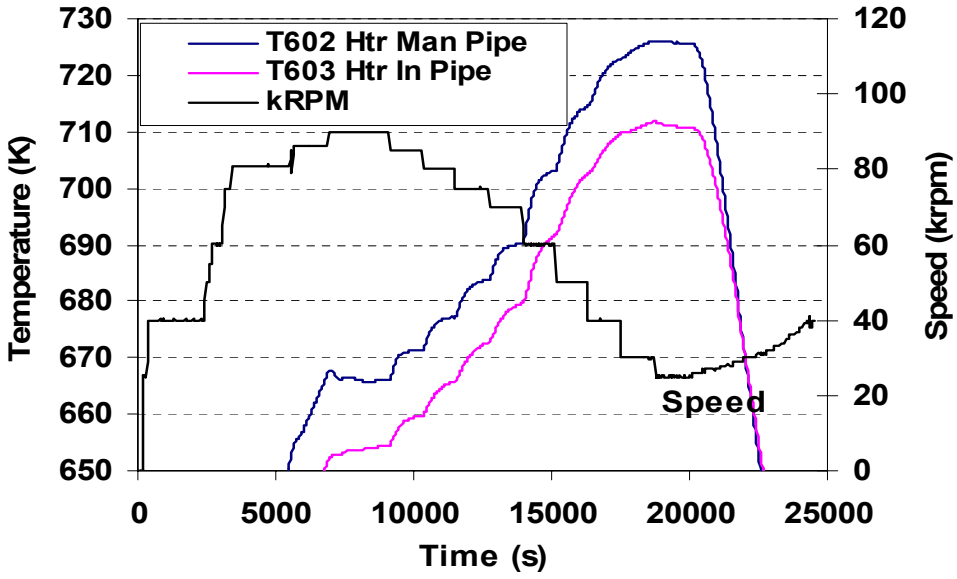

Figure 4-11: Measured duct temperature details and shaft speed for test TT5.

Overall we the equilibrium conditions are achieved within about one degree for nearly all of the shaft speed increment steps at the end of the 20 minute increments. However, the large flange at the exit of the heater never reaches equilibrium. The heat loss to this flange is a significant uncertainty in the measurements, but it can be estimated from the heat up rate. Heat loss to heating the two large heater flanges is estimated to be about 5 kW at the start of the steps (at 9,000 sec) and 0.7 kW at the end of the steps (at 20,000 sec). This amounts to about a 7% heat loss for all of the steady-state data points. Heat loss to heating all the ducts at the steady-state points at the end of each 20-minute step is estimated to be about 0.3 kW, excluding the heater flanges. In addition, there is some heat loss to the room, but it is believed to be small. All outer surfaces were insulated so that their external temperatures were less than 150 F. Heat loss via convection and radiation to the room from all the hot surfaces is estimated to be about 0.1 kW.

Figure 4-12 shows the gas pressures for test TT5. As the turbine speed increases the separation in pressure between high and low pressure sides increases. Note once the turbo-machinery is turned on (about t=300s) the high and low pressure values diverge. In addition, as the system heats, there is a slow increase in the average pressure of the system.

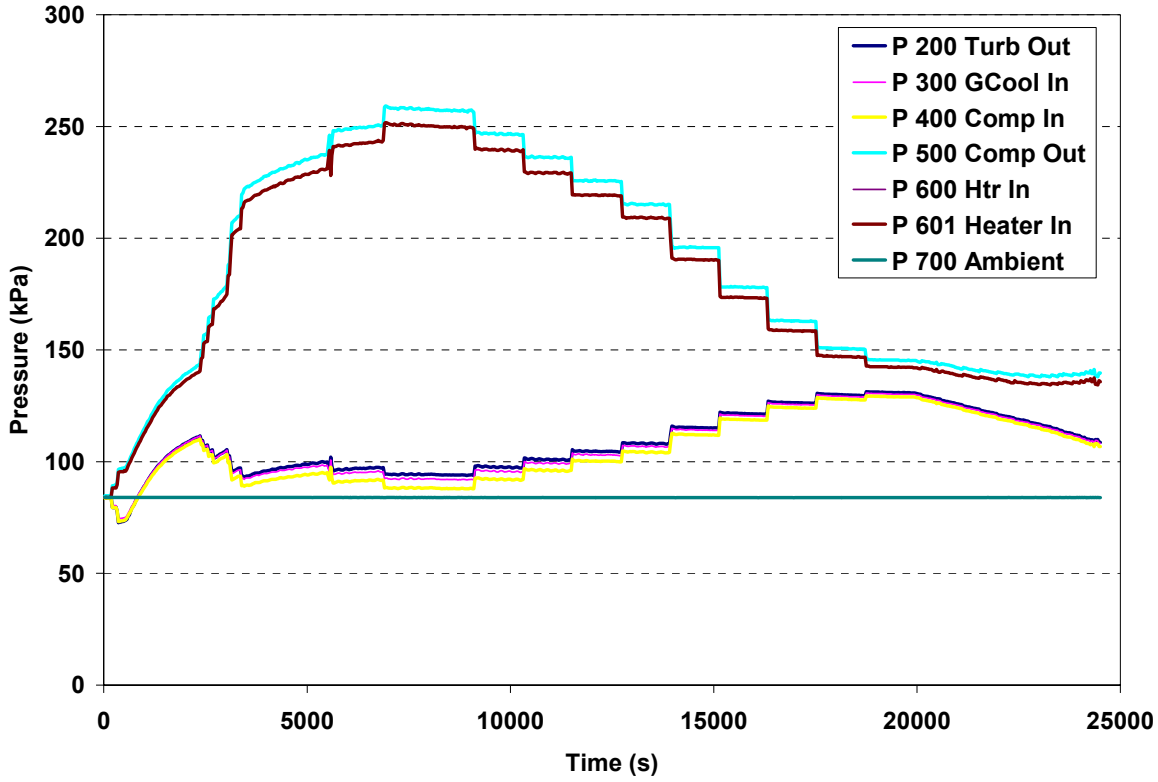

Figure 4-12: Gas pressures for SBL-30 run TT5 with TIT held at 880 K.

Figure 4-13 shows the details of the water coolant. The flow rate is very steady at 1.12 liters/second (17.8 gal/minute). The cooling water inlet temperature to the gas cooler was fairly constant with a peak value of 294 K. Notice that the water inlet temperature exhibits a oscillation of about +/- 1 K with a 200 second period. This oscillation is simply a consequence

of how the facility cooling water is supplied to our lab. Also note that as the water heats while passing through the gas chiller the oscillation magnitude is still observable (magenta line).

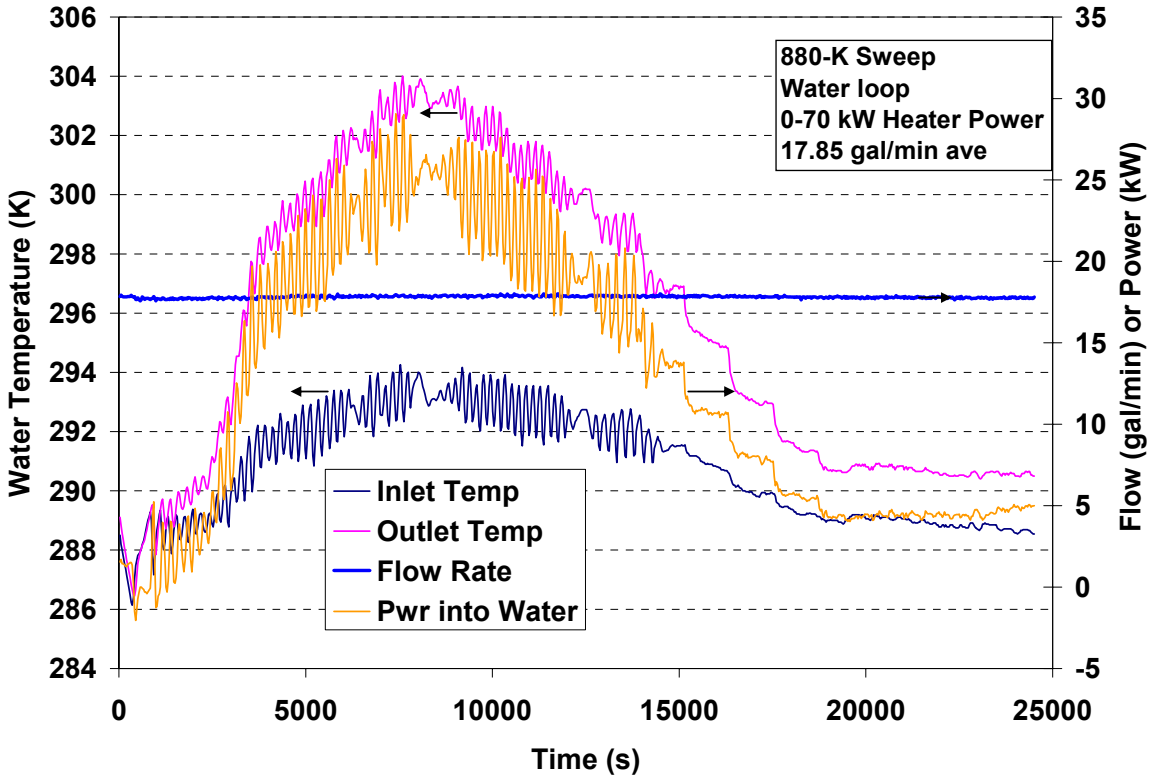

Figure 4-13: Coolant water conditions for SBL-30 run with TIT held at 880 K.

Figure 4-14 shows a comparison of the RPCSIM model predictions and the measured data for temperature of the gas. The "prediction" was actually a "blind" calculation made by running RPCSIM for the Sandia Brayton Loop after the data were acquired. The inputs to the model included the turbine speed as a function of time and the initial gas pressure, which were obtained from the experiment data. The turbine inlet temperature was kept close to 880 K(which was the actual measured TIT) via feedback loop in the model. In general, the agreement is fairly good. The small disagreement could easily be due to the uncertainties in the characteristic flow curves, in the recuperator model. Subsequent sections will show other comparisons that use the turbo-compressor shaft speed, initial gas pressure, water flow rate and inlet temperature and electrical power as the input variables. Again general agreement is seen but differences are clearly observable.

Figure 4-15 shows the similar results for system pressures. The calculated pressure at the end of the test is higher than the actual. This may be due to an error in the assumed volume of the system, or it may indicate an incorrect compressor curve. Or perhaps the leak is not adequately modeled.

Figure 4-17 shows the measured and predicted system powers.

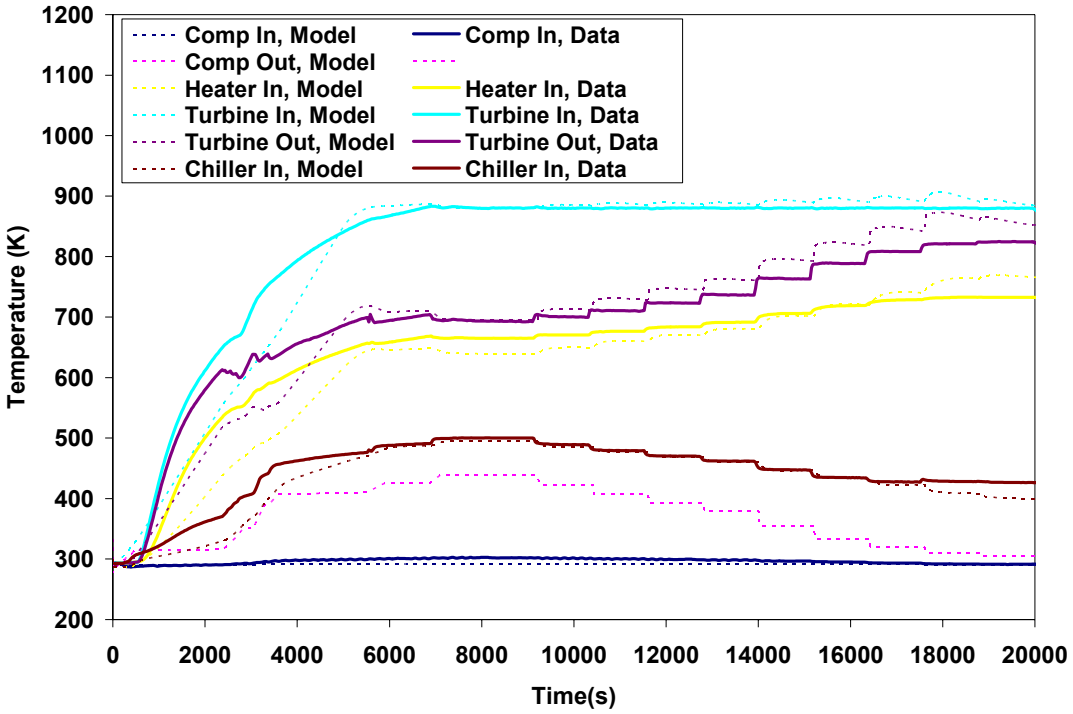

Figure 4-14: Measured temperatures compared with model predictions for test TT5. The solid lines are measured data and the dotted lines are RPCSIM predictions.

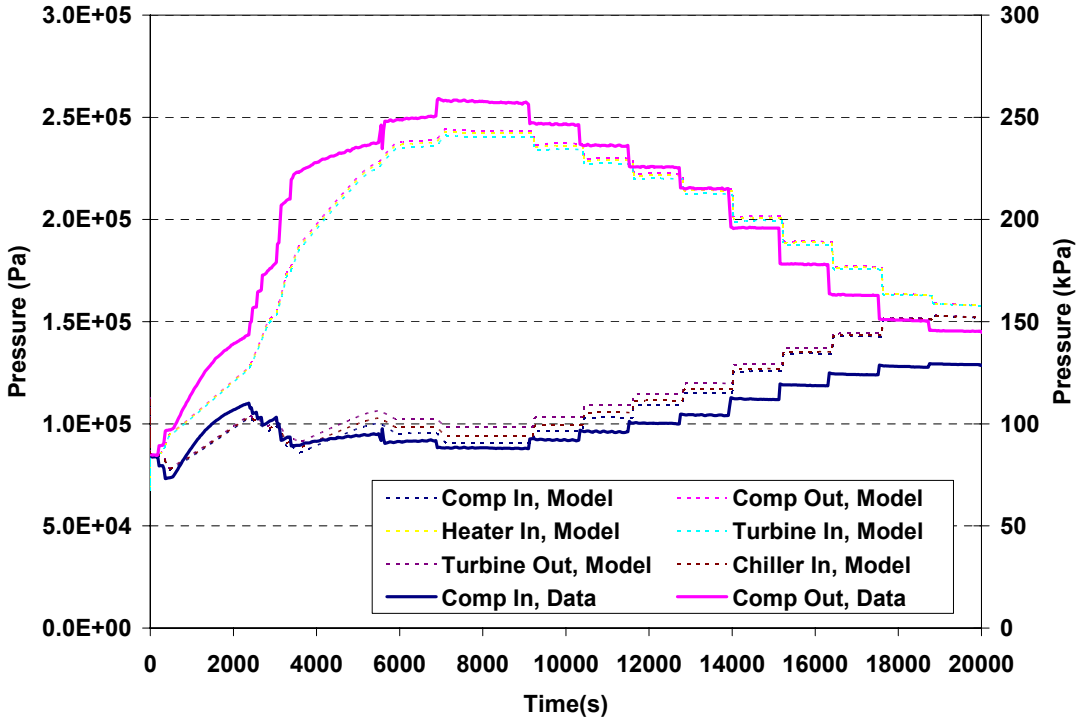

Figure 4-15: Measured pressures compared with model predictions for test TT5. The solid lines are measured data and the dotted lines are RPCSIM predictions.

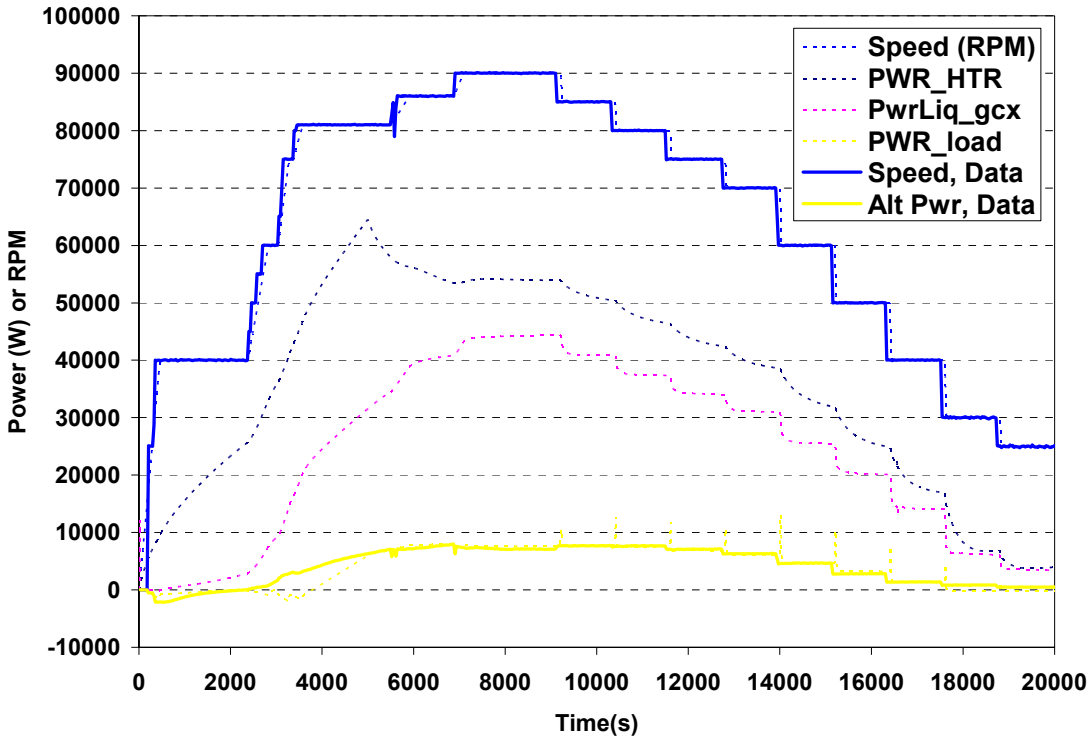

Figure 4-16: Measured power compared with model predictions for TT5. The solid lines are measured data and the dotted lines are RPCSIM predictions.

4.4.1.1.1 Impact of Power versus RPM "Operation Curve"

From these data we may construct a curve of the steady power produced by the alternator vs. speed of the turbomachinery with a fixed TIT of 880 K and a nearly fixed CIT of about 303 K. The results are shown in Figure 4-17. Also shown in the figure is the "heater power". This is the power that the gas picks up in flowing through the heater; it is close to the electrical power going into the heater (these estimates of heater power did not use the corrected flow.) It is determined from the temperature difference between the gas entering the heater and the gas just at the exit of the heater before it looses heat to the heater flange or the six exit pipes leading to the turbine inlet. The "net power in" is also shown. It is determined by the gas temperature increase from the inlet to the heater to the turbine inlet. It would be equal to the heater power if there were no flange heat up or wall losses between the heater and the turbine. The model predictions are also shown.

The agreement between the model and measures is good but differences are clearly visible. First and perhaps most striking is the fact that the turbo-machinery has two shaft speeds that it produces the same electrical power. For example the 7 kW of electrical power is produced at a TIT=880 K at 73,000 rpm and at 92,000 rpm. This effect is measured and observed and was predicted earlier in section 2.4.6.1. As described before this behavior is a consequence of the non-linear nature of the turbo-machinery equations which have multiple steady state solutions. Also observe that the heater power is less for the lower shaft speed. This means that the thermal efficiency of the system is greater at the lower shaft speed.

The Sandia Brayton loop is capable of operating over the full range of shaft speeds because it uses a feedback control loop that modifies the load to keep the shaft speed at the requested set point. The load feedback modifications are very rapid and not observable with the available data acquisition system. When we take a detailed look at the power fluctuations required to keep the shaft speed at the desired rpm we find that the modulations are small. They are on the order of +/- 25 watts about the 8000 W power production level. This is important because it shows that very small modulation or power feedback is required to keep the shaft speed at the desired set point. This has implications for control as it means that digital or analog control systems need not modulate the full power being generated but only a small fraction of the power, in this case on the or of 0.3% of generated power.

The second observation is that at low shaft speeds the hardware appears to be able to run produce positive power) at lower thermal power than the model predicts. This deviation in behavior can be seen as a change is slope below 40,000 rpm. See the dark blue alternator power curve slope change at 40,000 rpm. As will be described later much of this behavior is caused by the way the Capstone controller operates the alternator at low shaft speed (below 40,000 rpm). Essentially this slope change is purely a response by the controller which is programmed to add electrical power (i.e. motor the alternator) below 40,000 rpm to avoid a shaft resonance (reported by W. Treece formally of Capstone Inc.). As shown in Figure 4-17 the system can operate in a self-sustained manner over a wide range of input and output powers if the TIT is kept at around 880 K. The power produced by the alternator reaches a maximum at about 80,000 rpm and then decreases as speed is increased. This is the peak of the "power curve". The nominal operating power for this system is near this peak (perhaps at slightly higher speed so the system is passively stable). At 85 krpm, the electric power generated is 7.7 kWe. The heater power is 63.1 kWt and the net power in is 53.1 kWt. So the power generation efficiency is 12.2% or 14.5%, depending on whether wall and flange losses are considered.

Another observation is that at TIT= 880 K the Sandia Brayton loop begins to produce positive power at about 32,000 rpm, based on the dashed blue line model predictions shown Figure 4-17. If one ignores the slope change described above, a similar result is measured (solid blue line).

These measurements and observations are extremely important and have impacts on the design and operation of terrestrial closed Brayton gas cooled reactors. In terrestrial application it is imperative that the turbine and compressor shaft speed operate at a multiple of 3600 rpm. Typically a four pole generator runs at 1800 rpm after going through a speed reduction. If this is the case this means that the gas flow through the reactor (or primary heat exchanger) and the electrical power that is generated if essentially fixed for specific turbine inlet temperature (TIT). If the grid does not need the power that is being produced this will have the effect of increasing the grid voltage. It may also try to increase the grid frequency by a small amount. Thus the reactor driven CBC system has no way to follow the grid load without a separate feedback loop being provided to the CBC system. Typically, this can be accomplished in the long time frame by increasing or decreasing the CBC loop fill gas inventory. For short time power fluctuations, other control variables are needed such as bypass valves or throttle valves. These valves have the effect of reducing efficiency so will only be used for short time power fluctuations. This data is a reminder that even though the reactor is designed to be load following, the behavior of the entire power conversion system includes the rotating machinery

and the method of running and controlling the alternator/generator affects the load following capability and may require the addition of additional active hardware to reestablish a true load following capability. As of now, this behavior has not been fully explored with the hardware or the dynamic model; however, it will be the subject of future research and modeling.

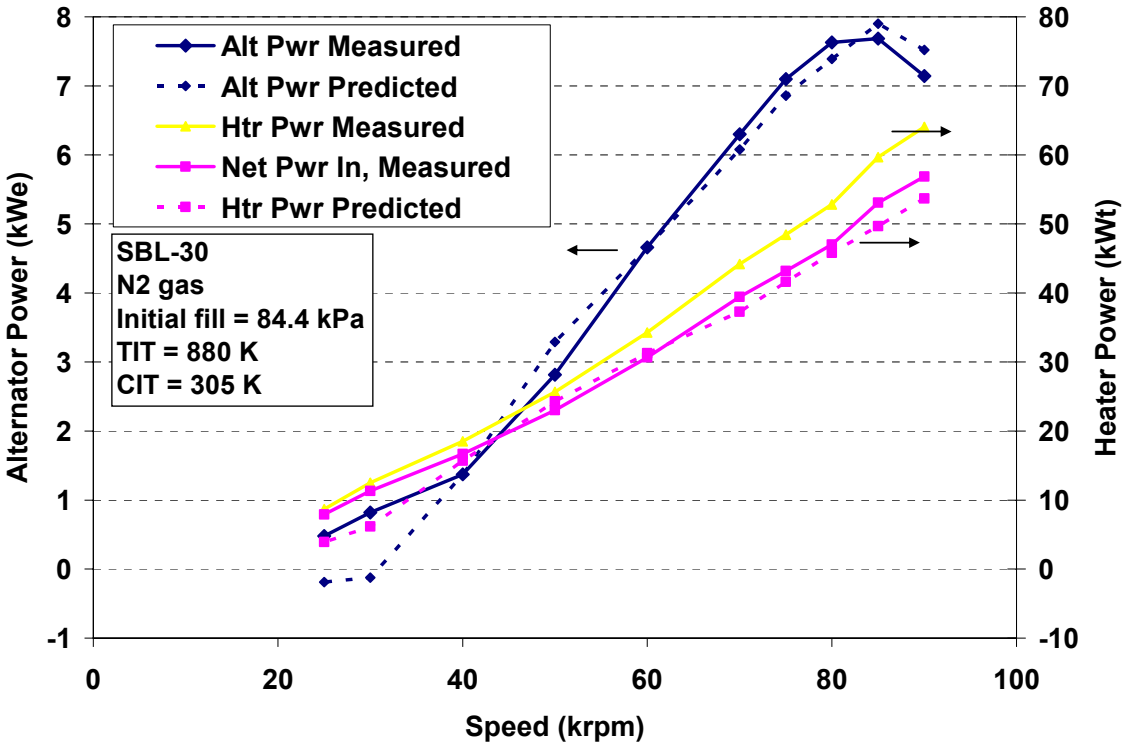

Figure 4-17: Heating power and alternator power vs. speed for TIT = 880 K.

4.4.1.2 750-K Turbine Inlet Temperature measured Test TT6

The previous section produced the alternator power operation curve at one turbine inlet temperature 880 K. After performing this test we recognized the need to fill in the rest of the data for other turbine inlet temperatures. Transient test TT6 was used to obtain this data. Essentially this test consisted of a sequence of runs that kept the TIT at 600 K, 650 K, 700 K, and 750 K. For this test an automatic feedback loop build into the Sandia controller was used to keep the turbine inlet temperature at the desired set point. While at this temperature the shaft speed was varied over a range (from 25,000 rpm up to 90,000 rpm) to determine the generated power. Figure 4-3 shows the results from the entire test. In this and the next three sections of the report the data obtained from TT6 is broken into segments. Each segment represents a time period over which the TIT was kept constant. The selected TIT's were 750 K, 700 K, 650 K and 600 K.

The first sequence of figures describes the data for the 750 K turbine inlet temperature that occurred from 16,000 seconds to 29000 seconds. The summary data for this time period is shown in Figure 4-18. Note that the TIT was kept constant at 750 K. During the last half of

this sequence the shaft speed was increased from 25,000 rpm to 90,000. The power produced by the alternator is shown as the light brown line in this figure, and shows the power increasing from about 500 We to 2.5 kWe. Figure 4-19 shows the gas pressures at the various location through the loop, and Figure 4-20 shows the extracted power versus shaft rpm operation curve.

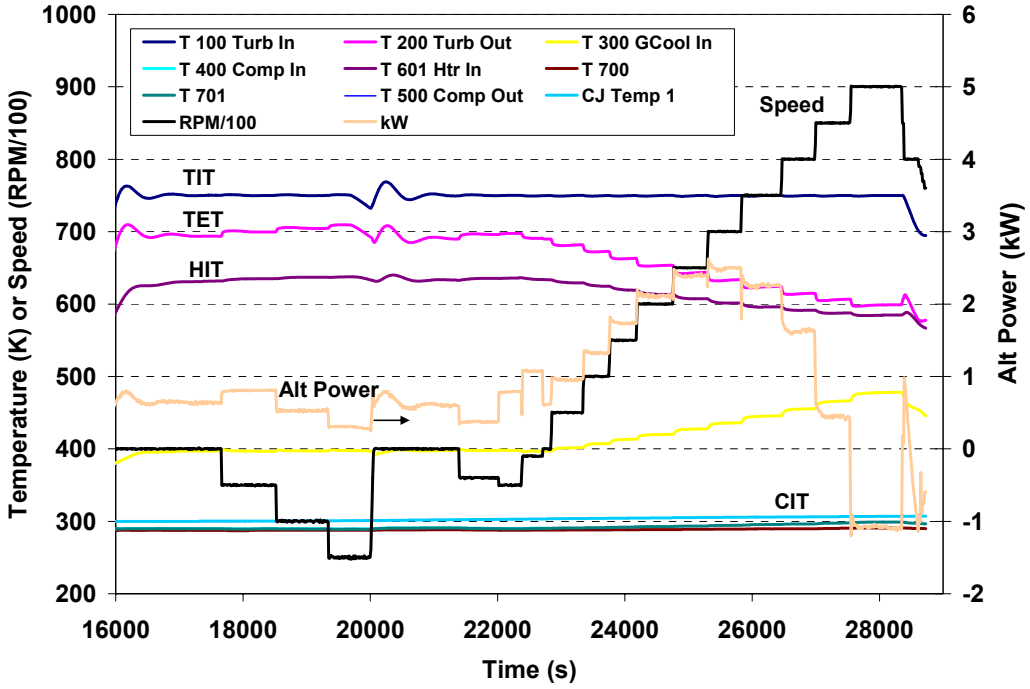

Figure 4-18: TT6 measured data to determine alternator power for a fixed turbine inlet temperature of 750K at various shaft speeds.

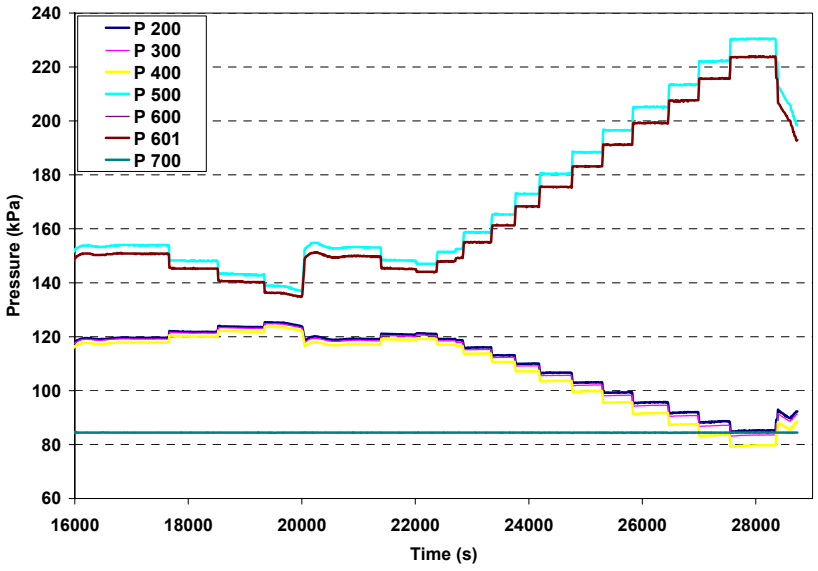

Figure 4-19: TT6 measured pressure data for the 750 K alternator power versus shaft rpm data.

Also shown in Figure 4-20 is the RPCSIM prediction for the generated power which is plotted as the dark blue dashed line. Note that the general shape and magnitude between the model and measurements are similar, however there are clear deviations. One deviation is the hysteresis effect observed at 35,000 and 40,000 rpm. We spent some time exploring this behavior and observed that as we decreased the rpm from higher shaft speeds to lower speeds, at 35,000 rpm there was a step increase of about 400 W in the reported generator power. However as the shaft speed was increased the reported generated power decreased by about 400 W between 39,000 rpm and 40,000 rpm. As mentioned before, this phenomenon has been described as an attempt by the Capstone controller to avoid a shaft speed resonance. While running the loop, the authors notice no obvious changes in sound or any other evidence of a disturbance within the loop.

Other contributing effects to the differences between the model and the measurement are probably due to differences between the actual characteristic flow curves and the real curves and also the accuracy of the alternator model. Currently the alternator model uses a linear fit that gives the efficiency as a function of rpm. This a very heuristic model and is not based on phenomenological models. The linear model currently reduces the mechanical power by 400 at 25,000 rpm and increasing to 800 W at 90,000 rpm.

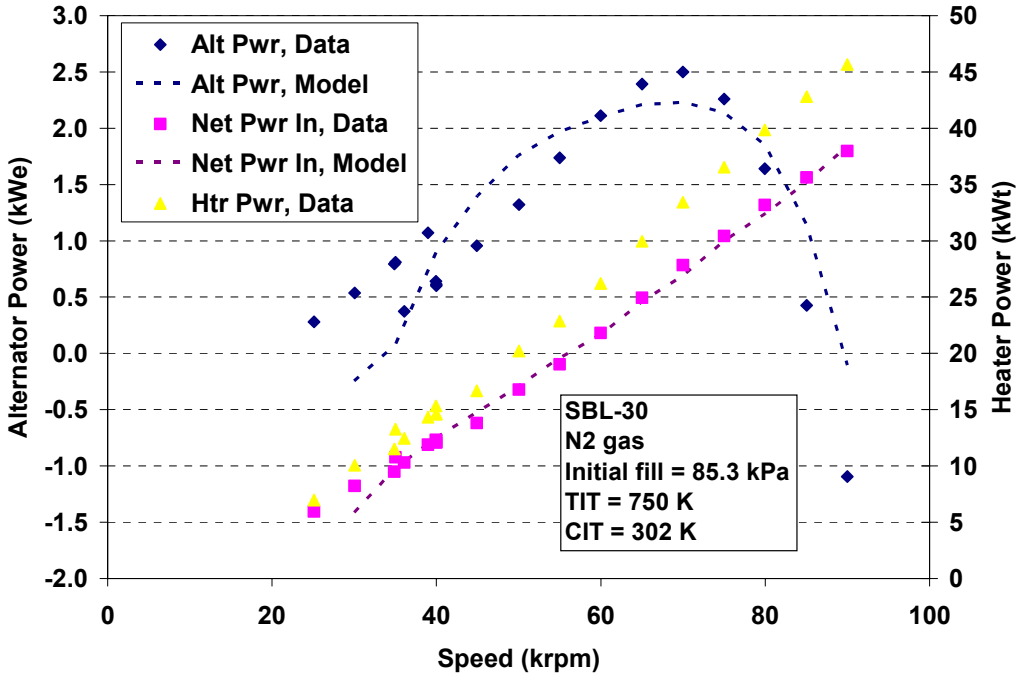

Figure 4-20: Extracted 750 K data of alternator power versus shaft speed for TT6.

4.4.1.3 700-K Turbine Inlet Temperature Measured in TT6

The next segment of data measured the generated power as a function of shaft speed at 700 K. The summary data is shown in Figure 4-21 and covers the time span from 28,000 seconds to 34,000 seconds. Again observe that the TIT was kept constant at 700 K while the shaft speed

was reduced from 80,000 rpm to 25,000 rpm. The measure alternator power is again shown as the light brown curve, which decreases in steps from about 700 W to 150 W near the end of the run. The measured gas pressure data is shown in Figure 4-22, and it has the usual shape.

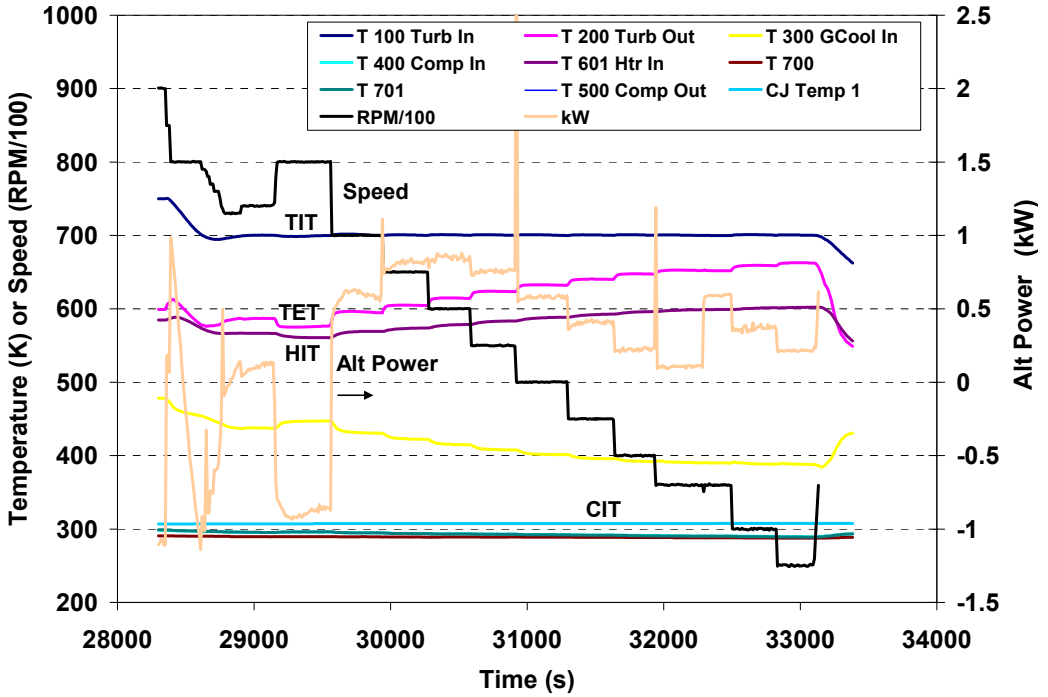

Figure 4-21: Summary thermal data segment of TT6 to measure alternator power versus shaft speed at 700 K.

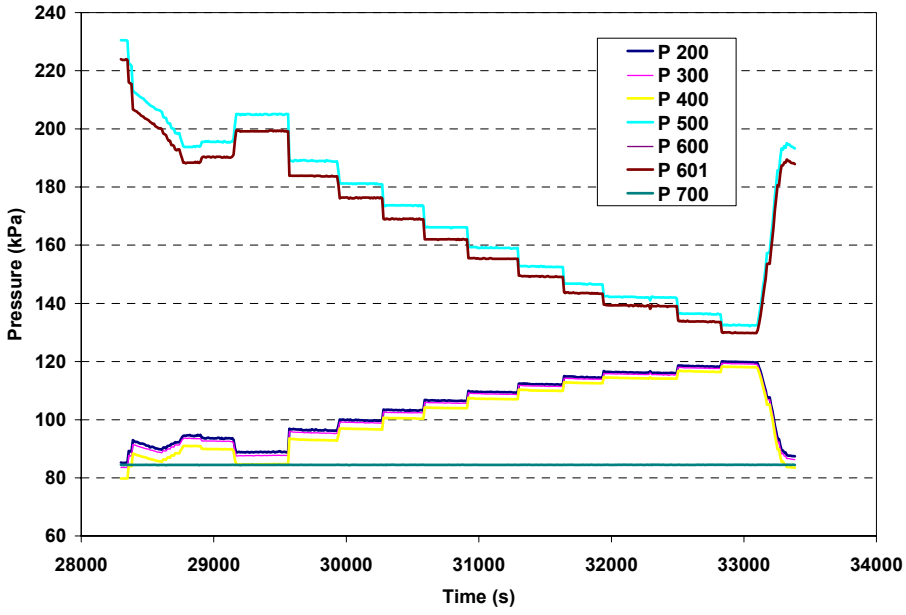

Figure 4-22: Pressure data for the TT6 segment kept at 700 K.

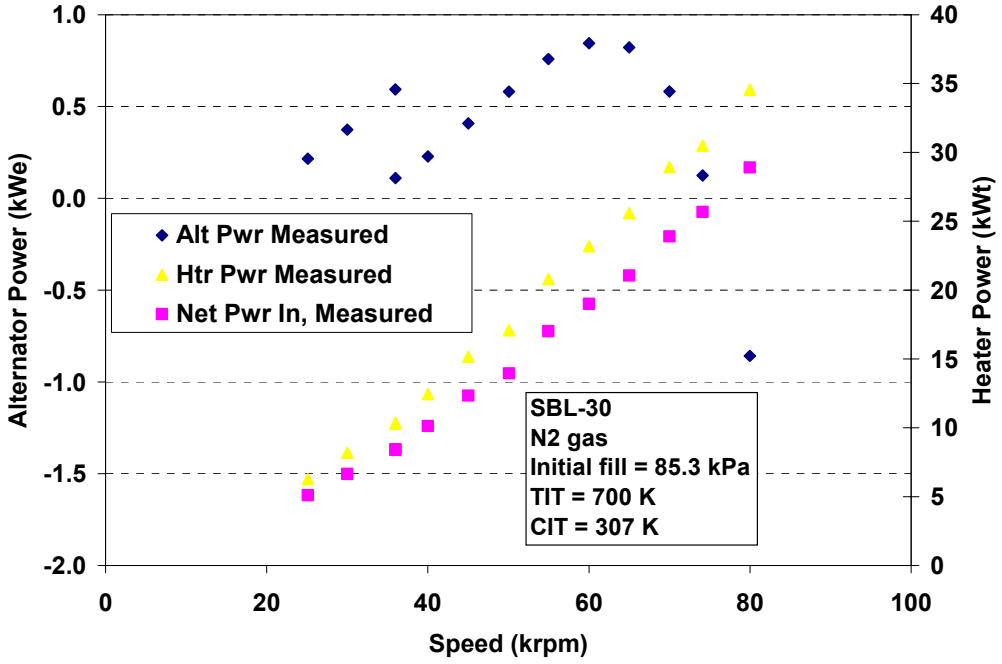

Figure 4-23: Extracted 700 K data of alternator power versus shaft speed for TT6.

The summary data for the generated power versus rpm curve is plotted Figure 4-23 for the turbine inlet temperature of 700 K. Note that it has the same shape as before and again exhibits the nonlinear nature of the CBC loop at high shaft speeds. The hysteresis effect is again illustrated at shaft speeds below 40,000 rpm.

4.4.1.4 650-K Turbine Inlet Temperature Measured in TT6

The next segment of data measured the generated power as a function of shaft speed at 650 K. The summary data is shown in Figure 4-24 and covers the time span from 4,000 seconds to 16,000 seconds. Again observe that the TIT was kept constant at 650 K while the shaft was reduced from 80,000 rpm to 25,000 rpm. The measure alternator power is again shown as the light brown curve, which decreases in steps from about 400 W to -1.800 W. The measured gas pressure data is shown in Figure 4-25 and has the usual shape showing increasing pressure differences with higher shaft speeds.

The summary data for the generated power versus rpm curve is plotted Figure 4-23 for the turbine inlet temperature of 650 K. Note that it has the same shape as before above 40,000 4pm but this time the peak is less pronounced but still observable. In fact the data is almost horizontal very close to zero power. This indicates that the TIT must be above 650 K before positive power can be produced at any speed. The hysteresis effect is again illustrated at shaft speeds below 40,000 rpm. Notice this time that the data is recorded at more shaft speeds thus the reported power jump at 35,000 for decreasing shaft speeds and 40,000 for increasing shafts speeds was measured much more thoroughly.

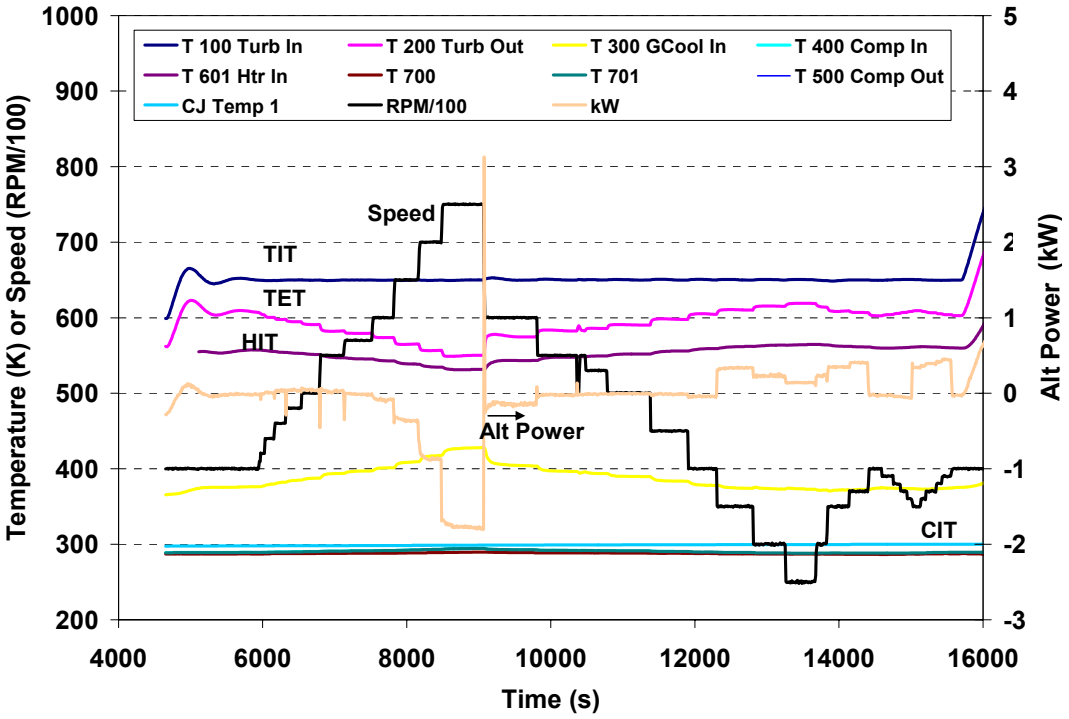

speed

Figure 4-24: Summary thermal data segment of TT6 to measure alternator power versus shaft speed at 650 K.

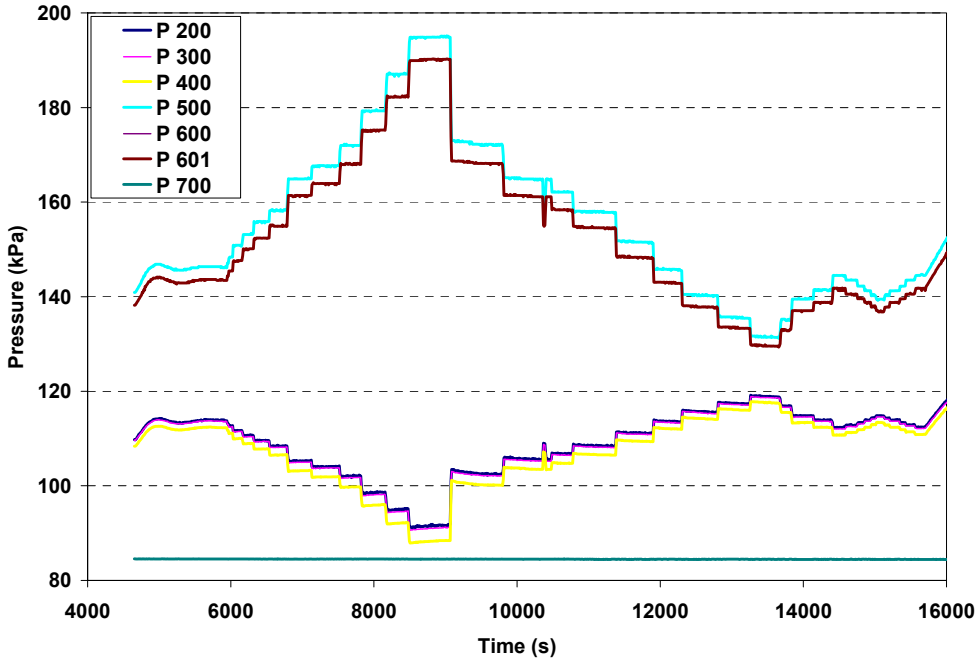

Figure 4-25: Pressure data for the TT6 segment kept at 650 K.

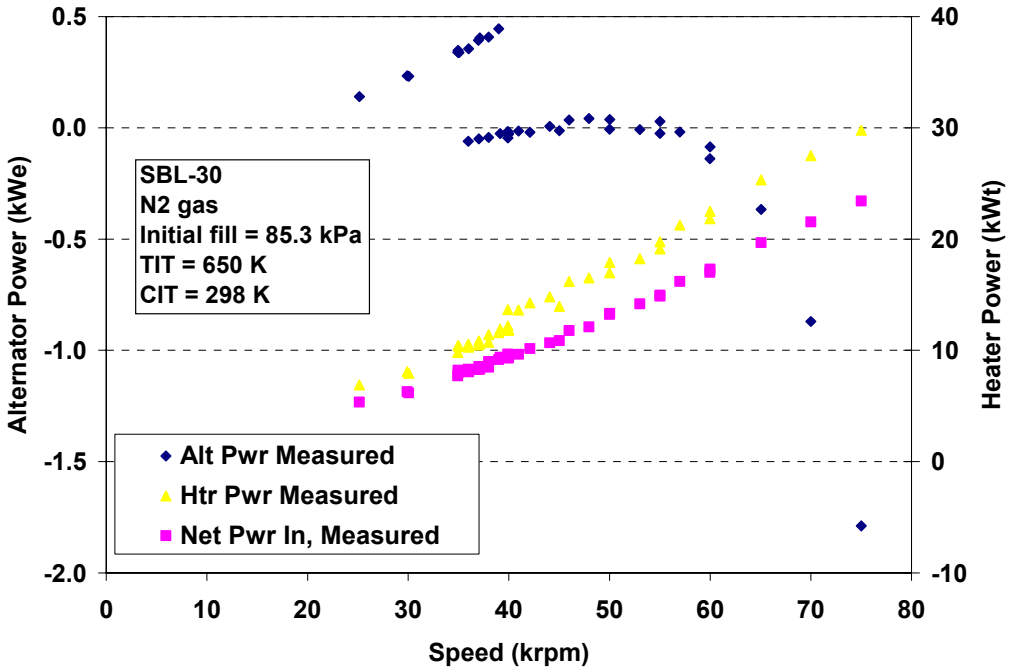

Figure 4-26: Extracted 650 K data of alternator power versus shaft speed for TT6.

4.4.1.5 600-K Turbine Inlet Temperature Measured in TT6

The next segment of data measured the generated power as a function of shaft speed at 600 K. The summary data is shown in Figure 4-27 and covers the time span from 3,000 seconds to 6,000 seconds. Again observe that the TIT was kept constant at 600 K while the shaft was varied from 35,000 rpm to 60,000 rpm. The measure alternator power is again shown as the light brown curve. The measured gas pressure data is shown in Figure 4-28. It has the usual shape showing increasing pressure differences with higher shaft speeds.

The summary data for the generated power versus rpm curve is plotted Figure 4-23 for the turbine inlet temperature of 600 K. Note that in this test run, the shape of the operational curve is different than previously measured. Now the shape of the alternator power curve above 40,000 rpm is always negative (and decreases from -250 W to -400 W. This indicates that the alternator must be motored to spin because insufficient power is being produced by the turbine compared to what is being consumed by the compressor. The negative slope for the operating curve was expected because the previous data showed that the TIT must be above 650 K before positive power can be produced at any speed.

The hysteresis effect is again illustrated at shaft speeds below 40,000 rpm. Notice this time that the data is recorded at more shaft speeds thus the reported power jump at 35,000 for decreasing shaft speeds and 40,000 for increasing shafts speeds was measured much more thoroughly.

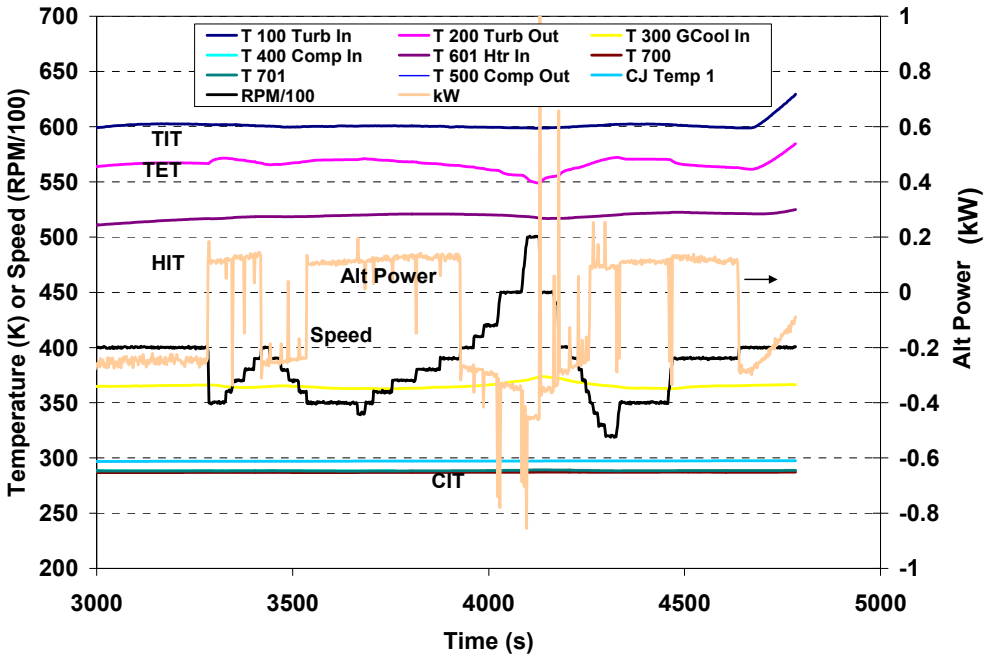

Figure 4-27: Summary thermal data segment of TT6 to measure alternator power versus shaft speed at 600 K.

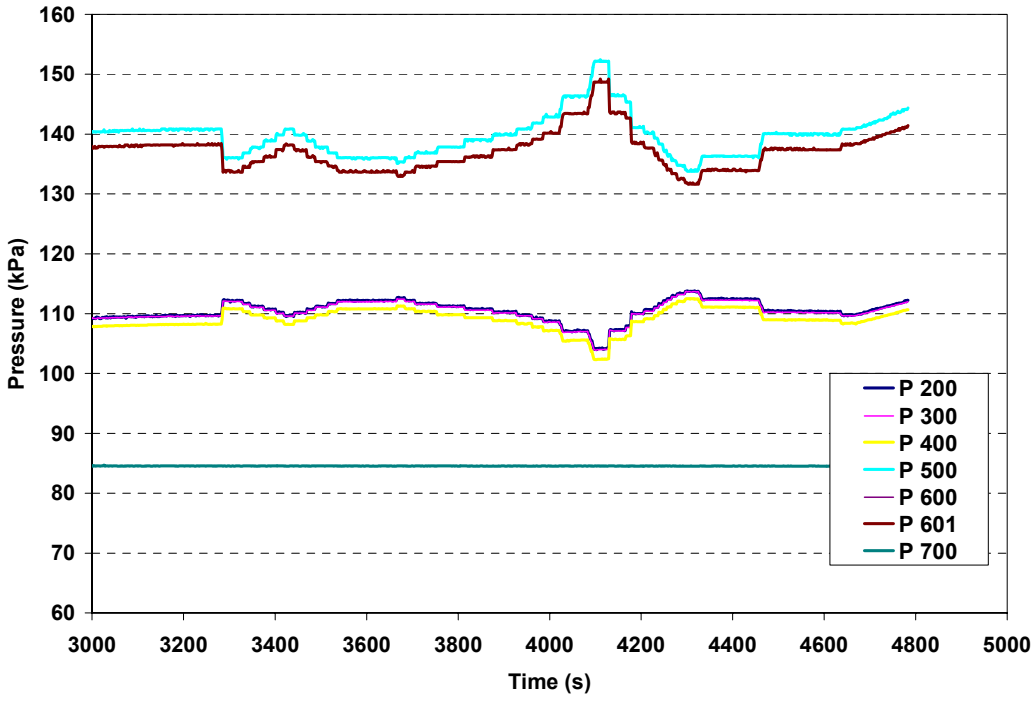

Figure 4-28: Pressure data for the TT6 segment kept at 600 K

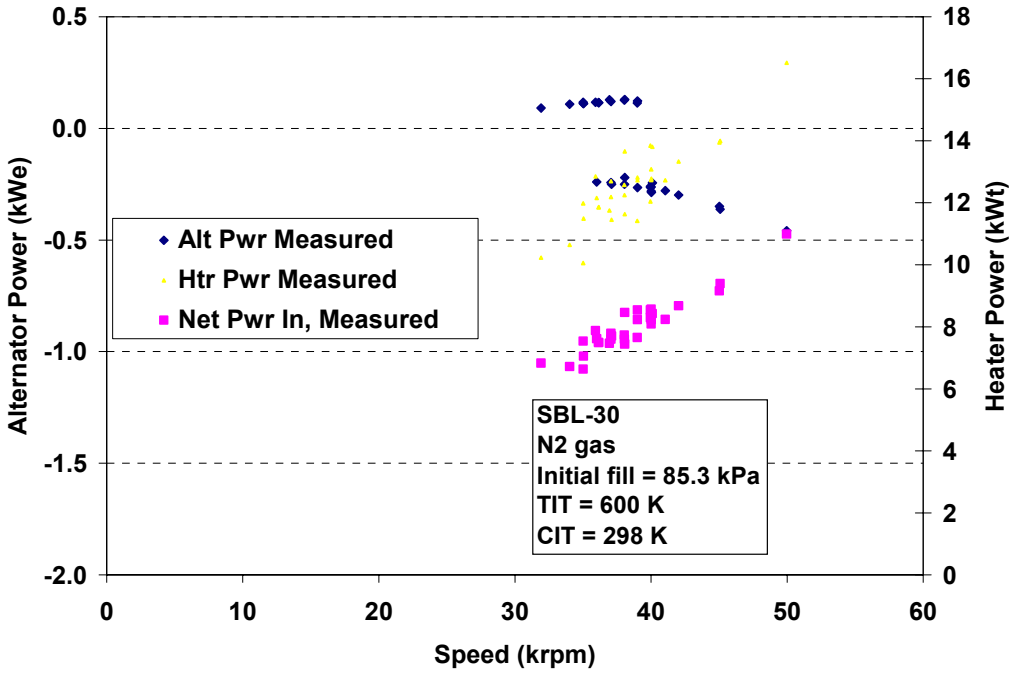

Figure 4-29: Extracted 600 K data of alternator power versus shaft speed for TT6.

4.4.2 Power vs. Speed Summary of Measured Operations Curves for the Sandia Brayton Loop

A summary of all data just described is shown in Figure 4-30. It shows the generated power as a function of shaft speed at the five turbine inlet temperatures of 600 K, 650 K, 700 K, 750 K, and 880 K. The trend and overall behavior is clear and closely resembles the predictions shown in Figure 2-28.

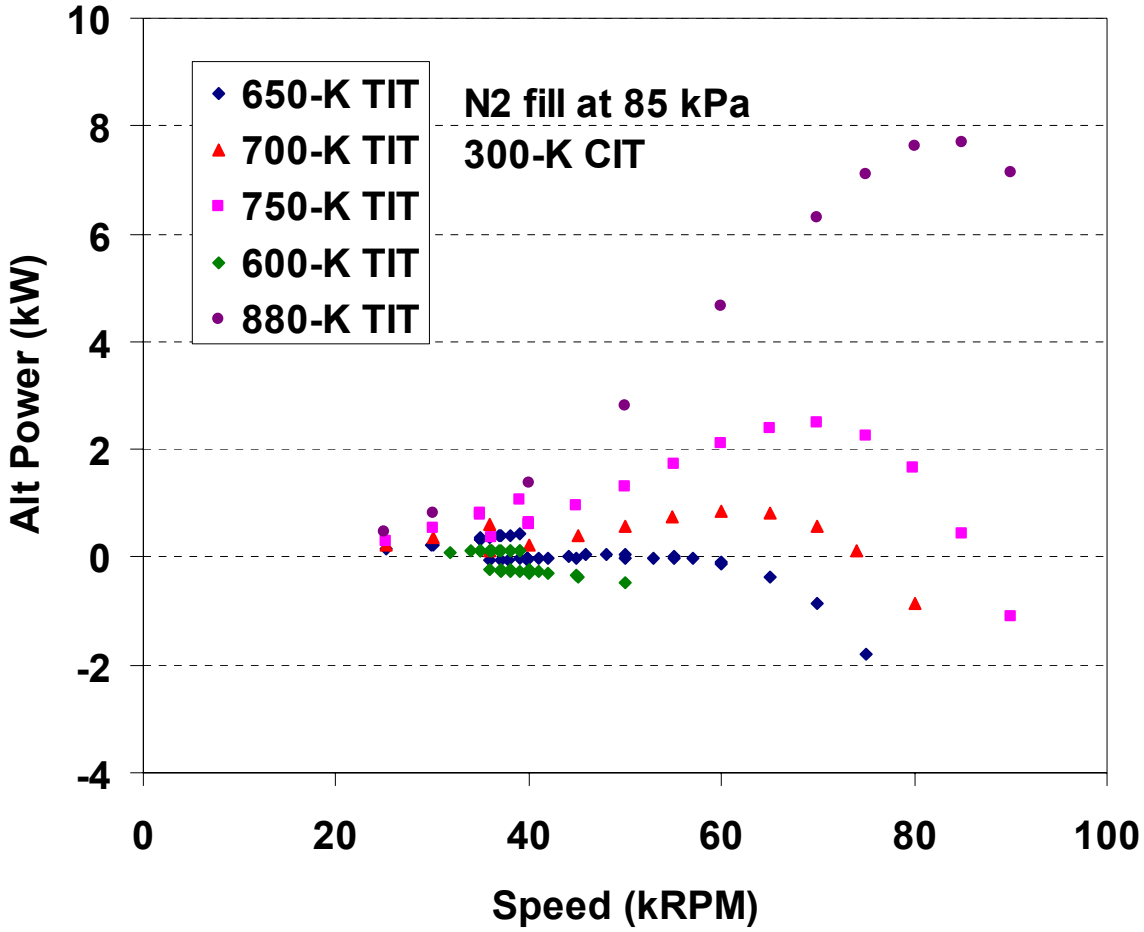

Figure 4-30: Summary data of all power versus speed measurements made in tests TT5 and TT6.

4.5 Reactor Shutdown Simulations

A GCR driving a Closed Brayton Cycle is one of the primary options for high-efficiency electricity generation for the next-generation commercial nuclear power plants (Pope 2003, and Peterson 2005). The main reason for the interest is the reactor's ability to produce high temperatures (up to 1175 -1200 K) which enables the reactor to produce electricity at high efficiencies (> 40%) using CBC systems and/or to use chemical decomposition processes to produce hydrogen. In addition several prototype reactors have been built and operated thus a valuable database for these types of reactors exist. In fact gas cooled reactors are the only reactors that have operated in sustained operations at these temperatures. Partially for these reasons the GCR was also the selected space reactor option for an electric propulsion spacecraft for a mission to Jupiter (Wollman, 2005). The down selection of the reactor type was made by the Naval Reactor Prime Contract Team funded by NASA.

An important issue regarding space reactors (where auxiliary power is not readily available) is how to shut down the reactor and remove the decay heat generated by the fission products in the reactor fuel. This chapter addresses this question for reactors that use a closed Brayton

loop as it power conversion system. Even though the analysis and tests were performed for gas cooled reactors, the results are equally valid for LMRs that are coupled to CBC power conversion systems. The results are presented by comparing experimental data obtained from the Sandia Brayton Loop (SBL-30) and predicted by RPCSIM, the dynamic simulation model. This data and analysis explores the power that can be removed from the structural thermal inertia to simulate heat removal following a reactor shutdown.

4.5.1 Decay Heat Removal Issue Description

Figure 4-31 shows the amount of decay power in a nuclear reactor vs. time since shutdown. The various curves portray the amount of time that the reactor had operated steadily at full power prior to shutdown (Hetrick, 1971). The power drops to about 3% of full power in about 20 seconds, and then it slowly declines after that. It takes about an hour to reach 1% of full power. Notice also that it takes a month or two to reach 0.1% of full power. For a commercial reactor one might depend on an external source of electrical power to run the compressor and keep the coolant flowing after shutdown. But eventually the externally-driven flow would need to be turned off. The situation is more demanding for a space reactor. There likely will not be an external source of power to motor the compressor after shutdown, or if batteries are used the duration might be severely limited. The space reactor systems will likely be designed to lose heat passively (via conduction and thermal radiation to space) at about 1% of full power. So the challenge is to remove heat via convection until that power level is reached.

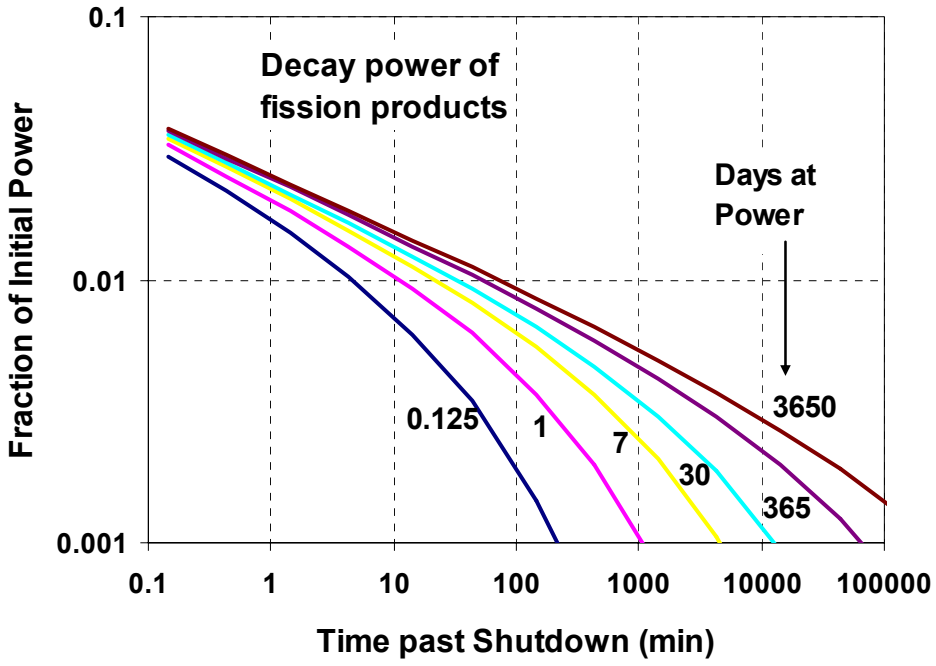

Figure 4-31: Decay power levels after shutdown.

A key question is how long can a CBC operate with small or negligible power being generated, and also at what shaft speed should the decay heat removal phase use. That is, how low long can a small but positive power be generated at a low flow rate which correspond to a low shaft

speed (at constant turbine inlet temperature)? Essentially we are asking how low can the power and flow (shaft speed) be reduced and keep the CBC self-sustaining.

As an aside, a system could be designed to operate at any thermal power level desired. But once a system is designed for set power (e.g. 1 MW of thermal power), it might not be self-sustaining at significantly lower power (e.g. below 0.2 MW). This is all a function of the compressor and turbine performance curves and the flow resistance in the CBC loop.

4.5.2 Sandia Brayton Loop Decay Heat Removal Test (TT5)

The SBL-30 can provide an illustrative example of the limitations of self-sustained flow in a CBC system. The decay heat removal test was performed in test TT5. In this test, which is shown in Figure 4-7, the turbine inlet temperature was brought to 880 K and kept at that temperature while the shaft speed was reduced from 90,000 rpm to 25,000 rpm. At about 20,000 seconds into the run the electrical heater power was turned off. Then the shaft speed was manually adjusted to keep the alternator power at 500 W.

Figure 4-32 shows the predicted power generated by the SBL-30 vs. turbine speed for a turbine inlet temperature of 880 K. As can be seen, the minimum speed needed to maintain self-sustained flow is 30,000 rpm. This is about 30% of the full speed that the system is designed for. The thermal power at this speed is predicted to be 8 kWt, which is about 13% of the full design power. So if the electrical heater were replaced by a reactor, there would be gap between the 13% of full power that the system can maintain self-sustained flow at and the 1% of full power where heat can be removal by radial conduction and radiation. However, this is the case only in steady state. Fortunately, transient effects and thermal inertia can be used to keep the CBC loop running while the decay heat reduces to levels below 1%. In effect the

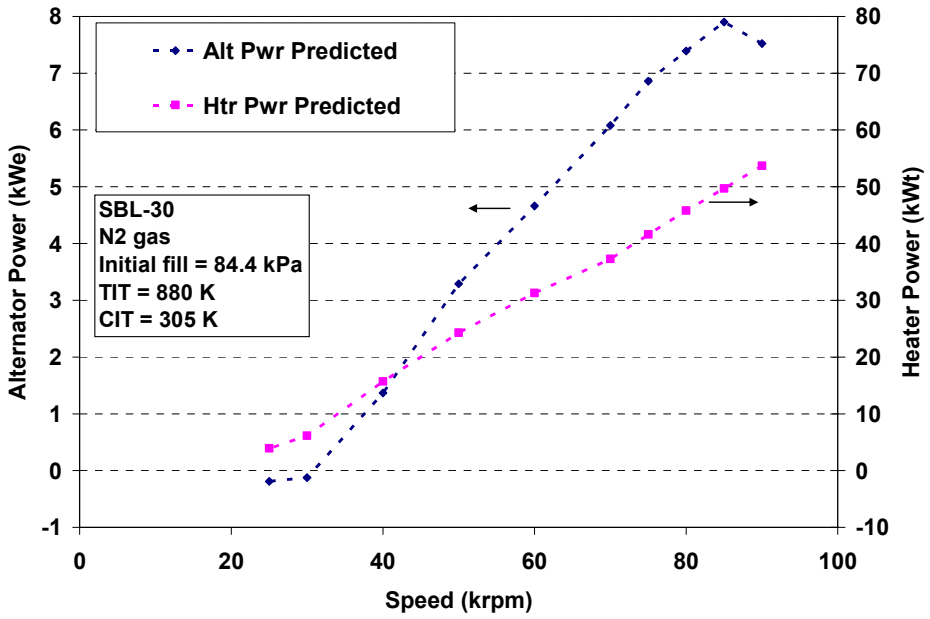

Figure 4-32: Predicted power produced by SBL-30 vs. turbine inlet temperature.

sensible heat stored in the reactor fuel, vessel, piping, and other components is used to temporarily keep the system running while the decay power decays to an acceptable level of around 1%. As these systems cool they will deliver a considerable amount of power into the gas flow which could maintain the flow in the CBC. How much power is delivered in this fashion, and how long it will last, is a function of the speed of the turbo-machinery.

To test this approach, the SBL-30 was operated with the electrical power off and the speed low for as long as possible at the end of the data run just discussed (starting at about 20,000 seconds). In addition, the speed was adjusted so that the alternator produced about 500 W_e (to simulate the power needed for reactor control in a stand-alone system). Figure 4-33 shows the gas temperatures for that time period. The turbine speed had to be increased slowly to maintain 500 W as the TIT and other temperatures decreased. The system produced 500 W of electrical power for 71 minutes after the heater was turned off. Had this been a reactor, the decay power would have decayed to about 1% of full power in that time. This power level would likely be low enough to remove by conduction and thermal radiation radially through the vessel and neutron reflectors for a space reactor.

When the TIT reached 666 K, the system stalled abruptly and began drawing power from the grid to maintain the gas flow. This rapid change in power was later determined to be caused by the Capstone CBC controller hysteresis effect that was described earlier.

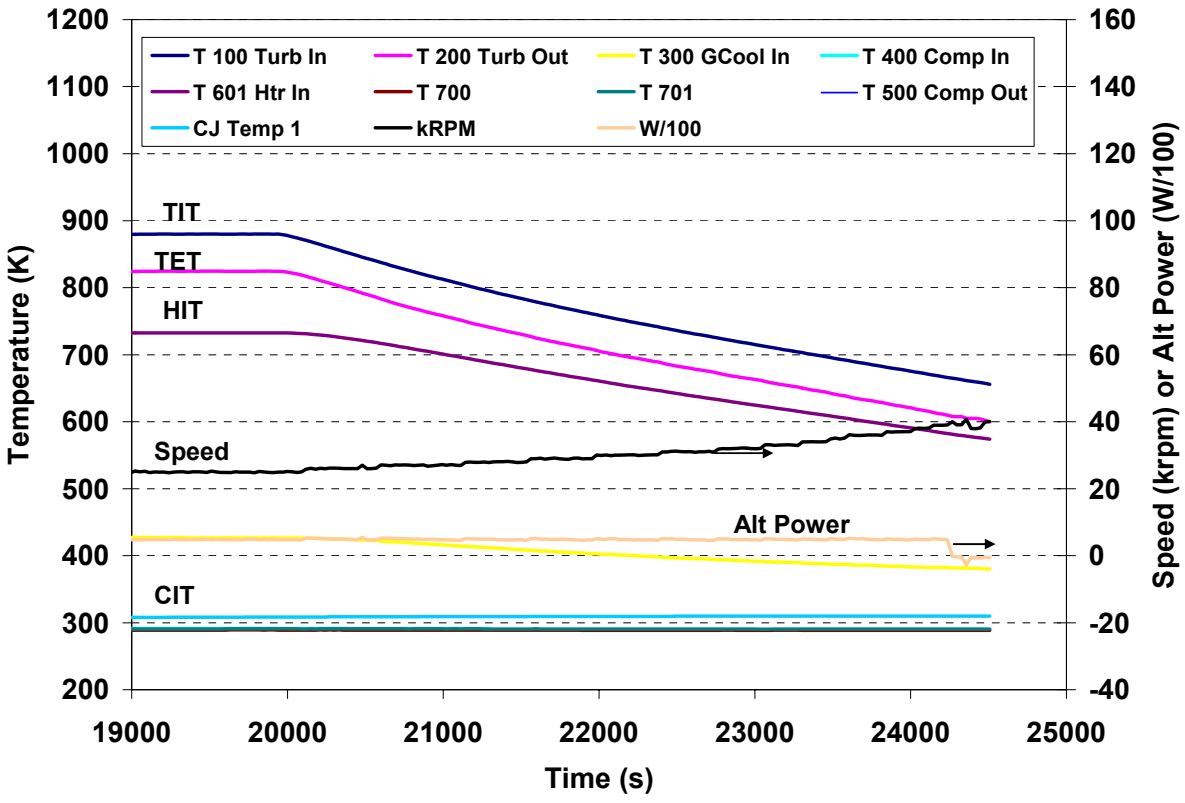

Figure 4-33: Gas temperatures for SBL-30 run with TIT held at 880 K.

4.6 Dynamic Model Predictions of TT5

The dynamic model RPCSIM was used to predict the transient behavior of the Sandia Brayton loop. The Simulink block diagram of the model of the Sandia Brayton Loop is shown in Figure 4-34. This version of the dynamic model is very similar to the model used for the gas cooled reactor except that the reactor has been replaced with an electrical heater and the space based radiator is replaced with a water to gas tube and shell heat exchanger. The turbo-machinery models are identical to the GCR model but the fits to the C30 turbine and compressor flow curves are used. Because of the large amount of power lost to the high temperature flange, the dynamic model of the heater included a flange model. Another difference is that the thermal conductivity of the gas and viscosity are kept constant, unlike the gas cooled reactor model where they are allowed to vary with temperature. Future versions of the RPCSIM SBL-30 model will be upgraded to include these temperature effects.

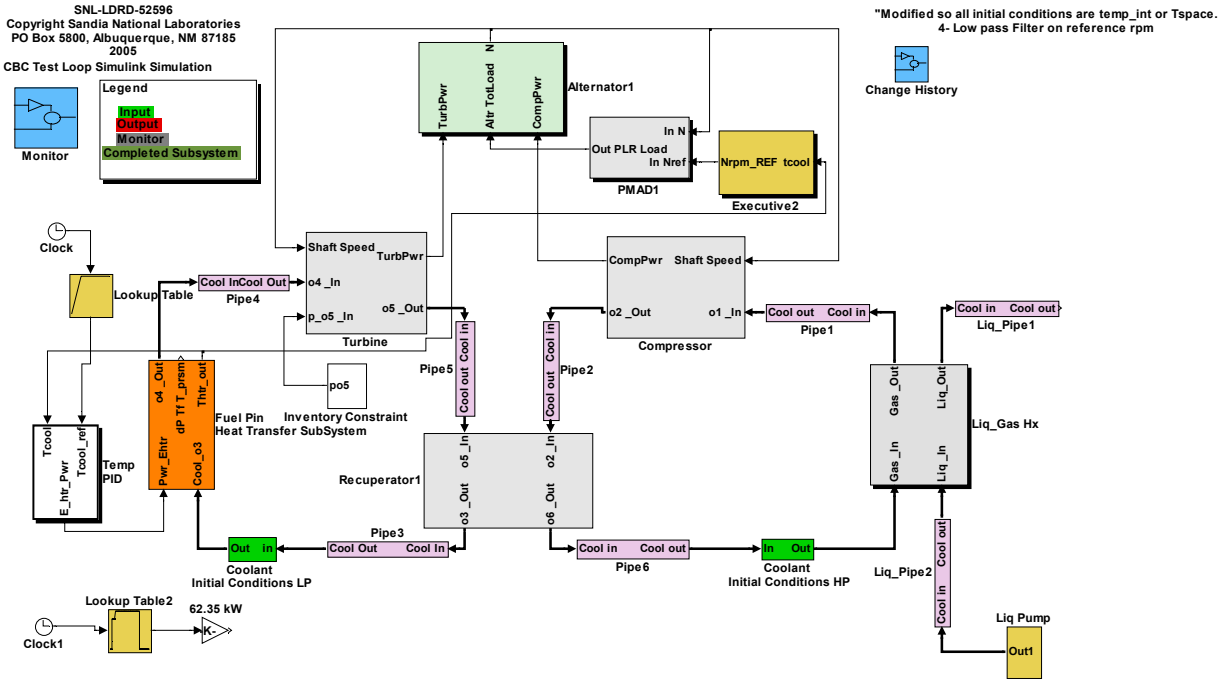

Figure 4-34: RPCSIM block diagram of the Sandia Brayton Loop.

This section of the report uses the RPCSIM Sandia Brayton loop model to predict the thermal behavior of the test loop. In earlier sections of this report some comparisons between the dynamic model and the measured data were made. In these earlier comparisons (see Figure 4-14 through Figure 4-17 and Figure 4-32), the SBL-30 RPCSIM model used a feed back Simulink module to adjust the heater power to keep the turbine inlet temperature at the actual measured TIT. As shown, when this was done the comparisons with the data were overall very good. In this section the SBL-30 RPCSIM model predictions were made by eliminating the feedback loop and simply by using the measured heater power, cooling water flow rate, water temperature, and turbo-alternator-compressor shaft speed. Essentially this phase of the modeling effort uses the measured heater power as input rather than measured turbine inlet temperature.

This type of modeling that is based on the measured heater power was performed for both tests TT5 and TT6, but only the results of TT5 are presented here. The reader is encouraged to compare the predicted results with the measured results that are reported Figure 4-7 through Figure 4-16. The data presented here focuses mainly on the long term transient behavior; as a consequence we are looking at the predictions to see if the heating rates and changes in flow and temperature approximate the actual measurements. Other data that is available looks at the short term behavior (1-10 seconds). Both types of predicted transient behavior generally follow the measured results in shape and magnitude but small differences can be observed. Most of these differences are believed to be caused by the difference in the measured and predicted flow curves as well as the assumption of constant properties for viscosity, thermal conductivity, and heat capacity.

While performing the simulations the authors found that it is important to include much of the geometric detail of the loop and some of the power electronics as well. The RPCSIM SBL-30 model includes all the structural masses, volumes, length, gas volumes, hydraulic diameters, and heat transfer areas that were described in tables Table 3-10 through Table 3-13. In addition accurate models of the heater and the gas chiller were also required (see tables Table 3-4,

Table 3-5, and Table 3-8. We also found that it was important to include models for the alternator, rectifier, regulator, and inverter. At the current time the models for the alternator, rectifier, and inverter are only heuristic. They do not consist of electrical phenomenological models, but they do account for loss effects that are shaft speed dependent and to account for losses or electrical demand to run the fans, inverters, rectifiers and regulators. Currently these models are very simple and do not fully describe all of the observed behavior of the Capstone electronics and controller. Nevertheless they do mimic the observed behavior in a "gross" sense. Typically the power losses appear to predict observed losses to within about 500-700 W. At high power production levels (>7 kWe) this relative error is small, however when we start to compare results at near zero power generation (as required by the decay heat removal tests, and by the determination of the self sustaining conditions) the errors appear to be relatively large. Nevertheless the overall predicted and measured behaviors clearly show similar trends and values.

The SBL-30 RPCSIM model predictions used the heater power transient shown in Figure 4-35. This figure shows the measured electrical heater power (E-Htr-Pwr, solid blue line) which is the main input used in these simulations and actually consists of the measured heater power. Notice that the heater power jumps up and down around +/- 5% about various power settings. During the test (TT5) these perturbations were used to manually keep the measured turbine inlet temperature at 880K. Figure 4-35 also shows the predicted thermal power (power transferred to the coolant in the heater) and the predicted power lost through the gas chiller. The difference between the thermal power in the heater and the power rejected in the gas chiller (neglecting losses to ducts and flanges) is the alternator. The actual alternator power (including the modeled loss effects) is shown in Figure 4-35 as the dark gray line. The measured alternator power for test TT5 can be compared with the model predictions. The

measured alternator power is shown as the tan line within the summary data illustration given in Figure 4-7.

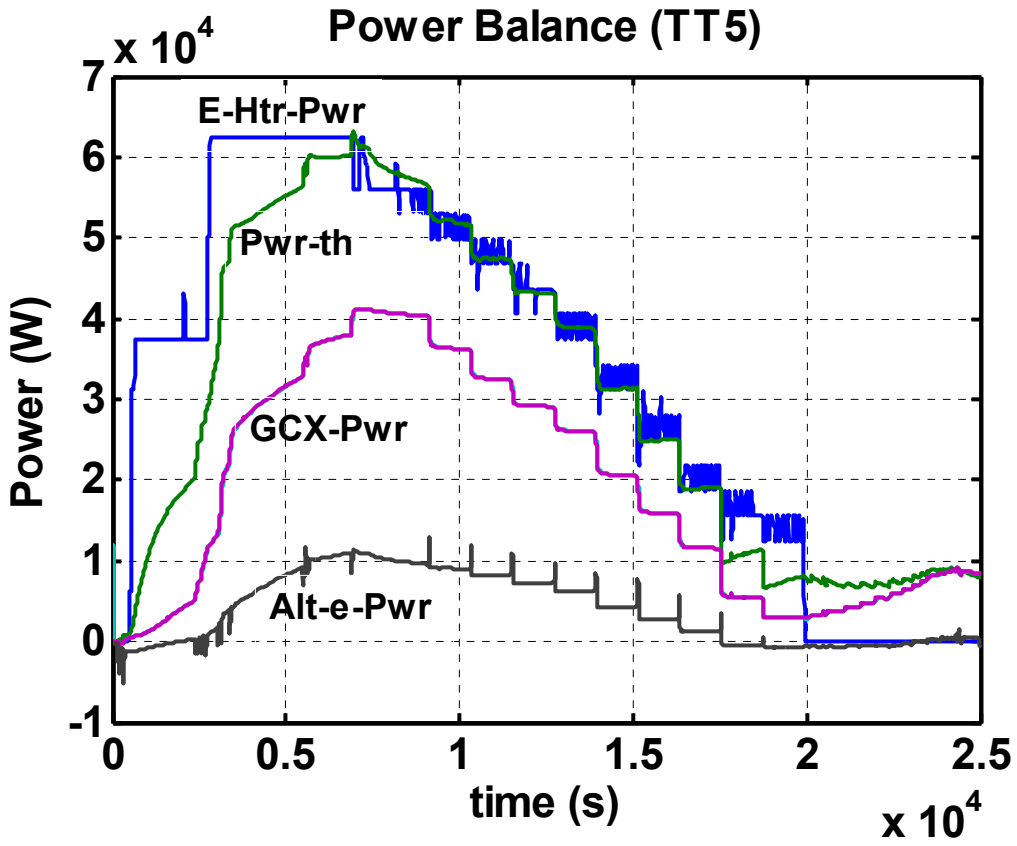

Figure 4-35: RPCSIM model power balance curves for TT5, given the input electrical power for the heater E-Htr-pwr and shaft speed. The Pwr-th curve shows the power transferred to the coolant. GCX-Power shows the wasted heat power rejected in the gas cooler heat exchanger and Alt-e-Pwr shows the power produced in the alternator.

The overall shape of the measured alternator power (tan line in Figure 4-7) compared with the predicted curve in Figure 4-35 are indeed very similar. Both curves peak at about 7000 seconds with the predicted peak alternator power of about 10 kW, while the measure alternator power was about 8 kWe. This difference (8 kWe versus 10 kWe) is thought to be due to the inaccuracies of the characteristic flow curves. After the peak both measured and predicted curves slowly decrease to small values as the rpm is lowered. Also observe that for each step reduction in rpm there is a spike in the alternator power. A reduction in rpm results in a momentary increase in alternator power. This spike in alternator power is followed by a rapid decrease to a power level that is generally less than before the step rpm change. Actually the cause and effect of this behavior is just the reverse of the previous statement. To reduce the rpm requires a momentary increase in load which is equivalent to a momentary spike in alternator (to slow the shaft speed down). As the shaft speed slows less flow goes through the heater/reactor which results in less power being transferred to the gas. To reach the new equilibrium point load (alternator power) must be reduced to match the difference in power

produced and consumed by the compressor at the lower flow/power conditions. The equilibrium point is lower because the flow rate is reduced at the slower shaft speed.

This spiking phenomenon was observed in the measured data but can't be seen in the summary plot as the data that is plotted only includes the measured data plotted at 30 second intervals and it therefore misses the transient power spike. The actual data which is recorded every second shows theses spikes. The spike occurs because the alternator power is proportional to the derivative of the rpm (see equation 2-44). In essence, to decrease rpm, the alternator load has to be temporarily increased to slow the shaft speed, then once the new rpm is achieved the alternator power must be decreased of backed off to a lower value to hold at this new rpm. Of course whether the load increases or decrease also depends on which side of the operating curve the system is starting from.

Also observe that during the decay heat removal portion of the transient (time > 20,000 seconds when the heater power was turned off) that the predicted alternator power levels are predicted to be small but negative, while the observed alternator power levels are small and positive. In the test (see Figure 4-7) the alternator power was kept at 500 W_e for 71 minutes after the heater power was turned off. In the model, the predicted alternator power is nearly constant but near zero as opposed to the 500 W_e value that was measured. It is not surprising that the model incorrectly predicts the alternator power at low levels because as mentioned the alternator and other electrical losses models are simple and do not include all effects. In addition the characteristic flow curves were developed to assure that the model was accurate at 30 kWe and high shaft speeds (near 96,000 rpm) not at low shaft speeds and near zero power. A 10% deviation between measured and predicted flow curves could easily account for these effects. The surprising observation is that the model really does capture virtually all of the measured phenomena both qualitatively and quantitatively (within about 10%).

As just mentioned the main differences between the observations and predictions are currently attributed to inaccuracies in the characteristic flow curves (see section 4.3). Other differences could also be contributing including the assumption that the gas is ideal, has a constant heat capacity, and constant values for viscosity and thermal conductivity, when in fact they vary substantially with temperature. Nevertheless, the trends and relative values of the model are generally within about 10% of the observed/measured values.

Because the code is fast running (at least 1/100 -1/1000 of real time or faster, on a 3 GHz Pentium PC) and produces reasonable results we feel that the dynamic simulation results are indeed remarkably close to the measured data. The run time of the code depends to a large extend on the fidelity used in the heater power. Very detailed heater power transients with 1 second resolution and power fluctuations that vary every second run at about 1/100 of real time, while simple transients that ramp slowly or have long periods of constant power can easily run 1/1000 of real time or even faster. Other dynamic simulation codes that were developed for the Gen IV program are not fast running and have not been compared with real data to date (Pope, 2003 and Peterson, 2005). The reason for the fast running time is that RPCSIM is not "Courant" limited.

The next figure is presented to illustrate the relationship between flow rate and shaft speed. Again this data can be compared with the data shown in the summary plot Figure 4-7. It is included here to show that to first order the flow rate is proportional to shaft speed. For every increase or decrease in rpm there is a corresponding increase or decrease in flow rate.

However, there is a secondary effect caused by the pressurization of the loop due to the heat up of the gas. As the gas heats up early in the transient (from 0 – 4000s) the system pressure increases (see following figures) which results in even more of an increase in flow.

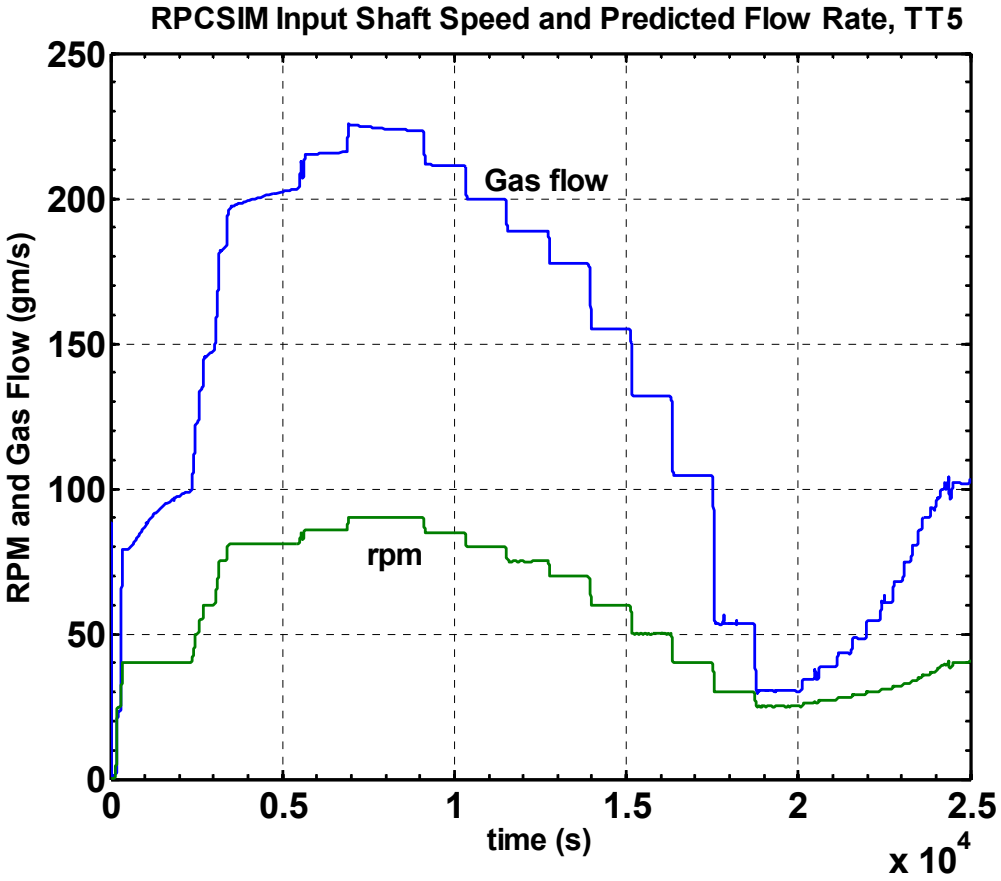

Figure 4-36: RPCSIM input shaft speed (rpm) and predicted gas flow rate for TT5.

The next figure (Figure 4-37) shows the predicted gas temperatures at the heater outlet (Htr-OT), the turbine inlet temperature (TIT), the turbine outlet temperature (TOT), the heater inlet temperature (HIT), the gas chiller inlet temperature (GCX-IT) and the compressor outlet temperature (COT). Again these values can be compared with the measured temperatures shown in Figure 4-7. As before the trends and values between the measured and predicted curves are very comparable and are generally within 10% of each other, but differences are apparent. For example the predicted TIT does not stay constant at 880 K, but fluctuates from a high value of 890 K to a low value of 830 K. At this time we aren't sure if these thermal differences are due to the flow curves, the assumption of constant properties or to energy balance issues that might cause the model to have greater/different heat losses than our measured thermal data indicates.

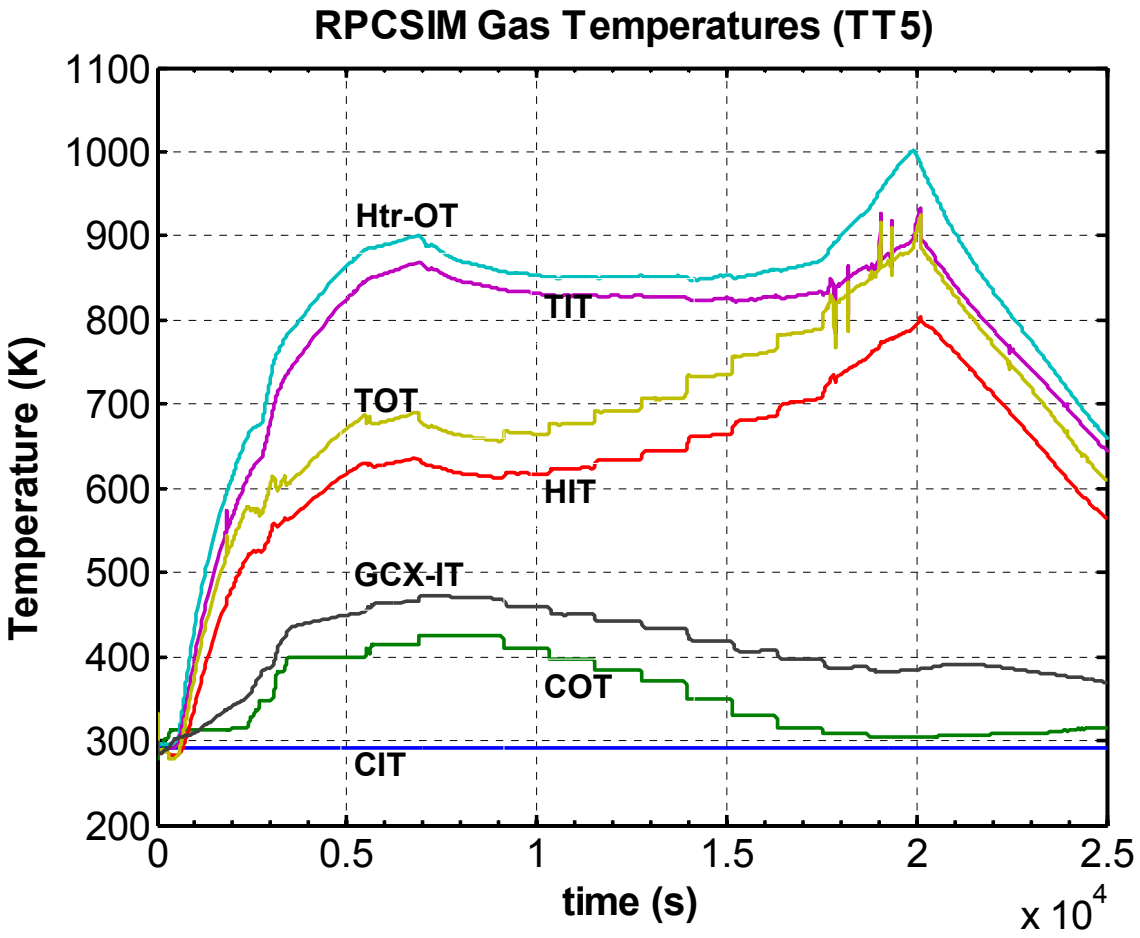

Figure 4-37: RPCSIM predicted gas temperatures for TT5 using measured input for the electrical heater power and the shaft speed.

The next set of data compares the predicted and measured pressure data. Figure 4-37 shows the predicted pressure in the loop. Note that there is a high pressure and low pressure leg of the loop. At the beginning of the transient the two legs are at the same pressure. When the turbo-machinery starts spinning (~250 s) the pressures begin to deviate. Then once the heater is turned on (~500 s) the pressures both begin to increase while still maintaining a difference. At about 2300s the shaft speed was greatly increased from 40,000 rpm to 80,000 rpm. Because the pressure ratio is proportional to the square of the shaft speed this plot shows a marked increase in the system pressures at this time. Notice that there is a tendency for the low pressure leg to decrease in pressure for large rapid increases in shaft speed. The reverse is also true.

For comparison purposes the reader should compare the pressures predicted in Figure 4-37 with the measured pressures shown in Figure 4-12. The comparison is really very good with both the magnitude and value being virtually the same. This comparison is also illustrated in Figure 4-39 where the predicted and measured pressure ratios are shown side by side. Again the two curves are virtually identical. However, a closer look reveals that the pressure drop through the system piping and ducting is still not being predicted as accurately as we would like. This will be further explored in future tests and by making further improvements to the model.

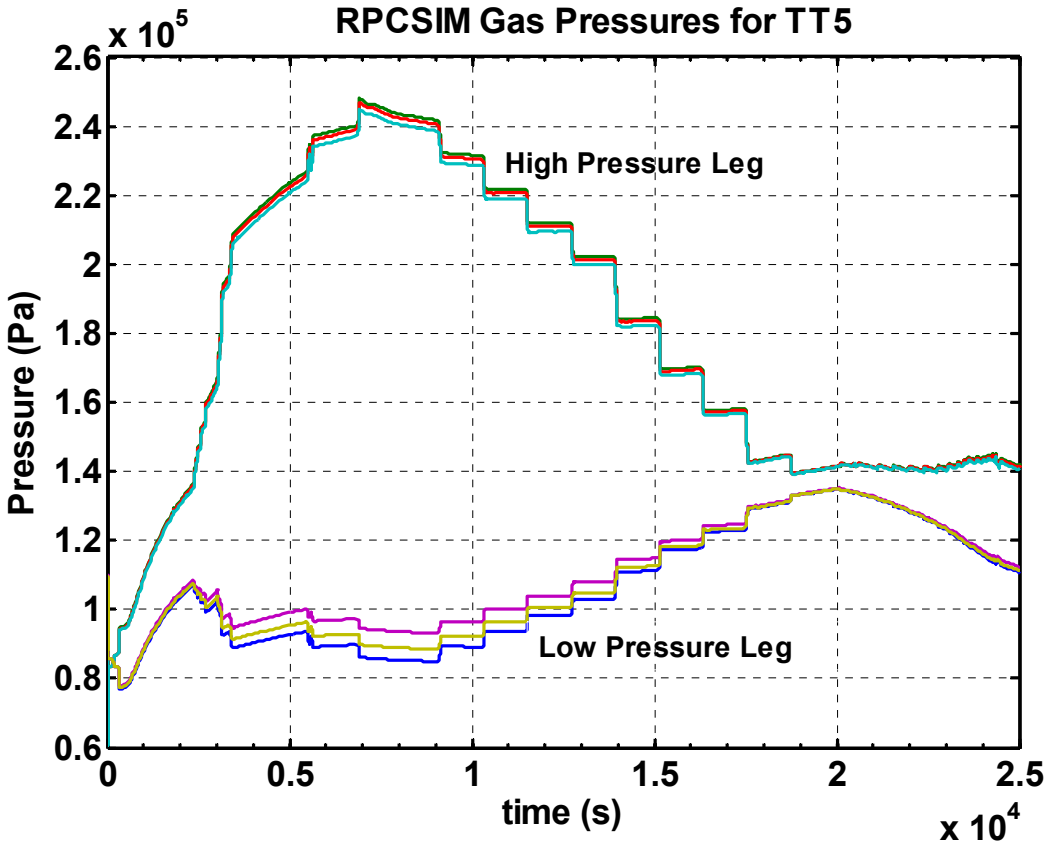

Figure 4-38: RPCSIM calculated gas pressures at each station around the loop for test TT5 given the input power and rpm. The curves show the high and low pressure legs, and the small deviations due to frictional pressure drop simulated by the model.

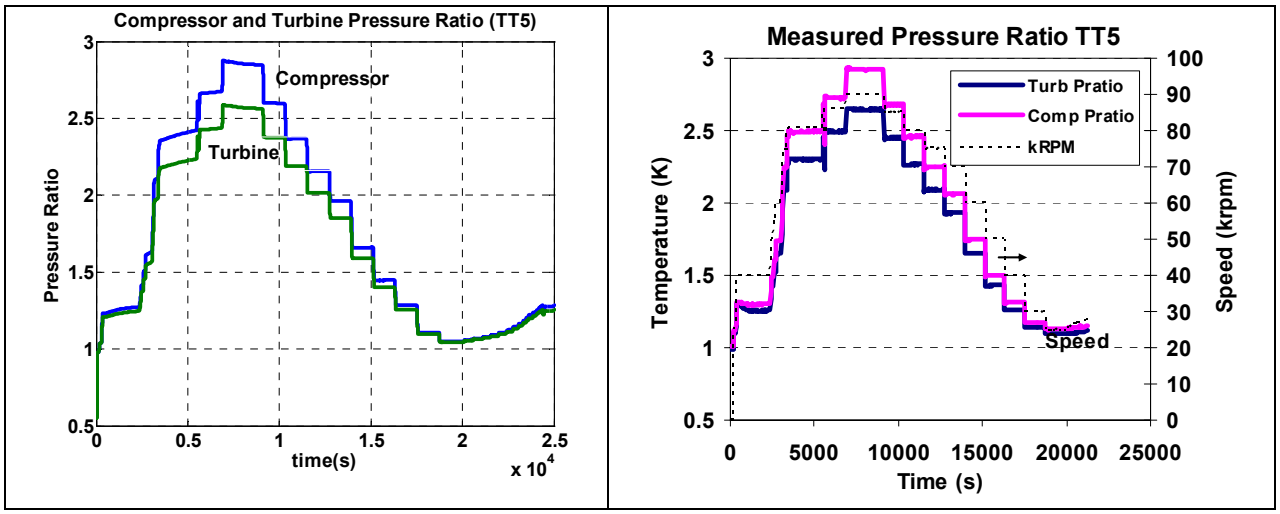

Figure 4-39: Predicted compressor and turbine pressure ratio for test TT5.

Overall this validation effort shows that the code RPCSIM model is quite good at predicting the major trends and even the values of the pressure and temperatures. All of the data is easily predicted to within 10% of the measured data and much of it is far more accurate on the order of 3-5%. Many of the actual detailed measured short term results are predicted faithfully as well, such as the spikes in the power when the shaft speed is changed and the rates of increase for the temperatures and pressures. We haven't fully investigated this short term detail as yet. Overall it appears that the results of the model are only as good as the for the characteristic flow curves. We've shown that clear differences between our flow curve predictions and measurements exist and are only good to about 10%. To further improve the model we must increase the fidelity of the flow curves, include temperature dependent properties for thermal conductivity, viscosity, and heat capacity. We also need to assure closely examine the energy balance throughout the loop and within each component. Performing these required additional tests and improving the models will be the focus of further efforts at Sandia within the Next Generation Program.

5 Summary and Conclusions

This report describes the results of a Sandia National Laboratories internally funded research program to study the coupling of nuclear reactors to gas dynamic Brayton power conversion systems. The research focused on developing integrated dynamic system models, fabricating a 10-30 kWe closed loop Brayton cycle, and validating these models by operating the Brayton test-loop. The closed Brayton cycle model was developed and implemented in SIMULINK™. Models for all the major components (turbines, compressors, reactors, ducting, alternators, heat exchangers, and space based radiators) were developed for gas cooled reactors, liquid metal reactors, and electrically heated simulators. Various control modules that use proportional-integral-differential (PID) feedback loops for the reactor and the power-conversion shaft speed were also developed and implemented. The simulation code is called RPCSIM (Reactor Power and Control Simulator).

An open-cycle commercially available Capstone C30 micro-turbine power generator was modified to provide a small inexpensive closed Brayton cycle test loop called the Sandia Brayton test-Loop (SBL-30). The SBL-30 test loop was operated at the manufacturers site (Barber-Nichols Inc.) and installed and operated at Sandia. A sufficiently detailed description of the loop was provided in this report along with the design characteristics of the turbo-alternator-compressor set to allow other researchers to compare their results with those measured in the Sandia test-loop.

The SBL-30 test loop was operated and compared with the modeled results to develop a more complete understanding of this electrically heated closed power generation system and to validate the model. The measured and predicted system temperatures and pressures are in good agreement, indicating that the model is a reasonable representation of the test loop. Typical deviations between the model and the hardware results are less than 10%. Both steady state and transient effects were measured in the Brayton loop and compared with dyanamic model predictions from RPCSIM. One of the most unique predictions and comparisons with the data are the shapes of the steady-state power curves. These curves show the electrical power that can be generated (and required reactor or heater power) as a function of turbine shaft speed. The curves reveal the non-linear nature of the closed CBC power conversion system which can generate the same power at two shaft speeds. Both solutions are equally valid steady-state solutions, however only the higher speed solution is inherently dynamically stable. Unfortunately, this solution is not where one would desire to operate the plant as it has lower efficiency than the lower speed solution. The CBC system can operate at the more efficient power versus rpm point only if a rapid electronic control system is used to dynamically keep the system running at the more optimum shaft speed.

Additional SBL-30 tests were performed to assess the capability of the Brayton engine to continue to remove decay heat after the reactor/heater is shutdown, to develop safe and effective control strategies, and to asses the effectiveness of gas inventory control as an alternative means to provide load following. In one test the heater power was turned off to simulate a rapid reactor shutdown, and the turbomachinery was driven solely by the sensible heat stored in the heater for over 71 minutes without external power input. This is an important safety feature for CBC systems as it means that the closed Brayton loop will keep cooling the reactor without the need for auxiliary power (other than that needed to circulate the waste heat rejection coolant) provided the heat sink is available.

References

ASME, “Measurement of Fluid flow in Pipes Using Orifice, Nozzle, and Venturi”, ASME MFC-3M-1989, Reaffirmed 1995, 1989.

Atomic Energy Commission, The ML-1 Mobile Nuclear Power Plant: The Army Gas Cooled Reactor Systems Program, National Reactor Testing Station, AEC brochure or report, circa 1963-1966.

Balje O. E., *Turbomachines: A Guide to Design, Selection and Theory,* John Wiley and Sons, New York, 1981.

Barber-Nichols Inc, 6325 West 55th Avenue, Arvada, CO 80002, http://www.barber-nichols.com, 2005.

Blair D. T. A. in J. M. Meek J. M. and Craggs J. D., Electrical Breakdown of Gases, J. Wiley & Sons, New York, NY, 1978.

Bird, R B., W. E. Stewart, and E. N. Lightfoot. *Transport Phenomena*, J. Wiley & Sons, New York, NY, p 259, 1969.

Bragg-Sitton S. and J.P. Holloway. “Reactor Start-up and Control Methodologies: Consideration of the Space Radiation Environment,” in *Proceedings of Space Technology and Applications International Forum (STAIF-2004)*, pp 614-622, February, 2004.

Brey, H. L. “Current Status and Future Development of Modular High Temperature Gas Cooled Reactor Technology,” IAEA, Tecdoc=(electronic version), 1999-2000.

Breismeister, Judith F. (Editor), "MCNP A General Neutron Particle Transport Code Version 4B," UC705 and UC700, LA-12625-M, Version 4B Manual, March 1997.

Brunhouse J. S. Jr. and G. W. Titus, “Nitrogen, Air Acceptable to Cool ML-1”, *Nucleonics*, February 1961.

Buckingham E. “On physically similar systems: illustrations of the use of dimensional equations”, *Physical Review* 4(4): 345, 1914.

CBC pressure safety data package (Lipinski, Wright, 2005).

Capstone Turbine Corporation, 21211 Nordhoff Street, Chatsworth, CA 91311, http://www.microturbine.com

Chapman, Alan J. Heat Transfer, Macmillan Company, NY, 1967.

El-Genk M.S., H. Xue, and D. Paramonov. “Start-up Simulation of a Thermionic Space Nuclear Reactor System,” in *Proceedings of the 10th Symposium on Space Nuclear Power Systems*, CONF-930103, M. S. El-Genk and M. D. Hoover, eds., American Institute of Physics, January, 1993.

Fuller R., Barber-Nichols Inc. Personal communication, 2005.

Galvas, M.R. “Fortran Program for Predicting Off-Design Performance of Centrifugal Compressors,” NASA TN D-7487, 1973.

Hetrick D.L., *Dynamics of Nuclear Reactors*, University of Chicago, 1971.

Holman, J. P.,*Heat Transfer*, McGraw-Hill, New York, NY, 2001.

Japikse, D. and N.C. Baines. *Introduction to Turbomachinery*, Concepts ETI Inc. and Oxford University Press, 1997.

Japikse, D. *Centrifugal Compressor Design and Performance*, Concepts ETI Inc. 1996.

Jet Propulsion Laboratory, California Institute of Technology, “Jupiter Icy Moons Orbiter,” www.jpl.nasa.gov/jimo, 2004.

Jones, Llewellyn. *Phil Mag*, **28**, p 192, 1939.

Keepin, Robert G. Physics of Nuclear Kinetics, Addison-Wesley Publishing Company, Inc.1965.

Kwan, S. Kwok. “Real-Time Dynamic Simulator for the TOPAZ II Reactor Power System,” CONF-9410181-3, SAND-94-2033C, 1994.

Lipinski R.J. and S.A. Wright. "A Gas-Cooled-Reactor Closed-Brayton-Cycle Demonstration with Nuclear Heating," in *Proceedings of Space Technology and Applications International Forum (STAIF-2005)*, February, 2005.

Mason Lee S., Richard K. Shaltens, and William D. Espinos. "Experimental Data for two Different alternator Configurations in a Solar Brayton Power System", NASA Technical Memorandum 107509, IECEC-97481, *Proceedings of the 32 Intersociety Energy Conversion engineering Conference*, Honolulu, Hawaii, July-August 1997.

Mason L., NASA, Glenn Research Center, personal communication, 2005.

Mason E. A. and Saxena S. C, *The Physics of Fluids*, 1, 361-369 (1958

Mathsoft Engineering and Education, Inc., 101 Main Street, Cambridge, MA 02142-1521, www.mathcad.com, 2005.

MatLab, The Mathworks, 3 Apple Hill Drive, Natick, MA 01760-2098, www.mathworks.com Trademark of MathWorks, Inc., 1994- 2005.

Meek J. M. and J. D. Craggs, *Electrical Breakdown of Gases*, J. Wiley & Sons, New York, NY, 878 pages, 1978.

NASA, Software Repository, https://technology.grc.nasa.gov/software/index.asp, 2005.

Paschen, F., "Uber die zum Funkenubergang in Luft, Wasserstoff und Kohlensqure bei verschiedenen Druken erforderliche Potentialdifferenz" Wied. Ann., 37, 69, 1889.

Postel, O. B. and M. A. Cappelli. "Vacuum emission and breakdown characteristics of a planar He–Xe microdischarge", *Applied Physics Letters,* Volume 76, Number 5 31 January 2000.

Pope M. A. Driscoll M. and Hejzlar P. "Reactor Physics Studies in Support of GFR Core Design*", Transactions of the American Nuclear Society, Proceeding of GLOBAL '03*, New Orleans, LA, Nov. 16-21, 2003.

Saito, S., et. al, "Design of High Temperature engineering Test Reactor (HTTR), JAREI 1332, 6 1994.

Simulink, The Mathworks, 3 Apple Hill Drive, Natick, MA 01760-2098, www.mathworks.com Trademark of MathWorks, Inc., 1994- 2005.

Structural Alloys Handbook, 1988 Ed, Battelle's Columbus Division, Columbus, OH , 1988.

Suid L. H., *The Army's Nuclear Power Program: The Evolution of a Support Agency*, Greenwood Press, NY 1990.

Takase, K. "Experimental Results of Heat Transfer Coefficients and Friction Factors in a 2D/3D Rib-Roughened Annulus", *Experimental Thermal and Fluid Science,* v. 13, pp 142-151, 1996.

Treece W, Personal communication, formally of Capstone Inc., Sep. 2005.

Walsh P.P. and P. Fletcher. Gas Turbine Performance, ASME Press, 1998.

Wasserbauer, C.A. and A.J.Glassman. "FORTRAN Program for Predicting Off-Design Performance of Radial-Inflow Turbines," NASA TN D-8063, 1975.

Watlow Electric Manufacturing Company, 12001 Lackland Road, St. Louis, Missouri, USA 63146, www.watlow.com, 2005.

Weitzberg, A. "Liquid Metal Cooled Reactor Concept for Nuclear Space Initiative Electric Propulsion Missions," Design Data Package to Department of Energy Office of Space and Defense Power systems Space Reactor Programs Team, October, 2002.

Wilke C. R*., Journal of Chemistry and Physics,* 18, 517-519 (1950).

Wilson D. G., *The Design of High-Efficiency Turbomachinery and Gas Turbines*, MIT Press, Cambridge, Massachusetts, 1988.

Wollman M, "The Reactor Module for Project Prometheus", proceedings of the "Space Nuclear Conference 2005", Embedded Topical Meeting at the 2005 ANS Annual Meeting", June 5-9, San Diego, 2005.

Wright S. A., “Preliminary Results of Dynamic System Model for a Closed-Loop Brayton Cycle Coupled to a Nuclear Reactor,” in *Proceedings of the 1st International Energy Conversion Engineering Conference*, 17 - 21 Portsmouth, VA, Aug. 17-21, 2003.

Wright, S.A. “Dynamic Model of a Space Reactor Brayton-Cycle System,” *Transactions of the American Nuclear Society Proceedings*, Washington, DC, November, 2003.

Wright, S. A. and Beets R., “Application of Digitally-Controlled-Reactor Architecture to Space Reactors”, *in Proceedings of the American Nuclear Society Meeting*, Washington DC, November, 2003.

Wright, S. A., and R. J. Lipinski. “Pin-Type Gas Cooled Reactor for Nuclear Electric Propulsion,” in *Proceedings* of *Space Technology and Applications International Forum (STAIF-2003)*, edited by M. El-Genk, AIP Conference Proceedings 654, New York, pp. 408-419, 2003.

Wright, S.A., R. Fuller, , R. J. Lipinsk, K. Nichols, and N. Brown. “Operational Results of a Closed Brayton Cycle Test-Loop,” in proceedings of *Space Technology and Applications International Forum (STAIF-2005)*, edited by M. El-Genk, AIP Conference Proceedings, New York, 2005.

Wright, S.A and Lipinski, R. J. “Gas Cooled Space Fission Electric Power and Propulsion Systems,” Design Data Package Prepared by Sandia National Laboratories for U.S. Department of Energy Office of Space and Defense Power Systems Space Reactor Programs Team, April 17, 2003a.

Wright S.A. and T. Sanchez. “Dynamic Modeling and Control of Nuclear Reactors Coupled to Closed-Loop Brayton Cycle Systems using SIMULINK^{TM} ,” in *Proceedings of Space Technology and Applications International Forum (STAIF-2005)*, February, 2005.

Yahalom R., *SP100 System Thaw Road Map*, SP-100 PIR -1194, January 1994.